The identification and characterisation of novel cytoplasmic ASC-1 complex protein interactions

Thesis submitted for the degree of

Doctor of Philosophy

at the University of Leicester

by

Ryan David Mordue BSc

Medical Research Council Toxicology Unit

University of Leicester

September 2019

The identification and characterisation of novel cytoplasmic ASC-1 complex protein interactions

Ryan Mordue, MRC Toxicology unit, University of Leicester, Leicester, LE1 9HN

Abstract

Cytoplasmic control of gene expression allows for a rapid reprogramming of specific cellular processes in response to stresses, such as exposure to agents that damage nucleic acids. These responses dictate cell fate in the absence of transcriptional regulation, by regulating the expression of proteins that permit a cell to promote cell survival pathways, or alternatively trigger cell death in situations where homeostasis cannot be restored. In general, cytoplasmic control of gene expression is achieved by the action of RNA-binding proteins, therefore, techniques that allow the analysis of the RNA-bound proteome, such as RNA-interactome capture (RIC), permit the identification of novel RNA-binding proteins (RBPs) that have a key regulatory role in these responses. Work within the Willis laboratory has previously identified Activating signal cointegrator 1 (ASC-1) complex subunit 3 (ASCC3) as a cytoplasmic protein that has increased affinity for RNA in response to UVB irradiation. ASCC3 is a member of the ASC-1 complex, which also includes ASCC2, TRIP4, and ASCC1.

In this thesis, the ASC-1 complex members were investigated using immunoaffinity purification and size exclusion chromatography-based approaches. The data show that ASCC3 has increased binding to RNA in a range of cell lines following exposure to UVB and 4NQO, and that the response of ASCC3 and the ASC-1 complex to nucleic acid damage is conserved. FLAG-tagged versions of ASCC3 were generated, and when used as a bait in immunoaffinity purification reactions, the deubiquitinase OTUD4 was identified as a novel interactor of ASCC3. Further studies showed that OTUD4 was part of the cytoplasmic ASC-1 complex, although this interaction may occur with only a small proportion of total cytoplasmic OTUD4. While OTUD4 did not influence control of global protein synthesis rates or cell proliferation, it demonstrated increased binding to polyribosomes following treatment of cells with 4NQO, suggesting that it may function in the ribosome quality control pathway.

Acknowledgments

Firstly, I would like to express my most sincere gratitude to Professor Anne Willis, for providing excellent supervision throughout my PhD studies, giving encouragement, freedom, and support when required most.

I would also like to give a special thank you to Dr Mark Stoneley, who was central to my in-lab training and supervision throughout this project, while also contributing his time for comments and proof-reading of my thesis. I would also like to thank Dr Robert Harvey, for his advice and suggestions towards my thesis; Dr Rebekah Jukes-Jones, for her advice and assistance regarding mass spectrometry; and Dr Claudia Langlais for her helping-hand with size exclusion chromatography.

In general, I would like to thank the whole Willis lab, especially the frequent visitors of the 'coffice', these people, their friendships, and their 'grumpy emails', have got me through tough times; I couldn't have done it without them.

Another thank you must be given to my friends and family, for ensuring my work-life balance led to healthy project progression.

A final very profound thank you is to my wife, Bethany, without her constant love, support, and encouragement, I really could not have done this without her.

Contents

List of figures

List of tables

List of abbreviations

4E-BP	eIF4E-binding protein
4HAQO	4-hydroxyaminoquinoline 1-oxide
4NQO	4-nitroquinoline 1-oxide
4HAQO	4-hydroxyaminoquinoline 1-oxide
6-4PPs	pyrimidine 6-4 pyrimidone photoproduct
8-oxoG	8-oxoguanosine
aatRNA	aminoacyl tRNA
ARE	AU-rich elements
ASC-1	Activating signal cointegrator 1
ASCC3	Activating signal cointegrator 1 complex subunit 3
ATF4	Activating transcription factor 4
ATP	Adenosine triphosphate
BCA	Bicinchoninic acid
BER	Base excision repair
BP	Base pairs
BSA	Bovine serum albumin
CAT-tail	Carboxy-terminal alanine and threonine tail
CDS	Coding sequence
CHX	Cyclohexamide
CLB	Cytoplasmic lysis buffer
Co-IP	Co-immunoprecipitation
CNP	Cyclic nucleotide phosphodiesterase

CPD	Cyclobutane pyrimidine dimers
CTD	Carboxy-terminal domain
CV	Column volume
DDR	DNA damage response
DMEM	Dulbecco's modified eagle's medium
DMSO	Dimethyl sulfoxide
DNA	Deoxyribonucleic acid
dNTP	Deoxynucleoside triphosphate
DR	Direct reversal
dsRNA	Double stranded RNA
DUB	Deubiquitinase
ECL	Enhanced chemiluminescence
EDTA	Ethlenediaminetetraacetic acid
eEF	Eukaryotic elongation factor
eEF2K	Eukaryotic elongation factor 2 kinase
EGF	Epidermal growth factor
eIF	Eukaryotic initiation factor
EJC	Exon-exon junction complex
eRF	Eukaryotic release factor
FBS	Fetal bovine serum
GCN2	General control non-derepressible-2
GDP	Guanosine diphosphate
GEF	Guanine exchange factor

GG-NER	Global genomic NER
GOI	Gene of interest
GTP	Guanosine triphosphate
HEPES	4-(2-hydroxyethyl)-1-piperazineethanesulfonic acid
hnRNP	heterogenous nuclear ribonuclearprotein
HR	Homologous recombination
HRI	Heme-regulated inhibitor
Hsf1	Heat shock factor 1
IFNG	Interferon gamma
IgG	Immunoglobulin
IRES	Internal ribosome entry site
ISR	Integrated stress response
JAMM	JAB1/MPN/MOV34 family
KB	Kilobase
kDa	Kilodaltons
KH	K homology
LB	Lysogeny broth
m7G	7-methyl-guanosine
MAV	Mitochondrial antiviral signalling protein
MDa	Megadalton
Met-tRNAi	Initiator methionyl tRNA
miRNA	microRNA
MIU	Motif interacting with ubiquitin

MOPS	3-(N-morpholino)proanesulfonic acid
MR	Mismatch repair
mRNA	Messenger RNA
mTOR	Mammalian target of rapamycin
MW	Molecular weight
MyD88	Myeloid differential primary response protein MyD88
NER	Nucleotide excision repair
NES	Nuclear export signal
NF-κB	Nuclear factor kappa-light-chain enhancer of activated B cells
NGD	No-go decay
NHEJ	Non-homologous end joining
NMD	Nonsense-mediated decay
NSD	Non-stop decay
ORF	Open reading frame
OTU	Ovarian tumour
OTUD4	Ovarian tumour deubiquitinase 4
PABP	Polyadenylate binding protein
PAGE	Polyacrylamide gel electrophoresis
PBS	Phosphate buffered saline
PEG	Polyethylene glycol
PERK	PKR-like endoplasmic reticulum kinase
PFA	Paraformaldehyde
PIC	Pre-initiation complex

PKR	Protein kinase R
RBP	RNA-binding protein
RG4	G-quadruplex
RIC	RNA interactome capture
RISC	RNA-induced silencing complex
RLR	RIG-I-like-receptor
RNA	Ribonucleic acid
ROS	Reactive oxygen species
RQC	Ribosome-associated quality control
SDS	Sodium dodecyl sulphate
SEC	Size exclusion chromatography
siRNA	Small interfering RNA
SNEB	Soluble nuclear extract buffer
ssDNA	Single stranded DNA
TAE	Tris-acetate-EDTA
TBE	Tris-borate-EDTA
TBS	Tris buffered saline
TBS-T	Tris buffered saline with tween-20
TC	Ternary complex
TCA	Trichloroacetic acid
TC-NER	Transcription coupled NER
TISU	Translation initiator of short 5’ UTR
TLR	Toll-like recpetor

Tris	Tris(hydroxymethyl)aminomethane
tRNA	transfer RNA
TUBEs	Tandem ubiquitin binding elements
Ub	Ubiquitin
UBA	Ubiquitin-binding associated
UCC	Ubiquitin COOH-terminal hydrolase
uORF	untranslated ORF
UPF	Regulator of nonsense transcripts
USP	Ubiquitin specific protease
$USP2_{CD}$	Ubiquitin specific protease 2 catalytic domain
UTR	Untranslated region
UV	Ultraviolet radiation
V	Volt
WT	Wild type
XRN1	5’-3’ exoribonuclease 1
XP	Xeroderma pigmentosum

1. Introduction

Maintenance of cellular homeostasis is important for cell health and survival. The regulation of gene expression enables cells to respond rapidly to internal and external stimuli, including conditions of cellular stress such as DNA damage, heat shock, or nutrient deprivation. In such cases, cells are able to change the repertoire of proteins produced to dictate cell fate, whether that be survival or programmed cell death (Spriggs *et al.* 2010). Gene expression is a continuum and it is regulated by a variety of mechanism to ensure that the required cellular response is achieved. Common regulatory nodes include, but are not limited to, transcription of pre-mRNA (Aramburu *et al.* 2014) splicing of pre-mRNA into mature mRNA (Marengo & Garcia-Blanco 2009), export of mRNA from the nucleus to the cytoplasm (Thomas & Lieberman 2013), regulated RNA trafficking and localisation in the cytoplasm (Di Liegro *et al.* 2014), and mRNA translational control (Jackson *et al.* 2010). Control of protein synthesis is particularly important as it allows for a rapid response to stimuli, since it does not require mRNA production and localisation (Sonenberg & Hinnebusch 2009).

1.1 Eukaryotic translation

Protein synthesis is one of the most expensive cellular processes in the context of energetic requirements (Buttgereit & Brand 1995) and equally importantly, it is also one of the most complex processes a cell undertakes. It is unsurprising therefore, that the production of a polypeptide chain by decoding mRNA is a highly regulated process. Eukaryotic translation occurs in three major phases: initiation, elongation, and termination. Initiation is thought to be the rate-determining step of protein production because it is subject to a large degree of regulation (Reeve *et al.* 2014). However, regulation during translation elongation has been shown to be equally important (Richter & Coller 2015).

1.1.1 Canonical cap-dependent eukaryotic translation initiation

Formation of an elongation-competent 80S ribosome at the start codon of the mRNA occurs during translation initiation. Translation initiation requires many eukaryotic initiation factors (eIFs) and the methionyl transfer RNA (Met-tRNAi), which is specialised for initiation. Major steps include scanning of the mRNA by the 43S pre-initiation complex (PIC), leading to formation of the 48S initiation complex at the AUG codon, followed by the joining of the 80S subunit.

1.1.1.1 Formation of the 43S pre-initiation complex

Before the PIC can be formed, a ternary complex (TC) must be assembled. The TC is comprised of three eIF2 subunits (α, β, γ), to which GTP and the Met-tRNAi are able to bind (Figure 1-1A) (Kimball 1999). The TC is then recruited to the 40S ribosomal subunit with the aid of eIF1, eIF1A,

eIF3, and eIF5 (Sonenberg & Hinnebusch 2009). This forms a complete 43S PIC which is prepared for recruitment to the mRNA (Figure 1-1A) (Merrick 1992).

1.1.1.2 43S PIC recruitment to mRNA

Before the 43S PIC is recruited to the mature mRNA, a number of eIFs must prepare the mRNA. The eIF4F complex contains the DEAD-box helicase eIF4A, its interaction partner eIF4B, the scaffold protein eIF4G, and the mRNA cap-binding factor eIF4E (Figure 1-1A). Interaction of eIF4E with eIF4G causes increased affinity to the 7-methyl-guanosine (m^7G) cap end of the mRNA (Gross *et al.* 2003). This interaction also causes a conformational change which aids the alignment of eIF4A in the orientation required for ATP-dependent helicase activity (Marintchev *et al.* 2009). Recognition of the 5' cap structure by eIF4E, and the RNA binding sites in eIF4G, allows the anchoring of eIF4A to the 5' untranslated region (UTR) of the mRNA (Figure 1-1B step 1). Helicase power of eIF4A is stimulated by its accessory proteins eIF4B and eIF4H, which unwinds regions of RNA structure in the 5' UTR (Pestova & Kolupaeva 2002). eIF4G bound to the 5' UTR of the mRNA interacts with polyadenylate-binding protein (PABP), and the 3' poly(A) tail at the opposite end of the mRNA. This forms an mRNA loop structure and prepares the mRNA for 43S PIC recruitment (Figure 1-1B step 2). The interaction of eIF4B with PABP has also been shown to contribute to the stability of the complex (Bushell *et al.* 2001). At this stage, the 43S PIC is recruited to the m^7G cap proximal region at the 5' end of the mRNA, through interaction of eIF3 with eIF4G, forming the 48S complex.

1.1.1.3 Ribosome scanning

Upon recruitment of the 43S PIC to the mRNA and formation of the 48S complex, the PIC scans in a 5' to 3' direction along the mRNA until detection of the start codon (Figure 1-1B step 3). The current model suggests that the 48S binds the mRNA in an "open" conformation, induced by eIF1 and eIF1A, and stabilised by eIF3 (Nanda *et al.* 2013). As described previously, unwinding of mRNA structure by eIF4A facilitates scanning, while non-cognate pairing of the Met-tRNAi anti-codon with the mRNA also aids the scanning process (Sonenberg & Hinnebusch 2009).

Kozak consensus is an optimal sequence of nucleotides surrounding the AUG for efficient recognition by the PIC. Kozak consensus is defined as GCC(A/G)CC**AUG**G, with a purine in the -3 position and G in the +4 position relative to the A of the AUG codon, which is assigned the +1 position (Kozak 1987).

An AUG codon present in a good Kozak consensus on the mRNA is recognised by the PIC through base pairing of the Met-tRNAi anti-codon (Figure 1-1B step 4). This recognition triggers a series of events, including the hydrolysis of the eIF2-bound GTP via eIF5 GTPase-activation, and

dissociation of eIF1 from the PIC (Maag *et al.* 2005). The position of the AUG from the mRNA 5' end and the Kozak context in which it sits are integral factors in determining the recognition by a scanning ribosome. AUG codons without good context can appear "leaky", with only a small chance of the PIC identifying the poor context AUG as a start codon. In these cases, the PIC will often continue scanning until it recognises an AUG in better context (Kozak 1991).

1.1.1.4 80S ribosome assembly

Dissociation of eIF1, eIF2-GDP and eIF5 from the PIC allows the joining of the 60S subunit mediated by eIF5B (Figure 1-1B step 5) (Nag *et al.* 2016). Displacement of eIF1A from the ribosomal P-site upon start codon recognition causes the C-terminal end of eIF1A to become available. The interaction of the eIF5B C-terminus with the C-terminus of eIF1A is required for efficient subunit joining. Once joining has occurred eIF5B hydrolyses GTP, resulting in dissociation of eIF5B and eIF1A, forming the 80S initiation complex (Figure 1-1B step 6) (Acker *et al.* 2006).

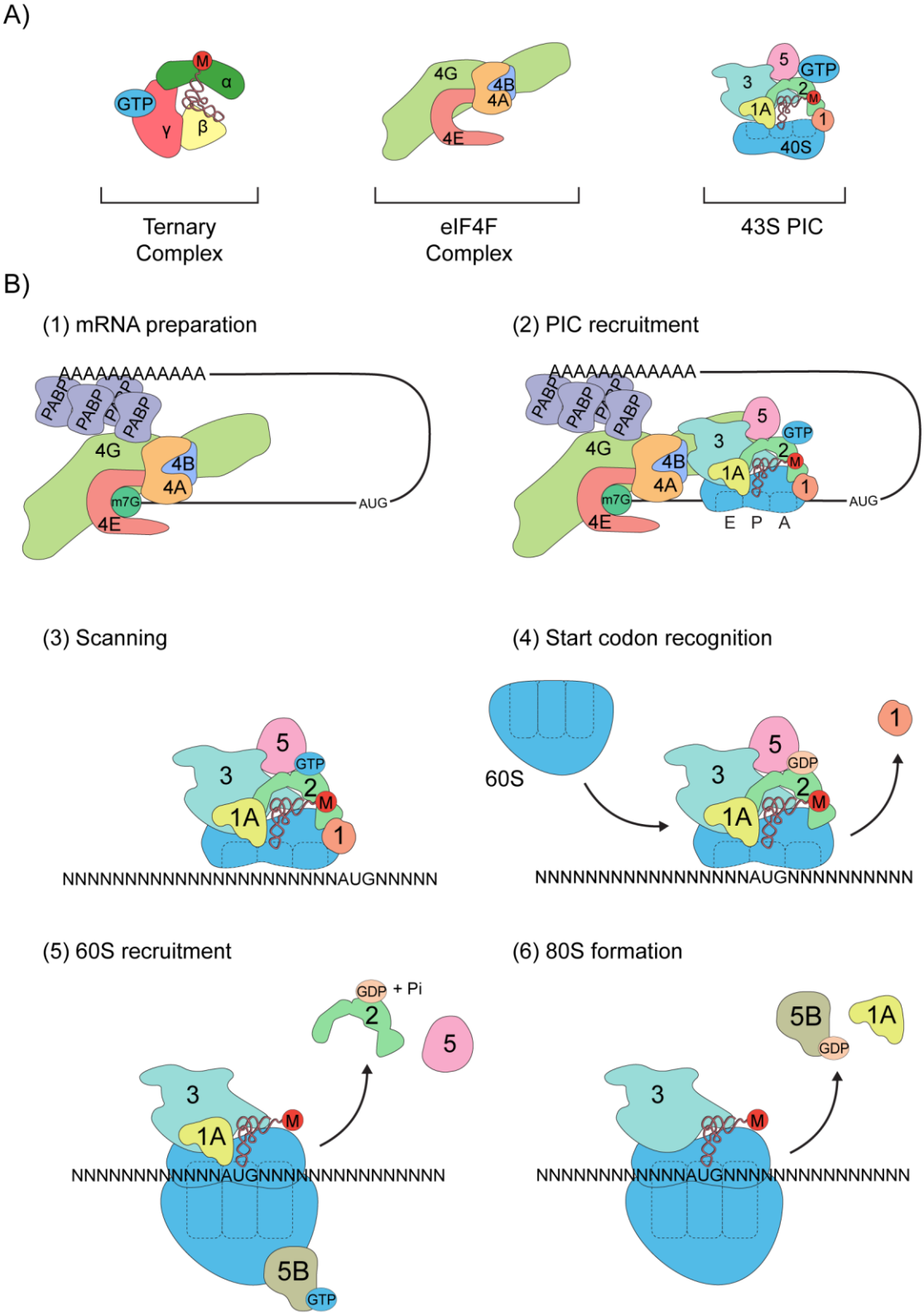

Figure 1-1. Schematic of eukaryotic translation initiation

To clarify, all eukaryotic initiation factor names have been abbreviated and are missing the eIF label. For example, eIF4G becomes 4G. A) Schematic of initiation complexes. The TC made up of eIF2 subunits as described in section 1.1.1.1, the eIF4F complex described in section 1.1.1.2, the 43S PIC as described in section 1.1.1.1. B) Schematic of eukaryotic translation initiation steps as described in section 1.1.1.

1.1.2 Cap-independent translation initiation

The majority of translation initiation occurs using cap-dependent initiation. However, under changes in cell condition such as viral infection, the conventional scanning mechanism can be bypassed through use of internal ribosome entry sites (IRES). IRESes are highly variable RNA structures which all achieve the same goal in promoting translation through cap-independent mechanisms (Stoneley & Willis 2004). Viruses use IRES structures in order to bypass the translational inhibition mechanisms that cells employ under conditions of stress caused by that of the virus. In the past decade the data have shown that up to 10% of mammalian mRNAs also contain an IRES structure (Stoneley & Willis 2004). In general, cellular IRESes are used to maintain the expression of key proteins under conditions of stress, including apoptotic and heatshock proteins, but are also required for development.

1.1.3 Eukaryotic elongation

Translation elongation is the reading of the mRNA strand and formation of the polypeptide chain once the initial Met-tRNAi has been incorporated. The basic principal of elongation stems from three steps, which are repeated until termination is required. The three steps consist of recruitment of the cognate aminoacylated tRNAs (aatRNAs) to the A-site, peptide bond formation, and finally the translocation of the ribosome to the next codon.

After 80S formation the Met-tRNAi is present in the ribosomal P-site, with both A- and E-sites unoccupied. Cognate and non-cognate aatRNA, as part of the ternary elongation complex, are then able to enter the A-site of the ribosome (Figure 1-2B step 1). The ternary elongation complex consists of GTP, aatRNA, and eukaryotic elongation factor (eEF) 1A (Figure 1-2A). However, only presentation of a cognate tRNA with the correct anti-codon is able to stabilise the interaction through conformational changes. This stabilisation leads to GTP hydrolysis and activation of ribosomal peptidyl transferase activity (Figure 1-2B step 2). The hydrolysis of GTP provides the energy for the formation of a peptide bond, deacetylation of the tRNA in the P-site, and transfer of the peptide chain to the tRNA in the A-site (Figure 1-2B step 3). Following peptidyl-transferase activity, eEF2-GTP is recruited to the ribosome; hydrolysis of the bound GTP to GDP stimulates ribosome translocation one codon towards the 3' end of the mRNA (Figure 1-2B step 6). This allows the release of the de-acetylated tRNA in the E-site, followed by the movement of the de-acetylated tRNA in the P-site into the E-site, and the peptide chain linked tRNA into the P-site. This also allows the eEF2 bound GDP to dissociate and be recycled (Figure 1-2B step 5), leaving the A-site free to accept the next ternary elongation complex and completing the elongation cycle. The cycle is continued until the ribosome encounters a stop codon (Dever & Green 2015).

1.1.4 Termination

Translation termination occurs when the translocating 80S ribosome encounters a stop codon (UAG, UAA, or UGA) in the mRNA sequence (as reviewed in (Jackson *et al.* 2012)). The stop codon is recognised by eukaryotic release factor (eRF) 1 which enters the empty A-site of the ribosome. Entry of eRF1 into the A-site leads to release of the polypeptide chain through hydrolysis of the ester bond linking the chain to the tRNA in the P-site. Activity of eRF1 is stimulated by eRF3.

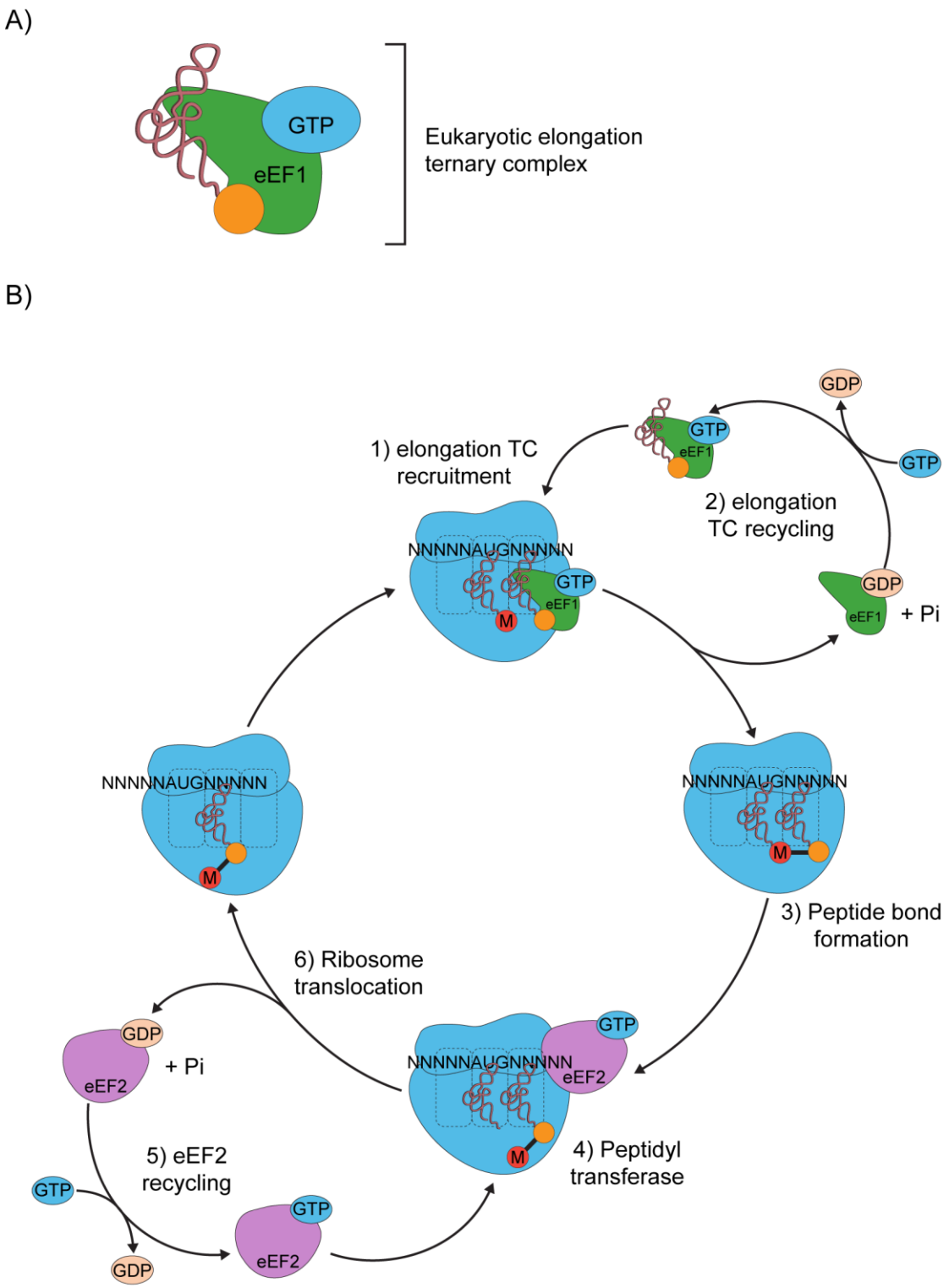

Figure 1-2. Schematic of eukaryotic translation elongation

A) The eukaryotic elongation ternary complex is formed of tRNA, eEF1, and GTP. These complexes shuttle in and out of the ribosome A-site until the cognate tRNA is detected. B) The eukaryotic translation elongation cycle. Showing entry of the cognate tRNA into the A-site, elongation TC recycling, peptide bond formation, peptide transfer, eEF2 recycling, and ribosome translocation.

1.2 Post-transcriptional regulation of gene expression

1.2.1 Regulation of translation initiation

Two major pathways are involved in the rapid inhibition of global protein synthesis at the level of translation initiation, one is the phosphorylation of the eIF2α leading to reduced TC availability, and the other is regulation of eIF4E availability through 4E binding proteins (4E-BPs).

1.2.1.1 Translation inhibition by eIF2α phosphorylation

Regulation of translation initiation can be achieved by targeting the availability of the TC, as reduced TC leads to reduced initiation and downregulation of global protein synthesis. The molecular mechanism for modulating TC availability is through preventing the recycling of eIF2-GDP (low affinity for Met-tRNAi) to eIF2-GTP (high affinity for Met-tRNAi) by the GTP exchange factor (GEF) eIF2B (Figure 1-3A) (Hinnebusch 2005; Wek *et al.* 2006). Phosphorylation of eIF2 at serine 51 of the alpha subunit allows for stabilised binding to eIF2B, therefore sequestering eIF2B and preventing turnover of eIF2-GDP to eIF2-GTP (Sudhakar *et al.* 2000).

Phosphorylation of eIF2α at serine 51 in mammals is carried out by four kinases, which are activated in response to specific cellular stresses, although some functions overlap. The kinases are heme-regulated inhibitor (HRI) which is activated in response to heme deficiency; protein kinase R (PKR), activated in response to interferons and double stranded RNA; PKR-like endoplasmic reticulum (ER) kinase (PERK), in response to ER stress; and general control non-derepressible-2 (GCN2), in response to amino acid starvation or UV irradiation (Hinnebusch 2005; Parker *et al.* 2006; Sudhakar *et al.* 2000; Wek *et al.* 2006).

1.2.1.2 Regulation of eIF4E by 4E-BPs

Global regulation of protein synthesis also occurs by controlling the bioavailability of eIF4E. There are a family of eIF4E-binding proteins (4E-BPs) that bind and sequester eIF4E, preventing eIF4F formation (Figure 1-3B) (Faller *et al.* 2015; Harvey *et al.* 2017; Sonenberg & Hinnebusch 2009; Spriggs *et al.* 2010). Activity of 4E-BPs are regulated through phosphorylation at four main residues: threonine 46, threonine 37, threonine 70 and serine 65 (Fadden *et al.* 1997). Hypophosphorylation of 4E-BPs increase affinity for eIF4E, leading to decreased translation initiation, while hyperphosphorylated 4E-BPs have a much weaker affinity. Activity of 4E-BPs is primarily regulated through the mTOR signalling pathway (Jackson *et al.* 2010). Factors which determine the activity of mTOR signalling involve hormones, growth factors, and pH, and therefore have a direct impact on global protein synthesis through changes in 4E-BP phosphorylation status.

1.2.2 Regulation of translation elongation

The overall rate of translation elongation is determined by two main factors; tRNA/eEF1A codon decoding, and eEF2-dependent ribosome translocation. Control of either of these steps is important for cell survival, division, and dysregulation which is associated with tumorigenesis. For example tRNA availability can control protein synthesis rates of specific mRNAs in tumours (Zhang *et al.* 2018). Under normal cellular conditions, reduced availability of the cognate tRNA to a specific codon can cause ribosome slowing on the mRNA, and it is now known that reduced elongation speed can now feedback into initiation and cause a global reduction in protein synthesis (Harvey *et al.* 2017). However, in some tumours, a distinct pool of tRNAs can be utilised to programme a subset of proteins which promote the tumour cell environment (Gingold 2014).

As previously described (Section 1.1.4) eEF2 aids ribosome translocation on the mRNA following peptidyl transferase activity. The ability of eEF2 to modulate this translocation step is reliant on its phosphorylation status. Phosphorylation of eEF2 at threonine 56 by its kinase (eEF2K) leads to complete inactivation of eEF2 through its inability to interact with the ribosome (Figure 1-3C). This single phosphorylation is therefore able to abolish ribosome translocation and elongation (Ryazanov *et al.* 1988). Tumour cells are known to exploit this pathway in order to adapt to nutrient deprivation (Leprivier *et al.* 2013).

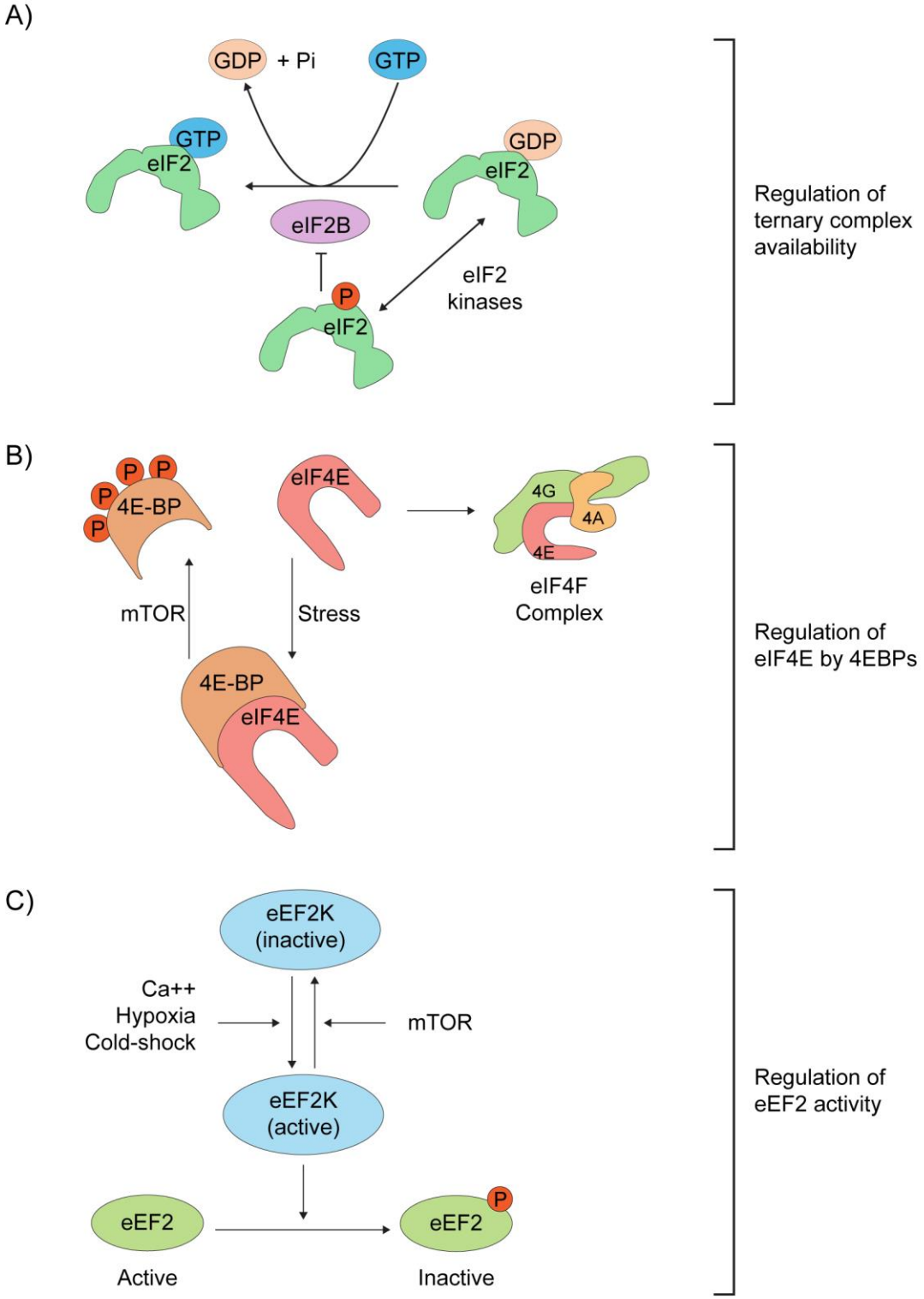

Figure 1-3. Regulation of translation following stress

Three major regulated steps of translation following cellular stress. A) TC formation can be reduced following phosphorylation of the alpha subunit of eIF2. Phospho-eIF2 binds eIF2B a prevent TC formation by preventing GDP-GTP exchange. B) Conditions of stress causes 4E-BP dephosphorylation by mTOR inactivation. 4E-BP then binds a sequesters eIF4E, preventing eIF4F complex formation. eEF2K becomes active during conditions of stress which phosphorylates and inactivates eEF2.

1.2.3 Translation of uORFs

Phosphorylation of eIF2α reduces protein synthesis on a global scale due to TC availability, but in turn causes up-regulation of a specific subset of transcripts, encoding most commonly for stress-response genes. These genes include key DNA damage and repair genes as part of the integrated stress response (ISR). The most studied example of an mRNA upregulated under these conditions is mammalian activating transcription factor 4 (*ATF4*). *ATF4* contains two upstream open reading frames (uORF). The second uORF overlaps the coding region, therefore, under conditions of high TC abundance (unstressed), allows for re-initiation at the second uORF and no translation of ATF4. Conditions of stress which activate the ISR and increase eIF2α phosphorylation cause decreased TC availability. This subsequently leads to reduced re-initiation at the second uORF and is more likely to re-initiate at the coding AUG, allowing for translation of ATF4 (Wek *et al.* 2006).

1.2.4 Stability and decay

The stability and decay of a given transcript can be largely governed by interactions between the mRNA structural components (including the 5'-cap structure, 5'UTR, coding sequence (CDS), 3'UTR, and poly(A) tail), and trans-acting factors (Guhaniyogi & Brewer 2001). While splicing (Section 1.2.5), structures within the mRNA (Section 1.2.6), and RNA-binding proteins (RBPs) (Section 1.2.8), all impact the stability and decay of their corresponding mRNAs, processes such as 5'-decapping, de-adenylation, and RNA degradation pathways play a more direct role on mRNA decay (Figure 1-4A). With some exceptions, the majority of all protein encoding mature mRNAs possess a N7-methylated guanosine, which is linked to the first nucleotide of the RNA via reverse 5' to 5' triphosphate linkage, known as the 5'-cap or 5'-m7G cap (Ramanathan *et al.* 2016). A poly(A) tail is also present on the great majority of these mRNAs, providing stability and efficient protein production. The cap structure is essential for mRNA cap-dependent translation (Section 1.1.1), preventing 5'-3' exonucleolytic activity by XRN1 and allowing mRNA circularisation through the interaction of eIF4G with PABP1 at the poly(A) tail, which subsequently protects the mRNA from 3'-5' degradation by the exosome (Guhaniyogi & Brewer 2001; Wiederhold & Passmore 2010). The deadenylation dependent arm of the mRNA degradation pathway provides two steps which can provide a point of gene expression regulation (Guhaniyogi & Brewer 2001). The first of these is shortening or removal of the poly(A) tail. While complete deadenylation results in degradation, shortening of the poly(A) tail causes reduced transcript specific translation and slows entry into the degradation pathway (Wiederhold & Passmore 2010). The second is decapping, which follows deadenylation as the next step in mRNA processing for degradation. While typically this reaction is only needed for

preparing the mRNA for 5'-3' degradation, a recent study in *Arabidopsis thaliana* has shown decapping contributes to the modulation of stress related transcription factors in an ABA-dependent manner (Wawer *et al.* 2018). The deadenylation independent decay pathway is caused by endonucleolytic activity within the transcript, and targeting of the mRNA fragments by the mRNA quality control pathways described further in section 1.3.1.

Stability and expression of a given mRNA can also be regulated by noncoding RNAs, including microRNAs (miRNAs) and short interfering RNAs (siRNAs). Consisting of around 21 to 26 nucleotides, miRNAs and siRNAs are processed in a dicer-dependent manner (Figure 1-4C). The regulatory function for both RNAs is exerted through the Argonaute (Ago) protein family (Liu & Lu 2012). Association of miRNAs or siRNAs with Ago proteins form RNA-induced silencing complexes (RISCs). RISC does not directly repress expression of their targeted transcript but recruits the Ccr4-NOT complex. This complex allows translational repression, as well as destabilisation of the targeted mRNAs, allowing them to modulate gene expression (Wilczynska & Bushell 2015). The expression profile for noncoding RNAs has been shown to be specific to the stress stimulus and cell type (Wang & Taniguchi 2013).

1.2.5 Splicing

Splicing of pre-mRNA occurs co-transcriptionally to generate mature mRNA by removing introns and joining exons (Figure 1-4D). The spliceosome is a well-studied RNA-protein machine which catalyses the splicing reaction. Genotoxic stress alters splicing by several distinct mechanisms, including changing the rate of transcription, while also sequestering and transactivating of splicing factors (Thomas & Lieberman 2013). Alternative splicing and production of antagonistic isoforms of many apoptotic genes suggests an important role in the response to DNA damage. In response to UV irradiation, hyperphosphorylation of RNA polymerase II at the carboxy-terminal domain (CTD) causes transcription elongation inhibition. The p53-independent kinetic coupling of RNA polymerase II elongation with alternative splicing allows for modulation of global alternative splicing in response to UV (Marengo & Garcia-Blanco 2009; Muñoz *et al.* 2009). RBPs also play an important role in splicing efficiency of specific targets. For example, splicing factor SKIP is required for p21 splicing, promoting cell survival following DNA damage (Chen *et al.* 2011). Regulation of p53 can also be achieved partly through splicing regulation. Interaction of EWS and YB-1, two RBPs, is required for the correct splicing of MDM2, the negative regulator of p53. In response to DNA damage, the EWS/YB-1 interaction is impaired, leading to eight of twelve exons being excluded from the MDM2 transcript, therefore limiting full-length MDM2 expression and contributing to cell survival following DNA damage (Dutertre *et al.* 2014).

1.2.6 mRNA structures

The CDS of a given mRNA is the primary method of transmitting genetic information from the cellular DNA. The untranslated regions at the 5' and 3' ends of these mRNAs are able to form considerable structures which can regulate the translation of their CDS.

1.2.6.1 TISU

While not typically considered a structure, some mRNAs with extremely small 5' UTRs can possess translation initiator of short 5' UTR (TISU) elements. TISU elements allow for scanning-free cap-dependent translation initiation and are present in some mRNAs. Functional classification of mRNAs bearing the TISU element reveals important cellular activities such as protein biogenesis and degradation, protein folding, RNA metabolism, and mitochondrial function (Elfakess & Dikstein 2008).

1.2.6.2 Physical structures

Base pairing in the mRNA UTRs can lead to formation of a variety of structures. These include pseudoknots, hairpins, RNA g-quadruplexes (RG4) and IRESes (Figure 1-4A). Modulation of translation by IRESes has already been described in section 1.1.2 as part of the cap-independent translation initiation mechanism. While the IRES demonstrates an example of positive regulation of translation of a given transcript, the other three structures mentioned here predominantly hold a negative regulatory effect. Common structures such as hairpins are most likely resolved by the ATPase-dependent duplex unwinding activity of eIF4A present in the eIF4F complex, and is thought to permit scanning of 48S ribosome (Parsyan *et al.* 2011). In support of this hypothesis, ribosome profiling following silvestrol (an inhibitor of eIF4A) treatment showed decreased translation efficiency of mRNAs with long 5'UTRs (Wolfe *et al.* 2014). DHX29 can also unwind structured 5'UTRs and has shown some compensatory role for the loss of eIF4A activity (Pisareva *et al.* 2008).

In vitro work has shown RG4 structures are perhaps the most stable RNA structure, and may be present in up to ~3000 human mRNAs (Leppek *et al.* 2018). Their ability to slow the scanning of the 48S ribosome of the 5'UTR has suggested that these may have a role in neuronal local translation (Schofield *et al.* 2015). The highly polarised nature of the neuron, with its distal axonal tips far reaching from the cell body, has led researchers to investigate localised translation in this cell type. Proteins such as FMRP are able to bind RG4 containing mRNAs then use motor proteins to transport them to the axonal tips where translation can occur (Schofield *et al.* 2015). The rapid changes in local monovalent cations within neurons and the sensitivity of

RG4 formation to monovalent cation concentration, suggests that this could play a role in localised translation of mRNAs containing RG4s upon neuron stimulation.

Pseudoknot structures may also play a role in translation regulation, but also may play a greater role in the regulation of global protein synthesis. The three dimensional structures are thought to reside in the 5'UTR of the interferon gamma (*IFNG*) mRNA, which signals in its own local feedback loop (Ben-Asouli *et al.* 2002). Translating ribosomes normally disrupt the pseudoknot and allow for IFN-γ translation in a positive feedback loop. When translation is reduced and the pseudoknot re-forms, the double stranded RNA (dsRNA) of the knot can stimulate PKR, which regulates ternary complex formation (as described in section 1.2.1.1) to repress IFN-γ expression (Cohen-Chalamish *et al.* 2009). Therefore as part of the IFN-γ feedback loop, the pseudoknot structure prevents excess interferon production by adjusting translation of its mRNA through local PKR activity (Leppek *et al.* 2018).

1.2.7 Stress granules

Protein synthesis can be globally regulated by the formation of cytoplasmic stress granules, which contain RBPs and translationally inactive mRNAs. Thus, stress granules are considered mRNA storage sites, as they contain mRNA in a translationally repressed state. However, their precise molecular function remains unclear. The RBPs present in stress granules commonly contain intrinsic disordered regions that promote their formation through the phenomenon of liquid-liquid phase separation, which is thought to help increase enzymatic activity at the outer shell by molecular crowding (Molliex *et al.* 2015; Sfakianos *et al.* 2016). While the specific requirements for entry into stress granules largely remains unknown, they are enriched for mRNAs which are long or less efficiently translated (Figure 1-4E) (Khong *et al.* 2017). Although some core protein components of stress granules have now been identified (e.g. G3BP1 and TIA-1), the protein combinations found is highly dependent on the stress stimulus (Aulas *et al.* 2017; Harvey *et al.* 2017).

1.2.8 RNA binding proteins

Stability and decay of transcripts contributes to the rapid adaption of protein synthesis levels in response to environmental conditions. The DNA damage response decreases transcription making it important to regulate the production of protein from the pre-existing pool of mRNAs (Ramachandran *et al.* 2011). Stability and translation rates of mRNAs are primarily regulated by RBPs and noncoding RNAs. AU-rich elements (AREs) are present in the 3'UTR of many mRNAs and are influential sequence elements for regulation. The ARE-binding protein, TIAR, has been

shown to repress translation of several mRNAs, including GADD45α, eIF4A, and eIF4E, especially in response to UV radiation (Mazan-mamczarz *et al.* 2006; Montecucco & Biamonti 2013). HuR is a well-studied RNA binding protein that controls expression of DNA damage response (DDR) genes in response to DNA damage. Normal conditions promote phosphorylation and nuclear retention of HuR by Cdk1. During the DNA damage response however, Cdk1 is phosphorylated and inactivated by Chk1 or Chk2 in response to ATM/ATR signalling (Kim *et al.* 2010). This allows cytoplasmic export of HuR, followed by stabilisation of target mRNAs, a well-studied example being *WEE1* (Kim *et al.* 2010; Lal *et al.* 2014). The specificity of HuR binding to mRNA is largely regulated by phosphorylation at specific sites by the major DNA damage kinases, and also by the presence of ARE on the mRNA (Lal *et al.* 2014). The direct binding of *WEE1* mRNA by HuR at its ARE leads to stabilisation and increased expression in response to DNA damage. Upregulation of WEE1 leads to increased γH2A.X levels, Cdk1 phosphorylation, and promotes cell cycle arrest at G_2-M transition (Lal *et al.* 2014).

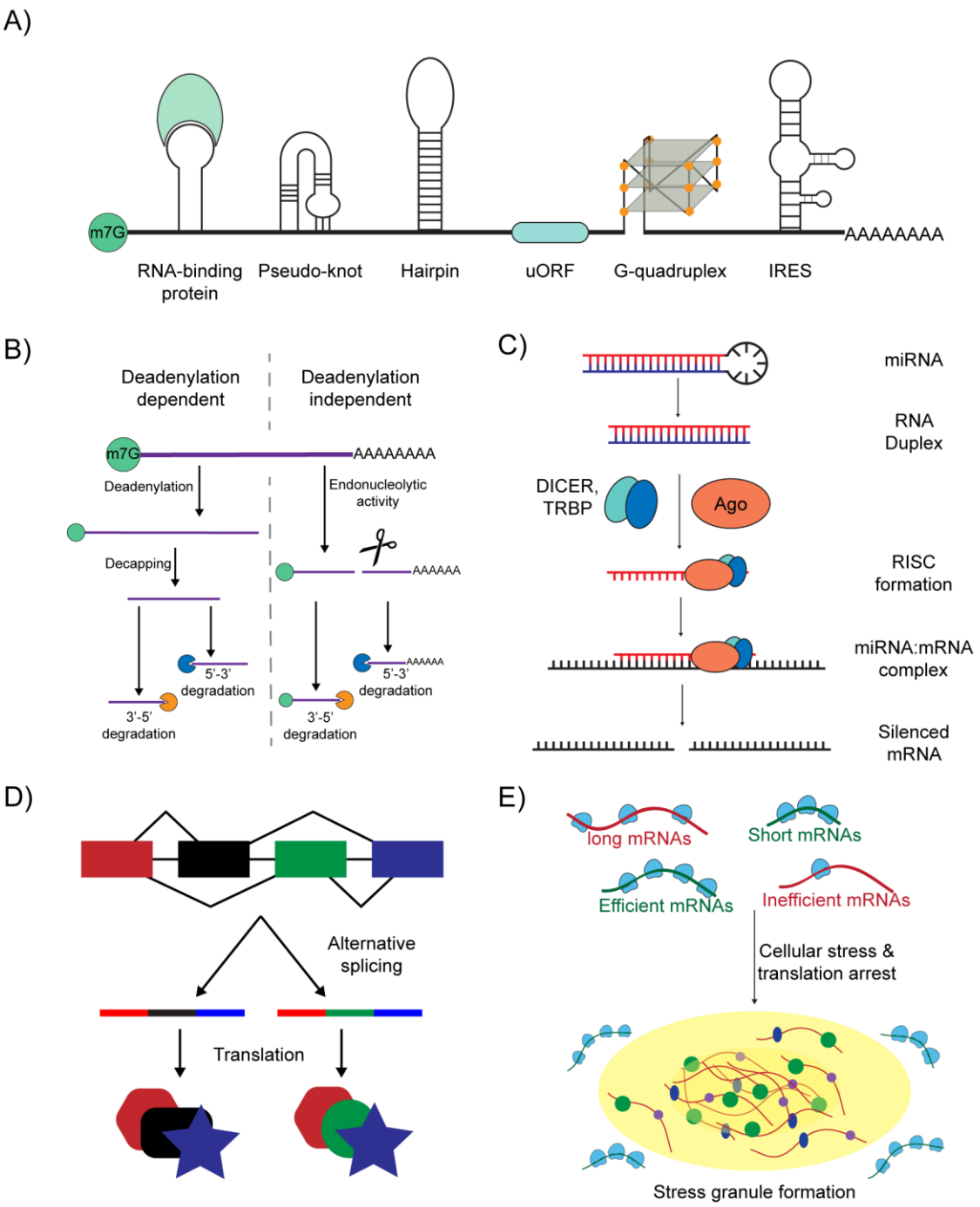

Figure 1-4. Mechanisms of post-transcriptional regulation of gene expression

Schematic detailing mechanisms of post-transcriptional regulation of gene expression described in section 1.2. A) RNA structures and motifs which can modulate the rate of translation on a given transcript. B) Typical mRNA decay pathways involving deadenylation dependent and independent pathways. C) Gene silencing by miRNAs. D) Alternative splicing of a gene can alter the functional properties of the translated protein. E) Stress granules can protect mRNAs from degradation which also reducing translation.

1.3 Ribosome-associated quality control

The energetic expenditure required to produce and degrade proteins makes it important to prevent unsuccessful protein synthesis. Therefore, cells have evolved various mechanisms for maintaining the integrity of the transcriptome and proteome. These mechanisms can be placed into two main categories: first, those involving mRNA integrity, and secondly, involving protein integrity. Interestingly, all these mechanisms intersect at the ribosome, and this ensures that defective mRNAs and products of translation are detected at the earliest opportunity.

1.3.1 Ribosome-associated mRNA quality control

There are three major mechanisms for recognising and removing aberrant mRNAs from the cell, which in turn prevents production of aberrant proteins. These mechanisms include: nonsense-mediated decay (NMD), which acts on mRNAs with premature stop codons; no-go decay (NGD), which is involved in truncated mRNAs and stalled ribosomes, and finally non-stop decay (NSD); focusing on mRNAs without the presence of a natural stop codon (Joazeiro 2017).

1.3.1.1 Nonsense-mediated decay

The function of NMD is to eliminate mRNA transcripts containing premature stop codons, to reduce gene expression errors. Many NMD target RNAs are derived from errors in splicing and translation initiation, but interestingly NMD can also target healthy mRNA transcripts following changes in cellular conditions to promote appropriate cell responses (Kurosaki & Maquat 2016).

NMD can be broadly described as a three-step pathway involving recognition, tagging, and degradation (Figure 1-5A). The most widely accepted model for the activation of the NMD pathway suggests that NMD substrates are recognised following the failure to remove the exon-exon junction complex (EJC), which remains bound to the mRNA following splicing errors (Popp & Maquat 2014). Normally the EJC is removed by the translating ribosome. However, the EJC complex will remain in instances where the EJC resides more than ~50-55 nucleotides downstream of the stop codon, providing a substrate for NMD. Following detection of the NMD substrate, the premature stop codon is tagged via the formation of the SURF complex, consisting of UPF1, SMG1, SMG8, SMG9, eRF1, and eRF3 at the terminating ribosome (Kashima *et al.* 2006). It has also been shown that phosphorylated UPF1 is a discriminating marker of cellular NMD targets (Kurosaki *et al.* 2014). The SURF complex is localised to the premature stop codon through interaction with UPF2, which is present at the premature stop codon through interaction with UPF3 or UPF3X. SMG1 is regulated by SMG8 and SMG9 in order to phosphorylate UPF1, which induces translational repression and recruits the endonuclease SMG6 and the SMG5-SMG7 heterodimer (Kashima *et al.* 2006). SMG6 cleaves the NMD target

mRNA in the vicinity of the premature stop codon (Izaurralde *et al.* 2008). In this state, the mRNA can no longer be used for protein synthesis, and thus the role of SMG5-SMG7 is to recruit decapping and/or deadenylation machinery to facilitate the exonucleolytic degradation of the 5'- and 3'-mRNA fragments remaining following NMD (Kurosaki *et al.* 2014). The 5'- cleavage product is degraded by the exosome in *S. cerevisiae* or DIS3L2 in mammals (da Costa *et al.* 2019) and the 3'-product degraded by XRN1.

1.3.1.2 No-go decay

mRNAs present within stalled ribosome complexes are the typical substrate for NGD (Figure 1-5B). Dom34 (Pelota in mammals) and Hbs1 are homologous to eRF1 and eRF3 respectively, indicating they function at the location of the ribosome A-site. Dom34/Hbs1 enters the A-site and together with ABCE1 causes ribosome splitting. The nascent peptidyl-tRNA is cleaved by Vms1 then the peptide extracted and degraded (Passos *et al.* 2009; Verma *et al.* 2018). Pelota-Hbs1 can stimulate endonucleolytic cleavage of the mRNA and promote its degradation (Passos *et al.* 2009). Ribosome density has been shown to affect the efficiency of NGD, likely indicating that the signal from ribosome collision enhances NGD activity. Like with NMD, the mRNA cleavage products are degraded by Xrn1 and the exosome (Harigaya & Parker 2010).

1.3.1.3 Non-stop decay

There are different mechanisms which lead to production of mRNAs lacking a stop codon. These mechanisms include erroneous polyadenylation, or endonucleolytic cleavage within the ORF, generating the non-stop mRNA lacking polyadenylation (Garzia *et al.* 2017). Translation of the poly(A) tail has been shown to cause stalling of ribosomes, which was originally thought to be caused by the positively charged consecutive lysine residues interacting with the negatively charged ribosome tunnel. In cases of mRNAs lacking the poly(A) tail, the ribosome becomes stuck at the very 3' end of the mRNA. In both cases the mRNA must be degraded to prevent energetic waste and aberrant protein accumulation (Saito *et al.* 2013).

It has been shown that the protein Ski7, a structural homolog to Hbs1 and eRF3, is able to bind and recruit the exosome in yeast. This process is absent in higher eukaryotes, which relies on the action of Pelota-Hbs1 for processing of non-stop mRNAs. Pelota-Hbs1 can directly interact with the exosome-Ski complex allowing for ribosome splitting and degradation of the aberrant mRNA (Figure 1-5C) (Saito *et al.* 2013).

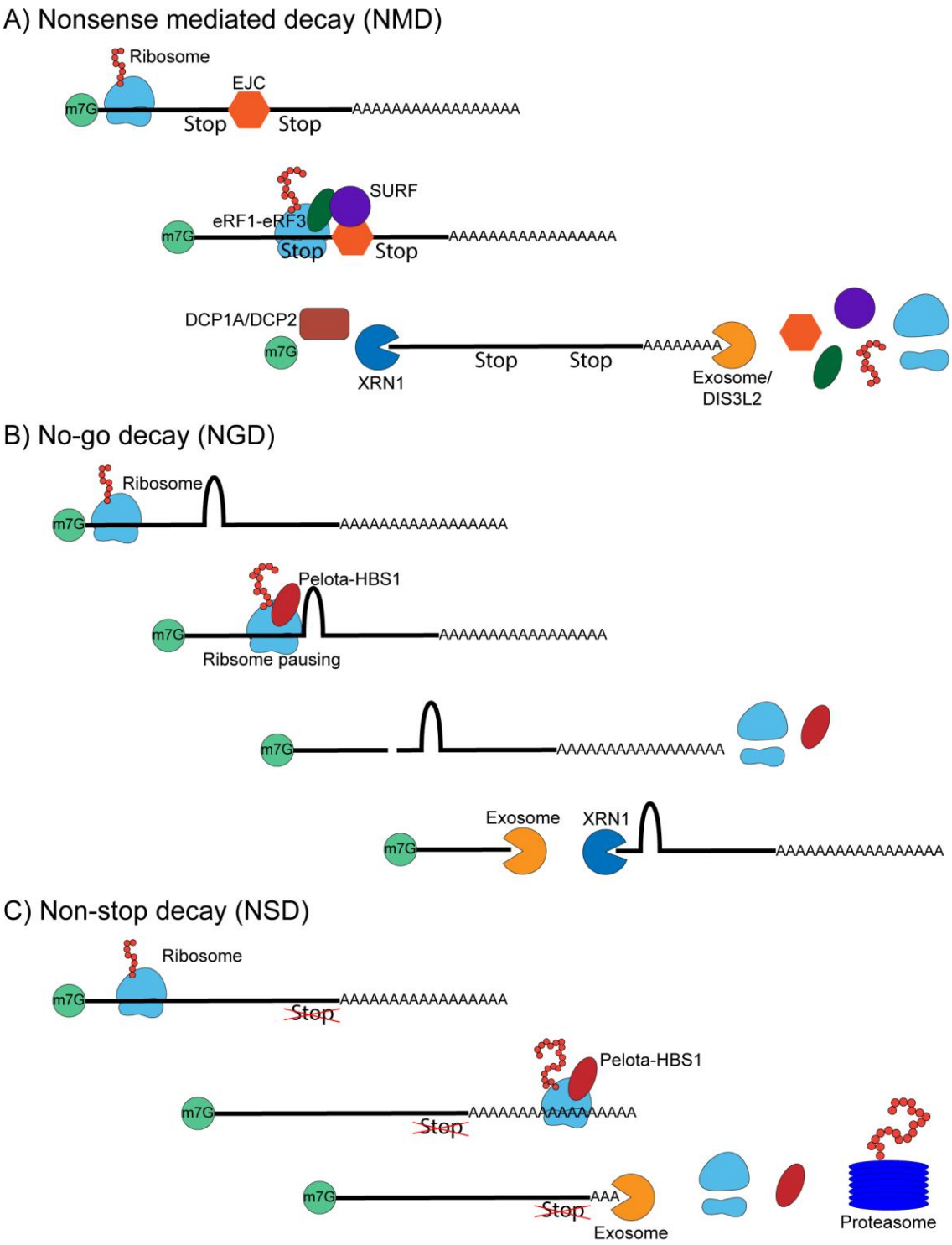

Figure 1-5. Ribosome-associated mRNA quality control

Schematic of mRNA quality control mechanisms. A) NMD depicts recognition of the EJC, followed by the recruitment of the SURF complex. The ribosome is dissociated, then mRNA de-capped and degraded. B) NGD shows the stalling of the ribosome and recruitment of DOM34 and Pelota. The ribosome is dissociated, and the mRNA cleaved. mRNA is degraded by the exosome and XRN1. C) NSD takes place on mRNAs without a stop codon. The ribosome runs onto the poly(A) tail and stalls, Pelota-HBS1 splits the ribosome and stimulates degradation of the peptide chain and mRNA.

1.3.2 Ribosome-associated protein quality control

Elimination of nascent chain polypeptides that are likely to form misfolded proteins, leading to accumulation and aggregation disease phenotypes, is clearly advantageous to a cell. A nascent chain may be marked by destruction before leaving the ribosome by two major mechanisms. First, co-translation quality control is used to monitor the folding status of the nascent chain as it is translated. Folding may be assisted by chaperones as the nascent chain is exposed, helping avoid defects in protein quality by sensing their folding ability. Second, ribosome-associated quality control (RQC) monitors the state of the translational machinery. For example, ribosome stalling leads to detection and degradation of defective components, e.g. aberrant mRNAs or defective ribosomes. Unlike co-translational quality control, RQC monitors the state of the translation machinery, predominantly the ribosome (Brandman & Hegde 2016).

1.3.2.1 Overview of the ribosome quality control pathway

The RQC pathway is employed to rescue and recycle stalled or blocked ribosomes in order to avoid an accumulation of non-functional complexes. Intricate studies have revealed the ability of the cell to remove and degrade aberrant nascent chains via the proteasome. Importantly, nascent chain removal and ribosome recycling is linked to the decay of aberrant mRNAs (Brandman & Hegde 2016; Karamyshev & Karamysheva 2018).

1.3.2.2 Ribosome stalling

There are several mRNA substrates which will initiate ribosome stalling (Figure 1-6A) which leads to degradation of the mRNA by NGD and recycling of the ribosome through RQC. Although translation typically resumes following a brief pause, there are certain types of pause which lead to translation abortion and execution of RQC.

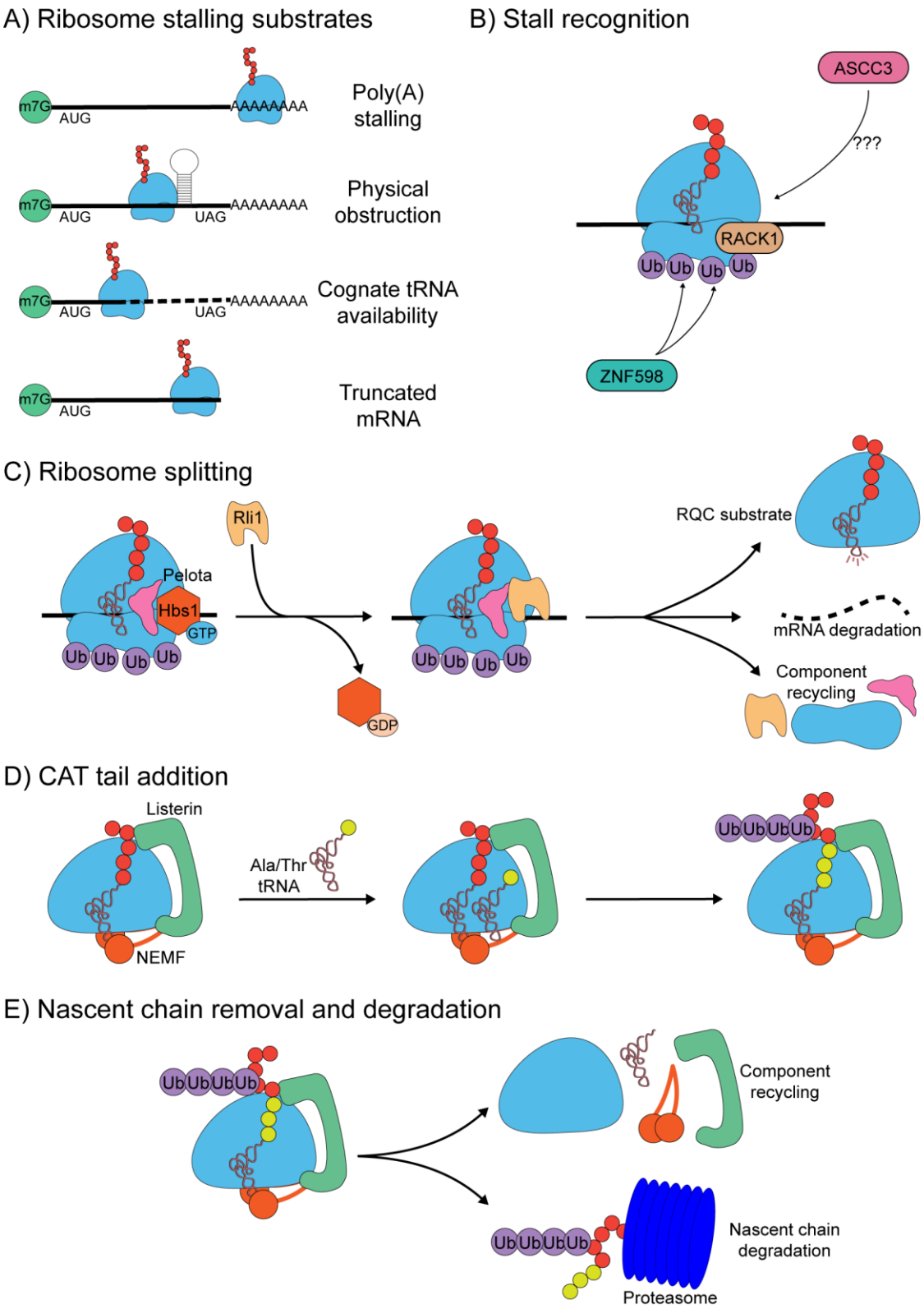

Figure 1-6. Ribosome-associated protein quality control

Schematic of RQC. A) Four known ribosome stalling substrates. B) ZNF598 and RACK1 coordinate ubiquitination of small ribosomal proteins upon recognition of a stall. The role of ASCC3 is implicated here but is still not fully understood. C) The ribosome is split by Pelota-Hbs1-Rli1. The mRNA is degraded, the 60S ribosome becomes the RQC substrate, and the rest of the components are recycled. D) If the nascent chain cannot be ubiquitinated, CAT-tailing is used to extend the nascent chain. E) The Nascent chain is removed, then degraded by the proteasome; the other components are recycled.

1.3.2.2.1 Codon choice and amino acid combination

Codon choice, and the up to 380 possible peptide bond formations between the peptidyl tRNA and the aminoacyl tRNA, can greatly affect the speed of the translating ribosome (Brule & Grayhack 2017). Many reporter systems used to study RQC contain repeats of the same sequence used to mimic the poly(A) tail of an mRNA transcript, which would normally be degraded by NSD. Using repeat sequence reporters, two major findings concerning ribosome stalling have been detailed. It is well established that the ribosome stalls on the poly(A) stretch (Figure 1-6A), which is partially influenced by the accumulation of positively charged consecutive lysine residues interacting with the negatively charged ribosome tunnel (Lu & Deutsch 2008). Consistent with these data, it has been shown that the length of the poly(A) sequence determines the effectiveness of the ribosome stall (Juszkiewicz & Hegde 2017). However, it has also been shown that a poly(AAA) stretch has a greater capability to stall ribosomes than a poly(AAG) stretch despite both encoding for lysine (Matsuo *et al.* 2017). These data demonstrate that whilst the conjugated amino acid may play an important role in stalling the ribosome, the mRNA sequence also has a role in this process. Interestingly, it was found that the poly(A) sequence can become 'slippery' for the ribosome when stalling factors are depleted, leading to skipping of individual nucleotides, continuation of translation, and formation of a frameshifted product (Juszkiewicz & Hegde 2017; Simms *et al.* 2017). There is also evidence for organism specific ribosome stalling in relation to codon choice and amino acid combination. Thus it has been shown in yeast that repeats of the CGA arginine codon is particularly potent in stalling ribosomes, whereas AAA and AAG are more effective in mammals (Sundaramoorthy *et al.* 2017).

Codon choice can affect ribosome stalling as encountering a rare codon or a codon with limited cognate tRNA availability can leave the A-site unoccupied for a prolonged period. This subsequently leads to a translating ribosome pausing on the mRNA until the cognate tRNA is delivered (Brandman & Hegde 2016). The empty A-site is thought to provide a molecular signature which can be recognised by the RQC machinery. The collision of a translating ribosome with a stalled lead ribosome is also a putative signal for the initiation of RQC (Ikeuchi *et al.* 2019), which will be discussed further on. These situations may arise when the kinetics of the tRNA recruitment is significantly slower than translocation rate. Thus, the rate of elongation is influenced by the availability of specific tRNAs, and the presence within the mRNA of codons that are decoded by rare tRNAs. Therefore cognate aminoacyl tRNA availability, will be related to the rate of translation when specific codons are prevalent (Brule & Grayhack 2017). Preferential codon usage has been shown to drive the expression of subsets of proteins e.g. those that control cell proliferation (Gingold *et al.* 2014).

Poly-proline motif catalysis is kinetically slow due to the challenging nature of the side chain. In eukaryotes eIF5A is thought to aid the translation efficiency of these stretches found within the proteome (Schuller *et al.* 2017). The activity of eIF5A is reliant on its unique hypusine modification (Park *et al.* 2010). It is possible that in the absence of eIF5A poly-proline motifs could potentially stall the ribosome and create targets for the RQC machinery (Buskirk & Green 2017).

1.3.2.2.2 mRNA structure and damage

Strong secondary structure including stem loops and pseudoknots within mRNA can induce physical stalling of ribosomes and activation of RQC (Figure 1-6A) (Brandman & Hegde 2016). Post-transcriptional covalent modifications to RNA, whether that be tRNAs, mRNAs or rRNAs, may also have a key role in forming stalled ribosome complexes (de Nadal *et al.* 2011). The modification of tRNAs can directly affect their charging and decoding activity, which in turn leads to changes in availability and the induction of ribosome stalling. Modifications to rRNA and mRNAs can also affect translation rates. Modification of RNA from chemical damage such as oxidation, depurination, or alkylation, and also damage from agents such as UV, which induce photochemical modifications and crosslinking, may also hinder ribosome progression on the mRNA (Wurtmann & Wolin 2009). For example, 8-oxoguanosine (8-oxoG) lesions in the mRNA were shown to reduce the rate of peptide bond formation by up to 3 orders of magnitude (Simms *et al.* 2014). Interestingly, 4-nitroquinoline-1-oxide (4NQO), a compound used to mimic a genotoxic response in this study, is thought to induce these modifications upon cell treatment (Arima *et al.* 2006).

1.3.2.3 Stalled ribosome recognition, ubiquitination and splitting

1.3.2.3.1 Stalled ribosome ubiquitination

The proteins required for recognition and processing of the stalled ribosome have been identified using yeast genetics and biochemical approaches. It was shown that depletion of Hel2 reduced ribosome stalling (Joazeiro 2017), with the mammalian homolog, ZNF598, demonstrating a similar effect in cultured cells (Garzia *et al.* 2017; Juszkiewicz & Hegde 2017; Sundaramoorthy *et al.* 2017). This was confirmed by ribosome footprinting analysis, which additionally suggested that Hel2/ZNF598 is one of the first factors to bind a stalled ribosome (Sitron *et al.* 2017). ZNF598 is a E3 ubiquitin-protein ligase and the data shows that the RING domain of ZNF598 is essential for its activity (Deshaies & Joazeiro 2009; Garzia *et al.* 2017; Juszkiewicz & Hegde 2017; Sundaramoorthy *et al.* 2017). In response to detection of stalled ribosomes ZNF598 ubiquitinates RPS10 and RPS20 (Figure 1-6B). Asc1 in yeast and RACK1 in

mammals are also required for early stall recognitions (Sitron *et al.* 2017). Data suggests that RACK1 facilitates stall resolution by mediating ubiquitination of RPS2, RPS3, and RPS20, however the E3 ubiquitin ligase remains unknown (Sundaramoorthy *et al.* 2017). These data suggest that RACK1 and ZNF598 are key to identification of RQC substrates and mark them for processing by facilitating ubiquitination of small ribosomal proteins.

1.3.2.3.2 The di-ribosome as the initiator of RQC

Recent studies have strongly implicated the di-ribosome as the initial marker for ribosome stalling, which acts as a structural unit for RQC (Ikeuchi *et al.* 2019; Juszkiewicz *et al.* 2018). As previously mentioned, di-ribosomes may be formed when a translating ribosome collides with a stalled ribosome. This leads to the translating ribosome becoming locked in a state consistent with an incomplete translocation step (Ikeuchi *et al.* 2019), and rotates the ribosome so that the two 40S subunits form an interface (Juszkiewicz *et al.* 2018). This creates a 40S-40S interface, which is preferentially bound and ubiquitinated by ZNF598 *in vitro* (Juszkiewicz *et al.* 2018). This is supported by similar work with preferential Hel2 ubiquitination of RPS20 of di-ribosome over mono-ribosomes (Ikeuchi *et al.* 2019).

1.3.2.3.3 Ribosome splitting

Research on the Hbs1-Pelota-ABCE1 pathway has led to an understanding of how ribosome splitting can be achieved. *In vitro* reconstitution assays showed that Dom34 (the yeast homolog of Pelota) and the GTPase Hbs1 can separate the stalled ribosomal subunits (Figure 1-6C). Initially the GTP-Hbs1-Pelota complex binds the stalled ribosome at the GTPase centre near the A-site of the ribosome. Hydrolysis of GTP promotes for dissociation of Hbs1 and enables Pelota to enter the A-site (Becker *et al.* 2011; Young *et al.* 2015). The binding of GTP-Hbs1-Pelota is thought to result from a lack of engagement by eEF1A-aminoacyl-tRNA or eRF1-eRF3 complexes with the ribosome (Defenouillère & Fromont-Racine 2017). ABCE1, an ATPase, is also involved in stalled ribosome splitting and recycling (Brandman & Hegde 2016). ABCE1 interacts with Pelota upon Hbs1 dissociation, which catalyses ribosomal subunit dissociation (Defenouillère *et al.* 2016). Splitting of the ribosome by ABCE1 leaves the nascent chain 60S subunit with an exposed peptidyl (P)-site tRNA at the inter-subunit interface as Dom34-Hbs1-ABCE1 mediated ribosome splitting does not lead to hydrolysis of the peptidyl tRNA bond. This provides the signal for the next step in the ribosome-associated quality control process (Shao *et al.* 2013; Shao & Hegde 2014).

1.3.2.4 Ribosome subunit and nascent chain processing

Unlike the 40S subunit which can be recycled immediately following ribosome subunit splitting, the nascent chain and peptidyl tRNA must be removed from the 60S subunit before being recycled. Listerin, which polyubiquitinates the nascent polypeptide, and its cofactor NEMF were identified as important in localisation of the nascent chain removal machinery to the dissociated 60S subunit (Chu *et al.* 2009; Shao *et al.* 2015). It has been proposed that NEMF binds the peptidyl-tRNA-60S complex which enables the recruitment of Listerin (Figure 1-6D) (Joazeiro 2017). The binding of Listerin-NEMF to the 60S subunit not only allows for activation of their catalytic activity, but also prevents the 40S subunit re-associating with the 60S subunit (Shao *et al.* 2015). Cryo-electron microscopy has shown NEMF binds across a large portion of the 60S subunit, which would normally interact with the 40S subunit. NEMF contains globular amino- and carboxyl- domains that interacts with the tRNA still present in the P-site following ribosome splitting (Shao *et al.* 2015). Studies demonstrating NEMF interaction with free tRNA at high concentrations *in vitro,* supports that tRNA is required for interaction with the 60S ribosome *in vivo* (Shao *et al.* 2015). A central domain in NEMF interacts with Listerin which spans over 100 Angstrom across the 60S towards the exit tunnel (Shao *et al.* 2015).

1.3.2.4.1 CAT-tailing for nascent chain degradation

Sequencing studies of tRNAs present in the A-site of post-stalled 60S subunits, along with amino acid analysis, have provided evidence of carboxy-terminal alanine and threonine tails (CAT-tails) on the nascent polypeptide (Figure 1-6D) (Kostova *et al.* 2017; Shen *et al.* 2015). This is dependent upon NEMF recruitment of Ala-tRNA and Thr-tRNAs to the A-site of the ribosome. NEMF positions the tRNAs close enough to the P-site to activate peptidyl transferase activity of the 60S subunit (Brandman & Hegde 2016). CAT-tail addition is thought to depend primarily on the ability of Ltn1 to ubiquitinate the pre-existing nascent chain on lysine residues close to the ribosome exit tunnel. In situations where lysine residues are not available for ubiquitination, CAT-tail addition is used to extend the nascent chain until a lysine residue presents itself for ubiquitination by Ltn1 (Kostova *et al.* 2017). Failed co-translational import of proteins into organelles is an instance where residues may be unavailable for ubiquitination by Ltn1, further enhancing the importance of CAT-tail formation to extend the nascent chain and allow ubiquitination (Izawa *et al.* 2017). Aside from potentially providing a ubiquitination site for Ltn1, the aggregative nature of CAT-tails and their ability to sequester cellular chaperones can also activate stress signalling via Heat shock factor 1 (Hsf1) (Brandman *et al.* 2012). To date, CAT tailing has not been detected in mammalian cells.

1.3.2.5 Nascent chain removal and ribosome subunit recycling

Nascent chain removal, degradation, and ribosome subunit recycling has predominantly been examined in yeast. Although homologous mammalian proteins exist, the experimental data is limited. As the process of recognition, splitting and processing of the stalled ribosome is highly homologous between mammals and yeast, assumptions are made that the overall mechanism of ribosome recycling is largely conserved.

The ubiquitin chains mark the nascent polypeptide chain for extraction and proteasomal degradation, and the 60S for recycling (Figure 1-6E). Results of several studies suggest Cdc48, Npl4, Ufd1 and Rqc1 are all involved in extraction of the ubiquitinated nascent chain (Defenouillere *et al.* 2013; Verma *et al.* 2013). The mammalian homologs of these proteins are thought to be VCP97, UFD1, NPLOC4, and TCF25 respectively (Brandman *et al.* 2012). Rqc1 is not required for ubiquitination of the nascent chain, but is thought to bind the polyubiquitin and recruit Cdc48 and its cofactors Npl4 and Ufd1 as a complex. The ATPase activity of the Cdc48 complex is then used to pull the nascent chain into a position for Vms1 to function (Verma *et al.* 2018). Vms1 (ANKZF1 in mammals), a homolog of Dom34 and eRF1 has also been shown to play a role in nascent chain release from the tRNA in the 60S subunit. Due to the homologous nature of Vms1 with Dom34 and eRF1, it was widely assumed that Vms1 hydrolyses the ester bond between the nascent chain and P-site tRNA. However, recent work has suggested that ANKZF1 acts as a bona fide endonuclease rather than a peptidyl-tRNA hydrolase (Yip *et al.* 2019). ANKZF1 is thought to act by trimming a few nucleotides from the 3' end of the tRNA in the P-site to release the nascent chain. The nascent chain can then be delivered to the proteasome by Cdc48. While the complete mechanisms of nascent chain removal and ribosome subunit recycling are not fully understood, in the absence of these factors, cells fail to remove RQC substrates (Defenouillère *et al.* 2016; Sitron *et al.* 2017; Verma *et al.* 2018; Young *et al.* 2015). In contrast to the 40S ribosomal subunit, which can be recycled immediately for pre-initiation complex formation following ribosome splitting, the nascent peptidyl-tRNA must be extracted before the 60S is ready to be recycled.

1.4 DNA damage

DNA damage activates a network of cellular pathways that sense, signal, and repair DNA lesions whilst monitoring genome integrity. The consequence of this activation is cell cycle arrest and DNA repair processes, taken together this is known as the DDR. In instances where the damaged DNA cannot be repaired, cells undergo programmed cell death to avoid the inheritance of mutated DNA (Mata *et al.* 2005; Sancar *et al.* 2004). DNA repair enzymes and surveillance

pathways are continuously monitoring host DNA, ready to activate signalling pathways that rapidly lead to the repair of detected damage. DNA integrity is constantly threatened by endogenously formed metabolic products such as reactive oxygen species and alkylating agents (Wood *et al.* 2001). In addition, DNA damage is commonly derived from environmental factors including ultraviolet (UV) light from the sun, and carcinogen exposure.

Many genes have been identified with roles in the DNA damage response, along with multiple gene-disease relationships (Lange *et al.* 2011; Ronen & Glickman 2001; Wood *et al.* 2001). For example, Xeroderma pigmentosum (XP) is a well-studied disease caused by defective DDR (Cleaver *et al.* 2009). This disease is specific to a defective global genomic nucleotide excision repair pathway (NER). XP cells are unable to remove UV radiation-induced DNA photoproducts, leading to a >1000-fold increased risk of developing skin carcinoma. XP is therefore a cancer predisposition syndrome, presenting a clear link between genotype and phenotype like many other DDR defective diseases (Cleaver *et al.* 2009; O'Driscoll 2012).

1.4.1 Ultraviolet light induced DNA damage

The UV component of sunlight is a major cause of DNA damage that can lead to the development of skin carcinoma. UV light consists of wavelengths between 400 nm and 100 nm and sits between x-rays and visible light on the light spectrum. UV wavelengths can be further sub-categorised into UV-A (400-315 nm), UV-B (315-280 nm), and UV-C (280-200 nm) (Madronich *et al.* 1998).

Exposure of cellular DNA to UV results in the formation of photoproducts, most commonly including pyrimidine-(6-4)-pyrimidone (6-4PPs) photoproducts and cyclobutane pyrimidine dimers (CPDs). 6-4PPs have a more lethal, potentially mutagenic effect, whilst CPDs are the more cytotoxic of the two lesions (Pascucci *et al.* 1997; Pfeifer 1997). The two photoproducts act by causing a distortion in the DNA double helix backbone structure, resulting in a loss of base pairing within the damaged region. Incorporation of incorrect DNA bases by error prone polymerases occurs because of this lost base pairing, resulting in missense mutations (Tremblay *et al.* 2009).

1.4.2 4-Nitroquinoline 1 - oxide induced DNA damage

The highly carcinogenic compound, 4-Nitroquinoline 1-oxide (4NQO), has demonstrated mutagenic capability in bacteria, fungi and vertebrates (Arima *et al.* 2006; Downes *et al.* 2014; Miao *et al.* 2006). Mutations occur through formation of bulky purine adducts which have been used to study DNA damage and repair, and to generate mutants for genetic screens. 4NQO does not directly damage DNA, but requires a four-electron reduction metabolism step into 4-

hydroxyaminoquinoline 1-oxide (4HAQO) (Arima *et al.* 2006). *In vitro* studies have shown that 4HAQO forms the majority of adducts on the second nitrogen of guanosine (~50%), but can also generate structures at carbon 8 and nitrogen 6 (~30% and ~10% respectively); this damage, if left unrepaired, can cause G:C to A:T transitions, potentially leading to pathological missense mutations (Downes *et al.* 2014). While in the past 4NQO was previously thought to damage guanine specifically, resequencing work shows that adenine residues are also damaged, albeit with a 19-fold lower preference to guanine (Downes *et al.* 2014).

1.5 DNA damage repair

Accurate transmission of genetic information through cellular generations is fundamental for the survival of organisms. The ability to pass on genetic information is determined by the accuracy of DNA replication and the prevention of heritable mutations through mechanisms of DNA repair (Sinha & Häder 2002). Surveillance mechanisms detect DNA lesions; signal their presence, then mediate DNA repair through various mechanisms (Carell & Epple 1998). The most studied pathways of DNA repair include nucleotide excision repair (NER), base excision repair (BER), homologous recombination (HR), non-homologous end joining (NHEJ), mismatch repair (MR), and direct reversal (DR) (Zhou & Elledge 2000).

1.5.1 UV and bulky adduct DNA damage repair

Specifically for UV irradiation, cells contain UV-absorbing pigments such as flavonoids in plants and melanin in animals and humans (Brenner & Hearing 2008; Kootstra 1994). The presence of these molecules, even under ideal circumstances, cannot completely prevent UV radiation reaching and damaging cellular DNA. Lesions induced by UV damage or other bulky adducts can be removed by a variety of mechanisms, including BER and NER (Sinha & Häder 2002).

1.5.1.1 Nucleotide excision repair

NER removes a variety of DNA distorting lesions, including both CPDs and 6-4PPs, and the bulky adducts generated following 4NQO treatment. This mechanism is highly conserved in eukaryotes, likely due to the inherent importance of removing damaged DNA. Recognition of damaged DNA leads to removal of a short single stranded DNA segment containing the lesion. The remaining undamaged single stranded DNA (ssDNA) is then utilised as a template, allowing the DNA polymerase to synthesise the complementary sequence. Ligation of the complementary sequence and re-formation of the DNA double helix completes the NER process. Two distinct helix distorting lesion recognition mechanisms exist in NER, these include global genomic NER (GG-NER) and transcription coupled NER (TC-NER) (Figure 1-7) (de Laat *et al.* 1999).

GG-NER is carried out primarily on non-transcribed regions of the genome, or the non-transcribed coding DNA strand of genes. The process occurs when XPC, stabilised by its partners hHR23B and CETN2, scans genomic DNA until it detects unpaired DNA created by 6-4PPs' helix distortion. The XPC-hHR23B-CETN2 complex then binds the lesion with preference for the undamaged single stranded DNA (Batty & Wood 2000). Without hHR23B, XPC has significant impairment in its ability to stimulate the repair process (Sugasawa *et al.* 1996). Small distortions of the helix, such as those caused by CPDs when compared to 6-4PPs, make poor substrates for XPC and therefore are recognised by the DDB1-DDB2 complex. The DDB1-DDB2 complex directly binds the CPD and acts as an auxiliary damage recognition factor. Kinking the DNA creates a larger region of ssDNA permitting XPC recognition of the damage area (Marteijn *et al.* 2014).

TC-NER has evolved to rapidly repair DNA lesions present in transcriptionally active regions of DNA. The pathway begins when an RNA polymerase stalls at the site of a bulky lesion, but it is important to note that this TC-NER does not require XPC. Instead CSA and CSB are required for further assembly of the TC-NER machinery, including the core NER machinery but also TC-NER specific proteins UVSSA and USP7. Normally CSA targets CSB for degradation by ubiquitination, but upon detection of a stalled RNA polymerase, UVSSA delivers USP7 to the TC-NER complex which deubiquitinates and stabilises CSB (Marteijn *et al.* 2014; Schwertman *et al.* 2012). The CSB-CSA complex also allows backtracking of the RNA polymerase which makes the DNA lesion accessible to the repair machinery (Marteijn *et al.* 2014; Mu & Sancar 1997; Wood 1997).

Following the recognition of DNA damage by either GG-NER or TC-NER, excision repair is carried out. The initial step involves the cooperative binding of RPA, XPA and the multi sub-unit transcription factor complex TFIIH (Sinha & Häder 2002). XPA and the single stranded binding protein RPA associate and bind the site of DNA damage, further aiding the recognition and recruitment of other components. TFIIH contains two helicases of opposite polarities, used for unwinding of the DNA duplex in the immediate vicinity of the lesion (Batty & Wood 2000). ATP hydrolysis allows the DNA helicases, XPD, and XPB, to act in the 5'-3' and 3'-5' direction respectively by approximately 25 base pairs. The nucleases XPG and ERCC1-XPF are recruited to the site of DNA damage, where they cleave 3' and 5' of the DNA damage respectively. This releases the small, damage-containing DNA oligonucleotides in complex with TFIIH (Mu & Sancar 1997; Wood 1997). RFC loads PCNA onto the DNA strand, allowing gap repair synthesis to be carried out by DNA polymerase δ/ε. A ligase then seals the gap to complete the repair process (Thoma 1999).

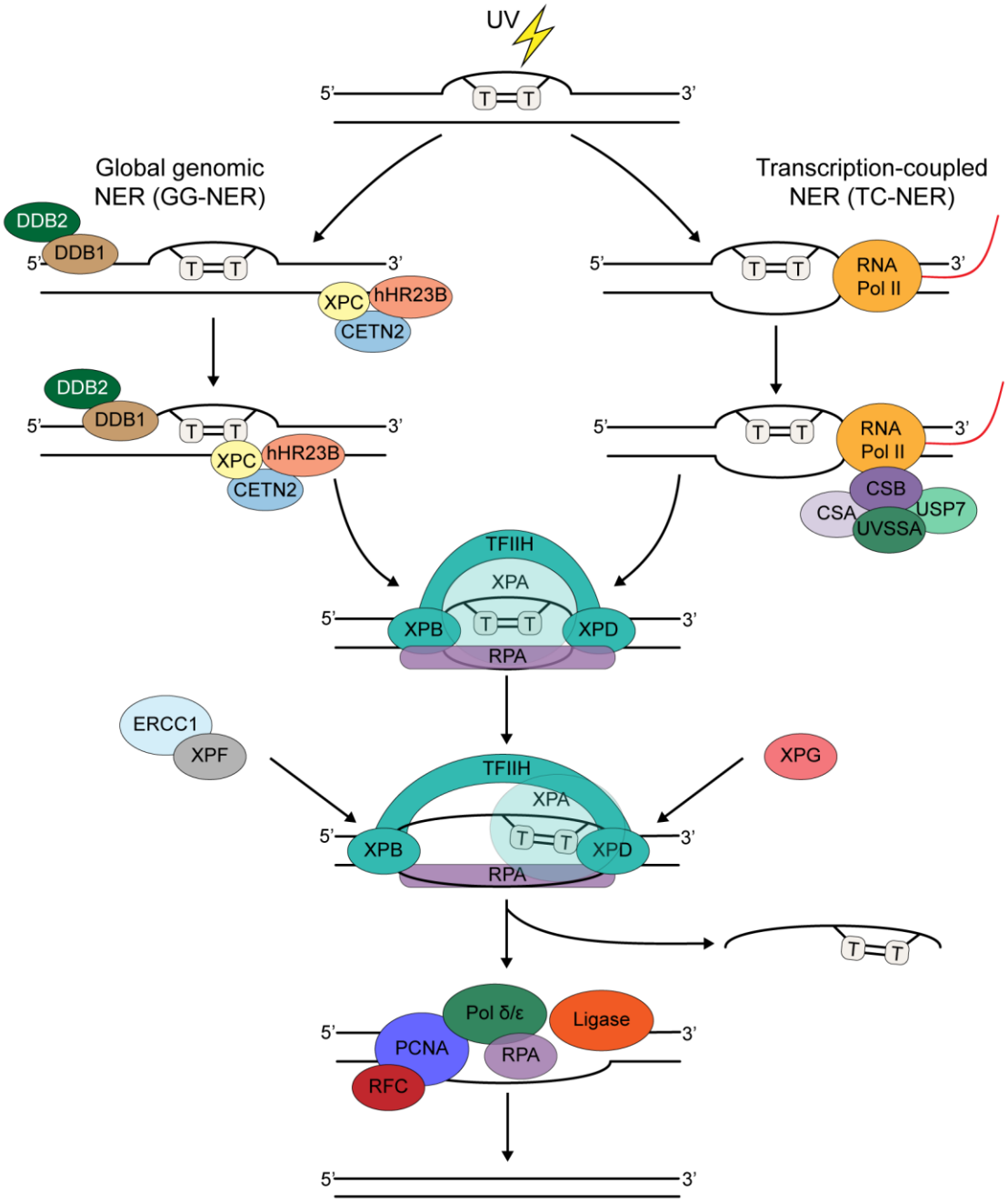

Figure 1-7. Nucleotide excision repair pathways

Schematic of the nucleotide excision repair pathway. Addition of a bulky adduct to DNA by UVB or 4NQO leads to loss of accurate base pairing. NER is used to repair the DNA by either the GG-NER pathway or TC-NER pathways. Recognition of the DNA lesion is the only step that differs between the pathways. Upon detection of the damage the NER machinery is recruited to unwind the DNA and cleave the region of damage. The NER machinery dissociates which allows synthesis of a new complementary strand and replacement of the damaged DNA by ligation.

1.6 ASCC3

1.6.1 Identification of ASCC3

Stress signals commonly influence cells to shut down global protein synthesis in order to fine-tune the translational response through a series of controlled mechanisms (as previously described). While there is information to describe how the cell achieves changes in translation in response to genotoxic insults, such as the physiologically relevant UVB irradiation (Collier *et al.* 2015; Powley *et al.* 2009), there is little information about the non-canonical RBPs involved in this process. One of the means to elucidate novel mechanisms of translational reprogramming is through analysis of the RNA-interactome. RNA-interactome capture (RIC) (Figure 1-8A) was used to determine changes in the RNA-interactome following UVB irradiation (Stoneley *et al*, unpublished data).

RIC relies on the 'zero-distance', or less than ~2 Å proximity between the RNA and protein to allow covalent bond formation by cross-linking during irradiation with a high dose of UVC at a low wavelength (254 nm) (Pinol-Roma *et al.* 1989). Although efficiency of cross linking is low, with only up to 1% of the total RNA bound proteins being cross-linked, the speed and covalent nature allows the generation of an *in vivo* "snapshot" of the RNA-protein interactome (Castello *et al.* 2015). To limit contamination from DNA-binding proteins and nuclear localised RNA-protein interactions, a cell fractionation step was employed to ensure predominantly cytoplasmic proteins were detected. Following cross-linking and cytoplasmic fractionation of cells, oligo d(T) beads was used to isolate the poly(A) RNAs present along with their respective RBPs. Due to the covalent linkages generated by the UVC treatment, stringent washes were employed to remove background interactions. Following elution of the RNA-protein complexes from the beads, the benefit of the covalent interaction during the purification becomes the challenge. Because the proteins cannot be dissociated from the RNA, a combination of RNAses were used to degrade RNA before identification of the proteins by SDS-PAGE, mass spectrometry, and western blotting.

Work within the Willis lab demonstrated changes in the RNA-interactome using RIC in response to UVB irradiation (Stoneley *et al,* unpublished data). Of the 383 identified proteins, 54 % showed no change in their RNA interaction, while 40.5 % showed decreased RNA-binding, and 5.5 % showed increased RNA-binding (Stoneley *et al*, unpublished data). One of these proteins, activating signal cointegrator 1 complex subunit 3 (ASCC3), had a high number of peptide counts and at the time of discovery had no defined cytoplasmic function, making it a novel candidate for post-transcriptional regulation following genotoxic stress. Validation of ASCC3 RNA-binding

demonstrated time-dependent and UVB dose-dependent changes in affinity for RNA (Figure 1-8B; Stoneley *et al*, unpublished data).

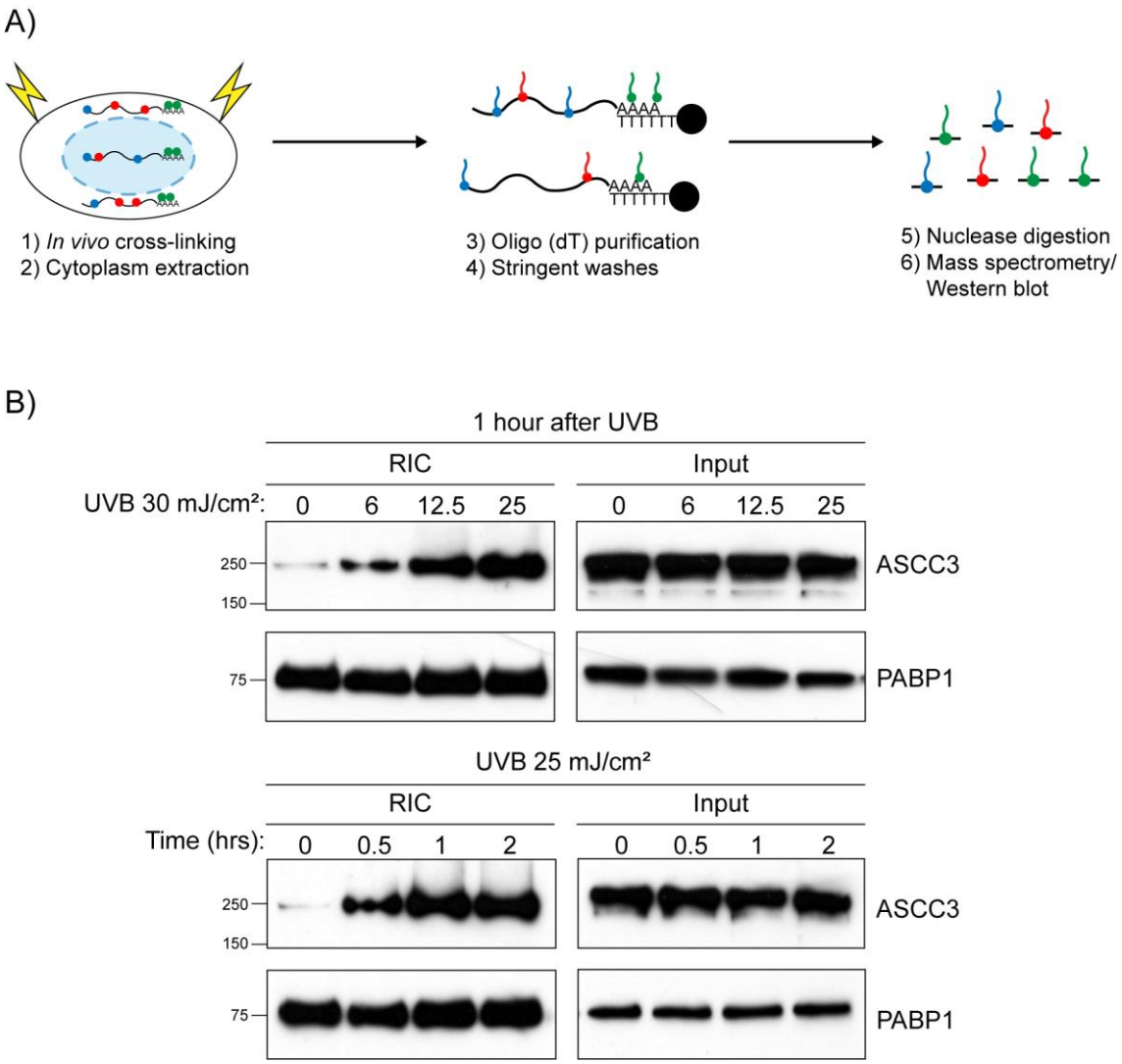

Figure 1-8. ASCC3 is an RNA-binding protein as determine by cytoplasmic RIC

A) Schematic of the RIC technique, showing crosslinking, fractionation, oligo (dT) purification and stringent washes, before identification of isolated proteins. B) ASCC3 was identified by cytoplasmic RIC in response to UVB irradiation. ASCC3 shows time and UVB dose dependency on its RNA binding capacity. Data kindly provided by Mark Stoneley.

1.6.2 The ASC-1 complex

The ASC-1 complex consists of 4 members: ASCC1, ASCC2, ASCC3, and TRIP4 (Dango *et al.* 2011; Jung *et al.* 2002). The amino acid sequence of individual ASC-1 complex components, was analysed using 'Interpro: protein sequence analysis and classification' database to identify protein domains (Figure 1-9A). Structural homology modelling was also carried using RaptorX structural prediction, but only ASCC3 was modelled well, which utilises Brr2 as a template (Figure 1-9B). ASCC1 domain analysis yielded two known domains; a K homology (KH) domain and a cyclic nucleotide phosphodiesterase (CNP). The KH domain was identified in the human heterogenous nuclear ribonucleoprotein (hnRNP) K and has since been shown to enable RNA binding (Baber *et al.* 1999). The CNP domain selectively cleaves 2'-3' cyclic phosphates to produce 2' products; the physiological substrate of these enzymes still remains a unknown (Myllykoski *et al.* 2012). ASCC2 is mostly disordered with a central CUE domain, which is structurally related to the ubiquitin binding UBA domain. The CUE domain has been proposed to aid ubiquitin chain growth through substrate stabilisation during ER-associated protein degradation (Bagola *et al.* 2013). TRIP4 contains an amino-terminal putative zinc finger domain, a relatively small, well studied motif which is thought to enable binding to nucleic acids. The carboxy-terminal of TRIP4 contains an ASCH domain, which is structurally related to the PUA domain, and which likely functions as an RNA-binding domain (Iyer *et al.* 2006).

ASCC3 is a member of the Ski2-like helicase family of DExD/H box RNA helicases (Caruthers & McKay 2002; Linder & Jankowsky 2011). ASCC3 represents a unique subclass of these helicases, containing tandem Ski2-like helicase cassettes; this subclass also includes BRR2 (Johnson & Jackson 2013; Santos *et al.* 2012) (Figure 1-9C). A Ski2-like helicase cassette typically consists of the DEAD/Helicase C domain or AAA+ ATPase domain and sec63 domain (Bleichert & Baserga 2007; Johnson & Jackson 2013) (Figure 1-9C). These domains can be further sub-classified into dual RecA domains, winged helix domain, and ratchet domain. Some SF2 helicases also contain a helix-loop-helix domain and fibronectin type III domain (Johnson & Jackson 2013). The structural similarities between ASCC3 and BRR2 (Figure 1-9C and 9D) may indicate that ASCC3 binds RNA with its N-terminal helicase domain (Santos *et al.* 2012), however, this would disagree with previously published RNA-binding domain mapping data (Liao *et al.* 2016), which suggests that ASCC3 binds RNA with its C-terminal helicase domain.

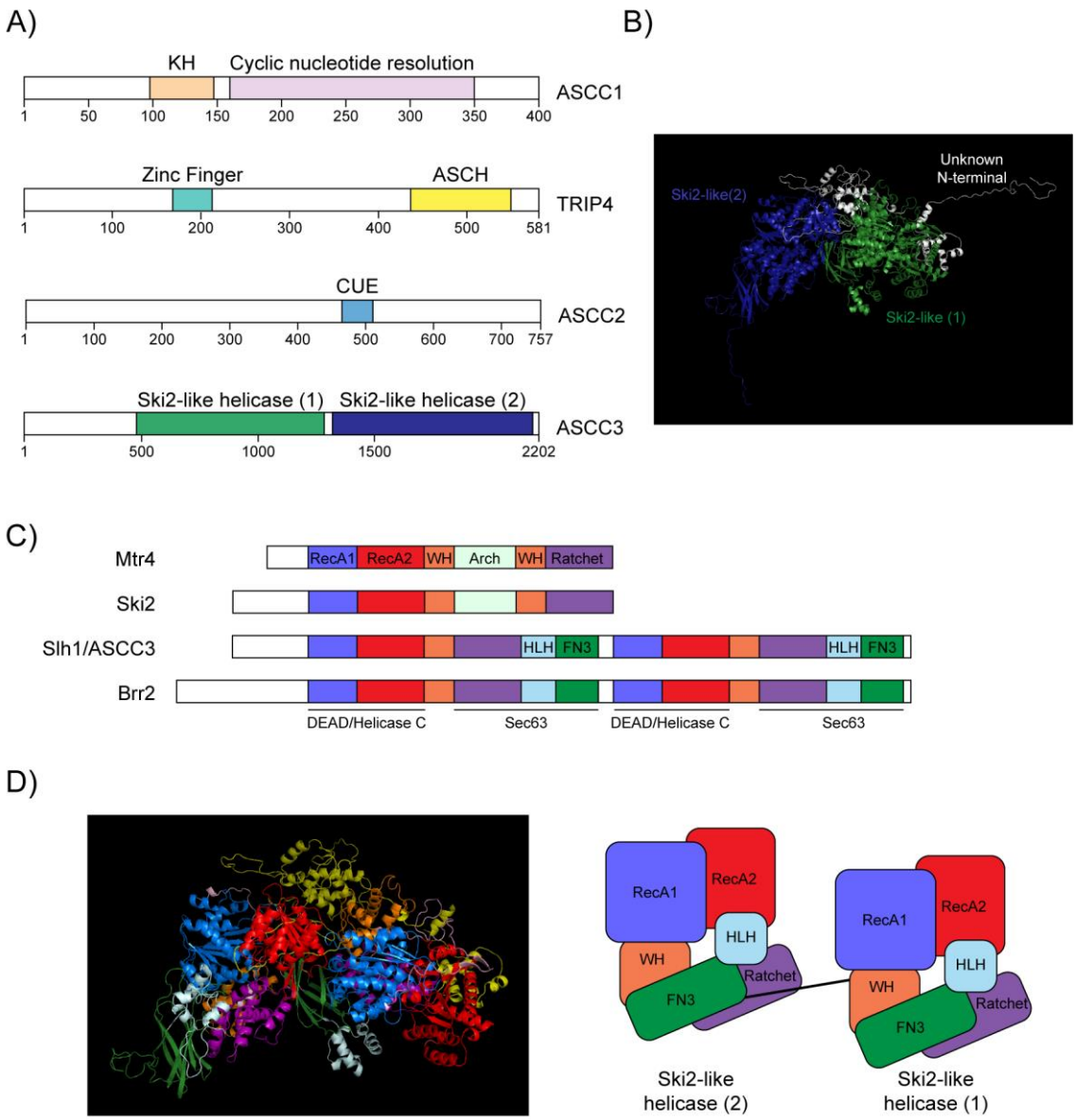

Figure 1-9. ASCC3 and the ASC-1 complex

ASCC3 is a member of the Ski2-like RNA helicase family and part of the ASC-1 complex. A) Domain analysis for each of the ASC-1 complex members using 'interpro: protein sequence analysis and classification'. B) Structural modelling showing location of each helicase cassette (colours comparable to that of part (A). Models produced using RaptorX structural prediction. C) Further domain analysis of ASCC3 and members of the Ski2-like RNA helicase family. D) ASCC3 structural model and cartoon highlighting the domains shown in part (C).

1.6.3 This history of the ASC-1 complex

TRIP4, also known as ASC-1, was originally identified through its binding to thyroid hormone receptors (Lee *et al.* 1995). This protein was then proposed to act as a transcription coactivator of nuclear receptors, and shuttle from the nucleus to the cytoplasm in response to serum deprivation, while playing a role in spermatogenesis (Kim *et al.* 1999; Lee *et al.* 2002). Like many other transcription coactivators, TRIP4 demonstrated inclusion into a protein complex. The three other proteins within this complex were later shown to be ASCC3, ASCC2, and ASCC1 (Jung *et al.* 2002).

The next major breakthrough regarding the role of the ASC-1 complex came from the identification of a function for ASCC3 in DNA alkylation damage repair (Dango *et al.* 2011). The data suggest that ASCC3 uses its helicase activity to unwind damaged DNA, allowing repair by ALKBH3, a nuclear demethylase. Localisation of the ASC-1 complex to the foci of DNA damage requires the recognition of K63-linked polyubiquitin chains by the CUE domain of ASCC2 (Brickner *et al.* 2017). Interestingly, OTUD4, a canonical deubiquitinase and member of the ovarian tumour deubiquitinase family, has also been implicated as a scaffold protein in alkylation DNA repair complex (Zhao *et al.* 2015). ASCC1 has also been shown to aid ASC-1 complex localisation to the site of DNA damage (Soll *et al.* 2018). A large multiomic analysis showed that ASCC3 becomes ubiquitinated and phosphorylated in response to UV irradiation, suggesting regulation by post-translational modifications (Boeing *et al.* 2016), this data also showed that ASCC3 was important in transcriptional recovery after UV damage. Further work demonstrated that exposure to UV irradiation can cause a shift from full-length to a shorter transcript of ASCC3, caused by alternative last exon splicing, which acts as a long non-coding RNA (Williamson *et al.* 2017).

The first indications that ASCC3 contributes to cytoplasmic regulation of gene expression came in yeast studies from experiments showing that Slh1 (ASCC3 in yeast), in combination with Ski2, modulates the expression of transcripts missing their poly(A) tail (Searfoss & Wickner 2000). A later study revealed a translational defect in cells lacking Slh1 and two DRG factors (Daugeron *et al.* 2011). This study also showed that Slh1 is associated with translating ribosomes. Slh1 was then identified in a screen for proteins that facilitate stalling on poly(A) tracts (Brandman *et al.* 2012). It demonstrated that deletion of Slh1 increased levels of pre-stall fragments, giving a similar result as Hel2 (ZNF598 in mammals) and Asc1 (RACK1 in mammals) (Brandman *et al.* 2012). This data was further clarified using reporter vectors capable of measuring stalling following deletion of Asc1, Hel2, Slh1, Ltn1 (Listerin in mammals), and Rqc2 (NEMF in mammals) (Sitron *et al.* 2017). These deletions demonstrated a decrease in ribosomes stalling, showing

that these proteins were essential for stalling of the ribosome (Sitron *et al.* 2017). The study placed Slh1 after Asc1 and Hel2 (stall recognition), but before Ltn1 and Rqc2 (RQC machinery recruitment) in the RQC pathway (Sitron *et al.* 2017). This was also the first evidence that Ykr023w (TRIP4 in mammals) and Cue3 (ASCC2 in mammals) have functions in RQC. Deletion of these components yielded a similar phenotype as that seen with Slh1 and Hel2 depletion (Sitron *et al.* 2017). These data were recapitulated in another study which also demonstrated that ASCC3 was co-purified with ZNF598 bound ribosomes (Matsuo *et al.* 2017). These works are now further highlighted with a greater understanding of the interaction of Slh1 with RQC substrates within recent studies. Ubiquitination of the small ribosomal proteins is a common theme amongst RQC substrates, and has been shown to be required for the interaction of Slh1 with RQC signatures (Matsuo *et al.* 2017), with independent studies all highlighting the importance of Slh1 ATPase activity for dissociation of non-functional ribosome subunits (D'Orazio *et al.* 2019; Matsuo *et al.* 2017; Sugiyama *et al.* 2019). Recent work suggests that Slh1 is required to prevent accumulation of collided ribosomes on NGD mRNAs; failure of this process leads to mRNA cleavage by CUE2, as shown by ribosome profiling data (D'Orazio *et al.* 2019). Complementary to this data, Slh1 interacts with and promotes subunit dissociation of ribosomes containing non-functional 18S rRNA (Sugiyama *et al.* 2019). Despite this data, the mechanism of Slh1 induced ribosomes subunit dissociation and the required helicase activity is still unknown. Further adding to the abundant repertoire of evidence for the involvement of the ASC-1 complex in RQC, a CRISPRi screen measuring cellular fitness identified ASCC3 and ASCC2 as having the largest effect in response to compounds that selectively stall human translation (Liaud *et al.* 2019).

1.7 Ubiquitin modifications and OTUD4

1.7.1 Ubiquitination

Ubiquitination is an evolutionary conserved post-translational modification that controls complex aspects of cell physiology (Clague *et al.* 2013). Ubiquitin, is a small 8.6 kDa, 76 amino acid regulatory protein encoded by four genes, *UBB, UBC, UBA52,* and *RPS27A* (Kimura & Tanaka 2010). Addition and removal of post-translational ubiquitin modifications are used to transmit signals, determining protein function, subcellular localisation, and alter protein-protein interactions. The process of ubiquitination occurs in three steps: firstly, activation by ubiquitin-activating enzymes (E1s); secondly, conjugation by ubiquitin conjugating enzymes (E2s); and finally ligation by ubiquitin ligases (E3s) (Figure 1-10A) (Zhang *et al.* 2017).

Ubiquitin modifications are highly dynamic and complex, such that not only can a protein undergo monoubiquitination, but multi-monoubiquitination and polyubiquitination may also occur. Eight linkage types are used between ubiquitin molecules to create ubiquitin chains, which generates additional complexity. Poly-ubiquitin linkages exist between the C-terminus of the donor ubiquitin molecule and any seven lysine residues, (lysine 6, 11, 27, 29, 33, 48, and 63), or the N-terminal methionine residue of the acceptor ubiquitin molecule (Figure 1-10B) (Komander 2009; Zhang *et al.* 2017). Branched and mixed poly-ubiquitin chains, along with phosphorylation and acetylation of ubiquitin molecules, creates another level of complexity surrounding ubiquitin modification (Herhaus & Dikic 2015; Meyer & Rape 2014). Each linkage type has been broadly assigned a cellular function, however, full understanding of the function of ubiquitination depends on the targeted protein and the plethora of ubiquitin molecule modification factors.

1.7.2 Deubiquitinases

Ubiquitin post-translational modification are reversed through the action of deubiquitinating enzymes (DUBs). There are approximately 100 different cellular DUBs with distinct six families based on the architecture of their catalytic domains: ubiquitin specific proteases (USPs), ubiquitin COOH-terminal hydrolases (UCCs), ovarian tumour proteases (OTUs), Josephins, motif interacting with ubiquitin (MIU), and JAB1/MPN/MOV34 family (JAMMs) (Komander *et al.* 2009; Mevissen & Komander 2017). Most DUBs are cysteine proteases, with some metalloproteases, and use a catalytic triad of conserved amino acids to remove ubiquitin molecules from their substrate (Clague *et al.* 2013). DUBs often remove specific ubiquitin chain linkages (Hospenthal *et al.* 2015; Mevissen *et al.* 2013), creating a complex network of ubiquitin removal which is still relatively unexplored. Moreover, DUBs also display tissue-specific expression and differential localisation within the cell (Clague *et al.* 2013).

1.7.2.1 The OTU family deubiquitinases

Phylogenetic analysis of the OTU family of DUBs revealed four sub-families; OTUDs, OTUBs, A20-like, and OTULINs, which are generally distinguished by the size of their catalytic domains. OTUD enzymes contain the smallest catalytic domain of approximately 150 amino acids, whereas OTUBs have a catalytic domain between 220-270 amino acids, and A20-like have the largest catalytic domain between 300-350 amino acids (Mevissen *et al.* 2013). The OTULIN subfamily are yet to be annotated in this manner. In regards to ubiquitin linkage specificity, OTU family members are the most intriguing, and often show preference towards one or a small set of linkage types (Mevissen *et al.* 2013). Therefore, these proteins are often used to regulate important signalling cascades, such as regulation of NF-κB signalling by A20, Cezanne, and

OTULIN (Aksentijevich & Zhou 2017), and OTUB1 in the DDR (Nakada *et al.* 2010). From the sixteen OTU family deubiquitinases, four distinct mechanisms of ubiquitin chain specificity have been described. In all of these mechanisms, the DUB interacts with the proximal ubiquitin molecule, and helps define the chain specificity through protein contacts (Mevissen *et al.* 2013; Mevissen & Komander 2017).

1.7.2.2 OTUD4

OTUD4 is a member of the OTU family of deubiquitinases, with the OTU domain is present in the N-terminal region of the protein and its catalytic cysteine as the 45th amino acid (Mevissen *et al.* 2013). Originally, studies suggested that OTUD4 was only able to degrade K48 ubiquitin chains (Mevissen *et al.* 2013), however, more recent work showed phosphorylation of serine residues in position 202 and 204 could change the specificity of the activity of OTUD4 from K48 to K63 ubiquitin chains (Zhao *et al.* 2018). The physiological role of OTUD4 was first determined in the nucleus as an interactor of modified XPC (Lubin *et al.* 2013), before being shown to interact with the nuclear ASC-1 complex, acting as a scaffold protein in alkylation damage repair (Zhao *et al.* 2015). The interaction between OTUD4 with the ASC-1 complex in the nucleus, while not important for this thesis, suggests a separate role for OTUD4 in the cytoplasm. In this regard, it has now been shown that in the cytoplasm, OTUD4 removes K63 ubiquitin chains of MyD88, an innate immune signal transducer for toll-like receptor (TLR) signalling, which negatively regulates NF-κB signalling (Zhao *et al.* 2018). It was then demonstrated that OTUD4 removes K48 ubiquitin chains from mitochondrial antiviral-signalling proteins (MAVs), preventing their degradation in response to prolonged viral infection (Liuyu *et al.* 2019). Taken together, these studies demonstrate the role of OTUD4 as a regulator of innate immune response proteins. Despite the identification of OTUD4 as an RNA-binding protein in HEK293 cells (Baltz *et al.* 2012) and RAW 264.7 macrophages (Liepelt *et al.* 2016), it was only recently that this function was studied in further detail. Data shows that OTUD4 localises to stress granules and has profound effects on proliferation and protein synthesis of HeLa cells (Das *et al.* 2019). In terms of disease association, OTUD4 has been linked to ataxia and hypogonadotropic hypogonadism in humans as well as to dorsoventral patterning in zebrafish (Margolin *et al.* 2013; Tse *et al.* 2009, 2013).

A)

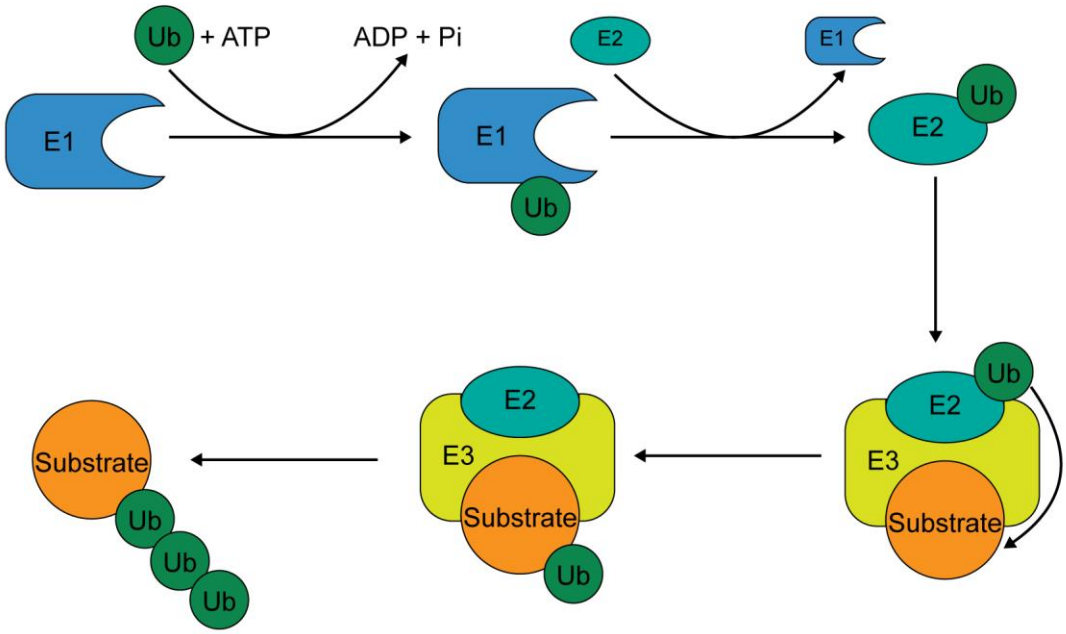

B)

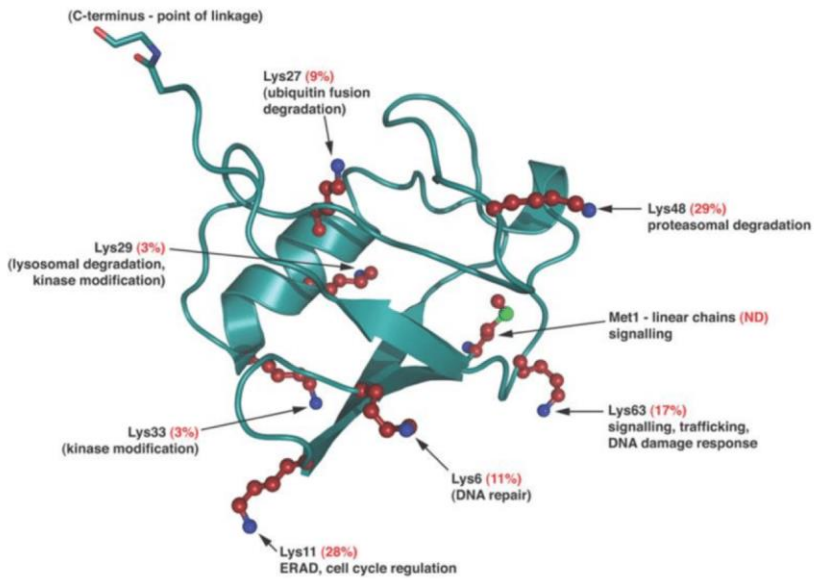

Figure 1-10. Ubiquitination and important ubiquitin residues

A) Schematic of the process of protein ubiquitination. The E1 enzyme activates the ubiquitin (Ub) molecule by binding one of its own cysteine residues. The ubiquitin is then passed from the E1 to an E2 enzyme before an E3 transfers it from the E2 onto the target protein. B) A ubiquitin molecule showing the position of the 7 lysine residues (red with blue nitrogen atoms), single methionine (with a green sulphur atom), and C terminal linkage point. Red numbers refer to the relative percentage abundance of each linkage in *Saccharomyces cerevisiae* (Xu *et al.* 2009). Image adapted from (Komander 2009).

1.8 Project aims

Control of gene expression is essential to maintain cellular homeostasis. Cellular stress often leads to a rapid global inhibition of protein synthesis, while utilising mechanisms (which circumvent the global inhibitory signal) to express proteins required to facilitate the desired response. Work within the Willis laboratory has previously shown some selective mRNAs containing uORFs are translated following UVB irradiation (Powley *et al.* 2009). While more recent developments in methods to study the RNA-bound proteome facilitated discovery of cytoplasmic ASCC3 as a novel, UVB-responsive, RNA-binding protein (Stoneley *et al*, unpublished data). At the time of discovery, ASCC3 had not been implicated in any gene expression regulatory processes. Therefore, the aims of this thesis are to understand the function of cytoplasmic ASCC3 as part of the ASC-1 complex, and to identify novel interacting partners in response to stress.

2. Materials and methods

2.1 Cell culture techniques

2.1.1 Growth and cryopreservation media

Cell Line	Culture Media	Cryopreservation Media
U2OS	DMEM (ThermoFisher #41966) 10 % FBS	95 % culture media 5 % DMSO
Flp-In™ T-REx™ HEK293	DMEM (ThermoFisher #41966) 10 % FBS 15 µg/ml Blasticidin 100 µg/ml Zeocin™	40 % culture media 50 % FBS 10 % DMSO
Flp-In™ T-REx™ HEK293	Freestyle™ 293 (ThermoFisher #12338) 5 % FBS 15 µg/ml Blasticidin 100 µg/ml Zeocin™	40 % culture media 50 % FBS 10 % DMSO
Stably transformed Flp-In™ T-REx™ HEK293	DMEM (ThermoFisher #41966) 10 % tet-free FBS 15 µg/ml Blasticidin 200 µg/ml Hygromycin	40 % culture media 50 % tet-free FBS 10 % DMSO
HeLa	DMEM (ThermoFisher #41966) 10 % FBS	40 % culture media 50 % tet-free FBS 10 % DMSO
Flp-In™ T-REx™ HeLa	DMEM (ThermoFisher #41966) 10 % FBS 5 µg/ml Blasticidin 100 µg/ml Zeocin™	40 % culture media 50 % tet-free FBS 10 % DMSO
Stably transformed Flp-In™ T-REx™ HeLa	DMEM (ThermoFisher #41966) 10 % FBS 5 µg/ml Blasticidin 200 µg/ml Hygromycin	40 % culture media 50 % tet-free FBS 10 % DMSO

Table 2-1 | Media and concentration of supplements for cell culture and cryopreservation

2.1.2 Maintenance of cell lines

2.1.2.1 Adherent cell culture

Cells were grown in sterilised plastic-ware with appropriate media (Table 2-1) in a humidified incubator maintained at 37 °C with 5 % CO_2. Cells were typically grown to approximately 80 % confluence before they were split. The split ratio and frequencies were variable between cell lines, but the methodology remains largely the same. Upon splitting, media was aspirated from the culture T175 flask and cells washed once with warmed PBS. Cells were then trypsinised using 1x Trypsin (0.05 % trypsin, 0.5 mM EDTA, 1x PBS) at 37 °C for the appropriate amount of time

for the given cell line. Upon cell detachment from the flask, culture medium was added to inactivate the trypsin. Cells were collected and centrifuged at 200 g for 5 minutes before re-suspending the cell pellet in culture medium. Cells were transferred to a fresh flask containing culture medium or plated as required for experimental approaches.

2.1.2.2 Suspension cell culture

Stably expressing Flp-In™ T-REx™ HEK293 cells were adapted to grow in suspension by lowering FBS concentration by 1 % per week until a final concentration of 5 % was achieved while maintaining viability. Cells were then introduced to Freestyle™ media with 5 % FBS and were seeded into 150 ml sterile flask and incubated at 160 rpm, 37 ^{o}C, 8 % CO_2, with humidity at 500,000 cells/ml. Cells were grown until a density of $1.5x10^6$ cells/ml was achieved then centrifuged at 200 g. Cells were counted and viability checked before being split into a new sterile flask.

2.1.3 Cryopreservation of cell lines

Cells were collected as described previously (Section 2.1.2) but were resuspended in the appropriate freeze medium (Table 2-1) at approximately $10x10^6$ cells/ml. 1 ml volumes were aliquoted into labelled cryopreservation vials were labelled. Cryopreservation vials were placed inside a Mr. Frosty™ freezing container (ThermoFisher) filled with 100 % isopryopyl alcohol as per manufacturer instructions to achieve a freeze rate of -1 ^{o}C/minute in a -80 ^{o}C freezer. Cryopreservation vials containing cells were then transferred from the -80 ^{o}C freezer 24 hours post-freezing to liquid nitrogen for long term storage.

2.1.4 Thawing of cryopreserved cells

Frozen stocks of cells were retrieved from liquid nitrogen storage and placed on dry ice temporarily for transport. Frozen cells were thawed quickly by shaking in a 37 ^{o}C water bath for 1-2 minutes. Cells were transferred dropwise into a 50 ml conical-bottom centrifuge tube containing 10 ml pre-warmed appropriate media. The cells were collected at 200 g for 5 minutes and cryopreservation media removed. The cell pellet was resuspended in fresh media and seeded in a T175 sterile flask.

2.1.5 Poly-L-lysine coating of plates

Sterile-filtered 0.01 % poly-L-lysine in water (Sigma #P4707) was applied to sterile flasks to ensure complete surface coverage under sterile conditions. After a 10-minute incubation at room temperature the excess solution was removed. The treated plates were then washed twice with sterile water. Residual water was then aspirated before the plates allowed to dry at room

temperature for 2 hours. From here the plates were ready for cell culture or can be stored at 4 ^{o}C for 4 weeks.

2.1.6 Cell transfection

2.1.6.1 Transfection of DNA (plasmids) using Lipofectamine™ LTX

Cells were counted and seeded in desired plates 24 hours prior to transfection. The number of cells seeded varied depending upon cell line and was calculated in order to reach ~80 % confluence on the day of cell harvesting. The transfection mix was prepared according to the manufacturer's instruction using 2.5 µl of Lipofectamine™ LTX (ThermoFisher #15338100) per 1 µg of DNA plasmid with Opti-MEM® (ThermoFisher #11058021) as the diluent (Note that the PLUS reagent was not used for any transfection). The amount of DNA transfected was dependent upon the plate growth surface area (Table 2-2). Upon transfection cells were incubated for 6 hours before media removal and refreshing with an appropriate volume of culture media.

Plate	Surface area (cm^2 per well)	DNA (total µg)
10 cm	55	13.75
6 cm	21	5.25
6-well	9.6	2.5
12-well	3.9	1.25

Table 2-2 | Transfection of cells with DNA

2.1.6.2 Transfection of siRNA using Lipofectamine™ RNAiMAX

2.1.6.2.1 Forward transfection

Cells were counted and seeded in desired plates 24 hours prior to transfection. The number of cells seeded varied depending upon cell line and was calculated in order to reach ~80 % confluence on the day of cell harvesting. Lyophilised siRNA was resuspended in 1x siRNA buffer, creating a 50 µM stock. Further dilutions of the siRNAs were carried out in 1x siRNA buffer. The transfection mix was prepared according to the manufacturer's instruction using Opti-MEM® with the amount of siRNA dependent on the efficiency of the knockdown. The volume of Lipofectamine™ RNAiMAX (ThermoFisher #13778075) used was directly proportional to the surface area of the well (Table 2-3). Cells were incubated with transfection mix for 6 hours prior to refreshing of the culture media. Cells were further cultured for 1-3 days prior to harvesting.

Plate	Surface area (cm^2 per well)	Lipofectamine™ RNAiMAX (µl)
10 cm	55	28
6 cm	21	11
6-well	9.6	5
12-well	3.9	2

Table 2-3 | Transfection of cells with siRNA

2.1.6.2.2 Reverse transfection

Cells were seeded at $1x10^6$ cells per 10 cm plate in 10 ml of culture media. 250 µl of Opti-MEM™ was mixed with 30 µl RNAiMAX and mixed with desired siRNA concentration. These mixes were incubated at room temperature for 5 minutes before mixing them together and incubating for a further 20 minutes at room temperature. This mixture was added to the 10 cm plate and the plate incubated for 24 hours at 37 °C, 5 % CO_2, with humidity. Following the 24-hour incubation the media was refreshed and cells incubated at 37 °C. 5 % CO_2, with humidity for a further 48 hours. The culture was refreshed again 1 hour before cells were harvested.

2.1.7 Monoclonal stable cell line generation

Stable cell lines were generated by co-transfecting pOG44 Flp recombinase expression vector along with pcDNA5/FRT/TO-Gene of interest (GOI) into the Flp-In™ T-REx™ cells using Lipofectamine™ LTX (Section 2.1.6.1). Ratios of pOG44 to pcDNA5/FRT/TO-GOI were used as per manufacturer instruction to achieve integration of the GOI into the chromatin. Cells were incubated for 24 hours post-transfection before introduction of selection antibiotics into the culture media. Media was changed every 3-4 days herein to allow cell expansion. When cells became confluent the cells were transferred to a 15 cm dish where culture continued. Upon visual formation of colonies, media was removed, and colonies isolated using cloning rings (Sigma #C1059). Individual colonies were transferred into individual wells of a 12-well plate. Clones were expanded and cryopreserved as in section 2.1.3.

2.1.7.1 Induction of stable cell line protein expression

Expression of the protein of interest was carried out through addition of 250 ng/ml doxycycline to the culture media for a minimum of 16 hours.

2.1.8 Immunofluorescence

Ethanol washed 13 mm cover slips were placed in wells of a 24-well plate. Cells were seeded into the wells to achieve approximately 70 % confluence and incubated overnight at 37 °C, 5 % CO_2, with humidity. The following day the media was carefully aspirated, and wells washed with

PBS. Cells were fixed with -20 °C methanol for 10 minutes before washing in PBS three times for five minutes. Cells were washed once more in PBS for 1 minutes before blocking in 3 % BSA in PBS for 1 hour at room temperature. Coverslips were carefully placed in a self-made humidity chamber before adding 50 µl of primary antibody in 3 % BSA-PBS for overnight incubation at 4 °C. Coverslips were washed three times in PBS for 1 minutes before addition of the appropriate secondary antibody in 3 % BSA-PBS for 1 hour at room temperature in the dark. Coverslips were washed again in PBS three times for 1 minute before staining with Hoechst (1:200 in PBS) and incubated for a further 1 hour at room temperature in the dark. Coverslips were washed twice in PBS and then left covered with PBS, these slips were now ready for mounting. Coverslips were mounted by applying mounting fluid to a slide and placing the coverslips cell-side down on the slide. Slides were dried for 16 hours in the dark before confocal microscopy.

2.1.9 Crystal Violet assay

HeLa cells were seeded at 500 cells/well in a 96 well plates with a final volume of 100 µl in their respective cell culture media (Table 2-1) and cells incubated overnight at 37 °C, 5 % CO_2, with humidity. The following day cells were transfected with the desired siRNA (Section 2.1.6.2.1) and incubated for 6 hours before a media refresh. A plate was taken at every desired time point and washed with ice cold PBS before adding 100 µl per well of 3 % PFA, 2 % sucrose for 15 minutes at room temperature to fix the cells. The fixing solution was removed, and cells washed a further 3 times in PBS before leaving the cells submerged in 100 µl PBS and storing at 4 °C until all time point plates were fixed. Once all the plates were fixed the PBS was removed and 100 µl of 0.05 % crystal violet, 5 % ethanol was added to each well for 15 minutes at room temperature. The crystal violet staining solution was removed, and plates washed in distilled water by submerging the plates multiple times until no background stain was visualised. Excess water was removed by flicking the plate and the plates were dried at room temperature. When dry 100 µl of 10 % acetic acid was added to each well and incubated overnight at room temperature. The plate absorbance was read the following day at 540 nm.

2.2 Cell treatments

2.2.1 UVB irradiation

Cells were grown to approximately 80 % confluence then the media was refreshed 1 hour prior to treatment. Media was aspirated and cells washed in ice-cold PBS prior to an appropriate treatment of UVB_{302} inside a UV oven.

2.2.2 UVC irradiation

Cells were grown to approximately 80 % confluence then the media was removed, and cells washed in ice-cold PBS prior to treatment. Residual PBS was aspirated, then cells treated with 150 mJ/cm^2 UVC$_{254}$ inside a UV oven.

2.2.3 4NQO treatment

Cells were grown to approximately 80 % confluence then the media was refreshed 1 hour prior to treatment. Cells were then treated with 20 µM 4NQO in culture media for 1 hour at 37 ^{o}C, 5 % CO_2, with humidity.

2.2.4 Cisplatin treatment

Cells were grown to approximately 80 % confluence then the media was refreshed 1 hour prior to treatment. Cells were then treated with 50 µM Cisplatin in culture media for 2 hours at 37 ^{o}C, 5 % CO_2, with humidity.

2.3 Protein techniques

2.3.1 Buffers and solutions

Buffer name	Buffer composition
Antibody binding buffer	50 mM Tris pH 8.0, 150 mM NaCl, 0.1 % Tween20
Antibody wash buffer	PBS + 0.1% Tween20
Cytoplasmic lysis buffer	10 mM HEPES pH 7.5, 10 mM NaCl, 0.35 M sucrose, 3 mM $MgCl_2$, 0.5 % NP-40, (+ 1x complete mini EDTA-free protease inhibitors)
DUB reaction buffer	50 mM HEPES pH 7.5, 150 mM NaCl, 2 mM EDTA, 5mM DTT
FLAG elution buffer	20 mM Tris pH 7.5, 150 mM NaCl, 0.1 % NP-40
His-tag elution buffer	200 mM imidazole, 150 mM Tris pH 6.8, 30 % glycerol, 720 mM β-mercaptoethanol, 5 % SDS
His-tag lysis buffer	6 M Guanidinium hydrochloride, 100 mM Na_2HPO_4/NaH_2PO_4, 10 mM Tris pH 8.0, 20 mM imidazole, 10mM β-mercaptoethanol, 10 mM N-ethylmaleimide

His-tag wash buffer	8 M urea, 100 mM Na_2HPO_4/NaH_2PO_4, 10 mM Tris pH 6.8, 20 mM β-mercaptoethanol
Hypotonic lysis buffer	20 mM HEPES pH 7.5, 10 mM NaCl, 3 mM $MgCl_2$
MOPS running buffer (20x)	50 mM MOPS, 50 mM Tris-base, 0.1 % SDS, 1 mM EDTA, pH 7.7
Oligo (dT) lysis/binding buffer	20 mM Tris pH 7.4, 500 mM LiCl, 0.5 % LiDS, 1 mM EDTA, 5 mM DTT
Oligo (dT) storage buffer	250 mM Tris pH 7.4, 20 mM EDTA, 0.1 % Tween20, 0.02% NaN_3
PBS (10x)	137 mM NaCl, 2.7 mM KCl, 1.5 mM KH_2PO_4, 10.2 mM Na_2HPO_4, pH 7.4
Polysome Gradient buffer (10x)	200 mM HEPES pH 7.5, 1 M NaCl, 50 mM $MgCl_2$, 1 mg/ml Cycloheximide
RBP capture elution buffer	20 mM Tris pH 7.4, 1 mM EDTA
RBP capture low salt buffer	20 mM Tris pH 7.4, 200 mM LiCl, 1 mM EDTA
RBP capture RNA digestion buffer	20 mM Tris pH 7.4, 2 mM $MgCl_2$
RBP capture wash buffer 1	20 mM Tris pH 7.4, 500 mM LiCl, 0.1 % LiDS, 1 mM EDTA, 5 mM DTT
RBP capture wash buffer 2	20 mM Tris pH 7.4, 500 mM LiCl, 1 mM EDTA
RIPA buffer	25 mM Tris pH 7.4, 140 mM NaCl, 1 mM EDTA, 1 % NP-40, 0.1 % SDS, 0.5 % sodium deoxycholate, (+ 1x complete mini EDTA-free protease inhibitors)
SDS-PAGE developer	3 % sodium carbonate *w/v*, 0.04 % formalin, 0.001248 % sodium thiosulfate *(w/v)*
SDS-PAGE gel fixing solution	30 % ethanol, 10 % acetic acid, 60 % H_2O
SDS-PAGE stop solution	4 % Tris *w/v*, 2 % acetic acid

SDS loading buffer (5x)	250 mM Tris pH 6.8, 50 % glycerol, 10 % SDS, 50 mM DTT
siRNA buffer	6 mM HEPES pH 7.5, 60 mM KCl, 0.2 mM $MgCl_2$
SEC buffer	20mM HEPES pH 7.5, 150 mM NaCl, 5 % Sucrose
Soluble nuclear extract buffer	20 mM HEPES pH 7.5, 150 mM NaCl, 1 % NP-40, 0.5 % deoxycholate, 0.1 % SDS, 1 mM $MgCl_2$, (+ 1x cOmplete mini EDTA-free protease inhibitors)
TBE buffer	100 mM Tris, 90 mM Boric acid, 1 mM EDTA
TCA wash buffer	70% Acetone, 20% Ethanol, 50 mM Tris pH 8.0
Transfer buffer	25 mM Tris, 192 mM Glycine, 20 % methanol (*v/v*)
TUBEs lysis buffer	50 mM Tris pH 7.5, 150 mM NaCl, 1 mM EDTA, 1 % NP-40, 10 % glycerol, 20 mM imidazole, -/+ 100 µg/ml TUBEs, (+ 1x complete mini EDTA-free protease inhibitors)
TUBEs wash buffer	20 mM Tris pH 7.5, 150 mM NaCl, 0.1 % Tween-20, 20 mM imidazole
Ubiquitin chain buffer	50 mM HEPES pH 7.5, 150 mM NaCl
USP2 stock buffer	50 mM HEPES pH 7.5, 150 mM NaCl, 100 mM EDTA, 1 mM DTT
Whole cell lysis buffer	10 mM Tris pH 7.5, 50 mM NaCl, 0.5 % NP-40, 0.5 % sodium deoxycholate, 0.5 % SDS, 10 mM Iodoacetamide, 20 mM N-Ethylmaleimide, (+ 1x complete mini EDTA free protease inhibitors)

Table 2-4. Table of Buffers and their composition

2.3.2 Antibodies and dilutions

Antibody	MW (kDa)	Species	Type	Supplier	Primary dilution	Secondary dilution
β-tubulin	55	Rabbit	Poly	Cell signal #2146	1:1000	1:10000
ASCC1	45	Rabbit	Poly	Abcam #ab157102	1:1000	1:5000
ASCC2	88	Rabbit	Poly	Bethyl #A304-020A	N/A	N/A
ASCC2	88	Rabbit	Poly	ThermoFisher #PA5-30849	1:1000	1:10000
ASCC3	250	Rabbit	Poly	Bethyl #304-014A	1:1000	1:5000
ASCC3	250	Rabbit	Poly	Bethyl #304-015A	1:1000	1:5000
ASCC3	250	Rabbit	Poly	Proteintech #17627-1-AP	1:1000	1:5000
BAG2	24	Mouse	Poly	Bethyl #A304-751A	1:1000	1:5000
FLAG	-	Mouse	Mono	Sigma #F1804	1:1000	1:5000
FLAG	-	Mouse	Mono	Sigma #F3165	N/A	N/A
GAPDH	37	Rabbit	Mono	Cell signal #2118	1:1000	1:5000
His-tag		Rabbit	Poly	Cell Signal #2365	1:1000	1:5000
MDM2	75/90	Mouse	Mono	Merck #04-1530	1:1000	1:5000
Mouse IgG1κ	-	Mouse	Poly	ThermoFisher #14-4714-82	N/A	N/A
Normal Rabbit IgG	-	Rabbit	-	Cell Signal #2729	N/A	N/A
OTUD4	124	Rabbit	Poly	Bethyl #A304-605A	1:3000	1:5000
OTUD4	124	Rabbit	Poly	Bethyl #A304-606A	1:1000	1:5000
OTUD4	124	Rabbit	Poly	Proteintech #25070-1-AP	1:1000	1:5000
OTUD4	124	Rabbit	Poly	Sigma #HPA036623	N/A	N/A
PABP1	70	Rabbit	Poly	Abcam #ab21060	1:1000	1:10000
PARP1	89	Rabbit	Poly	Cell Signal #9542	1:1000	1:10000
PTBP1	57	Mouse	Poly	In house	1:2000	1:10000
RPS2	31	Rabbit	Poly	Bethyl #A303-794A	1:1000	1:10000
RPS6	32	Rabbit	Poly	Cell signal #2217	1:1000	1:10000
RPL11	20	Rabbit	Poly	Abcam #ab79352	1:1000	1:10000
STK38	54	Mouse	Mono	Novus #H00011329	1:1000	1:5000
THRAP	109	Rabbit	Poly	Bethyl #A300-956A	1:1000	1:5000
TRIP4	67	Rabbit	Poly	Bethyl #A300-203A	1:1000	1:5000
TRIP4	67	Rabbit	Poly	Bethyl #A300-843A	1:1000	1:5000
Ubiquitin	8	Mouse	Mono	Cell signal #3936	1:1000	1:10000
UBR5	308	Rabbit	Mono	Cell signal #65344	1:1000	1:10000
USP2	68	Rabbit	Poly	Cell signal #8036	1:1000	1:10000

Table 2-5. Table of Antibodies, dilution factors, and relevant information

2.3.3 Cell lysis

2.3.3.1 Whole cell lysate preparation

Media was removed from the cells and plates washed with ice-cold PBS. Residual PBS was aspirated and Oligo (dT) lysis/binding buffer (complete with 1x cOmplete mini EDTA-free protease inhibitors and without DTT present in the buffer) applied in an appropriate volume. Cells were scraped with a cell scraper and collected in a 1.5 ml Eppendorf tube. The lysate was passed through a 21G needle (BD Plastipak) ten times followed by 10 passes through a 23G needle. The extract was centrifuged at 3000 g for 5 minutes at 4 ^{o}C. The supernatant was the whole cell extract and was used immediately or snap frozen in liquid nitrogen and stored at -80 ^{o}C.

2.3.3.2 Cytoplasmic cell lysate preparation

The media is removed from plated cells prior to washing with ice-cold PBS. Residual PBS was aspirated, and cytoplasmic lysis buffer applied in an appropriate volume. Cells were scraped with a cell scraper and collected in a 1.5 ml Eppendorf tube. The sample was then incubated on ice for 3 minutes prior to centrifugation at 1300 g for 5 minutes at 4 ^{o}C. The supernatant was then transferred to a fresh 1.5 ml Eppendorf tube; this was the cytoplasmic fraction. The nuclear pellet was discarded, and the cytoplasmic fraction used immediately, or snap frozen in liquid nitrogen and stored at -80 ^{o}C.

2.3.3.3 Nuclear cell lysate preparation

The cultured cells were treated as in section 2.3.3.2. At the point of fractionation, the cytoplasmic extract was discarded and nuclear pellet kept for further processing. The nuclear pellet was washed in cytoplasmic lysis buffer and centrifuged again for 5 minutes at 1300 g at 4 ^{o}C. The supernatant was discarded, and the pellet resuspended in soluble nuclear extract buffer. 25 units of Benzonase was added and sample incubated on ice for 1 hour. SDS was then added and the sample heated to 70 ^{o}C for 10 minutes. The cell debris were pelleted 17000 g for 5 minutes at 4 ^{o}C and the supernatant taken as the soluble nuclear extract.

2.3.3.4 Complete cell lysis

The cell culture media was removed from the 10 cm plates prior to washing with ice-cold PBS. Residual PBS was aspirated, and 1 ml complete cell lysis buffer added to each plate. Cells were scraped using a cell scraper into the buffer and transferred to a 1.5 ml Eppendorf tube. The lysate was passed through a 23G needle 30 times before centrifugation at 17000 g at 4 ^{o}C for 10

minutes. The supernatant was transferred to a fresh 1.5 ml Eppendorf tube and used immediately or snap frozen in liquid nitrogen and stored at -80 °C.

2.3.3.5 Hypotonic cell lysis – polysome profiling

Media was refreshed 1 hour prior to choice of stimulus for each confluent 15 cm plate. Following stimulus duration, cycloheximide (CHX) was added to the media to a final concentration of 0.1 mg/ml for 3 minutes at 37 °C, 5 % CO_2, with humidity. Media was removed and cells washed with room temperature PBS before adding 5 ml 1x trypsin and incubating at 37 °C, 5 % CO_2. Upon cell detachment plates were placed on ice, 10 ml ice cold PBS was used to resuspend the cells which were then transferred to a 50 ml falcon tube containing 35 ml ice-cold PBS. Cells were pelleted at 200 g for 5 minutes at 4 °C. The supernatant was removed, and the cells resuspended in 25 ml ice-cold PBS followed by centrifugation at 200 g for 5 minutes at 4°C. The supernatant was removed, then the cell pellet resuspended in 1 ml of 1x hypotonic lysis buffer and transferred to a 1.5 ml tube. Cells were centrifuged at 17000 g for 5 seconds at 4 °C and the supernatant removed. Cells were resuspended in 800 µl hypotonic lysis buffer containing 0.1 mg/ml CHX, NxGen® RNAse inhibitor (1000 U/ml), and 1x protease inhibitor cocktail (Sigma #P8340), followed by incubation on ice for 20 minutes. Cell solutions were passed twenty time through a 27G needle before centrifugation at 2000 g for 5 minutes at 4 °C. The supernatant was transferred to a new 1.5 ml tube and centrifuged at 17000 g for 10 minutes at 4 °C. The supernatant was transferred to a new 1.5 ml tube and NaCl concentration adjusted to 100 mM.

2.3.4 Protein quantification (Pierce BCA assay)

The BCA assay was conducted using clear 96-well micro titre plates with pre-prepared standards ranging from 20 – 2,000 µg/ml in duplicate. Protein samples were diluted 1:10 in sterile H_2O before 10 µl of each standard and samples were added to individual wells. To each well, 200 µl of pre-prepared Pierce BCA solution (50:1 of Reagent A to B) was added. The plate was incubated at 37 °C for 30 minutes prior to absorbance readings at 562 nm using a PowerWave XS2 plate reader (Bio-Tek instruments). The readings from the BCA standards were used to construct a standard curve, to which the protein concentration of samples could be calculated and normalised.

2.3.5 SDS-poly acrylamide gel electrophoresis (PAGE)

Samples were made up using 5x SDS loading buffer and DTT, then heated to 75 °C for 10 minutes to ensure linearization of proteins for separation by relative mass. A molecular weight marker and samples were loaded onto the gel after being normalised to either protein or RNA quantity. Typically, a pre-cast NuPAGE™ 4-12 % Bis-Tris gel (ThermoFisher) was used in the XCell

SureLock™ Mini-Cell (ThermoFisher) filled with 1x MOPS running buffer. Gels are run at 150 volts (V) until the dye front reaches the bottom of the gel.

2.3.5.1 Coomasie staining

Post SDS-PAGE, the gel was washed in distilled H_2O 3 times for 5 minutes each to remove excess MOPS running buffer. The solution of ProtoBlue Safe stain (National diagnostics) was mixed well before use. Prepare the staining solution by mixing stain with ethanol (9:1) and mixing then adding the stain solution to completely cover the gel. The gel was stained for 4-16 hours depending upon protein abundance and sensitivity. The stain was removed then the gel washed in distilled H_2O until background was removed.

2.3.5.2 Silver staining

The SDS-PAGE gel was soaked in SDS-PAGE gel fixing solution for 30 minutes at room temperature with agitation. The gel was then washed twice in 20 % ethanol and twice in distilled H_2O for 10 minutes each at room temperature with agitation. The gel was the sensitised in 0.02 % sodium thiosulfate for 2 minutes before rinsing with distilled H_2O. The gel was then soaked in 0.2 % silver nitrate for 20-60 minutes at 4 ^oC with agitation. The gel was then rinsed in distilled H_2O and the gel soaked in SDS-PAGE developer solution until protein bands were visualised. The gel was then transferred to SDS-PAGE stop solution for 30 minutes, followed by two 30-minute washes in distilled H_2O.

2.3.5.3 Gel drying

Gels were placed flat on a piece of saran wrap and excess H_2O blotted away. A piece of Whatman® paper was then placed on top of the gel and the whole assembly flipped to allow the gel to face upwards. The gel was then placed inside a Fisher brand gel dryer where the gel was dried for 2 hours at 80 ^oC with vacuum applied.

2.3.6 Transfer of proteins to a PVDF membrane

Proteins were transferred and immobilised from an SDS-PAGE gel (Section 2.3.5) to PVDF membranes using the wet transfer method using the Bio-Rad Mini-PROTEAN® Tetra cell with Mini Trans-Blot®. Prior to transfer the PDVF membrane was activated in methanol before being submerged in 1x transfer buffer. Three pieces of Whatman® paper and 3 transfer sponges were also pre-soaked in transfer buffer prior to cassette assembly. Transfer cassettes were then layered as follows: Black side of cassette, 2 sponges, 2 pieces of Whatman® paper, SDS-PAGE gel, activated PVDF membrane, 1 piece of Whatman® paper, 1 sponge, and finally the clear side

of the cassette. The cassette was placed in the transfer tank and filled with 1x transfer buffer. The transfer was carried out at 100 V for 1 hour at 4 °C or 30 V overnight at 4 °C.

2.3.7 Immunodetection of proteins

To detect the immobilised protein of interest on the PVDF membrane, an antibody specifically able to bind an epitope from the protein is used (Table 2-5). To prevent non-specific binding of the antibody to the membrane, the PVDF was blocked in TBS-T containing 5 % dried milk powder (Marvel) *w/v* for 1 hour at room temperature with rotation in a 50 ml Falcon tube (BD Plastipak). Once blocked the membrane was washed thrice in TBS-T for 10 minutes at room temperature with rotation. The PVDF membrane was then cut if multiple primary antibodies were to be used. Each region of the membrane was then incubated with TBS-T containing 5 % *w/v* dried milk powder and the appropriate dilution of the primary antibody (Table 2-5) overnight at 4 °C with rotation. Excess primary antibody was then removed by three TBS-T wash steps for 10 minutes each with rotation at room temperature. An appropriate dilution and species-specific secondary antibody (Table 2-5) conjugated to a horseradish peroxidase enzyme was then applied in TBS-T containing 5 % *w/v* dried milk powder. The membranes were then washed three times for 10 minutes each in TBS-T at room temperature with rotation to remove excess secondary antibody. The membrane was then incubated with 1:1 mixture of enhanced chemiluminescence (ECL) reagents (Bio-Rad, Amersham, ThermoFisher) for 5 minutes before being exposed to photographic film (Fuji RX X-ray). Signals were detected depending upon the strength of ECL reagent and abundance of protein within seconds and minutes.

2.3.8 Membrane stripping

Membranes were washed in PBS for 5 minutes with rotation before incubation with Restore™ western blot stripping buffer (Thermofisher) for 10 minutes. The membrane was then washed three time for 5 minutes each in TBST before proceeding to immunodetection (Section 2.3.7).

2.3.9 RNA binding protein interactome capture

RNA was crosslinked to protein using by treating cells with UVC as in section 2.2.2 before cell lysate preparation (Section 2.3.3). Lysis buffer included NxGen® RNAse inhibitor (1000 U/ml) to preserve RNA. For cytoplasmic lysates the LiDS was added to a final concentration of 0.5 %, LiCl to 500 mM, DTT to 5 mM, and EDTA to 1 mM and mixed for 5 minutes with rotation. Dynabeads™ Oligo (dT) magnetic beads (ThermoFisher #61002) were re-suspended before transferring an appropriate volume for the size of lysate into a fresh 1.5 ml Eppendorf tube. Storage buffer was removed by placing each tube on a magnetic rack and waiting for the magnet to pull the beads to one side of the tube. The supernatant was removed then the beads

resuspended in oligo (dT) lysis/binding buffer. Tubes were incubated at room temperature for 5 minutes with rotation. The buffer was then removed then the beads mixed with the previously prepared lysate. Samples were incubated for 1 hour at room temperature. Bead-RNA complexes were washed once with oligo (dT) lysis/binding buffer for 5 minutes with rotation, twice with oligo (dT) wash buffer 1 for 5 minutes with rotation, twice with oligo (dT) wash buffer 2 with no incubation time, and twice with oligo (dT) low salt buffer twice with no incubation time. At this point the samples were centrifuged at 2000 rpm for 10 seconds prior to being placed on the magnetic rack and residual oligo (dT) low salt buffer removed. Bead-RNA complexes were resuspended in 50 µl of oligo (dT) elution buffer before heating to 75 °C for 3 minutes to elute RNA. Samples were separated from the beads using the magnetic rack and transferred to a fresh 1.5 ml Eppendorf tube. RNA concentration was measured using a nanodrop 2000 before storage at -80 °C. Before SDS-PAGE and western blot analysis $MgCl_2$ was added to each tube to a final concentration of 2 mM, followed by addition of turbo nuclease (250 U/µl) (Sigma #T4330) and RNase A/T1 (100 U/µl) (Thermofisher #EN0551) for 2 hours at 37 °C. For analysis, all samples were normalised by sample RNA concentration.

2.3.9.1 Oligo (dT) bead reconditioning

Beads were re-suspended in 500 µl of 500 mM NaOH and incubated at room temperature with rotation for 5 minutes. NaOH was removed using a magnetic rack and beads were washed five time in oligo (dT) storage buffer. Beads were finally resuspended in storage buffer and stored at 4 °C. Beads were reconditioned twice without substantial loss of binding activity.

2.3.10 Immunoaffinity isolation

Antibodies specific to the native epitope of a protein of interest were conjugated to magnetic beads either through covalent or non-covalent interactions. These antibody-bead conjugations were then used to capture proteins from a lysate. It was possible to also isolate proteins in complex with the protein of interest (co-immunoprecipitation).

2.3.10.1 Non-covalent immunoaffinity isolation

Magnetic beads with conjugated protein A or protein G (ThermoFisher) were used to couple with rabbit and mouse antibodies respectively. 30 µl of magnetic bead slurry was transferred to two fresh 1.5 ml Eppendorf tubes and placed on a magnetic rack. Storage buffer was then removed and beads equilibrated with antibody binding buffer. Equilibration buffer was then removed and 3 µg of desired antibody and control isotype was added to a single tube along with 250 µl of antibody binding buffer. Antibody-bead mixes were incubated at 4 °C for two hours with rotation before being washed with antibody binding buffer to remove any antibody not

bound to the magnetic beads. Antibody-bead complexes were then incubated with desired lysate containing 500 µg of protein with a minimum volume of 400 µl to allow sufficient fluidity during the 3-hour incubation at 4 °C with rotation. Bead-immunocomplexes were then washed three times in antibody wash buffer at 4 °C for 10 minutes with rotation. Following the last wash, the bead-immunocomplexes were resuspended in 200 µl PBS and transferred to a fresh 1.5 ml Eppendorf tube. The PBS was aspirated and bead-immunocomplexes re-suspended in 2x SDS loading buffer before heating at 70 °C for 10 minutes to elute the protein. The beads were separated from the sample using a magnetic rack and sample transferred to a fresh 1.5 ml Eppendorf, DTT was added to a final concentration of 100 mM and samples heated at 95 °C for 5 minutes. Samples were then ready for SDS-PAGE (Section 2.3.5).

2.3.10.2 Covalent immunoaffinity isolation

Dynabeads™ antibody coupling kit (ThermoFisher) was used to couple antibodies to the magnetic beads through epoxy conjugation. Antibodies were coupled to beads at 7 µg per 1 mg of magnetic beads using manufacturer protocol. Upon coupling completion, the antibody-bead complexes were washed with cytoplasmic lysis buffer to condition the beads. The antibody-bead complexes were then incubated with cell lysate (1 mg of protein per 1.5 mg of magnetic beads) for 3 hours at 4 °C with rotation, followed by three 15 minute washes in epoxy bead antibody wash buffer before re-suspending in PBS and transferring to a fresh 1.5 ml Eppendorf tube. Elution of protein was carried out by two methods, but predominantly by re-suspending the bead-immunocomplexes in FLAG elution buffer containing 1 mg/ml 3xFLAG peptide (Sigma #4799), then shaking for 45 minutes at 1100 rpm at 4 °C in a thermoshaker. The elution step was carried out twice for optimal elution before adding 5x SDS loading buffer and DTT to 50 mM for SDS-PAGE (Section 2.3.5).

2.3.11 Mass Spectrometry

Protein samples were prepared in SDS loading buffer and run on an SDS-PAGE gel (Section 2.3.5), however samples were run ~2 cm into the gel unless isolating specific band of interest. The gel was stained (Section 2.3.5.1) and sent for mass spectrometry analysis at the Proteomics profiling group at the MRC Toxicology unit.

Briefly, SDS-PAGE gels were sliced, de-stained, and digested with trypsin (Promega) either overnight at 30 °C or for 3 hours at 37 °C. Tryptic peptides were extracted using 0.2 % trifluoroacetic acid/10 % acetonitrile and dried down. The dried peptides were solubilised in injection solvent (90 % formic acid (5 %)/10 % acetonitrile containing alcohol dehydrogenase (ADH) and bovine serum albumin (BSA) digests 20 fmol/µl internal standards). Samples were

analysed by LC-MS/MS using a Waters nanoAcquity LC system interfaced to a G2S-I mass spectrometer in positive ion mode (Waters). Peptides were separated using a M-Class Symmetry100 C18 5 µm trap column (1.8 µm x 20 mm) (Waters) and M-Class Symettry HSST3 1.8 µm C18 (75 µm x 250 mm) analytical column (Waters). A gradient was used consisting of aqueous formic acid 0.1 % (A) and acetonitrile (B). Mass spectrometry data were acquired using Masslynx 4.1 software using both data independent (DIA) and data directed acquisition (DDA) Peptide spectra were processed by Proteinlynx GlobalServer 3.02 (Waters) software identified through comparison to the nonredundant SwissProt database. Data were visualised and further analysed using Scaffold (Proteomic Software, Oregon).

2.3.12 Polysome profiling

2.3.12.1 Preparing sucrose gradients

Sucrose gradients were prepared using 15 %, 23.75 %, 32.5 %, 41.25 %, and 50 % *w/v* sucrose solutions in 1x polysome gradient buffer (Table 2-4), 2 ml of 50 % sucrose was added to a 12 ml polyallomer centrifuge tube (Sorvall) and allowed to freeze at -80 ^{o}C for a minimum of 30 minutes. Upon freezing 2 ml of 41.25 % sucrose was added on top of the pre-existing frozen 50 % sucrose layer. This layer was frozen as before, and further layers added sequentially in descending order by repeating the process. Prior to use, gradients were removed at least 24 hours in advance and stored at 4 ^{o}C to equilibrate. Lysates (Section 2.3.3.5) were thawed and carefully loaded onto the pre-chilled sucrose gradients. Loaded gradients were placed into a pre-cooled SW41 Ti rotor (Beckman) and were centrifuged at 38000 rpm for 2.5 hours at 4 ^{o}C under vacuum in a Sorvall WX Ultra Series centrifuge. Following centrifugation gradients were stored at 4 ^{o}C until ready to load onto a gradient density fractionation system in which a 0.05 % bromophenol blue 60 % sucrose solution was pumped into the bottom of the tube at 1 ml/minute. This causes the displaced sample containing sucrose solution to be pumped through a UA-6 UV/Vis detector. The sample absorbance was measured continually at 254 nm as it passes through the detectors. The sample being displaced was collected in 1-minute intervals using a Foxy Jr fraction collector. 15 % of the collected fraction was transferred to a fresh tube and the protein precipitated as in section 2.3.15. The other 85 % was snap frozen in liquid nitrogen and stored at -80 ^{o}C.

2.3.13 Size exclusion chromatography

Cytoplasmic lysates were prepared from cells and protein concentration measured by BCA assay (Section 2.3.3.2 and 2.3.4). Before samples were loaded onto the column, they were clarified at 17,000 g at 4 ^{o}C for 15 minutes.

All columns were stored at 4 °C in 20 % ethanol to prevent microbial growth. Before use, the column was flushed with 5 column volumes (CV) of ultrapure water followed by 2 CV of size exclusion chromatography (SEC) buffer. Samples were taken up into a syringe and injected into the injection port being careful not to introduce air into the system. Upon introduction of the sample, the ÄKTA run was started, maintaining a constant flow rate collecting fractions of equal volume. Further details about the columns used, their respective chromatography system, flow rate, pressure limit, fraction collection and loop size can be found in Table 2-6.

Column	Chromatography system	Flow Rate (per minute)	Max Pressure (MPa)	Fraction collection	Loop volume (µl)
Superose 6 10/300 GL	ÄKTApurifier	400 µl	1.7	50 x 500 µl	250
Superose 6 increase 3.2/300	ÄKTAmicro	30 µl	1.2	60 x 50 µl	50
HiPrep™ 16/60 Sephacryl® S-500 HR	ÄKTApurifier	150 µl	0.6	70 x 2 ml	2000

Table 2-6. SEC column information

2.3.14 TCA protein precipitation

Trichloroacetic acid (TCA) protein precipitation is described as if precipitating protein from a 1 ml sample. In a 1.5 ml Eppendorf tube 250 µl of 100 % TCA was added to each sample. The samples were vortexed and incubated at 4 °C for a minimum of 30 minutes. Samples were centrifuged at 17000 g for 10 minutes at 4 °C before discarding the supernatant. The pellet was washed in 300 µl of 1x TCA wash buffer (Table 2-4) twice before removing the supernatant and allowing the pellet to air-dry in the fume hood for 10 minutes. The pellets were resuspended in 90 µl 2x SDS-loading buffer before adding 10 µl of 1 M DTT. Samples we're heated at 95 °C for 5 minutes with a brief vortex at every minute for SDS-PAGE western blot analysis (Section 2.3.5 – 2.3.7).

2.3.15 Methanol-Chloroform protein precipitation

Methanol-chloroform protein precipitation is described as if precipitating protein from a 150 µl sample. In a 1.5 ml Eppendorf tube 600 µl of methanol was added to each 150 µl sample and

mixed. 150 µl of chloroform was then added to each tube and vortexed, followed by addition of 450 µl of ultrapure water and mixing by vortex. Samples were centrifuged at 17,000 g for 10 minutes at room temperature before the aqueous phase was removed leaving the protein at the interface. 650 µl methanol was added to each sample and samples inverted three times before centrifugation at 17000 g for 10 minutes at room temperature to pellet the protein. All remaining liquid was discarded then the pellets were air dried for 5 minutes at room temperature in the fume hood. Pellets were resuspended in 80 µl 2x SDS loading buffer and incubated at 1200 rpm for 30 minutes at 37 °C in the thermoshaker to solubilise the protein. DTT was added to a final concentration of 100 mM before SDS-PAGE.

2.3.16 6xHis tag protein purification

Cells were seeded at $4x10^6$ cells per 10 cm plate and were attached to the plate by incubating overnight at 37 °C, 5 % CO_2, with humidity. The following day cells were transfected with the plasmid containing the His-tagged protein (Section 2.1.6.1). Following a 6-hour incubation with the plasmid at 37 °C, 5 % CO_2, with humidity, the media was refreshed to include doxycycline, then the cells incubated at 37 °C, 5 % CO_2, with humidity overnight. The following day the cells are treated with 10 µM MG132 in culture medium for 4 hours prior to cell lysis. Plates were washed twice in ice cold PBS before the addition of 1 ml His-tag lysis buffer. Cells were scraped and collected in a 1.5 ml Eppendorf tube, the lysates were sonicated three times with 30 second breaks. Each round of sonication was carried out for 15 seconds with 5 pulses. Lysates were centrifuged at 17,000 g for 10 minutes at 4°C and the supernatant transferred to a 15 ml falcon tube. At this stage a small amount of sample is taken was an input. 4 ml of lysis buffer was added to each 1 ml lysate and mixed and kept on ice while the beads were equilibrated. Beads were equilibrated by taking 150 µl of Dynabeads™ His-tag isolation and pulldown beads (ThermoFisher #10103D) per sample and removing solvent. Beads were washed in His-tag lysis buffer then resuspended in 75 µl His-tag lysis buffer. Beads were then added to the lysate placed on ice. Lysate-bead mixes were incubated at 4 °C for four hours on a rotating wheel for gentle agitation. The beads were collected to the side of the tube using a magnetic rack and the supernatant removed. Samples were washed once in 4 ml His-tag lysis buffer for 5 minutes with gentle agitation at room temperature. Samples were then washed once in 4 ml His-tag wash buffer for 5 minutes with gentle agitation at room temperature before being washed a further two times in His-tag wash buffer plus 0.1 % triton X-100 for 5 minutes each with agitation at room temperature. His-tagged proteins were eluted by incubating the beads in 75 µl of His-tag elution buffer for 20 minutes at room temperature with agitation. The supernatant was

collected and transferred to a fresh 1.5 ml Eppendorf before being mixed with 5x SDS loading buffer. Samples were analysed by SDS-PAGE western blot (Section 2.3.5 – 2.3.7).

2.3.17 TUBEs purification

Cells were seeded at $1.5x10^6$ cells per 10 cm plate and incubated overnight at 37 °C, 5 % CO_2, with humidity. Cells were treated the following day as in section 2.2 before lysis in 500 µl 1x TUBEs lysis buffer. Cells were scraped from the plate and collected in a 1.5 ml Eppendorf tube. Samples were incubated for 15 minutes on ice before centrifugation at 14,000 g for 10 minutes at 4 °C. The supernatant was transferred to a fresh 1.5 ml Eppendorf tubes and the pellet discarded. His-tag isolation and pulldown beads (ThermoFisher #10103D) were prepared by washing 100 µl beads per sample with 500 µl of TUBEs wash buffer four times for 5 minutes each with rotation. Equal amount of protein from each sample (1 mg) was added to each of the prepared His-tag beads and incubated at 4 °C for 2 hours with rotation. Beads were washed three times in 1 ml TUBEs wash buffer at 4 °C for 10 minutes with rotation. Before resuspension in 72 µl of 2x SDS loading buffer and incubation at 70 °C for 10 minutes to elute proteins. The supernatant was transferred to a fresh 1.5 ml Eppendorf tube and DTT concentration adjusted to 100 mM. Samples were heated for 10 minutes at 70 °C before analysis by SDS-PAGE and western blotting.

2.3.18 Puromycin incorporation

Cells were seeded at $1.0x10^5$ cells per well in 6 wells plates with a final volume of 2 ml culture media and incubated overnight at 37 °C, 5 % CO_2, with humidity. The following day cells were siRNA treated and cells incubated overnight at 37 °C, 5 % CO_2, with humidity. The following day media was refreshed, and plates incubated for 72 hours at 37 °C, 5 % CO_2, with humidity. One well was treated with 0.1 mg/ml cycloheximide as a translational inhibition control for 3 minutes before addition of 10 µg/ml puromycin and incubation at 37 °C, 5 % CO_2, with humidity for 10 minutes. Media was aspirated and wells washed with ice-cold PBS before lysis in 100 µl freshly prepared RIPA buffer. Cells were scraped into a 1.5 ml Eppendorf tube before centrifugation at 17,000 g at 4 °C for 10 minutes. The supernatant was collected and transferred to a fresh 1.5 ml Eppendorf tube. Samples were made up in SDS-loading buffer to 1x and DTT to 50 mM before analysis by SDS-PAGE and immunoblotting.

2.3.19 In vitro deubiquitination assay

Lyophilised biotinylated tetra-ubiquitin chains (BostonBiochem #UCB-310) were resuspended in ubiquitin chain buffer to a final concentration of 500 µg/ml. $USP2_{CD}$ stock (50 µM) (BostonBiochem #E-504) was serially diluted 1:10 in USP2 stock buffer to create dilutions of 5,

0.5 and 0.05 µM. Reactions were made up using DUB reaction buffer, 1, 0.1, or 0.01 µM $USP2_{CD}$, and 1 or 0.2 µg of ubiquitin chains to a final volume of 20 µl. The reactions were carried out at 37 °C for 2 hours before addition of 7 µl of 5x SDS loading buffer and 3 µl of 1 M DTT. Samples were heated at 40 °C for 20 minutes before SDS-PAGE. Gel was transferred to PVDF and blocked in TBS-T containing 5 % dried milk powder (Marvel) *w/v* for 1 hour at room temperature with rotation in a 50 ml Falcon tube (BD Plastipak). Streptavidin-HRP conjugate (1:10000) was used to detect ubiquitin chains by ECL (Section 2.3.7).

2.4 Nucleic acid techniques

2.4.1 Bacterial cell culture

Colonies were picked using a sterile pipette tip from an LB-agar plate and placed in a 20 ml universal tube containing 5 ml LB media with appropriate antibiotic. The cultures were incubated at 37 °C for 16 hours at 200 rpm to allow bacterial growth.

2.4.2 Glycerol stocks

After bacterial cell growth (Section 2.4.1), 500 µl of overnight culture was added to 500 µl of sterile 50 % glycerol solution in a 1.5 ml cyrovial. The solution was mixed by inverting before placing at -80 °C for storage. To recover bacteria from the stock a sterile loop was used to scrape frozen bacteria off the top of the cryovial and was streaked onto and LB-agar plate with appropriate antibiotic.

2.4.3 Transformation into Chemically competent E. coli

An aliquot of competent cells was thawed on ice, 1-50 ng of plasmid DNA or 2.5 µl of DNA ligation reaction product was added to 50 µl of chemically competent cells and incubated on ice for 30 minutes. The cells were then heat shocked at 42 °C for 60 seconds and returned to ice for 2 minutes. The cells were then added to 500 µl LB in universal 20ml tubes and incubated at 37 °C with shaking at 200 rpm for 60 minutes. 50-150 µl of cell solution was then plated out onto LB-agar plates containing the appropriate antibiotic at incubated at 37 °C overnight.

2.4.4 Plasmid amplification

Single colonies of *E. coli* containing the plasmid of interest was grown in 5 ml LB supplemented with the ampicillin to a final concentration of 100 µg/ml. The cells were centrifuged at 4000 g and the supernatant discarded. To purify the plasmid on a small scale minipreps were performed using Promega Wizard® Plus SV Miniprep kit. For large scale purification and transfection into mammalian cells maxipreps were performed using the Qiagen HiSpeed plasmid maxi kit.

2.4.5 Agarose gel

Agarose gels were made up to 0.8-2 % *(w/v)* agarose in 1x TAE containing 1x SYBR safe. DNA samples were prepared by mixing the sample with 6x DNA loading buffer (Merck #69180-1ml) to a final concentration of 1x. 5-20 µl of sample is loaded per well for a small gel comb, or up to 50 µl for a large gel comb. Gels were run in a tank containing 1x TAE for 30-60 minutes at 80 V. Bands were visualised by UV using a Syngene GeneFlash gel-imaging system. If bands needed to be purified, the gels were imaged using an Invitrogen SafeImager 2.0 and excised using a scalpel. DNA was purified from the agarose using QIAGEN QIAquick Gel extraction kit.

2.4.6 Primer design

Primer design has fundamental implications on DNA amplification by PCR. Basic primer design rules were followed as meticulously as possible for all primers which were ordered from Sigma. Basic guidelines for designing primers include:

- Primers for PCR sequencing were approximately 18-25 nucleotides in length.
- Primers for site directed mutagenesis were approximately 36 nucleotides in length.
- Primer GC content should be between 40 and 60 %, with the 3' end of the primer ending in a C or G.
- The 3' end of the primer should be an exact match to template DNA.
- Restriction enzyme sites should be added at the 5' of the primer with at least 6 extra nucleotides to allow for efficient cutting.
- Avoid runs of the same nucleotide or nucleotide repeats when possible.
- Avoid regions of secondary structure or inter-primer homology to allow for efficient annealing. Sigma OligoEvaluator™ was used to monitor secondary structure potential.
- Primer pairs should have a similar Tm (within a 5 ^{o}C difference)
- Assure the primers are specific to the desired region and won't bind any other regions of the template DNA.

2.4.7 High-fidelity PCR

Generation of DNA fragments from cDNA was completed using Q5 high-fidelity polymerase (NEB #M0491). PCR reactions were carried out in a final volume of 50 µl containing 1 x reaction buffer, 200 µM of each dNTP, 0.5 µM forward and reverse primers, 1 ng of cDNA template, and 0.5 µl of high-fidelity polymerase. When required 1x Q5 GC enhancer was also added to the reaction buffer. The reaction was incubated as shown in Table 2-7. Completed reactions were stored at 4 ^{o}C until samples were examined on an agarose gel. If reactions were successful, DNA was purified using QIAquick PCR purification kit (QIAGEN).

Step	Temperature	Times	Step
1	98 °C	45 s	Initial denaturation
2	98 °C	10 s	Denaturation
3	62 °C	30 s	Annealing
4	72 °C	30 s per kb	Primer extension
5	Repeat steps 2-4 for 20-35 cycles		
6	72 °C	300 s	Final extension
7	4 °C	Infinite	Hold

Table 2-7. Steps of a typical PCR reaction

2.4.8 Restriction enzyme digestion

All restriction enzymes used were purchased from New England Biolabs. Restriction digestion of plasmids or DNA fragments was performed in a 30 µl reaction containing: 1x NEB enzyme buffer, 2 µg of plasmid DNA, and 1 µl of desired restriction enzyme. Reactions were incubated at 37 °C for 2 hours before purification using the QIAGEN QIAquick PCR purification kit or running the sample on an appropriate percentage agarose gel (Section 2.4.5) and excising the band from the gel.

2.4.9 DNA ligation

DNA ligations were performed using T4 DNA ligase (NEB #M0202) in a 10 µl reaction at 16 °C overnight. Reaction composition was made up using 1x T4 DNA ligase buffer and 1 µl T4 DNA ligase. For each ligation two reactions were set up using 25 ng of digested vector with a 1:1 and 1:3 molar ratio of vector to insert.

2.4.10 Gibson Assembly

Gibson assembly allows the assembly of multiple DNA fragments, regardless of end compatibility or fragment length. The assembly allows scar-less cloning in a short space of time. DNA fragments were constructed so they contained in-frame homologous ends. Gibson assembly reactions were set up to a final volume of 20 µl including 10 µl of 2x Gibson assembly master mix (NEB #E2611), 50ng of linearized vector DNA, then a 3:1 molar ratio of each insert DNA to vector. The reactions were incubated at 50 °C for 60 minutes before 2 µl of each assembly was transformed into DH5α. Colonies were picked and analysed by diagnostic digest or sequencing.

2.4.11 Site directed mutagenesis

Primers designed for site directed mutagenesis contained the single point mismatch between position 6 and 9 from the 5’ end. The 5’ ends of the primers should overlap, but at least 8 non-overlapping bases should be present at the 3’ end of the primers. The mutagenesis process was carried out by whole plasmid PCR using Phusion® High-fidelity DNA polymerase (NEB #M0530). PCR was carried out (Section 2.4.7) before adding 1 µl of DpnI (NEB #R0176) to the reaction. The

reaction was then incubated at 37 ^{o}C for 75 minutes to digest the methylated template DNA. 10 µl of 6x loading buffer was the added and run on an agarose gel and purified (Section 2.4.5). 2.5 µl of each purified DNA was transformed into DH5α (Section 2.4.3). Colonies were picked and analysed by diagnostic digest or sequencing.

2.4.12 Nucleic Acid quantification

To calculate the amount of DNA or RNA in a sample a ND-2000 spectrophotometer (Nanodrop) was used. The quantity of DNA is calculated based on its absorbance at 260 nm using the Beer-Lambert law: $A=\varepsilon cl$, where A is absorbance at 260 nm, ε is the extinction coefficient, C is the concentration, and l is the path-length. The generally accepted extinction coefficient for double stranded DNA is 50 ng-cm/µl. The purity of DNA was assessed based on the ratio of absorbance at 260 nm/280 nm, with pure DNA having a ratio of approximately 1.80. The generally accepted extinction coefficient for RNA is 40 ng-cm/µl and a 260 nm/280 nm absorbance ratio of 2.0 generally accepted as being pure.

3. Creation and optimisation of an inducible stable cell line to study the ASC-1 complex

3.1 Introduction

ASCC3 was identified as an RNA-binding protein (Liao *et al.* 2016), and recently the Willis laboratory has shown that in the cytoplasm its interaction with RNA is substantially increased in response to UVB irradiation of the cells (Stoneley *et al,* unpublished data). Previous studies to determine the function of the ASC-1 complex have predominantly focused on its nuclear role. Thus, this complex was initially identified as a transcriptional coactivator (Jung *et al.* 2002; Kim *et al.* 1999) and more recent data has shown that it also has a role in DNA repair following alkylation damage (Brickner *et al.* 2017; Dango *et al.* 2011; Soll *et al.* 2018). The cytoplasmic role of the ASC-1 complex has also been explored; recent studies have suggested that the ASC-1 complex has a role in RQC (D'Orazio *et al.* 2019; Ikeuchi *et al.* 2019; Liaud *et al.* 2019; Matsuo *et al.* 2017; Sitron *et al.* 2017), although the function of the complex in this regard requires further investigation.

3.1.1 Aims

To further study the role of ASCC3 as a component of the ASC-1 complex, and identify novel protein interactors, an inducible stable cell line was generated. This chapter highlights generation of the stable cell line and the work carried out to ensure that exogenous ASCC3 functions in a similar manner to endogenous ASCC3.

3.2 ASCC3 as an RNA binding protein

In our studies of the role of ASCC3 in the cytoplasmic response to UVB exposure, the non-transformed breast epithelial cell line MCF10A was used (Stoneley *et al*, unpublished data). It was therefore important to investigate whether these data could be recapitulated in cell lines derived from different tissues, in addition to determining whether ASCC3 could be over-expressed in these cell lines. A panel of three cell lines was chosen, HeLa, HEK293, and U2OS, all of which had Flp-In T-REx cell line variants available and could be used to produce inducible stable cell lines.

To assess the RNA binding of ASCC3 in these cell lines, cytoplasmic RIC was performed after one hour following four conditions: untreated, UVB 30 mJ/cm^2 treated, cross-linked with UVC 150 mJ/cm^2, and a combination of UVB and crosslinking (Figure 3-1). As expected, no ASCC3 or PABP was detected by immunoblot in samples which have not undergone UVC crosslinking. Crosslinking with UVC demonstrated detection of PABP and a low level of ASCC3. ASCC3

detection increased in samples which had been UVB irradiated and crosslinked. There were no significant changes in total expression of ASCC3 or PABP in these samples, as demonstrated by the immunodetection of the input. Similar data were obtained with all three cell lines used and show that ASCC3's increase in RNA affinity following UVB exposure can be recapitulated across multiple cell types. The well-characterised ability of HEK293 cells to express high levels of exogenous protein (Thomas & Smart 2005), with its rapid basal proliferation rate, led to this cell line being chosen for further study.

3.3 Cellular fractionation and localisation of ASCC3

As previously discussed, ASCC3 has both nuclear and cytoplasmic functions. Therefore, to ensure that the RNA-binding observed in Figure 3-1 was solely occurring in the cytoplasm, fractionation experiments were performed, using appropriate cytoplasmic and nuclear marker proteins.

Whole cell, cytoplasmic, and nuclear HEK293 cell extracts were immunoblotted for β-tubulin and GAPDH (as cytoplasmic markers) and PARP and histone H3 (as nuclear markers) (Figure 3-2A). PARP and histone H3 were found almost exclusively in the nuclear extract, whereas β-tubulin and GAPDH were present in the cytoplasmic extract. Colloidal coomassie and silver staining of SDS-PAGE gels shows equal protein loading of these samples (Figure 3-2B). These data show that the cytoplasmic extracts used in these RIC assays are not contaminated with nuclear proteins. HEK293 cells demonstrate a nuclear and cytoplasmic population of ASCC3, therefore, all future experiments employed fractionation in order to focus on the cytoplasmic role of ASCC3 unless otherwise stated.

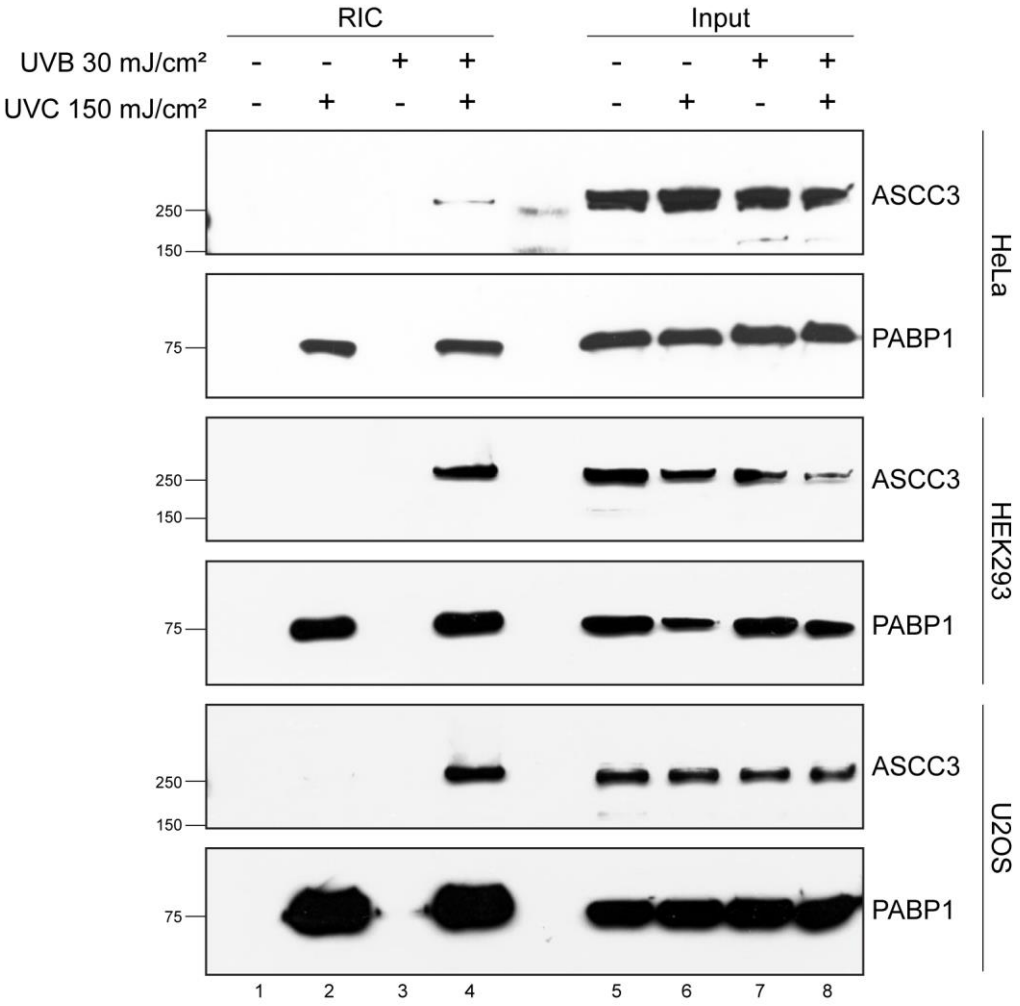

Figure 3-1. RNA-binding of ASCC3 following UVB irradiation in HeLa, HEK293, and U2OS cell lines
HeLa, HEK293, and U2OS cell were all subjected to RIC analysis under four conditions and extracts separated by SDS-PAGE and immunoblotted with the antibodies shown. Proteins are not detected by RIC without UVC cross-linking (compare lane 1 and 2) and UVB does not cause background cross-linking (lane 3). ASCC3 increased its affinity for RNA in response to UVB (lane 4) and these treatments did not affect the overall cytoplasmic expression level of ASCC3 (lanes 5-8).

A)

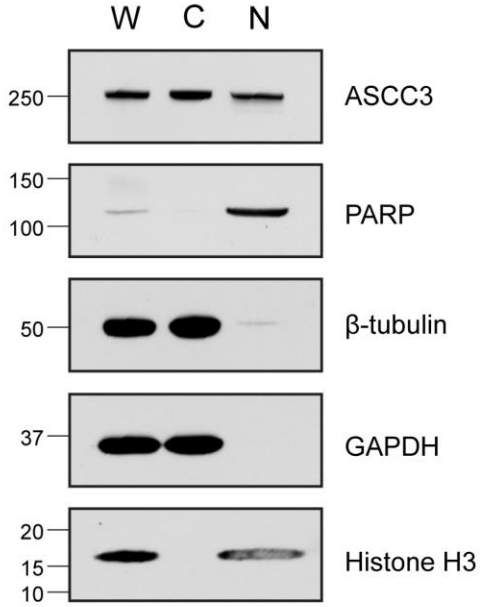

B)

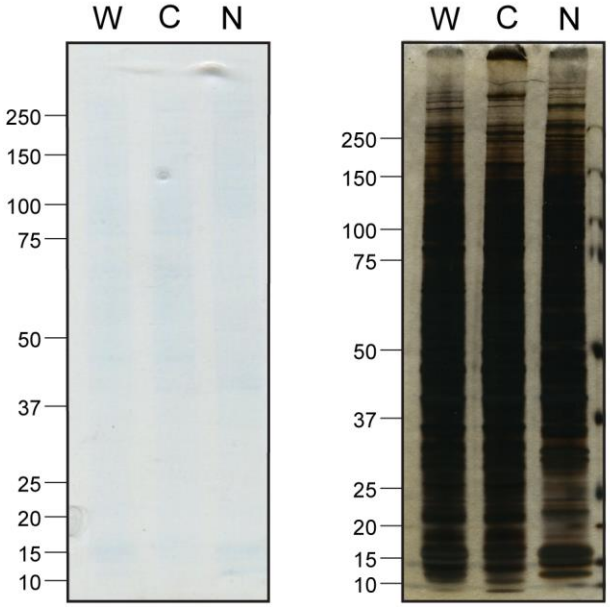

Figure 3-2. Cytoplasmic/nuclear fractionation of HEK293 cells

Analysis of the cytoplasmic and nuclear fractions of HEK293 cells. W=whole cell, C=cytoplasmic fraction, N=Nuclear fraction. A) Western blot analysis of fractionated HEK293 cells, showing ASCC3 expression in both nucleus and cytoplasm. β-tubulin and GAPDH were used as marker of the cytoplasm, whereas PARP and histone H3 were used as markers of the nucleus B) Colloidal Coomassie and silver stain analysis of the whole cell, cytoplasmic, and nuclear HEK293 lysates, showing equal protein loading and small differences in protein profiles between fractions.

3.4 Creation of the ASCC3 constructs

The cDNA encoding full-length ASCC3 was subcloned into the plasmid vector pcDNA5/FRT/TO with a 3xFLAG tag (Figure 3-3A). The FLAG tag was inserted at the C-terminus of ASCC3 to ensure that only the full-length product would be detected, but additionally because the N-terminus of Brr2, a protein which is structurally similar to ASCC3, has been shown to be important for its function (Absmeier *et al.* 2015b, 2015a).

The 3xFLAG tag was first inserted into the pcDNA5/FRT/TO vector. A restriction enzyme digest of the resulting plasmid showed a 153 base pair excised fragment of the correct size, whereas constructs with no insert resulted in excision of a 90 base pair fragment (Figure 3-3B). Due to the large size of ASCC3 (6606 base pairs) the open reading frame was subcloned into this new vector as two fragments. Primers were designed to overlap a naturally existing NheI site near the centre to the protein, allowing sequential insertion of the two helicase domains. Correct insertion of the ASCC3 N-terminal helicase domain resulted in excised fragment sizes of 1317, 2107, and 5126 bases (Figure 3-3C). The C-terminal helicase domain integration and successful completion of the pcDNA5/FRT/TO – ASCC3–3xFLAG plasmid was examined by the excision of a 3175 base pair fragment (Figure 3-3D). The successfully constructed plasmid was sequenced to confirm the correct insert orientation and size.

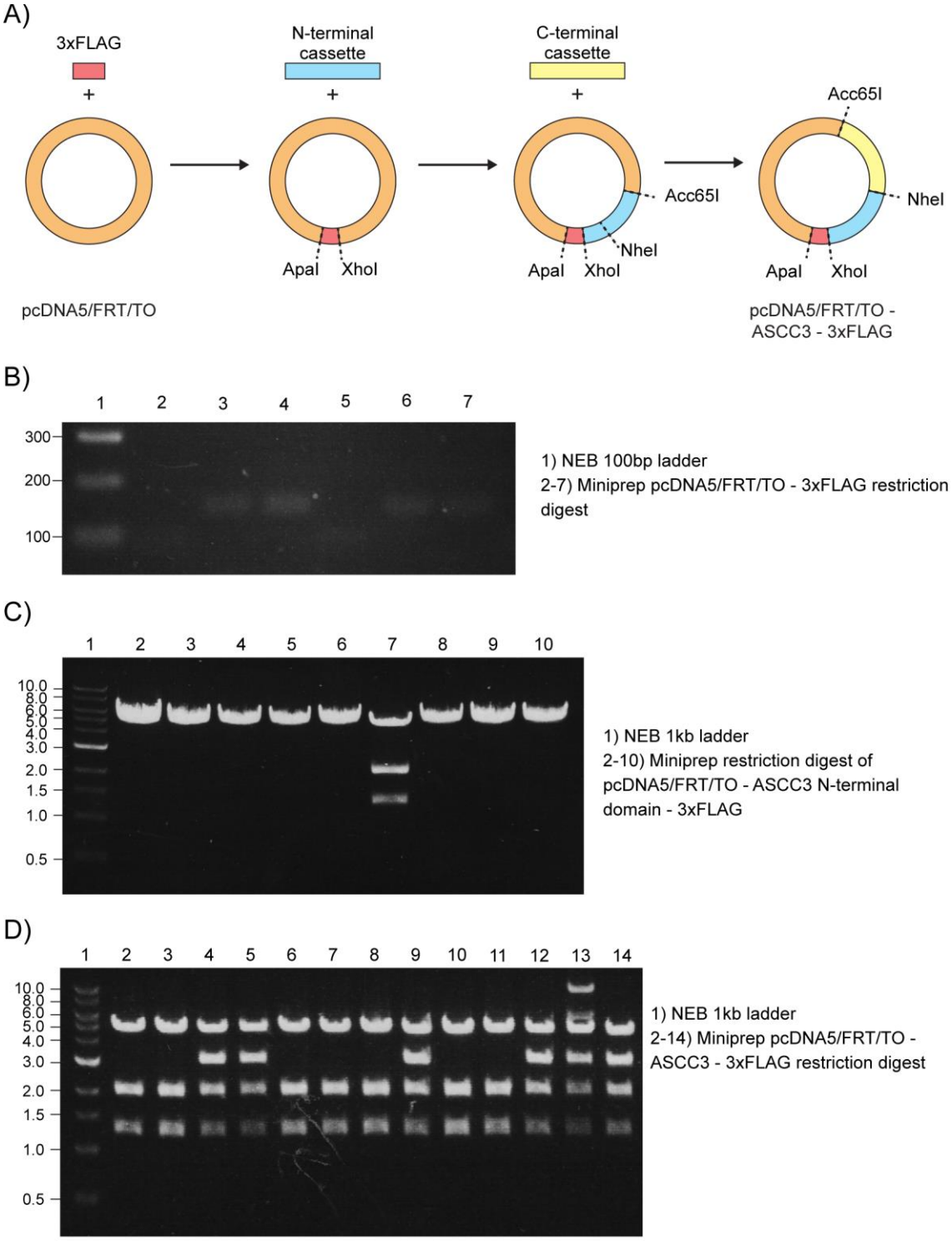

Figure 3-3. Construction of pcDNA5/FRT/TO - ASCC3-3xFLAG

A) Schematic demonstrating sequential insertion of ASCC3 DNA fragments in the pcDNA5/FRT/TO vector using common restriction enzymes. B) 2% agarose gel showing NEB 100 base pair (bp) ladder (lane 1) and restriction digest of six pcDNA5/FRT/TO – 3xFLAG miniprep clones using ApaI and HindIII (lane 2-7). C) 0.8% agarose gel showing NEB 1 kilobase (kb) ladder (lane 1) and restriction enzyme digest of nine pcDNA5/FRT/TO – N-terminal helicase domain–3xFLAG miniprep clones using HindIII and XhoI (lane 2-10). D) 0.8% agarose gel showing NEB 1 kb ladder (lane 1) and restriction enzyme digest of thirteen pcDNA5/FRT/TO – ASCC3–3xFLAG miniprep clones using HindIII and XhoI (lane 2-14).

3.5 Expression and localisation of the ASCC3 constructs

Three additional constructs were then generated containing the N-terminal helicase domain (amino acids 1-1300), a truncated N-terminal helicase domain (amino acids 401-1300), and the C-terminal helicase domain only (amino acids 1301-2202) (Figure 3-4A). These four constructs were transiently transfected into Flp-In T-REx HEK293 cells. Cell extracts from either the whole cell, cytoplasmic, or nuclear fractions were generated, proteins were separated by SDS-PAGE and immunoblotted with the FLAG antibody (Figure 3-4B). Constructs containing full-length ASCC3, the N-terminal helicase domain, the truncated N-terminal helicase domain, and the C-terminal helicase domain expressed polypeptides of 250, 150, 100, and 100 kDa respectively, which corresponded to their expected molecular weights. Each expression product was present in both cytoplasmic and nuclear fractions (Figure 3-4B). Gel staining demonstrates equal protein loading of the samples (Figure 3-4C), showing any differences in intensity of FLAG product are due to expression rather than loading.

3.6 Affinity purification of ASCC3–3xFLAG proteins

As previously stated, ASCC3 is a member of the ASC-1 complex, which is composed of ASCC3, ASCC2, TRIP4, and ASCC1. Thus, it was important to understand whether ASCC3-3xFLAG can also interact with other complex components. The full-length ASCC3-3xFLAG construct was transiently expressed in HEK293 cells, before isolation of the cytoplasmic extract. Expressed proteins were then immunoaffinity isolated by FLAG M2-protein G immunocomplexes by their 3xFLAG tag. Isolated proteins were analysed by immunoblotting for FLAG, ASCC2, TRIP4, and ASCC1, to determine whether these proteins interacted (Figure 3-5). These data show that a proportion of the full-length tagged ASCC3 can interact with each of its known binding partners (Figure 3-5A). Further examination of these data demonstrates that purified ASC-1 complex components are not enriched when compared to the input. This suggests that there is sub-stoichiometric complex formation, which may affect overall protein function.

In addition, similar experiments were performed using the three truncated ASCC3 proteins to delineate the binding regions for ASCC2, TRIP4, and ASCC1 (Figure 3-5B and 3-5D). Removal of the C-terminal helicase domain of ASCC3 resulted in loss of the TRIP4 and the ASCC1 interaction, but the ASCC2 interaction was maintained (Figure 3-5B). Deletion of the predicted disordered region (amino acids 1-400) from the N-terminal helicase domain resulted in co-isolation of ASCC2, however, the intensity of purified ASCC2 is decreased when compared to the complete N-terminal helicase domain (Figure 3-5C). The C-terminal helicase domain of ASCC3 co-purified TRIP4 and ASCC1, while losing its interaction with ASCC2 (Figure 3-5D). Overall, all constructs

successfully co-purified other ASC-1 complex components this allowed for generation of a simple model for complex formation (Figure 3-6); the exact contact points between the proteins remains unknown.

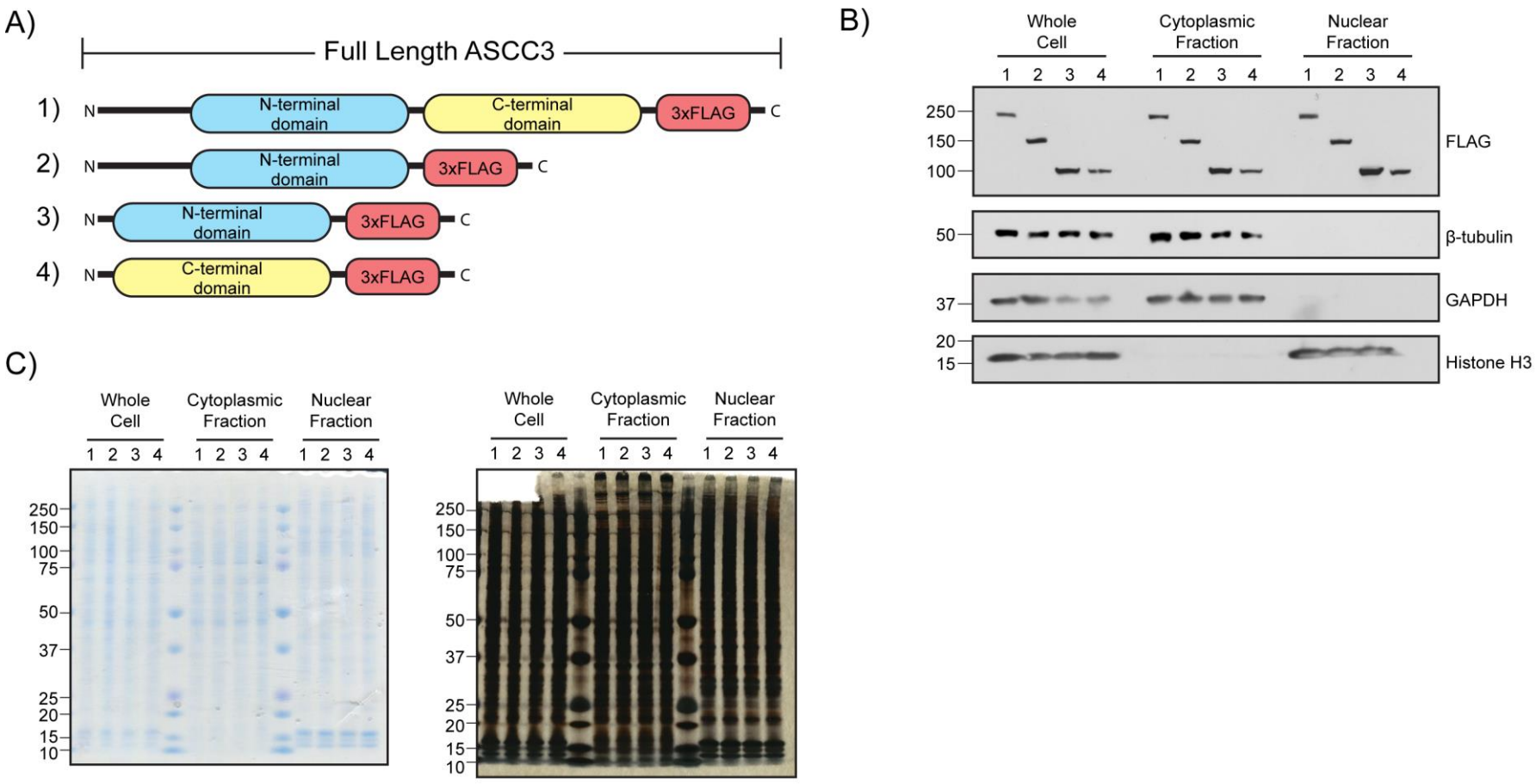

Figure 3-4. Expression of ASCC3-3xFLAG proteins

ASCC3 was cloned as full-length, N-terminal helicase domain, truncated N-terminal helicase domain, and C-terminal helicase domain into the pcDNA5/FRT/TO vector. These constructs were expressed in HEK293 and checked for cellular localisation. A) Schematic depicting the domains of ASCC3 for each generated construct. Construct number is a reference to the samples in B and C. B) Western blot analysis showing the transient expression of the four ASCC3 constructs and their expression in whole, cytoplasmic, and nuclear lysates (lanes 1-4, 5-8, and 9-12 respectively). A blotting error for histone H3, shows no presence in the nuclear fraction of construct 4. C) Coomassie and silver staining of the samples from B, showing the protein profile and loading for these samples.

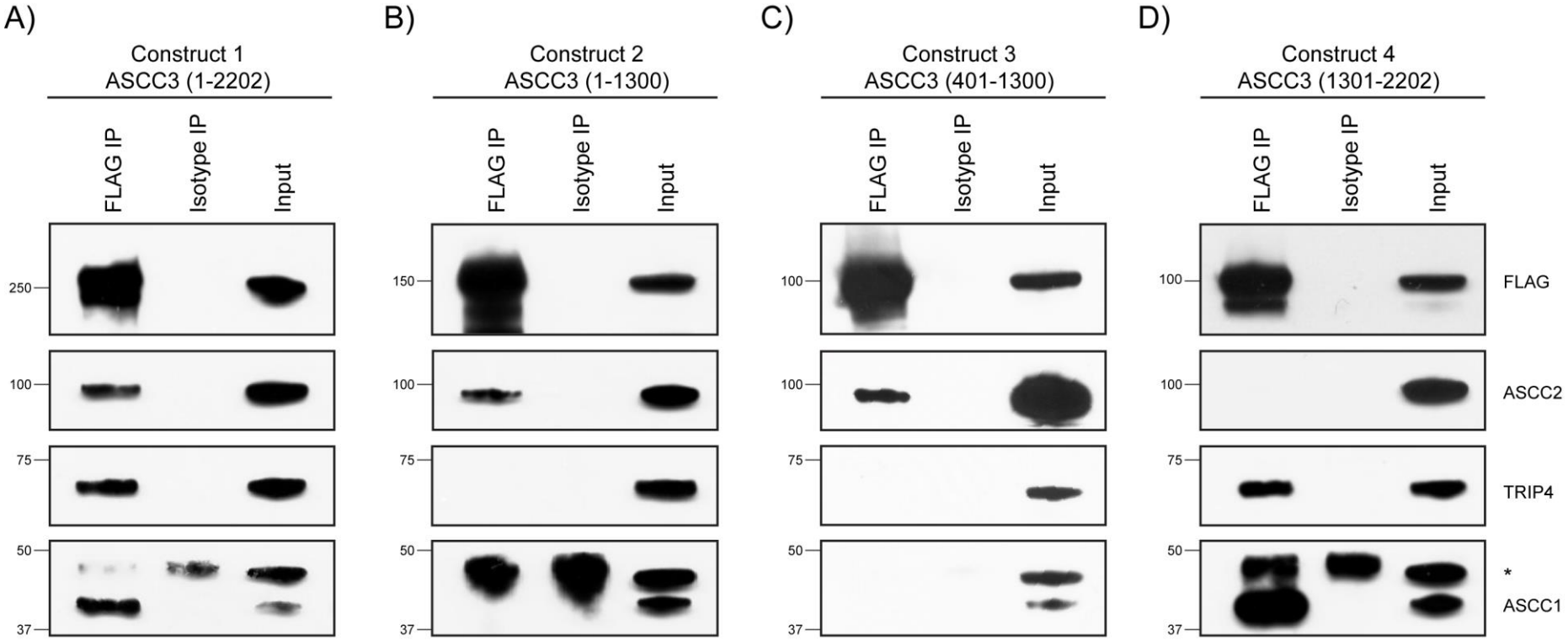

Figure 3-5. Immunoaffinity purification of ASCC3-3xFLAG products

Constructs displayed in Figure 3-4A were transiently expressed before immunoaffinity isolation of the fragments by FLAG monoclonal antibody. Numbers in brackets depict the amino acids of ASCC3 expressed by the construct. A) Full-length ASCC3 co-purified ASCC2, TRIP4 and ASCC1. B) The ASCC3 N-terminal helicase domain co-purified ASCC2 but no TRIP4 and ASCC1. C) The ASCC3 N-terminal helicase domain missing the 400 amino acid N-terminal region of predicted disorder maintained an interaction with ASCC2, but the level of interaction was reduced. D) The ASCC3 C-terminal helicase domain showed co-purification of TRIP4 and ASCC1 but did not interact with ASCC2. * = non-specific band.

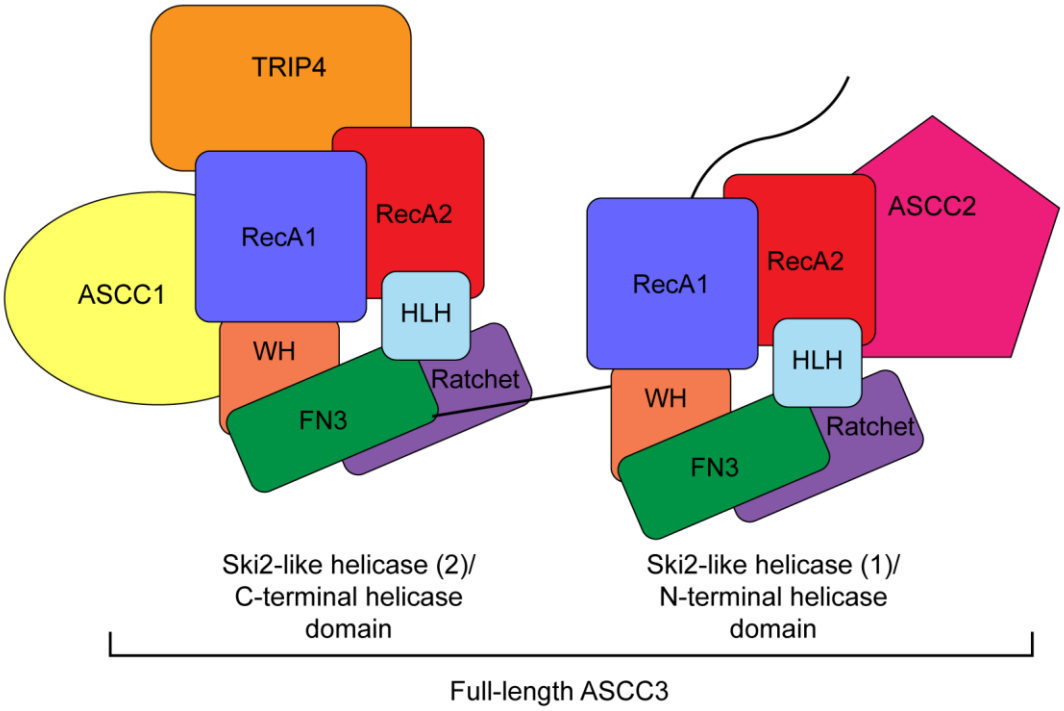

Figure 3-6. Proposed model of ASC-1 complex formation

Schematic of the ASC-1 complex adapted from Figure 1-9 to include the observations from Figure 3-5. Data suggests the ASC-1 complex forms by ASCC2 binding the N-terminal helicase domain, whereas TRIP4 and ASCC1 bind the C-terminal helicase domain of ASCC3. The exact contact points between the proteins remain unknown.

3.7 RNA-binding activity of ASCC3–3xFLAG proteins

Having determined that ASCC3-3xFLAG can associate with the other ASC-1 complex components, it was then important to determine whether the exogenous protein could recapitulate the increased RNA-binding activity that was observed following UVB irradiation by endogenous ASCC3 (Figure 3-1). In the first instance, ASCC3-3xFLAG was transiently transfected into HEK293 cells and the RNA-binding capacity was examined by RIC and immunoblotting. Although RNA-binding for full-length ASCC3 was detected, there was no increase in RNA-binding in response to UVB irradiation (Figure 3-7). PABP1 detection shows equal RNA loading for RIC samples, while inputs show this was not caused by discrepancies in protein loading. This result was also obtained using the plasmid constructs which encoded the N-terminal helicase domain and C-terminal helicase domain of ASCC3. The exogenous ASCC3 N-terminal helicase domain immunoblot was re-probed with an ASCC3 antibody that recognised an epitope in the C-terminal helicase domain, which showed that endogenous ASCC3 was able to increase RNA-binding in response to UVB irradiation in these experiments (Figure 3-7). This demonstrates that transient expressed ASCC3 has reduced RNA-binding fitness when compared to endogenous ASCC3.

3.8 Generation of an ASCC3–3xFLAG inducible stable cell line

Transiently expressed ASCC3-3xFLAG did not show similar binding characteristics to the endogenous ASCC3 (Figure 3-7), while inefficient co-purification of other ASC-1 complex components was also observed (Figure 3-5). These issues may be caused by the over-expression of ASCC3 in the transient system. Therefore, to create a system that more closely simulates the endogenous protein, an inducible stable cell line was generated for full-length ASCC3-3xFLAG.

Generation of a Flp-In T-REx HEK293 inducible stable cell line requires co-transfection of pcDNA5/FRT/TO containing the gene of interest (GOI) with pOG44 plasmid (Figure 3-8A). Flp-recombinase is expressed from pOG44 and catalyses the homologous recombination between FRT sites that are present in the chromatin of the cells and the plasmid. Successful integration of the GOI into the chromatin is denoted by hygromycin resistance and Zeocin sensitivity. Under normal conditions, expression of the GOI is prevented by the Tet repressor (TetR) binding the Tet operator ($TetO_2$) (Figure 3-8B), but tetracycline or doxycycline releases the TetR from the $TetO_2$ allowing expression of the GOI (Ahler *et al.* 2013).

Five clones were successfully collected and expanded, before examining the expression of ASCC3-3xFLAG in the cytoplasm by immunoblot (Figure 3-8C). In the absence of doxycycline in the culture media, ASCC3-3xFLAG could not be detected by FLAG antibody in the cytoplasmic extracts for any clones. Cytoplasmic extracts, which had been generated from clones cultured

with 10 ng/ml doxycycline in the media, showed ASCC3-3xFLAG expression. ASCC3-3xFLAG could not be detected in extracts generated from untransformed Flp-In T-REx HEK293 cells (WT) incubated with doxycycline. To further assess successful integration of ASCC3-3xFLAG coding sequence into the cells, clones were cultured in media containing Zeocin. Clone 1, 4, and 5 were unable to grow in media containing Zeocin, while clone 2 and 3 appeared Zeocin resistant and were therefore discarded (data not shown). Although the exact mechanism of maintaining Zeocin resistance following integration of the GOI remains unclear, the most likely cause is read-through of the GOI onto the pre-existing Zeocin resistance gene.

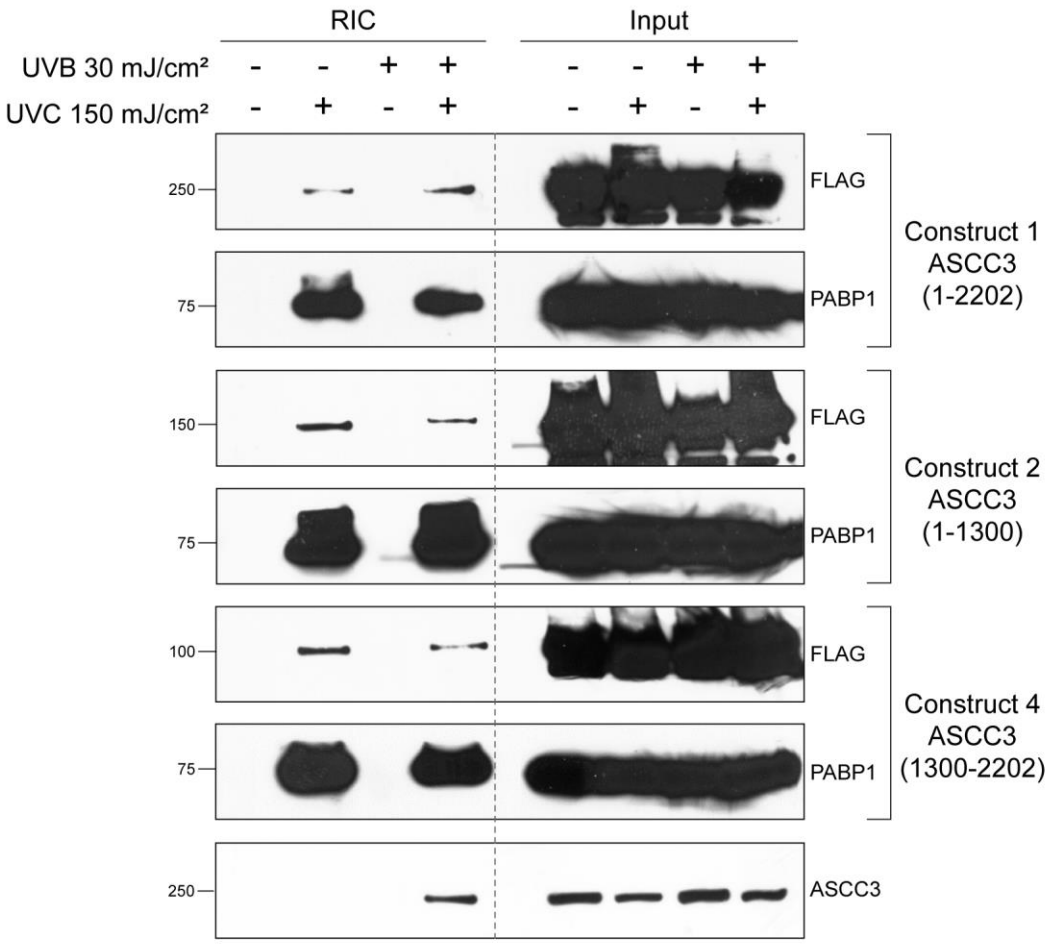

Figure 3-7. RNA-interactome capture of ASCC3-3xFLAG proteins

RIC performed following transient transfection of ASCC3 constructs. All ASCC3 protein products fail to increase RNA-binding in response to UVB irradiation. Input protein levels show no changes in protein expression, while PABP1 RIC detection shows equal levels of RNA loading, indicating that the failed increase of RNA-binding by ASCC3 protein-products is not a result of loading discrepancies. Re-probing the immunoblot for endogenous ASCC3 showed the ability to increase its RNA-binding in response to UVB, demonstrating the treatment had facilitated the desired response.

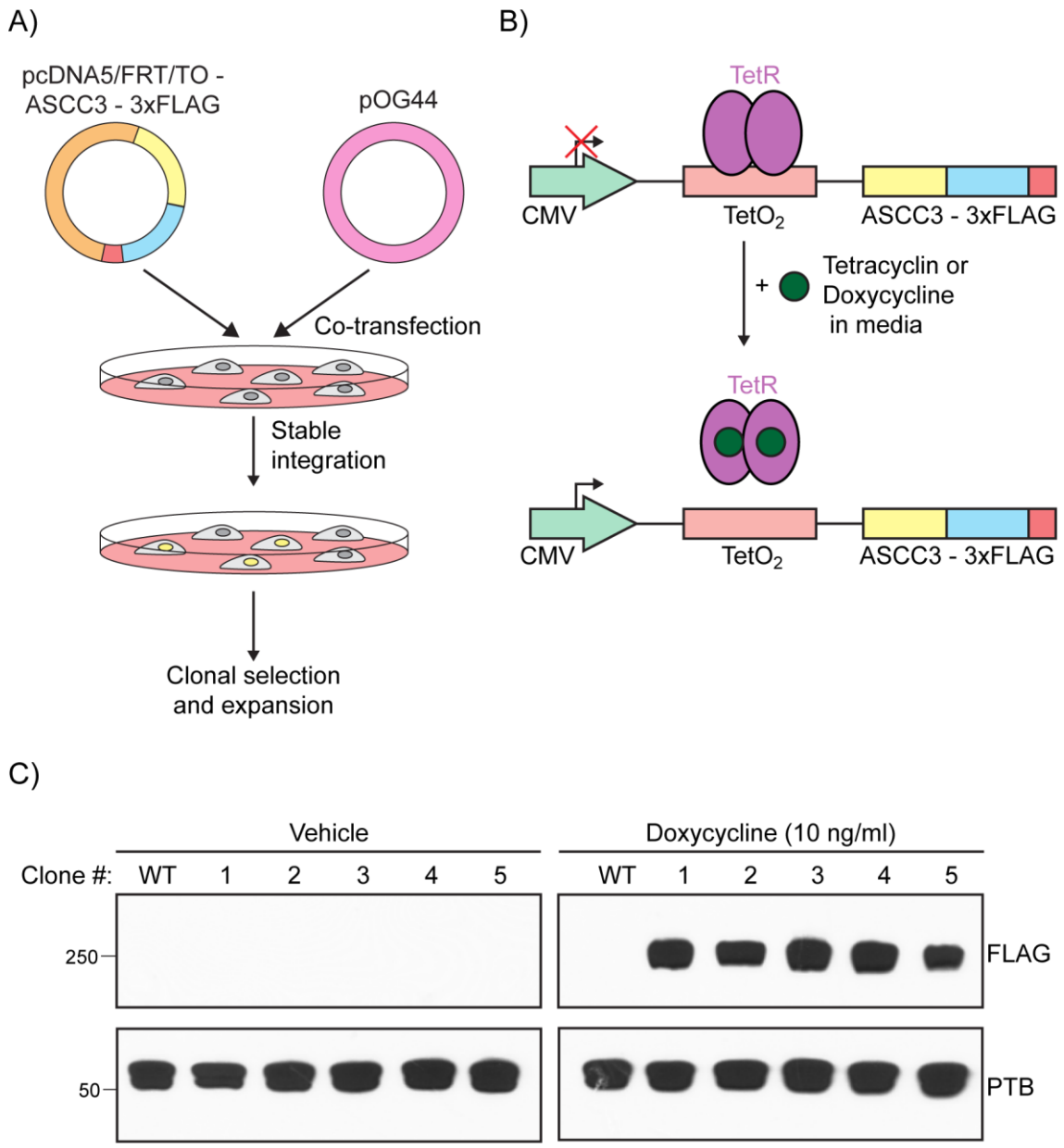

Figure 3-8. Generation of an ASCC3-3xFLAG inducible stable HEK293 cell line

A) Schematic of the process for generating the ASCC3 – 3xFLAG inducible stable cell line using the Flp-In T-REx system. Flp-In T-REx HEK293 cells are co-transfected with pcDNA5/FRT/TO containing the GOI and pOG44. The GOI is stably integrated into the chromatin, allowing selection with hygromycin B antibiotic. B) Schematic for the expression system of the inducible stable Flp-In T-REx cell lines. These cells constitutively express the tetracycline repressor (TetR) that blocks transcription of the downstream GOI by binding the tetracycline operator (TetO2). Addition of tetracycline or doxycycline to culture media dissociates the TetR from the TetO2, allowing transcription of the GOI. C) FLAG immunoblot of five ASCC3 clones following induction with doxycycline. ASCC3-3xFLAG was detected in all clones following addition of doxycycline (10 ng/ml) to the media.

3.9 ASCC3 – 3xFLAG clonal selection

Following the generation of an inducible stable HEK293 cell line for ASCC3-3xFLAG, three clones successfully demonstrated expression of ASCC3-3xFLAG following addition of the doxycycline to the media (Figure 3-8C) and showed Zeocin sensitivity. As previously discussed, transiently expressed ASCC3-3xFLAG did not demonstrate increased RNA-binding in response to UVB irradiation (Figure 3-7). Therefore, to examine the RNA-binding of stably expressed ASCC3-3xFLAG, each clone was cultured in media containing 250 ng/ml doxycycline to induce ASCC3-3xFLAG expression and RIC followed by immunoblotting was performed (Figure 3-9A). In the absence of UVC crosslinking, ASCC3-3xFLAG and PABP1 could not be detected in RIC samples by immunoblot. Upon UVC crosslinking, ASCC3-3xFLAG and PABP1 could be detected by immunoblot; ASCC3-3xFLAG showed increased RNA-binding in response to UVB irradiation while PABP1 remained the same. Input samples demonstrated no changes in protein expression. Immunoblot of endogenous ASCC3 also shows the same RNA-binding correlation as exogenous ASCC3-3xFLAG. To identify a clone for further progression, the RNA binding of exogenous ASCC3 in response to UVB irradiation was compared between the clones. Densitometry analysis comparing RNA-bound PABP1 to exogenous ASCC3-3xFLAG (Figure 3-9B) demonstrated that ASCC3-3xFLAG from clone 1 had the most robust response to UVB when compared to clone 4 and 5, therefore clone 1 selected for further studies.

It was proposed that transiently expressed ASCC3-3xFLAG was unable to increase RNA-binding in response to UVB due to its over expression. Therefore, it was important to assess the expression level of stably expressed ASCC3-3xFLAG and ensure the same issue was not replicated. The manufacturer guidelines for the Flp-In T-REx HEK293 system recommends culture media containing 1000 ng/ml doxycycline for expression of exogenous proteins; however, at this concentration there was reduced cell proliferation (data not shown). This result is consistent with previous studies showing that doxycycline can induce changes in metabolic pathways (Gossen *et al.* 1995) and inhibition of mitochondrial function (Ahler *et al.* 2013), which subsequently leads to changes in the proliferation rate of cell lines. Notably, 250 ng/ml doxycycline in cell culture media has no effect on cell proliferation. Extracts were taken from HEK293 cells stably expressing ASCC3-3xFLAG, which were cultured with doxycycline concentrations ranging from 250-0 ng/ml (Figure 3-9C). Detection of ASCC3-3xFLAG by FLAG immunoblot showed no changes in FLAG detection across concentrations between 250-5 ng/ml doxycycline. Cells cultured with 2.5 ng/ml doxycycline showed reduced detection of ASCC3-3xFLAG and below this concentration ASCC3-3xFLAG could not be detected. The levels of endogenous ASCC3 as detected by immunoblotting correlated with the expression of exogenous

ASCC3-3xFLAG. This demonstrated limited titratability of exogenous ASCC3-3xFLAG protein expression with doxycycline.

To determine whether expression level of exogenous ASCC3-3xFLAG had an impact on RNA-binding following UVB irradiation, RIC was performed on cells that were cultured with either 2.5 or 250 ng/ml doxycycline present in the media. (Figure 3-9D). The exogenous ASCC3-3xFLAG in the UVC crosslinked RIC samples showed increased RNA-binding in response to UVB irradiation at both concentrations, however, detection of ASCC3-3xFLAG from samples cultured in 2.5 ng/ml doxycycline was reduced when compared to samples cultured in 250 ng/ml doxycycline. A concentration of 250 ng/ml doxycycline was chosen to induce expression of ASCC3-3xFLAG for subsequent experiments.

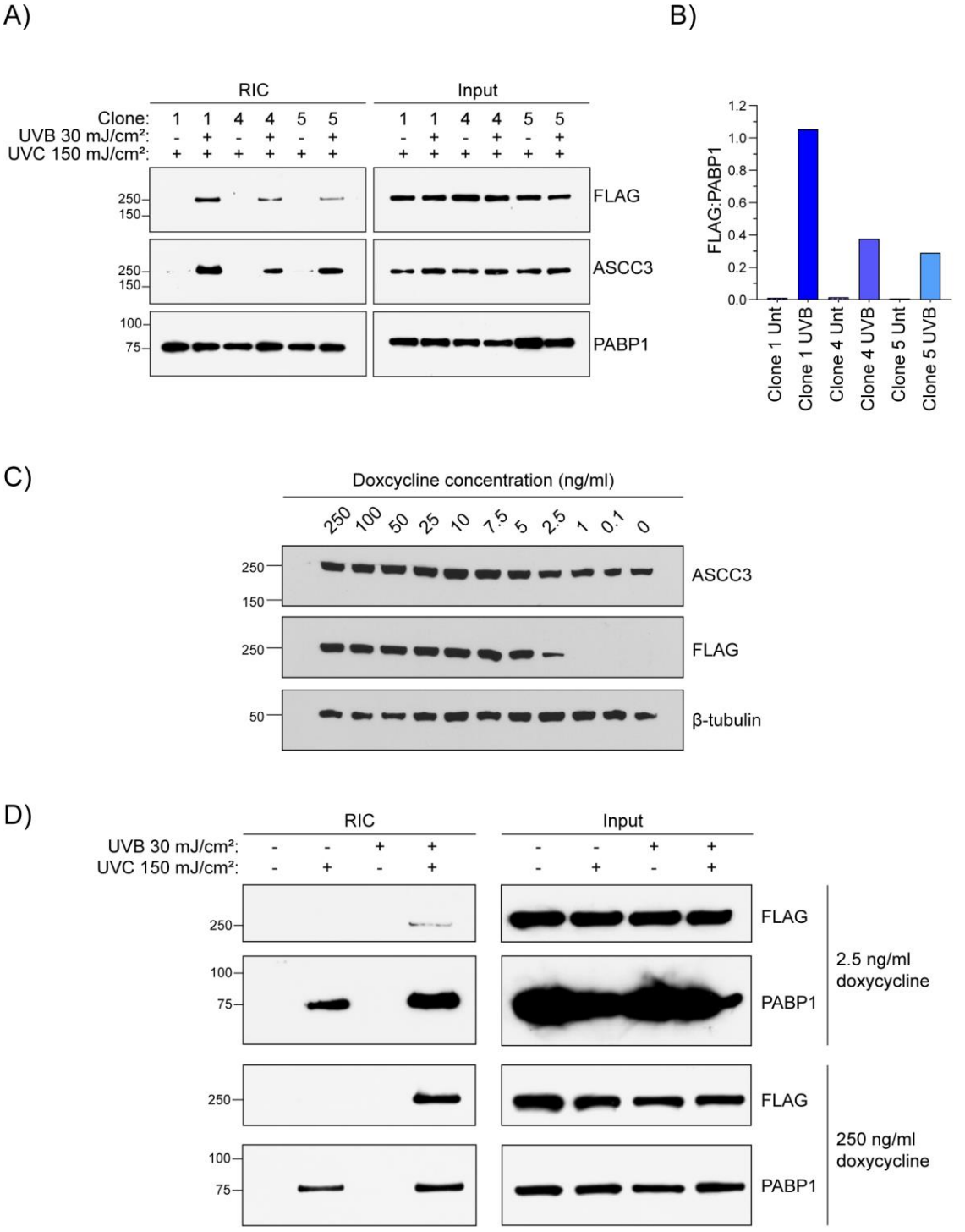

Figure 3-9. ASCC3-3xFLAG clone selection and expression optimisation

A) Immunoblot of samples from RIC, performed on clone 1, 4, and 5 showing ASCC3-3xFLAG from all clones increased RNA-binding in response to UVB irradiation. B) Densitometry analysis comparing RNA-bound PABP1 to exogenous ASCC3-3xFLAG, indicates that ASCC3-3xFLAG from clone 1 had the largest increased RNA-binding in response to UVB. Clone 1 was selected for continuation of the project. C) Doxycycline titration from 250-0 ng/ml showing that exogenous ASCC3 expression requires a minimum of 2.5 ng/ml doxycycline for detection by FLAG immunoblot. Changes in endogenous ASCC3 detection are relatively small across the range of doxycycline concentrations. D) Immunoblot of samples from RIC, performed on ASCC3-3xFLAG inducible stable cells with 2.5 and 250 ng/ml doxycycline in the culture media. 250 ng/ml doxycycline demonstrates more robust exogenous ASCC3 RNA-binding in response to UVB irradiation than 2.5 ng/ml doxycycline.

3.10 ASCC3–3xFLAG stable cell line characterisation

Previous work showed that exogenous ASCC3-3xFLAG expressed from inducible stable HEK293 cells was able to increase its RNA-binding in response to UVB irradiation. It was important to understand whether the expression conditions of exogenous ASCC3-3xFLAG could be further optimised. To determine the time required for ASCC3-3xFLAG to become functional, RNA-binding activity was monitored by RIC from ASCC3-3xFLAG HEK293 cells incubated in media containing 250 ng/ml doxycycline for 24, 48, and 72 hours (Figure 3-10A). Immunoblot levels of RNA-bound ASCC3-3xFLAG following UVB irradiation did not change significantly at these time points. These data suggest that 24 hours is sufficient to produce the maximum amount of functional ASCC3-3xFLAG.

To ensure that exogenous ASCC3-3xFLAG is representative of endogenous ASCC3 for other assays, it was important to recapitulate the RNA-binding kinetics of exogenous ASCC3-3xFLAG with endogenous ASCC3 (Stoneley *et al*, unpublished data). Firstly, the time-dependent RNA-binding of ASCC3-3xFLAG was examined by RIC in response to UVB (30 mJ/cm^2) irradiation (Figure 3-10B). ASCC3-3xFLAG was not bound to RNA at 0 minutes, but binds RNA within 30 minutes of UVB treatment, which further increases up to one-hour. The RNA-binding of ASCC3-3xFLAG does not increase further at two hours, signifying that the binding response is saturated within one-hour post-UVB exposure. Secondly, the dose-dependent RNA-binding of ASCC3-3xFLAG was examined by RIC one-hour post-UVB irradiation (Figure 3-10C). ASCC3-3xFLAG RNA-binding was detected in untreated cells, however, the amount of RNA-bound ASCC3-3xFLAG was significantly increased in 15 mJ/cm^2 UVB treated cells. This was further increased in 30 mJ/cm^2 UVB irradiated cells. Overall this demonstrated a time-dependent and dose-dependent relationship between ASCC3-3xFLAG RNA-binding and UVB irradiation, which subsequently recapitulates data previously seen for endogenous ASCC3 (Figure 1-8B) and therefore shows that ASCC3-3xFLAG is representative of endogenous ASCC3 for future work.

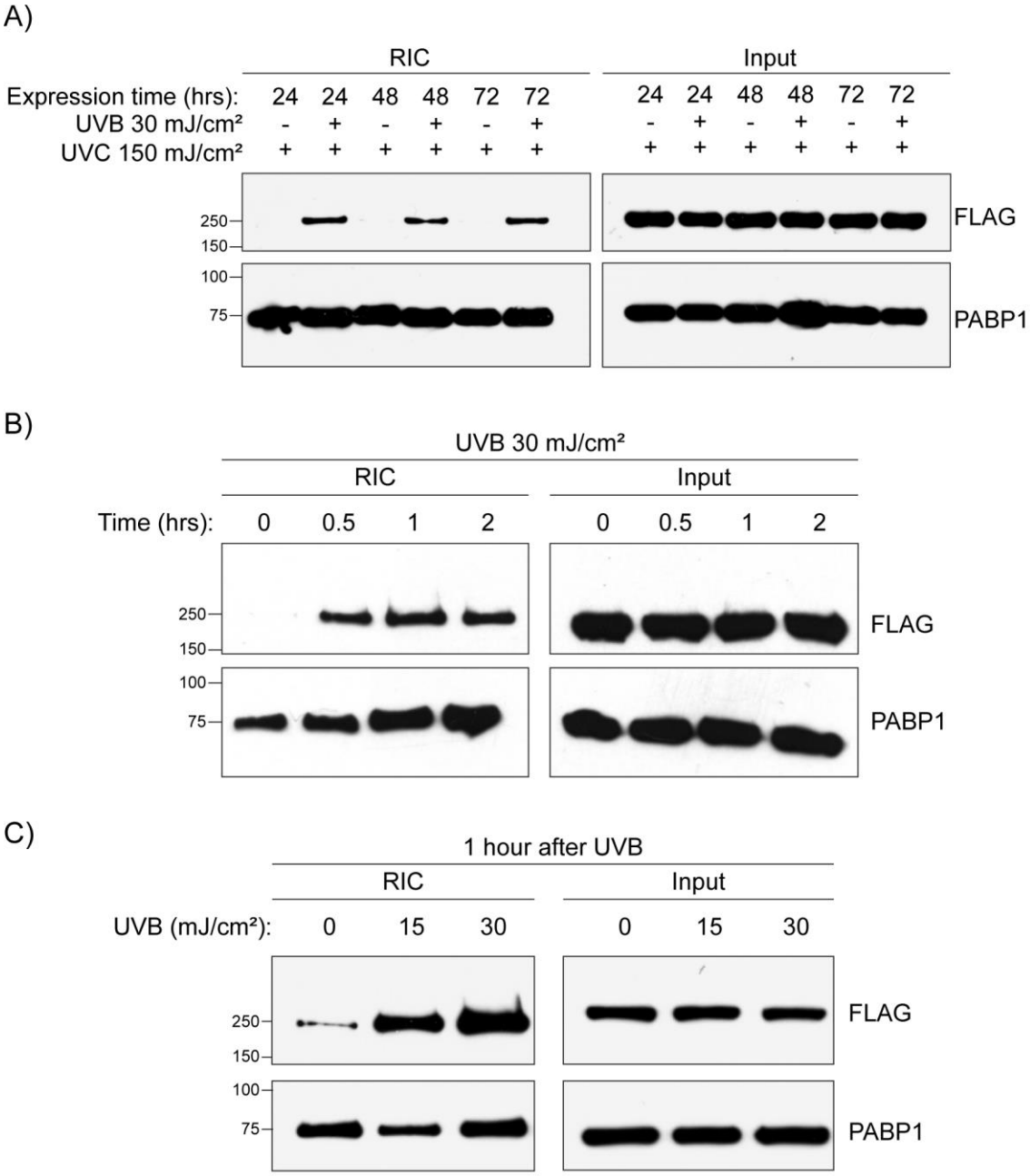

Figure 3-10. ASCC3-3xFLAG cell line characterisation

A) Immunoblot of samples from Flp-In T-Rex HEK293 cells expressing exogenous ASCC3-3xFLAG which had been cultured for 24, 48, or 72 hours with 250 ng/ml doxycycline before UVB treatment and RIC. Levels of RNA-bound exogenous ASCC3 did not change depending on incubation time with doxycycline. B) ASCC3-3xFLAG immunoblot of RIC samples for time points of 0, 0.5, 1, and 2 hours following 30mJ/cm^2 of UVB. Exogenous ASCC3 binds RNA from 0.5 hours, this binding increases at 1 hour, but is saturated and maintained at 2 hours. C) ASCC3-3xFLAG immunoblot of samples treated with 0, 15, or 30 mJ/cm^2 UVB, showing dose dependent RNA-binding.

3.11 ASCC3 responds to other genotoxic stresses

In addition to increasing affinity for RNA following UVB irradiation, ASCC3 also demonstrated the same RNA-binding kinetics in response to other DNA damage agents. These agents include UVC, 4NQO, hydrogen peroxide, cisplatin, mitomycin C, methyl methanesulphonate, however, thapsigargin, amino acid starvation, camptothecin, Etoposide, and Actinomycin D had no effect on ASCC3 RNA-binding (Stoneley *et al*, unpublished data). Two reagents, cisplatin and 4NQO, showed the most significant increase of ASCC3 RNA-binding (Stoneley *et al*, unpublished data). To examine whether these reagents could be used for further analysis of the ASC-1 complex using the inducible stable HEK293 cell line, RIC was performed to assess the RNA-binding of ASCC3-3xFLAG in response to these agents (Figure 3-11). Untreated samples demonstrated no detection of endogenous or exogenous ASCC3 in both non-crosslinked and crosslinked samples. Treatment of samples with cisplatin followed by UVC crosslinking demonstrated increased detection of ASCC3 in a similar manner as seen with UVB exposure (Figure 3-11A). Surprisingly, RNA-binding of endogenous and exogenous ASCC3 were both increased in response to cisplatin treatment without cross-linking. RIC is performed under conditions of high ionic strength and in the presence of a denaturing concentration of an anionic detergent to completely remove non-specific interaction. Therefore, the mechanism by which this interaction is maintained without covalent interaction remains to be determined. An additional series of bands is also present above RNA-bound endogenous and exogenous ASCC3 which is not seen with UVB irradiation. This could represent a series of post-translational modifications present on ASCC3; alternatively, this may also indicate the presence of incompletely digested RNA attached to the protein. The experiment was then performed to understand the effect of 4NQO on ASCC3 RNA-binding, these data recapitulated that shown with cisplatin (figure 3-11B).

To ensure that the optimal reagents are chosen herein, the RNA-binding response of ASCC3 must was directly compared using UVB, 4NQO, and cisplatin. RIC was performed on cell extracts from cells treated with each reagent for one-hour, with one sample left untreated. Direct comparison of these reagents showed that UVB was the weakest inducer of ASCC3-3xFLAG RNA-binding, while 4NQO was the strongest (Figure 3-11C).

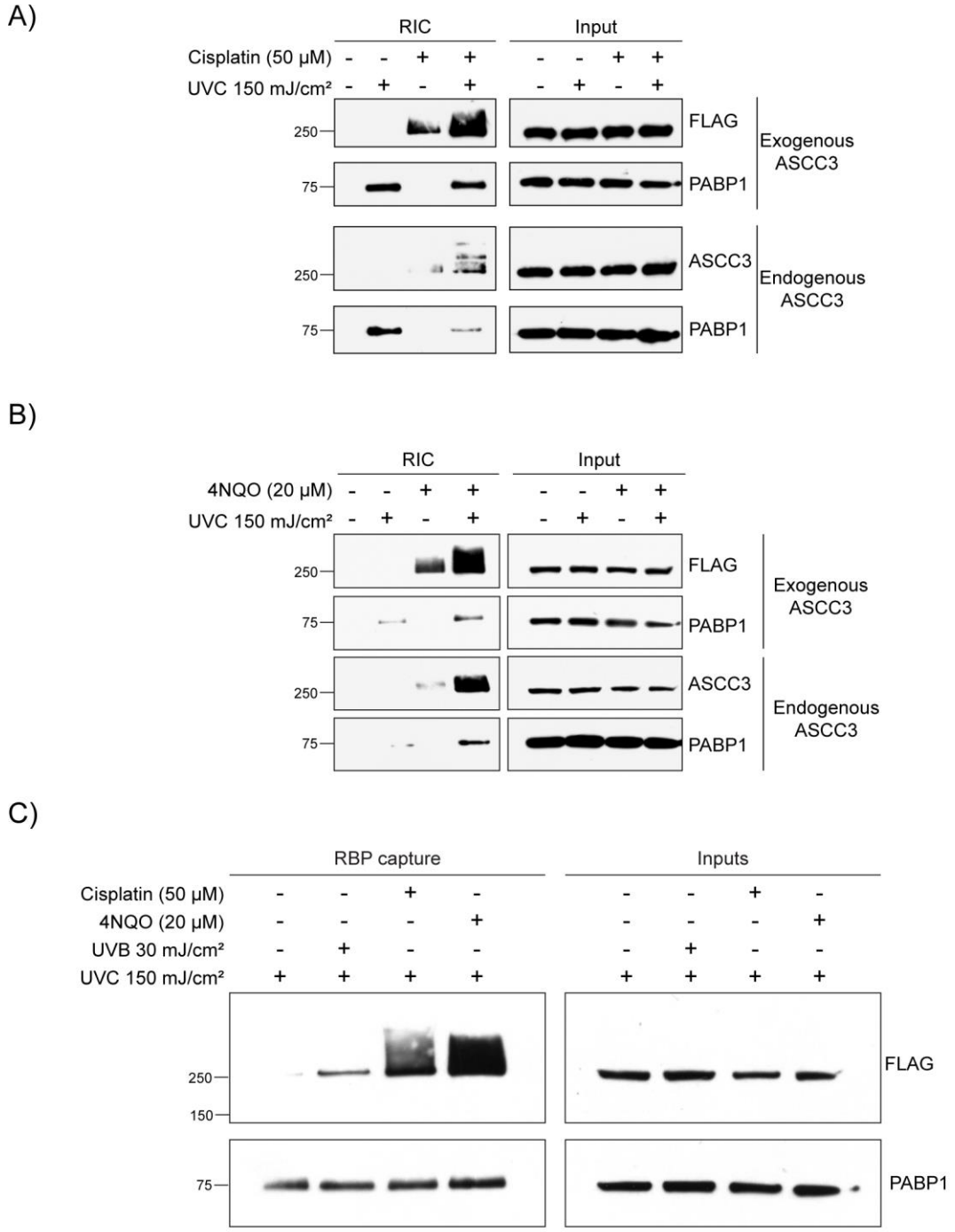

Figure 3-11. ASCC3 is a genotoxic stress-responsive RNA-binding protein

A) Immunoblot for endogenous and exogenous ASCC3 from RIC samples following cisplatin treatment. Cisplatin caused a large increase in ASCC3 RNA-binding. B) Immunoblot for endogenous and exogenous ASCC3 from RIC samples following 4NQO treatment. Treatment with 4NQO caused a large increase in ASCC3 RNA-binding. C) Immunoblot of RIC samples comparing untreated, UVB, cisplatin, and 4NQO treatments, showing 4NQO and cisplatin induces a stronger increased affinity for RNA by ASCC3-3xFLAG when compared to the UVB treated sample.

3.12 Discussion

The main aims of this chapter were to develop and optimise a system for expression of exogenous ASCC3-3xFLAG which could be used to further characterise the ASC-1 complex. ASCC3 has been identified as an RBP with increased affinity for RNA in response to UVB irradiation and other reagents known to damage nucleic acid (Stoneley *et al*, unpublished data). ASCC3 has also previously been identified in other large scale RIC studies as an RBP (Liao *et al.* 2016) and with increased RNA-affinity in response to ionising radiation (Milek *et al.* 2017). However, the specificity of this response is not understood, with more than 250 other proteins also demonstrating similar increases in affinity for RNA (Milek *et al.* 2017). Previous attempts to isolate the ASC-1 complex using antibodies directed towards endogenous ASC-1 components were successful under control conditions, however, similar isolations under stressed conditions resulted in poor recovery of the complex (Stoneley *et al*, unpublished data). This suggests that conformational rearrangements of the ASC-1 complex following conditions of stress results in masking of the antibody epitope.

To establish a system that could be used for viable expression of tagged exogenous ASCC3, the ability of endogenous ASCC3 to increase its affinity in response to UVB was examined in U2OS, HeLa, and HEK293 cells, showing that this response was uniform across all cell lines examined (Figure 3-1). HEK293 cells were chosen to continue the study due to their ability to express high levels of exogenous proteins and fast proliferation rates (Thomas & Smart 2005). Successful cytoplasmic fractionation of HEK293 cells, as determined by using nuclear and cytoplasmic markers (Figure 3-2), was carried out to ensure this study focused on the cytoplasmic role of ASCC3, as opposed to the already pre-determined nuclear role of ASCC3 in DNA alkylation damage repair (Dango *et al.* 2011). Tagged ASCC3 constructs were created (Figure 3-3), which included full-length and truncated variants of ASCC3 (Figure 3-4A). BRR2, another Ski-2 like RNA helicase with a high degree of similarity to the structure of ASCC3 (Figure 1-9D), has previously been shown to contain a predicted N-terminal region of disorder to be important for regulation of its two helicase domains (Absmeier *et al.* 2015a, 2015b). Therefore, as not to interfere with any potential regulatory function of ASCC3, and as a method of detecting only full-length protein, ASCC3 was tagged at its C-terminus. Transient expression of these proteins showed nuclear and cytoplasmic populations (Figure 3-4B), further highlighting the importance of fractionation to study the cytoplasmic ASC-1 complex. Transiently expressed full-length ASCC3-3xFLAG demonstrated interaction with ASCC2, TRIP4, and ASCC1 (Figure 3-5A). The N-terminal helicase domain could only interact with ASCC2 (Figure 3-5B), an interaction that was maintained upon removal of the unstructured N-terminal region (Figure 3-5C), these data differ

from that previously published about the interaction of ASCC3 and ASCC2, which shows that this interaction is fully dependent on the unstructured N-terminal region of ASCC3 in the nucleus (Brickner *et al.* 2017). However, this difference could be due to the distinct roles of this protein between the cytoplasm and the nucleus. The C-terminal helicase domain interacted with TRIP4 and ASCC1, but not ASCC2 (Figure 3-5D) which is different from previous work that showed that TRIP4 interacts with the N-terminal helicase domain of ASCC3 (Jung *et al.* 2002). Importantly, the previous studies were carried out using a yeast 2-hybrid system, as opposed to immunoaffinity co-purification used in this thesis and may offer an explanation to this discrepancy. Overall, these ASCC3-3xFLAG proteins interacted with ASC-1 complex components, allowing a predicted model for ASC-1 complex formation (Figure 3-6). However, the interactions between these proteins were not enriched in the transient system, which may indicate that there was sub-stoichiometric complex formation caused by over expression. RIC assays showed that the ASCC3-3xFLAG proteins did not increase their affinity for RNA in response to UVB (Figure 3-7), which is normally observed with endogenous ASCC3 (Figure 3-1). This could be caused by the sub-stoichiometry issues seen previously by immunoaffinity purification (Figure 3-5).

An inducible stable HEK293 cell line was generated for full-length ASCC3-3xFLAG to better control its expression (Figure 3-7). Clone 1 was selected for further study after examining Zeocin sensitivity (data not shown) and exogenous ASCC3-3xFLAG by RIC in response to UVB (Figure 3-9A). Clone 1 demonstrated the most robust RNA-binding response to UVB, as determined by densitometry analysis (Figure 3-9B). Analysis of exogenous ASCC3-3xFLAG RNA-binding was carried out using the highest and lowest concentrations of doxycycline which did not affect cell growth, and where ASCC3-3xFLAG was still detectable by immunoblot (Figure 3-9B and 3-9C), showing that detection of RNA-bound ASCC3-3xFLAG was enhanced at a higher concentration. Expression of ASCC3-3xFLAG for longer than 24 hours demonstrated no increase in functional activity by RIC (Figure 3-10). Exogenous ASCC3-3xFLAG observed similar UVB dose-responsive and time-dependent RNA-binding kinetics when compared to endogenous ASCC3 from MCF10A cells (Figure 3-10B and 3-10C, Figure 1-8B; Stoneley *et al*, unpublished data), further indicating that exogenous ASCC3-3xFLAG behaves in a similar manner as its endogenous counterpart. Cisplatin and 4NQO are two reagents which previously demonstrated increased ASCC3 RNA-binding when compared to untreated cells (Stoneley *et al*, unpublished data). Both reagents were able to increase the RNA-binding of exogenous ASCC3-3xFLAG (Figure 3-11A and 3-11B). When compared to UVB, cisplatin and 4NQO showed a more significant proportion of RNA-bound ASCC3-3xFLAG (Figure 3-11C).

To conclude, these data describe the process taken to develop and optimise an inducible stable cell line expressing 3xFLAG tagged full-length ASCC3. Steps were taken to ensure that expressed exogenous ASCC3-3xFLAG behaved with very similar characteristics to the endogenous protein. This now allows the investigation of novel protein interactors of ASCC3, and to understand how these interactions change following conditions of stress.

4. Identification of novel ASCC3 protein-protein interactions

4.1 Introduction

As previously discussed (Chapter 3), ASCC3 is cytoplasmic RNA-binding protein that increases its affinity for RNA in response to UVB irradiation (Stoneley *et al,* unpublished data). Moreover, it was shown that the cytoplasmic change in ASCC3-RNA affinity was emulated across multiple cell lines from various tissues (Figure 3-1). The ASC-1 complex consists of ASCC3, ASCC2, TRIP4, and ASCC1 (Jung *et al.* 2002), however, previous attempts to isolate the ASC-1 complex using endogenous antibodies to ASCC3 had not been successful under conditions of stress (Stoneley *et al*, unpublished data), suggesting that large conformational changes were masking the antibody epitope. For this reason, an inducible stable HEK293 cell line expressing ASCC3-3xFLAG was created and characterised. By tagging the end of ASCC3, it increases the likeliness that the epitope is available following changes in complex conformation.

4.1.1 Aims

The aim of the work in this chapter was to use immunoaffinity purification and size exclusion chromatography (SEC) (Cai *et al.* 2012; Kirkwood *et al.* 2013) to isolate ASCC3-3xFLAG expressed from the HEK293 inducible stable cell line to identify novel protein-protein interactors.

4.2 Interaction of ASCC3–3xFLAG with the ASC-1 complex

In these studies, the interaction of ASCC3-3xFLAG with the ASC-1 complex was explored using a transient system (Figure 3-5). These data showed that full-length ASCC3-3xFLAG was able to interact with ASCC2, TRIP4, and ASCC1, however, it also revealed that the ASC-1 complex components were not enriched when compared to the input. This suggested that ASCC3-3xFLAG was forming a sub-stoichiometric ASC-1 complex. An inducible stable HEK293 cell line was generated for ASCC3-3xFLAG (Figure 3-8), which showed improved RNA-binding when compared to the transient system (Figure 3-9). It was therefore important to determine whether the ASCC3-3xFLAG protein expressed from a stable cell line was able to be incorporated into the ASC-1 complex when compared to a transient expression system.

To determine whether exogenous ASCC3-3xFLAG protein was incorporated into the ASC-1 complex, immunoaffinity isolation of ASCC3-3xFLAG was carried out, then examined for co-purified ASC-1 complex members by immunoblot (Figure 4-1A). Purification of ASCC3-3xFLAG demonstrated co-purification of ASCC2, TRIP4 and ASCC1. These data show that TRIP4 and ASCC1 are enriched when compared to the input, however, ASCC2 was not and may suggest that sub-stoichiometric complex formation is still persistent.

To further analyse the integration of ASCC3-3xFLAG into the ASC-1 complex, SEC was performed using a Superose 6 10/300 GL column with two inducible stable HEK293 cell cytoplasmic lysates; one generated from cells where expression of ASCC3-3xFLAG was induced by doxycycline and the other was a control uninduced lysate. SEC separates molecules based on size and is advantageous for isolating protein complexes with weaker interactions. SEC analysis of the uninduced cytoplasmic lysate demonstrated co-localisation of ASCC3, ASCC2, TRIP4, and ASCC1 between an elution volume of 2.8-3.6 ml (Figure 4-1B), which was recapitulated in the lysate that expressed ASCC3-3xFLAG. The co-localisation of ASCC3-3xFLAG with ASCC2, TRIP4, and ASCC1 at the same elution volume as the endogenous ASC-1 complex suggests that ASCC3-3xFLAG was successfully integrated into the ASC-1 complex. The co-elution of the ASC-1 complex between 2.8-3.6 ml coincides with the initial detection of protein from the UV trace (data not shown); the column used is recommended for separation of complexes between 5000-5 kDa and therefore suggests that the ASC-1 complex is co-eluting with high molecular weight complexes. Overall these data show that ASCC3-3xFLAG can integrate into the endogenous ASC-1 complex, however, the efficiency of this integration remains unexplored.

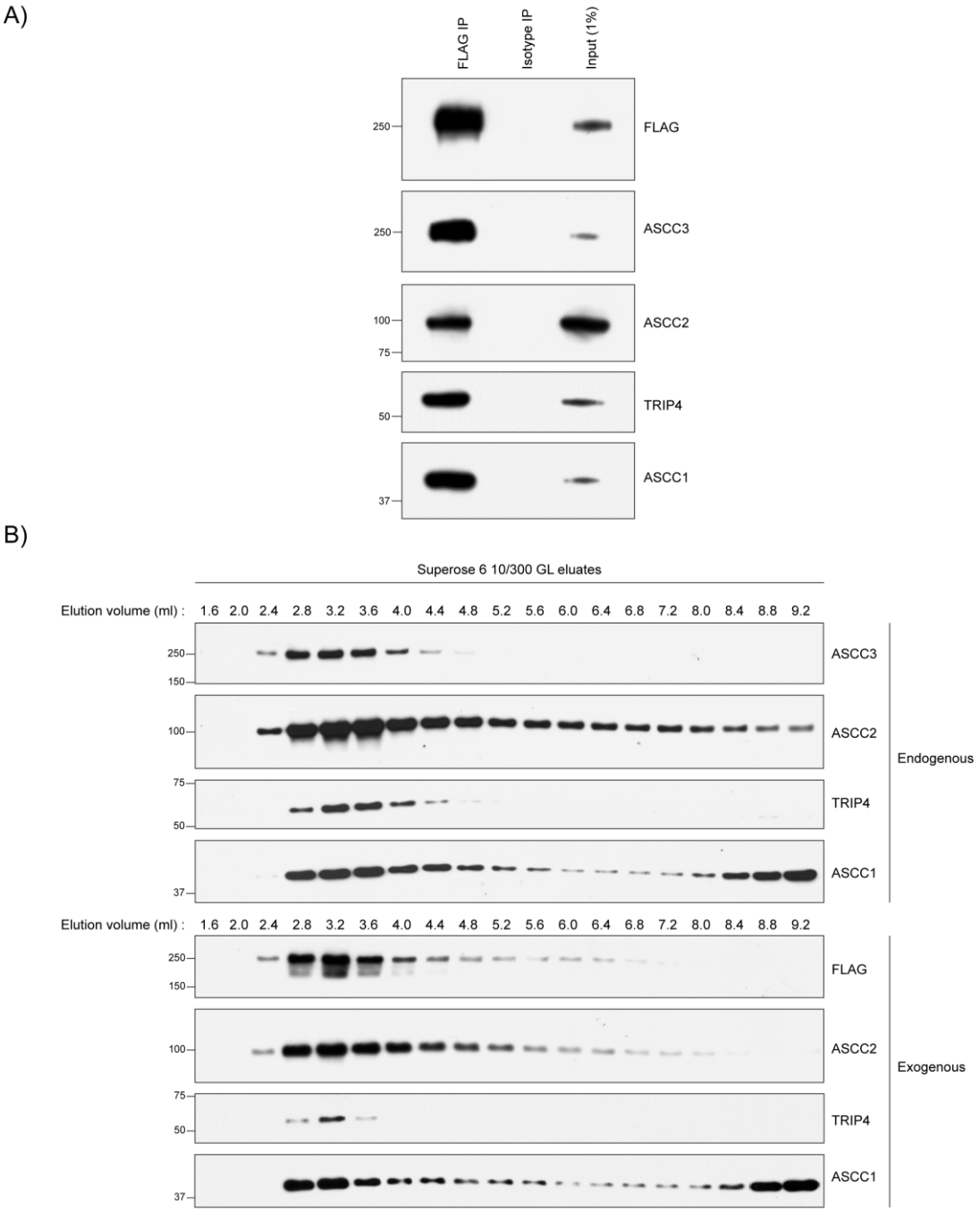

Figure 4-1. Analysis of exogenous ASCC3-3xFLAG in ASC-1 complex formation

A) Affinity purification of ASCC3-3xFLAG co-purifies ASCC2, TRIP4, and ASCC1 B) SEC of ASC-1 complex containing either endogenous or exogenous ASCC3. Both variants of ASCC3 co-localise with the other members of the ASC-1 complex at elution volumes containing high-molecular weight complexes.

4.3 ASC-1 complex is a sub-complex of a higher order macromolecular complex

As shown previously, the ASC-1 complex appears to co-elute in high molecular weight SEC fractions, however, the column used does not provide sufficient resolution of higher molecular weight complexes to draw definitive conclusions. Columns such as Sephacryl S-500 are readily used for separation of macromolecules, but require large, concentrated lysates for analysis. HEK293 cells have previously demonstrated efficient adaptation of suspension cell culture (Tsao *et al.* 2001), allowing greater quantities of cells to be grown efficiently. Therefore, ASCC3-3xFLAG inducible stable HEK293 cells were adapted to grow in suspension, providing greater material for analysis by Sephacryl S-500 SEC. To further increase SEC resolution, system pressure was decreased and separation-time extended.

A cytoplasmic extract from inducible stable HEK293 cells with expressed ASCC3-3xFLAG was separated by the method previously described. The UV protein trace indicated that protein elution began at 22 ml, while ASC-1 complex was detected at an elution volume between 46-54 ml as determined by immunoblotting (Figure 4-2). The ASC-1 complex has recently been shown to have a role in RQC (Matsuo *et al.* 2017; Sitron *et al.* 2017), therefore immunoblotting was also carried out to detect ribosomal complexes using antibodies to RPS6 and RPL11 respectively. The 80S ribosome has an approximate molecular weight of 4.3 MDa (Yoshikawa *et al.* 2018) and this can be used to obtain information about the size of the ASC-1 complex, and whether it interacts with the ribosome. RPS6 and RPL11 were eluted at volumes between 46-58 ml and 46-52 ml respectively (Figure 4-2) and these co-eluted with the ASC-1 complex. The ASC-1 complex distribution is much more similar to that of the 40S subunit, as detected by the RPS6 antibody, raising the possibility that the ASC-1 complex associates with the 40S and 80S ribosome. However, these data do not demonstrate a direct interaction between the ASC-1 complex and the ribosome; but may indicate that the ASC-1 complex is a small sub-complex that can interact with another, much larger macromolecular complex. ASCC1 also displays a population eluting at 72-76 ml, that may suggest that the interaction between ASCC1 and the ASC-1 complex is more transient than other components, resulting in pools of monomeric and complexed ASCC1.

To further estimate the size of eluted protein complexes from the column, molecular weight standards were used so that the elution volumes could be alighted with a defined molecular weight (Table 4-1). The available standards ranged between 2000-43 kDa, and a plot of log-molecular weight against elution volume was generated (Figure 4-3). A line of best fit was used to extrapolate the molecular weight of unknown protein complexes from their elution volume.

Extrapolation of the ASC-1 complex elution volume (46-54 ml) provides determines an estimated molecular weight range of between 9100-3000 kDa (Figure 4-3). However, Blue dextran, a 2000 kDa dye molecule, eluted at 52ml (table 4-1), which infers a 4600 kDa molecular weight, demonstrating that extrapolation of molecular weight from elution volumes of this plot was inaccurate (Table 4-1). Molecular weight of a molecule is not the only factor that determines its elution volume; the globular state of the molecule, molecule stability, and buffer conditions all impact flow through the column and determined elution. While the exact molecular weight of the ASC-1 complex remains unknown, it is apparent that this complex co-localises in SEC elution volumes that is not equivalent to a 1:1:1:1 ratio of ASCC3, ASCC2, TRIP4, and ASCC1 (~450 kDa).

Standard	Molecular weight (kDa)	Sephacryl S-500 elution volume (ml)	Extrapolated molecular weight (kDa)
Blue Dextran	2000	52	4630
Thyroglobulin	669	72	460
Ferritin	440	76	289
Catalase	232	82	145
Aldolase	159	84	115
Ovalbumin	43	86	91

Table 4-1. Table of SEC standards eluted on a Sephacryl S-500 column and predicted elution volumes

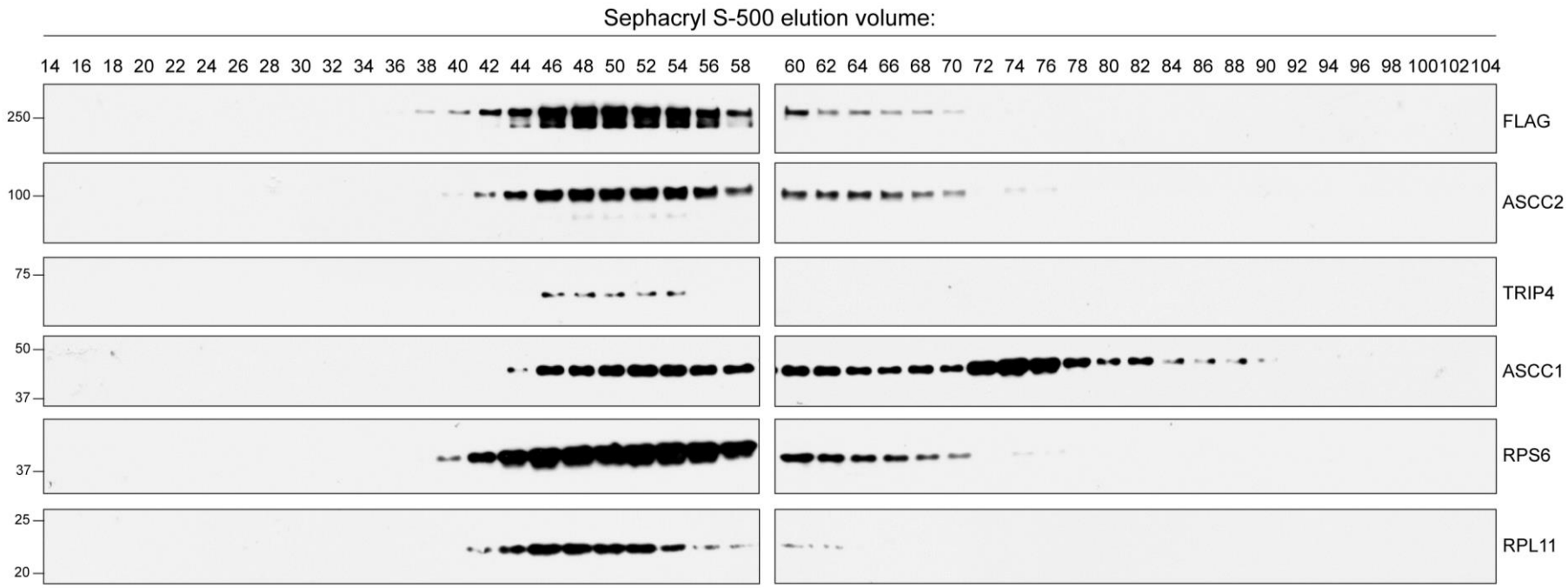

Figure 4-2. Sephacryl S-500 SEC analysis of ASC-1 complex

Immunoblot analysis of SEC separated into 2 ml eluate fractions, probing for ASC-1 complex components, RPS6, and RPL11. The ASC-1 complex is co-localised between 46-54 ml. RPS6 is present between 46-56 ml and RPL11 is present between 46-54 ml.

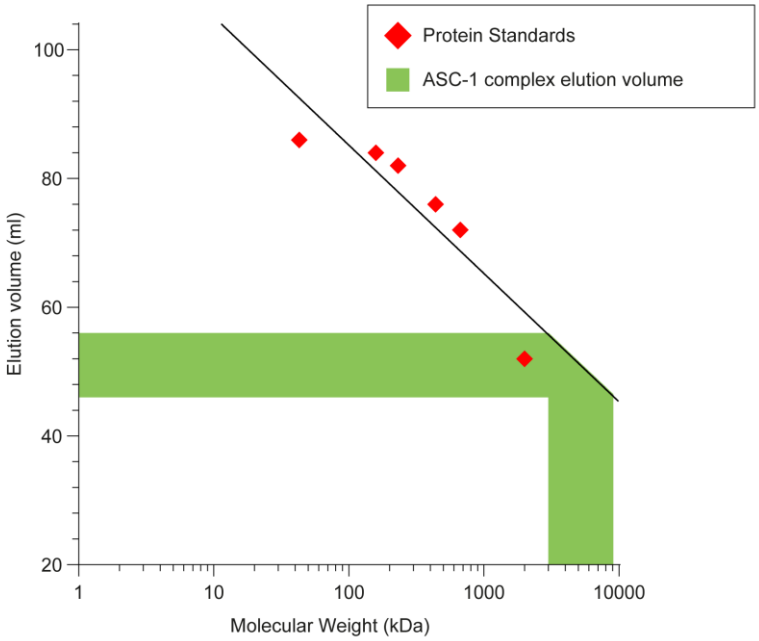

Figure 4-3. The ASC-1 complex analysed by SEC

Standard curve generated from molecular weight standards (Table 4-1). A semi-log line of best fit was generated and unknown values extrapolated. The ASC-1 complex extrapolation showed in green shows a range of ~9100-3000 kDa for an elution volume between 46 and 54 ml.

4.4 Optimisation of ASCC3–3xFLAG covalent purification

Immunoaffinity purification-mass spectrometry is a well-established technique that is commonly used to determine interacting partners of a protein of interest (Cai *et al.* 2012). Optimisation of the technique is required to accurately assess these interactions while limiting identification of non-specific interactions. Immunoglobulin (IgG) heavy and light chains are well known contaminants of this technique (Antrobus & Borner 2011) and can lead to peptide saturation during mass spectrometry analysis. To reduce the presence of IgG chains in the eluate of purified ASCC3-3xFLAG, the FLAG antibody used for immunoaffinity isolation was covalently attached to M-270 epoxy magnetic beads before the carrying out the purification. Although the conditions required for antibody coupling were predetermined, the method for the elution, nuclease digestion, and stability of the complex was unknown. To determine whether ASCC3-3xFLAG could be isolated using the FLAG epoxy beads, the initial immunoaffinity purification was carried out using conditions optimised for non-covalent affinity purification. SDS-PAGE combined with colloidal Coomassie and silver staining demonstrated strong purification of ASCC3-3xFLAG, however, bands for ASCC2, TRIP4, and ASCC1 could not be identified by staining (Figure 4-4A). Immunoblot analysis for ASCC2, TRIP4, and ASCC1 showed that these components were purified, and that they were still enriched when compared to the input (Figure 4-4B). Overall, these data together suggest that much of the ASCC3-3xFLAG is not incorporated into a complex, but a small proportion interacts with the endogenous ASC-1 complex.

4.4.1 Nuclease treatment

As previously shown, ASCC3 is an RBP whose affinity for RNA increases in response to UVB (Figure 3-1). To ensure that the interactions identified by immunoaffinity purification were through protein contacts, nuclease digestion was examined to remove nucleic acid based indirect interactions. Three nucleases were examined for their ability to affect the detection of the ASC-1 complex following immunoaffinity purification. These nucleases included: Benzonase, a non-biased nuclease that digests RNA and DNA; RNase A, which cleaves single stranded RNA at C and U residues; and DNase I, although DNA was not present in this sample this would control for addition of a recombinant protein to the sample. To determine the effect of these nucleases a single immunoaffinity purification of ASCC3-3xFLAG was carried out, before dividing into four equal samples. The unbound fraction was removed, and the beads digested with one enzyme for 1 hour at 4°C. Degradation products were removed by washing prior to analysis of eluted proteins by silver staining (Figure 4-4C) and immunoblotting of ASCC3-3xFLAG, ASCC2, and ASCC1 (Figure 4-4D).

Analysis of the samples by silver stain demonstrated that the amount of ASCC3-3xFLAG was relatively unchanged following nuclease digestion. A small decrease was observed with Benzonase treatment when compared to the other nuclease treated samples (Figure 4-4C), that was also demonstrated by detection of ASCC3-3xFLAG, ASCC2, and ASCC1 by immunoblot (Figure 4-4D). However, individual DNase or RNase treatment did not recapitulate this change, therefore, it is unlikely that the nuclease activity of Benzonase is causing this change. The exact mechanism by that Benzonase causes this change in ASCC3-3xFLAG purification remains unknown. Overall, as DNA is already excluded from these sample by fractionation and RNA is the only product required for degradation, RNase A was selected as the nuclease for digestion of the RNA in the immunoaffinity purified ASCC3-3xFLAG samples before mass spectrometry analysis.

4.4.2 Triple-FLAG tag elution optimisation

In order to reduce the level of IgG heavy and light chains present in the eluate, and to ensure proteins eluted are associated with ASCC3-3xFLAG and not the beads, peptide based competitive elution of ASCC3-3xFLAG was employed rather than denaturing elution. Initially, temperature and time were examined as factors for elution of ASCC3-3xFLAG using a 3xFLAG peptide. ASCC3-3xFLAG was eluted for 1 hour at 4 ^{o}C, 1 hour at room temperature, and 30 minutes at room temperature by peptide competition and compared to one sample with denaturing elution by silver stain analysis (Figure 4-5A) and immunoblot (Figure 4-5B). Silver stain analysis demonstrated minor changes in ASCC3-3xFLAG elution under these conditions, but elution in all cases was significantly impaired when compared to denaturing elution. Extra bands were visualised following elution at room temperature for 1 hour, that may indicate proteolysis of isolated proteins. Immunoblotting recapitulated this result, showing that denaturing elution was far more efficient that peptide-based methods (Figure 4-5B). Analysis of proteins that remain associated with the beads following peptide elution was carried out using a further round of denaturing elution. This demonstrated that some ASCC3-3xFLAG, ASCC2, TRIP4, and ASCC1 remained bound to the epoxy beads following peptide elution. Work within the Willis laboratory had already determined that peptide based elution can be enhanced by addition of non-ionic detergents such as NP-40 (Piñeiro *et al.* 2018), therefore addition of 0.1% NP-40 to the elution buffer was examined (Figure 4-5C). Eluted proteins were initially examined by silver staining and demonstrated that addition of NP-40 enhanced recovery of ASCC3-3xFLAG from the beads when compared to a sample eluted with TBS (Figure 4-5C). Furthermore, a denaturing elution of the same beads demonstrated a significant decrease in residual ASCC3-3xFLAG still bound to the beads when compared to the TBS eluted sample. Immunoblot analysis

of the ASC-1 complex components still associated with the epoxy beads following peptide elution also supported these data, showing that less ASCC3-3xFLAG, ASCC2, TRIP4, and ASCC1 remain bound to the beads following addition of NP-40 to the buffer (Figure 4-5D). The levels of TRIP4 detected also suggested that two 45-minute elution steps were more efficient at removing isolated proteins than a single 90-minute elution. Overall these data suggest that ASCC3-3xFLAG can be recovered from the FLAG epoxy beads without recovery of IgG chains by peptide elution. Optimal peptide elution conditions were determined as two 45-minute elutions in a buffer containing 0.1 % NP-40.

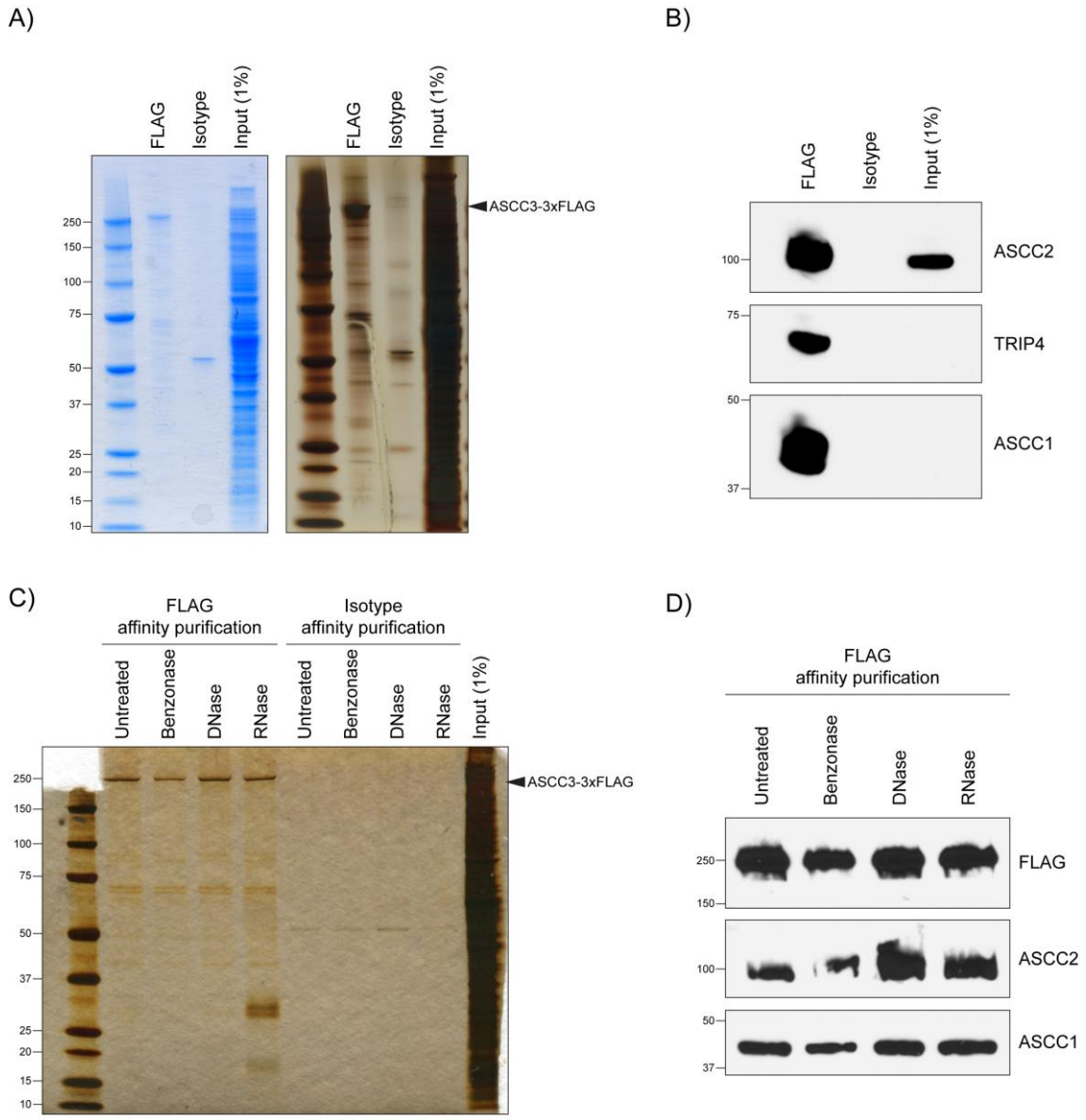

Figure 4-4. FLAG covalent immunoaffinity purification of ASCC3-3xFLAG and nuclease optimisation

A) Coomassie and silver stain analysis of magnetic bead-antibody covalently conjugated immune-complexes used for immunoaffinity purification of ASCC3-3xFLAG. Initial purification shows the ability to purify exogenous ASCC3 by this method. B) Immunoblot analysis of (A), probing for ASCC2, TRIP4, and ASCC1. C) Comparison of Benzonase, DNase I, and RNase A nucleases to test ASC-1 complex stability in the absence of nucleic acid by silver staining. Benzonase appears to show a lower level of exogenous ASCC3 purification, but RNase A and DNase I had no effect on ASCC3-3xFLAG recovery when compared to untreated. D) Immunoblot analysis of (C), probing for FLAG, ASCC2, and ASCC1.

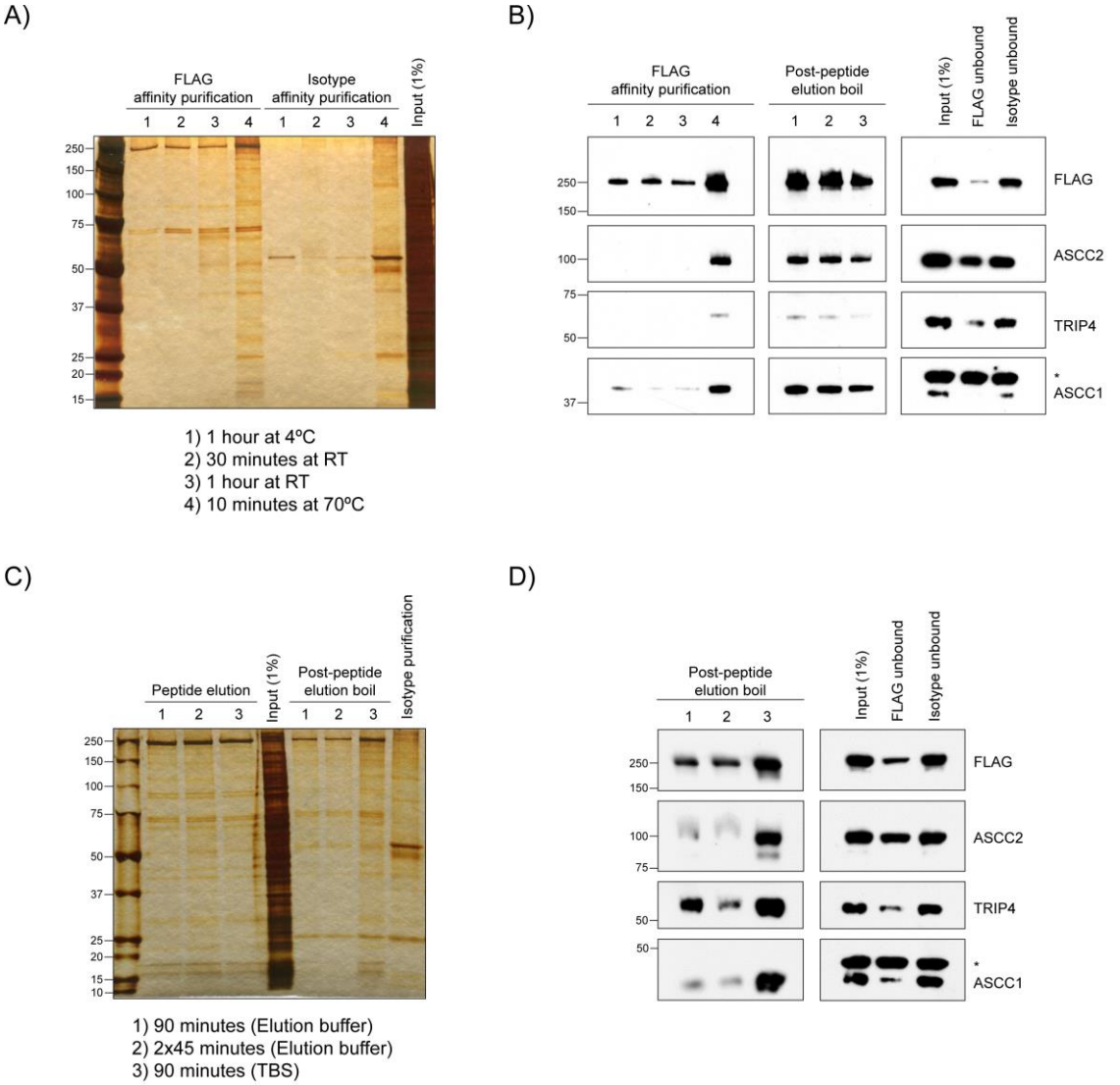

Figure 4-5. FLAG covalent immunoaffinity purification competitive elution optimisation

A) Silver stain analysis of competitive peptide elution methods compared to traditional denaturing boil elution. Demonstrating inefficient recovery of ASCC3-3xFLAG using peptide elution. B) Immunoblot analysis of (A) demonstrating the inefficient elution by peptide when compared to denaturing elution. Inputs and unbound fractions also show the efficiency of the purification. C) Silver stain analysis of elution buffer optimisation. Addition of 0.1% NP-40 shows reduced exogenous ASCC3 remaining on the beads following elution. D) Immunoblot analysis of (C) showing the amount of protein remaining on the beads following competitive peptide elution. Two 45-minute rounds of elution appeared to be optimal for competitive peptide-based elution. * = non-specific band.

4.4.3 Wash buffer optimisation

In order to reduce non-specific background interactions between ASCC3-3xFLAG and other proteins, the wash buffer for immunoaffinity isolation was optimised. Increasing wash stringency often includes increasing salt concentration or adding/increasing the concentration of detergents (Moser *et al.* 2009). To maintain protein interactions, the lysis buffer is often used as the wash buffer. As the lysis buffer used for isolation of the cytoplasmic fraction already contains 0.5% NP-40, that is composed of polyethylene glycol (PEG) structures, increasing this concentration may reduce the effectiveness of mass spectrometry as PEG is a hydrophobic agent that can give rise to ion suppression (Scheerlinck *et al.* 2015). Therefore, the salt concentration was optimised to increase the stringency of the purification. The stability of the complex was examined by sequentially increasing the salt (sodium chloride (NaCl)) concentration in each subsequent wash, from 0.15 M to 1.0 M (Figure 4-6A). The proteins present in these washes were TCA precipitated and resuspended in SDS-PAGE loading buffer, before analysis by silver stain and immunoblotting to determine at which NaCl concentration the ASC-1 complex would begin to dissociate. Analysis of the stained gel demonstrated that most protein is removed following the initial wash in a buffer containing 0.15 M NaCl, with only a residual amount of protein detected in subsequent washes from 0.25-1.0 M NaCl (Figure 4-6A). Interestingly, at this concentration ASCC3-3xFLAG, ASCC2, TRIP4, and ASCC1 are all detected by immunoblot (Figure 4-6A), implying that this complex is stable under conditions of high NaCl. A further increase of the NaCl concentration to 2 M, demonstrated similar results, with most non-specific binding removed by 0.15 M NaCl and only small amounts in subsequent washes (Figure 4-6B). All components of the ASC-1 complex were still observable in the immunoaffinity purification following washes containing up to 2 M NaCl (Figure 4-6B). Overall, these data suggest that the ASC-1 complex is highly stable under conditions of high salt.

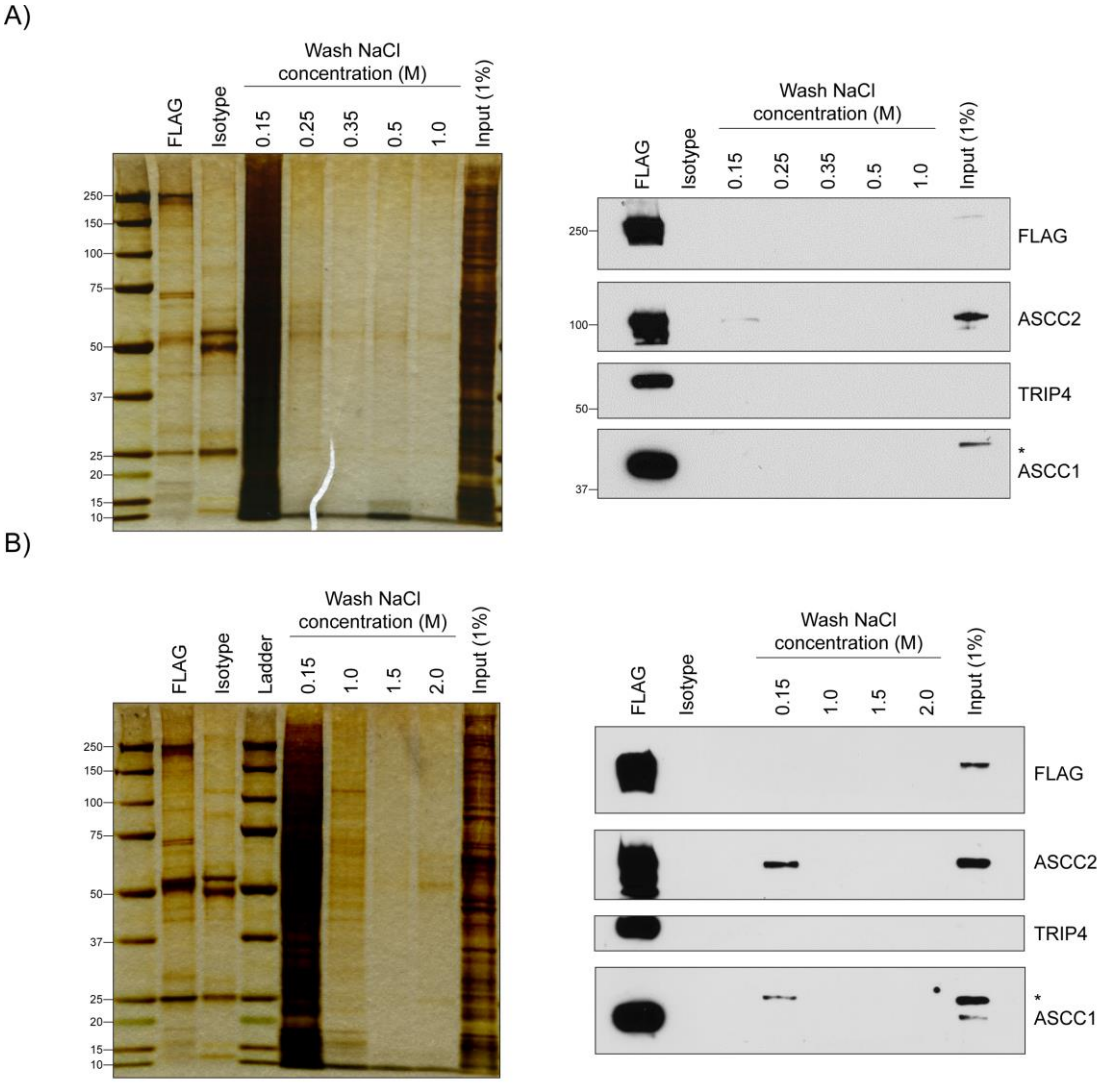

Figure 4-6. FLAG covalent immunoaffinity isolation wash buffer optimisation

A) Silver stain analysis of subsequent increases in the NaCl concentrations up to 1 M in the wash buffers showing the removal of non-specific proteins across the increasing NaCl concentrations. Immunoblot analysis shows the ASC-1 complex remains stable up to 1 M NaCl present in the wash buffer. B) Silver stain analysis of increasing wash buffer NaCl concentration up to 2 M NaCl. Immunoblot analysis of the samples in the silver stain showing the complex is stable following 2 M NaCl washes. * = non-specific band.

4.5 Identification of novel ASC-1 complex protein interactors

Following the optimisation of the wash buffer (Figure 4-6), nuclease digestion (Figure 4-4), and elution conditions (Figure 4-5), the immunoaffinity purification and mass spectrometry analysis of eluted samples was performed in order to determine novel protein interactors of ASCC3.

4.5.1 High stringency affinity purification

To identify proteins that interact with ASCC3-3xFLAG, ASCC3-3xFLAG was immunoaffinity purified using the conditions that had previously been optimised (Section 4.4) and the eluate was examined by mass spectrometry. Silver stain analysis displayed the major 250 kDa band of exogenous ASCC3 and a ladder of co-purified protein bands when compared to the isotype control (Figure 4-7A). The sample was then subjected to mass spectrometry analysis which identified 17 proteins with a minimum of 3-fold enrichment in the FLAG eluate when compared to the isotype control, 3 proteins that showed a 3-fold enrichment in the isotype control when compared to the FLAG purified sample, and 11 proteins that were not significantly enriched in either purification (Figure 4-7B). The components of the ASC-1 complex were the most significantly enriched proteins identified by ASCC3-3xFLAG immunoaffinity purification showing at least a 38-fold enrichment when compared to the isotype control (Figure 4-7C). Other proteins that showed enrichment and with a high number of peptide counts were: OTUD4, THRAP3, BAG2, UBR5, and STK38 (Figure 4-7C). ASCC3-3xFLAG immunoaffinity purification was repeated and immunoblotting was performed to validate the mass spectrometry data (Figure 4-7D). All components of the ASC-1 complex were enriched in the purification when compared to the input. Other proteins that were also detected in the co-purification were UBR5 and OTUD4. STK38 was also detected, but at a much lower level and also appeared in the isotype control. BAG2 and THRAP3 were not detected in the co-purification by immunoblot. UBR5 is an E3 ubiquitin ligase that plays a role in the regulation of the ubiquitin-proteome system in cancer and development (Shearer *et al.* 2015). OTUD4 is a deubiquitinating enzyme, that has previously been shown to have a nuclear role, interacting with ASCC3 and regulating alkylation DNA damage repair, and has only more recently been suggested to have a function in control of mRNA translation and innate immune signalling (Das *et al.* 2019; Zhao *et al.* 2015, 2018). Candidate proteins UBR5 and OTUD4 were present in the FLAG purification but were not depleted from the FLAG unbound fraction when compared to the input. Since OTUD4 and UBR5 are ubiquitin modifying enzymes they may have more transient interactions with their partner proteins. This may explain their reduced depletion in the unbound fraction when compared to the input and isotype control. Alternatively, these proteins may be present in more than one cellular complex.

The contaminant repository for affinity purification (CRAPome) is a series of compiled negative control datasets. These datasets can be utilised to identify contaminants and non-specific interactions in affinity purification-mass spectrometry data (Mellacheruvu *et al.* 2013). Submission of the significantly enriched proteins from this mass spectrometry data showed THRAP3, HSPA8, STK38, BCLF1, and IRS4, to be present in at least 25 % of all the affinity purification datasets (Table 4-2). These data do not demonstrate directly that these proteins are contaminants, but highlights proteins with this potential. Other proteins that scored highly were MAP18, BAG2, and MYCBP.

Protein	Uniprot ID	Number of experiments (found/total)	Number of experiments found (%)
ASCC3	Q8N3C0	39 / 411	9.5
ASCC2	Q9H1I8	5 / 411	1.2
TRIP4	Q15650	2 / 411	0.5
OTUD4	Q01804	40 / 411	9.7
ASCC1	Q8N9N2	5 / 411	1.2
MAP1B	P46821	94 / 411	22.9
THRAP3	Q9Y2W1	178 / 411	43.3
BAG2	O95816	96 / 411	23.4
UBR5	O95071	19 / 411	4.6
HSPA8	P11142	396 / 411	96.4
STK38	Q15208	168 / 411	40.9
BCLAF1	Q9NYF8	171 / 411	41.6
PRRC2B	Q5JSZ5	34 / 411	8.3
IRS4	O14654	152 / 411	37.0
RNF219	Q5W0B1	17 / 411	4.1
MYCBP	Q99417	72 / 411	17.5
INA	Q16352	83 / 411	20.2

Table 4-2. Protein contamination data from the CRAPome for affinity purification hits

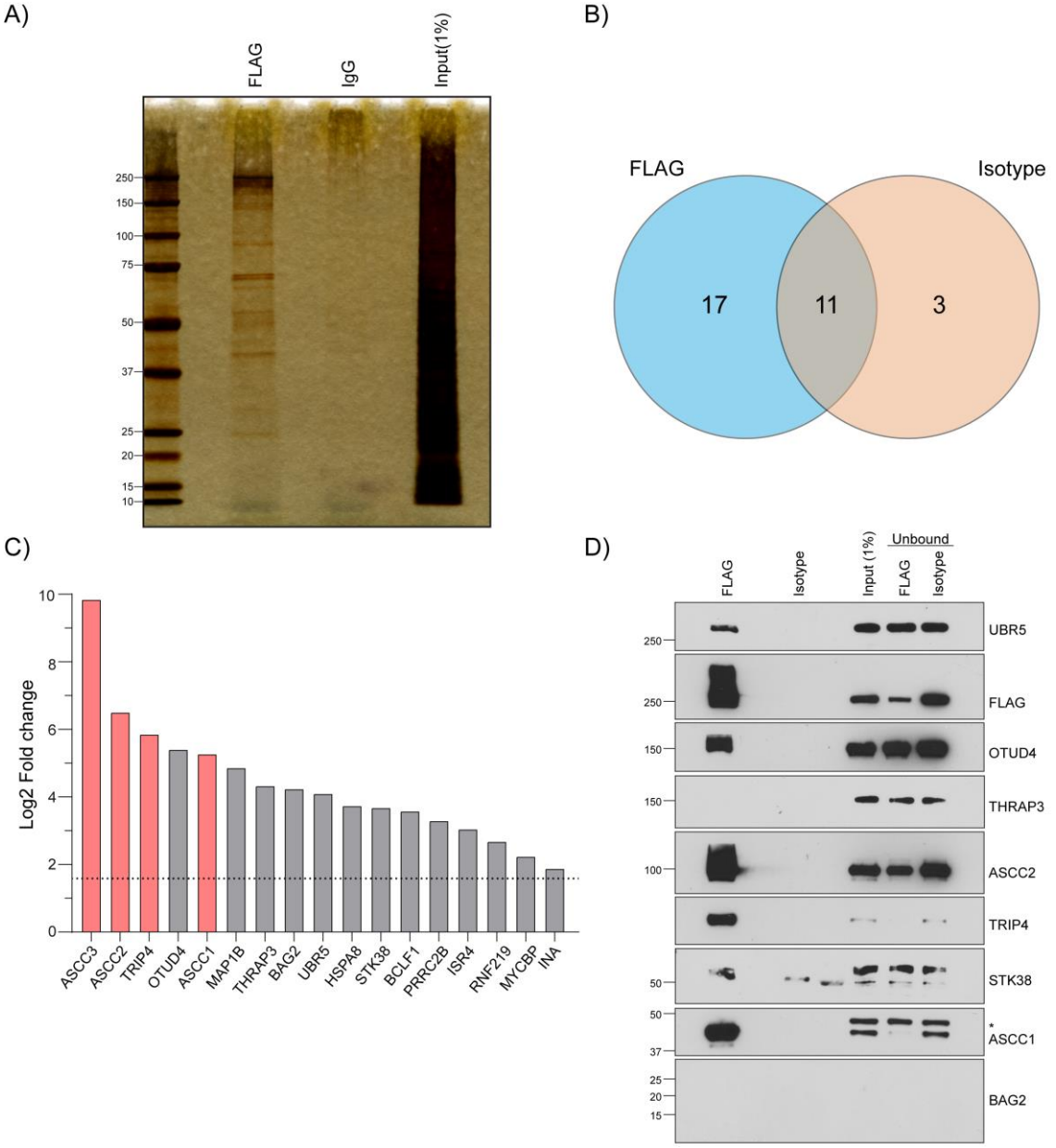

Figure 4-7. Identification of ASCC3-3xFLAG immunoaffinity purified protein by mass spectrometry

A) Silver stain analysis of ASCC3-3xFLAG co-affinity purified protein compared to isotype control. B) Venn diagram showing number of proteins enriched by at least 3-fold for each affinity purification. C) Bar graph showing log2-fold change of proteins that show at least a 3-fold enrichment in the FLAG purified sample when compared to the IgG. All data has been normalised to the internal standard and passed through a cut-off of at least 3-fold enrichment compared to the input. D) Immunoblot analysis of the top 5 protein candidates following data analysis. UBR5 and OTUD4 appear enriched in the affinity purification, while THRAP3, STK38, and BAG2 are not. * = non-specific band.

4.6 Comparing ASC-1 complex interactors following UVB irradiation

Previous attempts to identify changes in the protein interactions of ASCC3 with endogenous ASC-1 components following UVB irradiation using an ASCC3 specific antibody were unsuccessful (Stoneley *et al*, unpublished data). One possibility to explain this issue is that there could be large conformational rearrangements induced in the ASC-1 complex or ASCC3 following stress induction, which alters epitope availability. To determine whether it was possible to detect changes in interaction of ASCC3 with complex members and additional binding partners following stress, immunoaffinity purification of ASCC3-3xFLAG was carried out from cells which were either untreated or exposed to UVB. Cytoplasmic cell extracts were generated then mass spectrometry was performed on these samples. Because these interactions may be more transient in origin, the NaCl concentration was decreased from 2 M to 0.25 M for this immunoaffinity purification. Lowering the concentration of NaCl in the wash buffer will decrease the stringency of the interactions, although a significant number of non-specific interactions and contaminants will be removed (Figure 4-6A). To identify proteins that changed their ASCC3-3xFLAG interaction following UVB irradiation, peptide counts for proteins that were enriched when compared to the isotype control were then compared between untreated and UVB treated samples. The data show that no proteins changed their interaction with ASCC3-3xFLAG by at least 2-fold in response to UVB irradiation (Figure 4-8A and 4-8B). As the conditions used were not sufficient to identify new protein interactors or changes in existing protein interactors, further optimisation was required.

The mass spectrometry data were examined to determine whether the proteins identified were present in the CRAPome database (Table 4-3), in order to assess their potential as non-sepcific protein interactors. THRAP3, HSP90AA1, RBM10, eIF4B, ACTB, HSPA8, MEP50, RPS3, and PRMT5 all showed at presence in at least 40 % of all affinity purification in the CRAPome data base, suggesting that these are non-specific interactions. However, OTUD4 was present again as a significantly enriched interactor of ASCC3-3xFLAG in untreated and UVB irradiated conditions, further suggesting that OTUD4 is an ASCC3 interactor that also potentially binds to the ASC-1 complex. SVIL and HSPA1A are cytoskeletal and heat shock proteins respectively and therefore are most likely non-specific interactions.

Protein	Uniprot ID	Number of experiments (found/total)	Number of experiments found (%)
THRAP3	Q9Y2W1	178 / 411	43.3
SVIL	O95425	26 / 411	6.3
HSP90AA1	P07900	272 / 411	66.2
ASCC1	Q8N9N2	5 / 411	1.2
RBM10	P98175	175 / 411	42.6
ASCC2	Q9H1I8	5 / 411	1.2
eIF4B	P23588	167 / 411	40.6
ASCC3	Q8N3C0	39 / 411	9.5
ACTB	P60709	363 / 411	88.3
HSPA1A	P0DMV8	N/A	N/A
HSPA8	P11142	396 / 411	96.4
TRIP4	Q15650	2 / 411	0.5
MEP50	Q9BQA1	162 / 411	39.4
OTUD4	Q01804	40 / 411	9.7
RPS3	P23396	266 / 411	64.7
PRMT5	O14744	175 / 411	42.6

Table 4-3. CRAPome protein contamination data for protein hits in untreated and UVB irradiated affinity purification

Data from the CRAPome shows that eIF4B, is present in 40.6% of affinity purification data sets and suggests that eIF4B is a likely non-specific protein interaction of ASCC3-3xFLAG. However, the previous data suggesting the interaction between ASCC3 and the ribosome (Matsuo *et al.* 2017) and as a UVB responsive RNA binding protein (Figure 3-1; Stoneley *et* al, unpublished data) made eIF4B a putative candidate. Immunoblot analysis of OTUD4 and eIF4B from these mass spectrometry samples showed enrichment of OTUD4 in both FLAG purification samples, and an enrichment of eIF4B in the UVB treated ASCC3-3xFLAG purification (Figure 4-8C). However, detection of eIF4B proved difficult by immunoblot, as demonstrated by the overexposed ASCC3-3xFLAG, OTUD4, and ASCC1 (Figure 4-8C). Moreover, previous work from the Willis laboratory focussing on iCLIP of eIF4B allowed access to optimised immunoaffinity purification data of eIF4B (Quintas *et al*, unpublished data). However, no members of the ASC-1 complex were observed in this mass spectrometry data set. These data in combination with poor detection by immunoblot did not make eIF4B an ideal candidate binding partner.

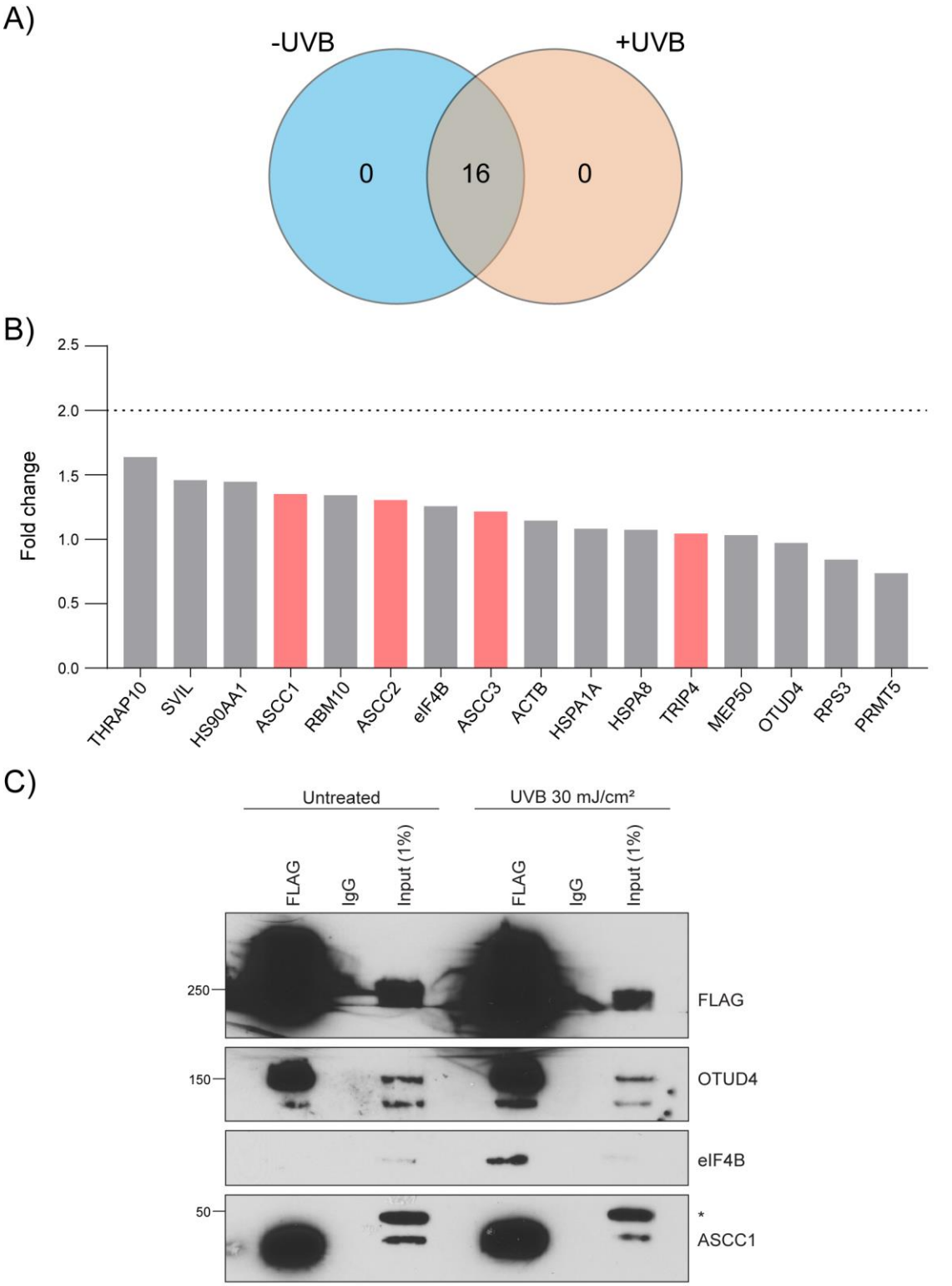

Figure 4-8. Identification of ASCC3-3xFLAG immunoaffinity purified proteins in response to UVB

A) Venn diagram displaying the number of proteins with at least a 2-fold change in interaction of exogenous ASCC3 between untreated and UVB 30 mJ/cm² irradiated samples. B) Bar graph displaying 16 proteins identified by mass spectrometry with the fold-change difference of protein peptide count between UVB irradiated and untreated samples. Known ASC-1 complex members are highlighted in red. Dotted lines represents the 2-fold change cut-off. C) Immunoblot analysis of exogenous ASCC3 immunoaffinity isolation showing enrichment of ASCC1 and OTUD4. Probing of eIF4B shows potential interaction but poor immunoblot detection. * = non-specific band.

4.7 Discussion

The overall aim of the work in this chapter was to identify novel interacting partners of ASCC3. Previous attempts to isolate ASC-1 complex using antibodies directed against endogenous components were only successful under control conditions, but not under conditions of cell stress e.g. following UVB exposure. Therefore, it was necessary to develop an alternative system to capture the ASC-1 complex. Thus, ASCC3 was triple FLAG tagged (ASCC3-3xFLAG) before the protein was expressed transiently, but the data showed that the expression of ASCC3-3xFLAG in a transient system led to poor enrichment of ASC-1 complex components (Figure 3-5). Therefore, an inducible stable cell lines was generated (Figure 3-8) and FLAG immunoaffinity purification of ASCC3-3xFLAG from the inducible cell system showed enrichment of ASCC2, TRIP4, and ASCC1, suggesting formation of the ASC-1 complex (Figure 4-1A). SEC was used to examine the incorporation of ASCC3-3xFLAG into the endogenous ASC-1 complex, and the data showed that ASCC3 and its protein partners ASCC2, TRIP4, and ASCC1 co-eluted together (Figure 4-1B). Interestingly, these data also demonstrate that the ASC-1 complex was associated with very high molecular weight complexes. Further analysis showed that ASC-1 complex was present in the same fractions as the ribosome, which is consistent with previous data showing that Slh1 (yeast homolog of ASCC3) interacts with the ribosome (Daugeron *et al.* 2011; Matsuo *et al.* 2017) (Figure 4-2).

There were a number of technical challenges that had to be overcome in this research, including IgG contamination, the co-purification of contaminant proteins, and non-direct proteins binding due to interactions with RNA, therefore, immunoaffinity purification was optimised using M-270 epoxy magnetic beads. The initial data showed that IgG heavy and light chains were significantly depleted by the covalent interaction between the antibody and the epoxy beads (Figure 4-4A), while also demonstrating co-purification of ASCC2, TRIP4, and ASCC1 by this technique (Figure 4-4B). Optimisation of nuclease digestion demonstrated that ASCC2 and ASCC1 does not require RNA to interact with ASCC3-3xFLAG (Figure 4-4D). Comparison of Benzonase and RNase A with a DNase I control, showed Benzonase had a small effect on ASCC3-3xFLAG recovery when compared to RNase A and DNase I (Figure 4-4C). The reason for this difference is still not understood, therefore, RNase A was chosen as the nuclease for ASCC3-3xFLAG immunoaffinity purification. To isolate proteins interacting with ASCC3-3xFLAG, 3xFLAG peptides were used to competitively elute ASCC3-3xFLAG and interacting proteins from the antibody. It was found that addition of 0.1 % NP-40 to the elution buffer enhanced elution of ASCC3-3xFLAG (Figure 4-5C and 4-5D) (Piñeiro *et al.* 2018). The stability of the ASC-1 complex was examined and the data show that this complex is stable at high NaCl concentrations (Figure 4-6).

Mass spectrometry analysis of immunoaffinity purified ASCC3-3xFLAG identified 31 proteins; 17 of which were enriched when compared to the isotype control (Figure 4-7B and 4-7C). Proteins which demonstrated the most significant peptide counts and fold-increase were examined by immunoblot. These proteins included OTUD4, THRAP3, BAG2, UBR5, and STK38, however, only OTUD4 and UBR5 were confirmed as co-purified proteins (Figure 4-7D). Interestingly, OTUD4 and UBR5 are a deubiquitinase and E3 ubiquitin ligase respectively, which may suggest ubiquitin modification controls ASC-1 complex function. Moreover, ASCC3 ubiquitination has been shown to change in response to UV exposure (Boeing *et al.* 2016) and resolution of stalled ribosomes has been shown to rely on ubiquitin modifications (Juszkiewicz & Hegde 2017; Sundaramoorthy *et al.* 2017).

Comparison of ASCC3-3xFLAG immunoaffinity purification data from untreated and UVB treated samples showed no differences in the proteins that were co-purified (Figure 4-8A and 4-8B). Therefore, although this work does not identify changes in ASCC3-3xFLAG protein interactions, it may suggest that interactions following UVB are weak, transient, or depend on post-translational modifications which are removed during purification. Interestingly, OTUD4 bound ASCC3-3xFLAG and was detected in both immunoaffinity purifications (Figure 4-8C). A possible interaction between eIF4B was also examined, however, eIF4B immunoblot analysis was inconclusive, and eIF4B did not bind any ASC-1 complex components when analysed by mass spectrometry (Quintas *et al*, unpublished data).

To conclude, these data describe the process taken to investigate the role of ASCC3 in the ASC-1 complex, and suggest that the ASC-1 complex may be a sub-complex of a much larger macromolecular complex, which likely contains the ribosome. Even following optimisation of immunoaffinity purification, it was not possible to identify changes in ASCC3-3xFLAG protein interactions following UVB irradiation, but these data did confirm OTUD4 as an interacting partner. This made OTUD4 the primary candidate for a novel-protein interactor of the ASC-1 complex in the cytoplasm, and this interaction was investigated further in this thesis.

5. OTUD4: a component of the ASC-1 complex

5.1 Introduction

Mass spectrometry data of ASCC3-3xFLAG immunoaffinity isolation reproducibly shows OTUD4 as a protein that is co-purified. Immunoblot analysis of these samples also confirms this interaction to be true. Functionally, OTUD4 is able to interact with the ASC-1 complex in the nucleus, and acts as a stabilisation factor for alkylation damage repair factors (Zhao *et al.* 2015). The interaction of OTUD4 with the ASC-1 complex in the nucleus suggests that this interaction also has a functionally important role in the cytoplasm. In this regard, it has been shown that in the cytoplasm, OTUD4 acts to removes K63 ubiquitin chains of MyD88, a signal transducer for TLR signalling (Zhao *et al.* 2018), and removes K48 ubiquitin chains of MAVS in the RNA-antiviral response (Liuyu *et al.* 2019). These functions may relate to the ability of OTUD4 to bind RNA (Baltz *et al.* 2012; Das *et al.* 2019; Liepelt *et al.* 2016), although, at the time of study, the interaction of OTUD4 with RNA was still yet to be studied in detail.

5.1.1 aims

The aims of this chapter were to further validate the inclusion of OTUD4 in the ASC-1 complex using immunoaffinity purification, siRNA complex stability experiments, and SEC. Additionally the functional properties of OTUD4 were explored in the context of RNA-binding, polysome association, proliferation, protein synthesis, and nuclear export.

5.2 OTUD4 antibody optimisation

5.2.1 OTUD4 siRNA knockdown

Detection of OTUD4 by immunoblot analysis was necessary before further characterisation of this protein could be carried out. There were three commercially available antibodies for OTUD4 immunoblot detection (Table 5-1) with others available for other applications. To determine the specificity of these antibodies, siRNAs were used to deplete OTUD4 in HeLa cells. Three siRNAs specific for OTUD4 were individually titrated from 50 to 2.5 nM and protein knockdown compared to 10 nM scrambled negative control DsiRNA treated cells. In the first instance, to assess depletion of OTUD4, antibody #2 (Table 5-1) was used and each siRNA was shown to deplete OTUD4 after 72 hours (Figure 5-1A). Moreover, quantification and normalisation of OTUD4 suggested depletion occurred in a concentration dependent manner (Figure 5-1B). The observed reduction of OTUD4:β-tubulin ratio for the scrambled negative control DsiRNA treated samples, compared to the untreated (RNAiMAX only) samples was not significant (Figure 5-1C).

5.2.2 OTUD4 antibody optimisation

Since all three siRNAs tested individually reduced the expression of OTUD4 over the course of 72 hours, a combination treatment was used to examine the specificity of the three commercially available OTUD4 antibodies (Table 5-1). Titration of the combined OTUD4 siRNA from 50 to 2.5 nM showed efficient depletion of OTUD4 and was detected with all three antibodies (Figure 5-2). Antibody #1 detected numerous non-specific bands in the scrambled negative control DsiRNA treated sample, but also showed efficient depletion of the specific OTUD4 band following siRNA knockdown (Figure 5-2, black arrow). Antibody #2, while detecting the specific ~150 kDa OTUD4 band which was depleted by siRNA treatment, also detected low-level non-specific bands. However, detection required more sensitive ECL reagents and longer antibody incubation times when compared with antibody #1. Antibody #3 detected a single band of the correct molecular weight, which was depleted by OTUD4 siRNA, however, detection was extremely poor.

Antibody	Supplier	Catalogue number
Antibody #1	Bethyl	A304-605A
Antibody #2	Bethyl	A304-606A
Antibody #3	ProteinTech	25070-1-AP

Table 5-1. OTUD4 antibodies

Antibody #1 and #3 were examined further, using a range of incubation conditions to optimise the detection of OTUD4. The same HeLa cytoplasmic cell extract was analysed in multiple lanes by SDS-PAGE and immunoblotted for OTUD4 using the conditions displayed (Figure 5-3). Antibody #1 detected the correct ~150 kDa band in all conditions (Figure 5-3A, black arrow) but also detected non-specific bands when used at a 1:1000 dilution overnight at 4°C. Reducing the antibody concentration to 1:2000 and to 1:3000, showed decreased detection of the non-specific bands while maintaining a strong signal for OTUD4 in both cases. Incubation of these antibodies at 1:1000 and 1:2000 at room temperature for 1-hour also decreased detection of non-specific bands, however, detection of OTUD4 was also reduced at a dilution of 1:2000. Antibody #3 produced a weak OTUD4 signal at a 1:1000 dilution factor, while showing an improved signal at 1:500 (Figure 5-3B). Room temperature incubation at concentrations between 1:500-1:1000, and incubation times of 1-2 hours showed no improvement of OTUD4 detection. Although antibody #3 shows greater specificity for OTUD4, the quantity of antibody

required, and the challenging detection of OTUD4 made antibody #1 the optimal choice for detection of OTUD4.

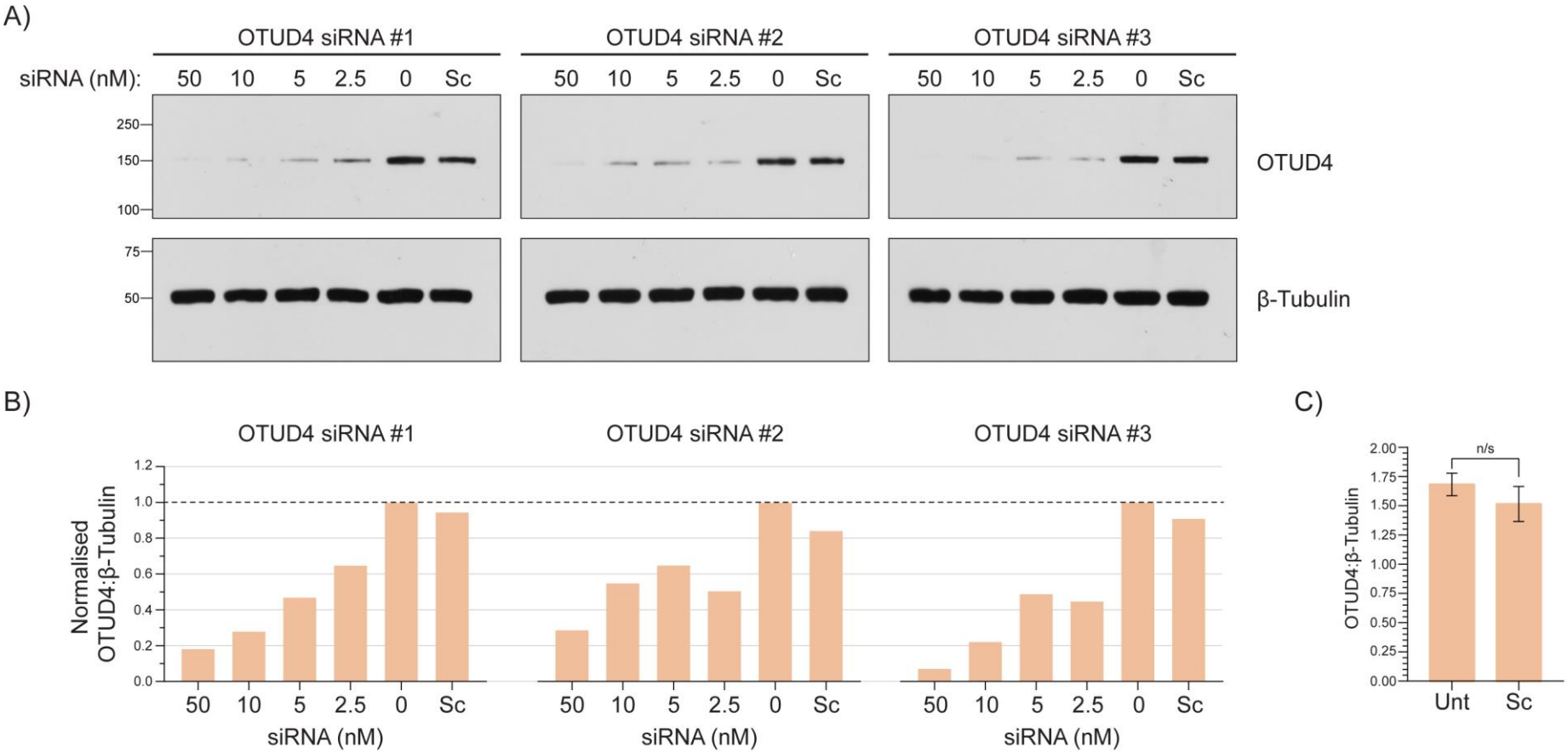

Figure 5-1. Knockdown of OTUD4 using siRNA

A) OTUD4 immunoblot analysis of cell lysates from HEK293 cells treated with titrating concentrations of 3 OTUD4 siRNAs from IDT. Each siRNA shows dose-dependent depletion of OTUD4 when compared to untreated and DsiRNA scramble (10 nM) treated cells. Equal protein concentration is shown by β-tubulin loading. B) Densitometric analysis of immunoblots from (A). Pixel density is acquired by area under the curve analysis using ImageJ, each OTUD4 density is normalised to its β-tubulin loading control, which is then adjusted to the untreated sample (0 nM siRNA) displayed by the dotted line. C) Comparison of OTUD4-β-tubulin ratios in untreated and scramble treated cells. Unpaired student t-test shows this change is non-significant.

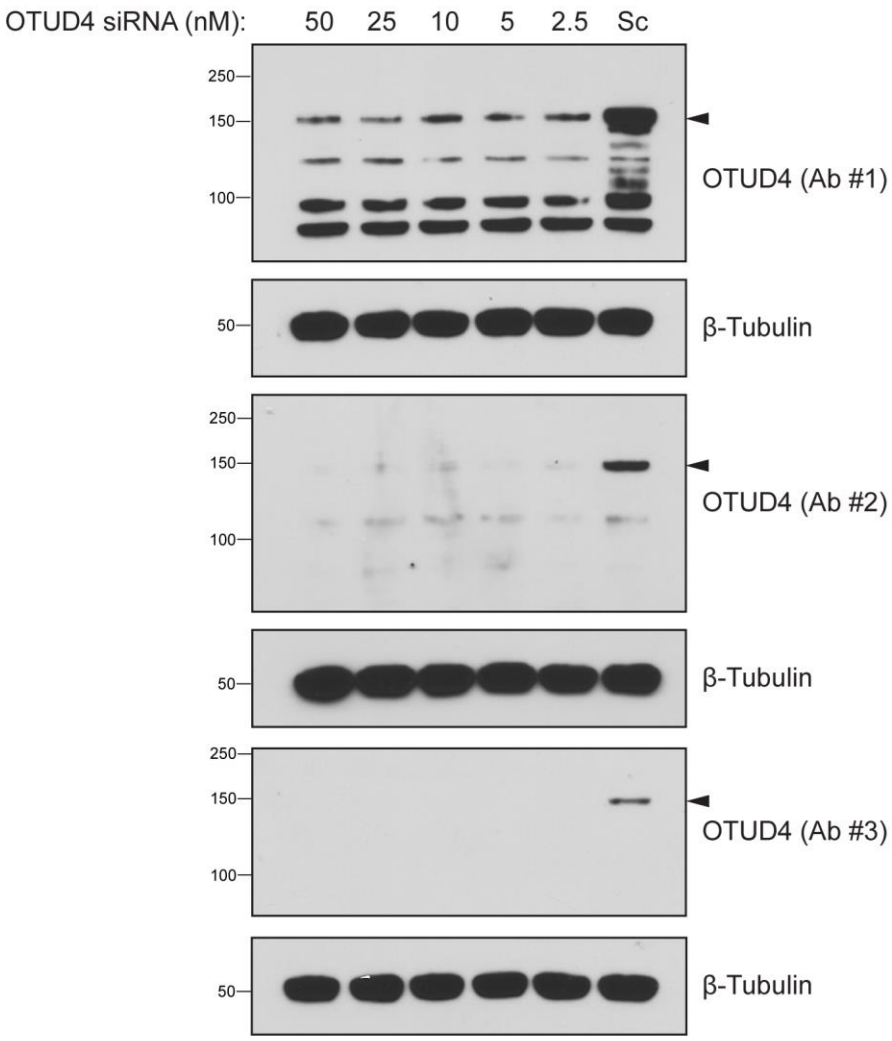

Figure 5-2. Examination of OTUD4 antibody specificities by immunoblot detection
Combination OTUD4 siRNA treatment was titrated from 50-2.5 nM in order to deplete OTUD4 from the samples while examining the antibodies for OTUD4 ease of detection. Antibody 1 (Ab #1) shows detection and depletion of the OTUD4 band at ~150 kDa, while also displaying multiple non-specific bands. Antibody 2 (Ab #2) shows depletion of OTUD4 by siRNA with some low-level non-specific band detection. Antibody 3 (Ab #3) detects only a single band which is depleted by siRNA treatment. Even loading for all samples is demonstrated by β-tubulin distribution.

A)

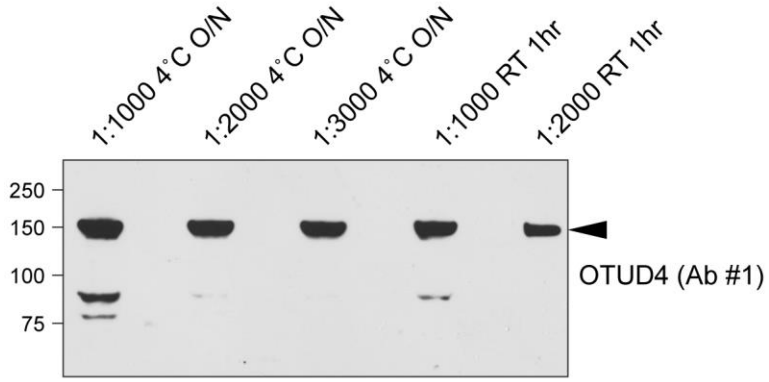

B)

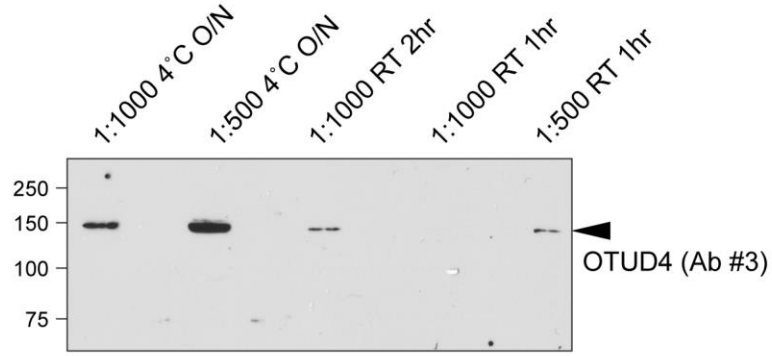

Figure 5-3. Immunoblot of OTUD4 antibody incubation optimisation

Detection of OTUD4 from the same equally loaded sample using five different antibody incubation conditions for two different antibodies. A) Ab #1 shows reduced background bands in every condition when compared to the original 1:1000 4 °C overnight, with optimal detection at 1:3000 at 4°C overnight (O/N). B) Ab #2 shows improved detection by increasing the concentration at 4 °C, but room temperature incubation shows decreased detection of OTUD4. Optimal detection is at 1:500 at 4 °C O/N.

5.3 OTUD4 RNA-binding

To date OTUD4 has been identified as a putative RNA-binding protein in HEK293 cells and macrophages (Baltz *et al.* 2012; Liepelt *et al.* 2016). However, the RIC screen carried out in the Willis laboratory to compare control to UVB exposed MCF10A cells did not reveal any peptides from OTUD4 (Stoneley *et al*, unpublished data). RIC was performed to examine the RNA-binding capability of OTUD4 and to determine whether its affinity for RNA changed in response to UVB. Comparison of control and UVB treated RIC samples from HEK293 cells showed that there were no changes in OTUD4 RNA-binding following UVB irradiation (Figure 5-4A). ASCC3 and PABP1 were used as positive and negative control respectively for RNA-binding in response to UVB. As expected, ASCC3 RNA binding was enhanced in response to UVB, whereas PABP1 binding was maintained.

Detection of OTUD4 following RIC has proven to be challenging. Thus, while the original experiments suggest OTUD4 was an RNA-binding protein in the cytoplasm, these data have yet to be fully confirmed. Analysis of OTUD4 RNA-binding from whole cell extracts of HEK293 and U2OS showed OTUD4 bound RNA in both cell lines (Figure 5-4B). OTUD4 was also shown to bind RNA in the cytoplasmic fraction of HeLa cells, however, inconsistency of the commercially available PABP1 antibody resulted in poor PABP1 detection, and therefore these studies lack an appropriate control (data not shown). However, taken together, these data suggest that OTUD4 can function as an RNA-binding protein, despite the absence of a recognised RNA-binding domain present within the protein.

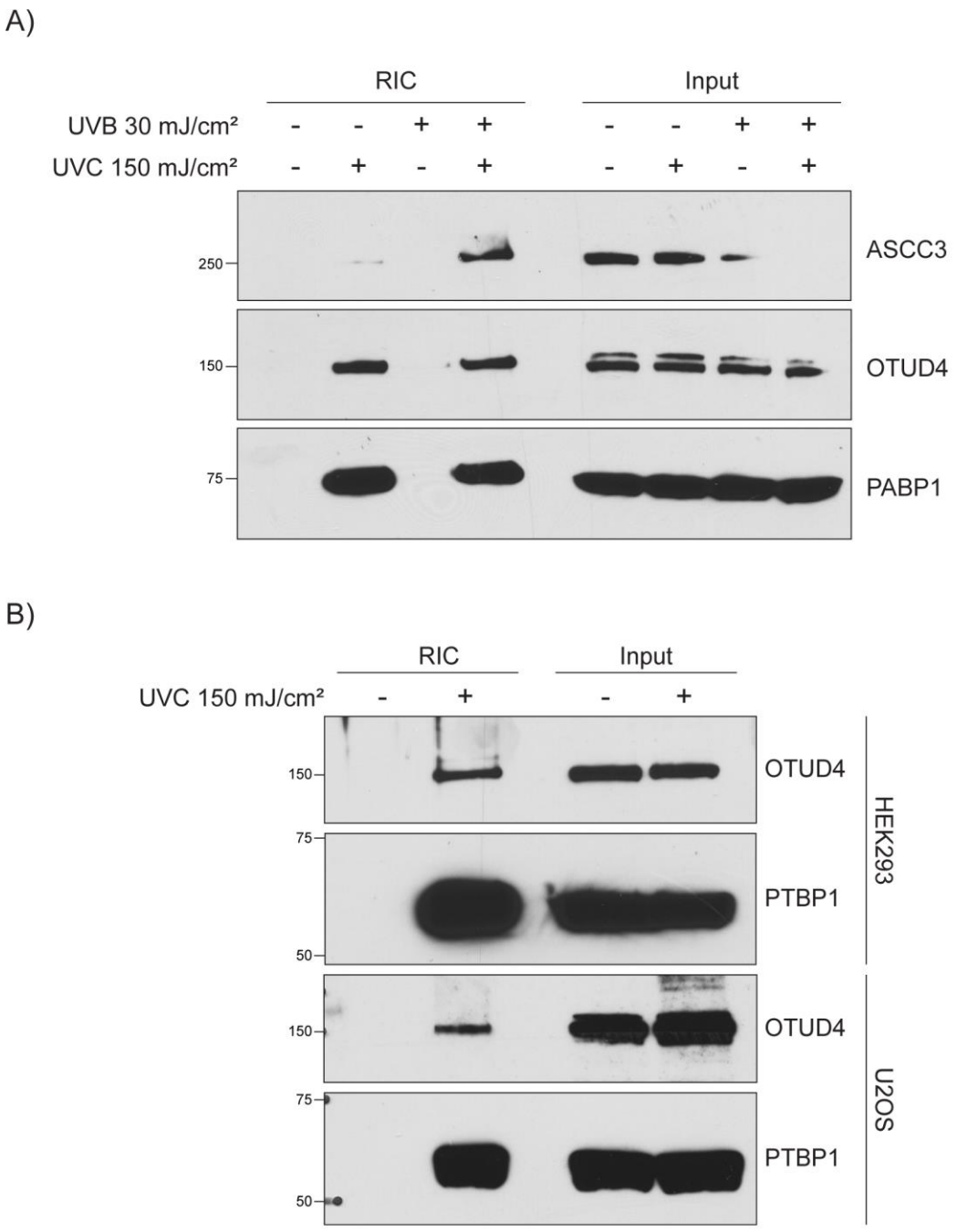

Figure 5-4. RNA-binding of OTUD4

A) Cytoplasmic RNA interactome capture analysis of untreated and UVB irradiated HEK293 cells. Immunoblot shows ASCC3 increases RNA-binding in response to UVB while OTUD4 RNA interaction does not change in response to UVB treatment. B) Whole cell RNA-interactome analysis of OTUD4 from HEK293 and U2OS cells shows detection of OTUD4 when cross-linking the cells with UVC.

5.4 OTUD4 as part of the ASC-1 complex

5.4.1 OTUD4 localisation

To ascertain if OTUD4 was a potential component of the ASC-1 complex, immunoaffinity isolation was used to determine if OTUD4 interacted with monomeric ASCC3 or ASCC3 as part of the ASC-1 complex. Since the main focus of our work is on the cytoplasmic role of the ASC-1 complex, initial experiments were carried out to determine whether OTUD4 was present in the cytoplasm. HeLa and HEK293 cells were fractionated and the distribution of OTUD4 between the nucleus and cytoplasm was analysed (Figure 5-5A). Successful fractionation was demonstrated by the enrichment of β-tubulin and GAPDH predominantly in the cytoplasmic fraction. Histone H3, as expected was predominantly in the nuclear fraction, however, this region of the immunoblot was overexposed. OTUD4 was identified as present in both the nucleus and cytoplasm. While the functional role for OTUD4 in the nucleus has already been explored (Zhao *et al.* 2015), the cytoplasmic function was yet to be fully determined.

5.4.2 Non-covalent affinity purification

Non-covalent immunoaffinity purification of OTUD4 was carried out to determine if endogenous OTUD4 could interact with the endogenous ASC-1 complex. Immunoaffinity purification of OTUD4 using antibody #1 from HeLa cytoplasmic extracts showed a small amount of OTUD4 was purified, with a small amount of ASCC3 and ASCC2 also co-purified (Figure 5-5B). ASCC2 was not detected in the input or unbound fractions which made it difficult to assign the band in the immunoaffinity purification as ASCC2. Comparison of the OTUD4 unbound to the input demonstrated that OTUD4 was not efficiently depleted, which may explain the reason for the small amount of ASCC3 detected. A combination of masking by IgG light chains and poor antibody-antigen interaction meant TRIP4 and ASCC1 were also not detected. Overall, OTUD4 co-purifies ASCC3 and also purifies what could be ASCC2, however, the affinity purification of OTUD4 is inefficient.

5.4.3 OTUD4 construct creation

To overcome complexities of immunoaffinity purification with OTUD4 antibodies an OTUD4-3xFLAG inducible stable cell line was generated in Flp-In T-REx HeLa cells. While the cell line is different from that used to generate the ASCC3-3xFLAG inducible stable HEK293 cell line, the overall procedure is otherwise identical. A FLAG-HA-OTUD4 plasmid was obtained from Addgene (#22594), however, the first 195 nucleotides were missing from the N-terminus of OTUD4 in this construct (Sowa *et al.* 2009). It was concerning that these missing 195 nucleotides (65 amino acids) encodes the catalytic cysteine residue at position 45, such that the proteins

produced from this plasmid construct are catalytically inactive. For addition of the first 195 nucleotides and the cloning of the constructs, Gibson assembly was used, which relies on multiple overlapping fragments of DNA in a single tube reaction in three steps: firstly, the exonucleolytic activity creates 3' overhangs, allowing annealing of the homologous single stranded DNA ends; secondly, the polymerase activity fills the gaps within the annealed fragments; and finally the ligase activity seals the DNA nicks (Figure 5-6A). Linearization of the vector prior to adding the DNA is crucial to create the final product. Two DNA fragments of 294 nucleotides were designed, containing the first 195 nucleotides for wild-type and catalytically inactive (Cys45Ala) OTUD4. PCR amplification was used to generate a larger quantity of the designed fragments and the OTUD4 CDS from the FLAG-HA-OTUD4 plasmid (Figure 5-6B), before Gibson assembly was carried out. Each assembled construct (pcDNA5/FRT/TO-OTUD4(WT)-3xFLAG or pcDNA5/FRT/TO-OTUD4(C45A)-3xFLAG) was transformed before colonies were isolated, expanded, and digested (Figure 5-6C). Successfully assembled constructs showed fragments of 4485, 3254, and 754 base pairs (Figure 5-6C). Clones 1, 3, and 5 for OTUD4(WT)-3xFLAG and clones 1, 4, 5, and 7 for OTUD4(C45A)-3xFLAG showed the correct band profile and showed the correct sequence (Figure 5-6C). Plasmids for clone 5 of each construct were transiently expressed in Flp-In T-Rex HEK293 and Flp-In T-REx HeLa by adding 250 ng/ml doxycycline to the media. 3xFLAG tagged products were detected by FLAG immunoblot at the expected molecular weight (Figure 5-6D).

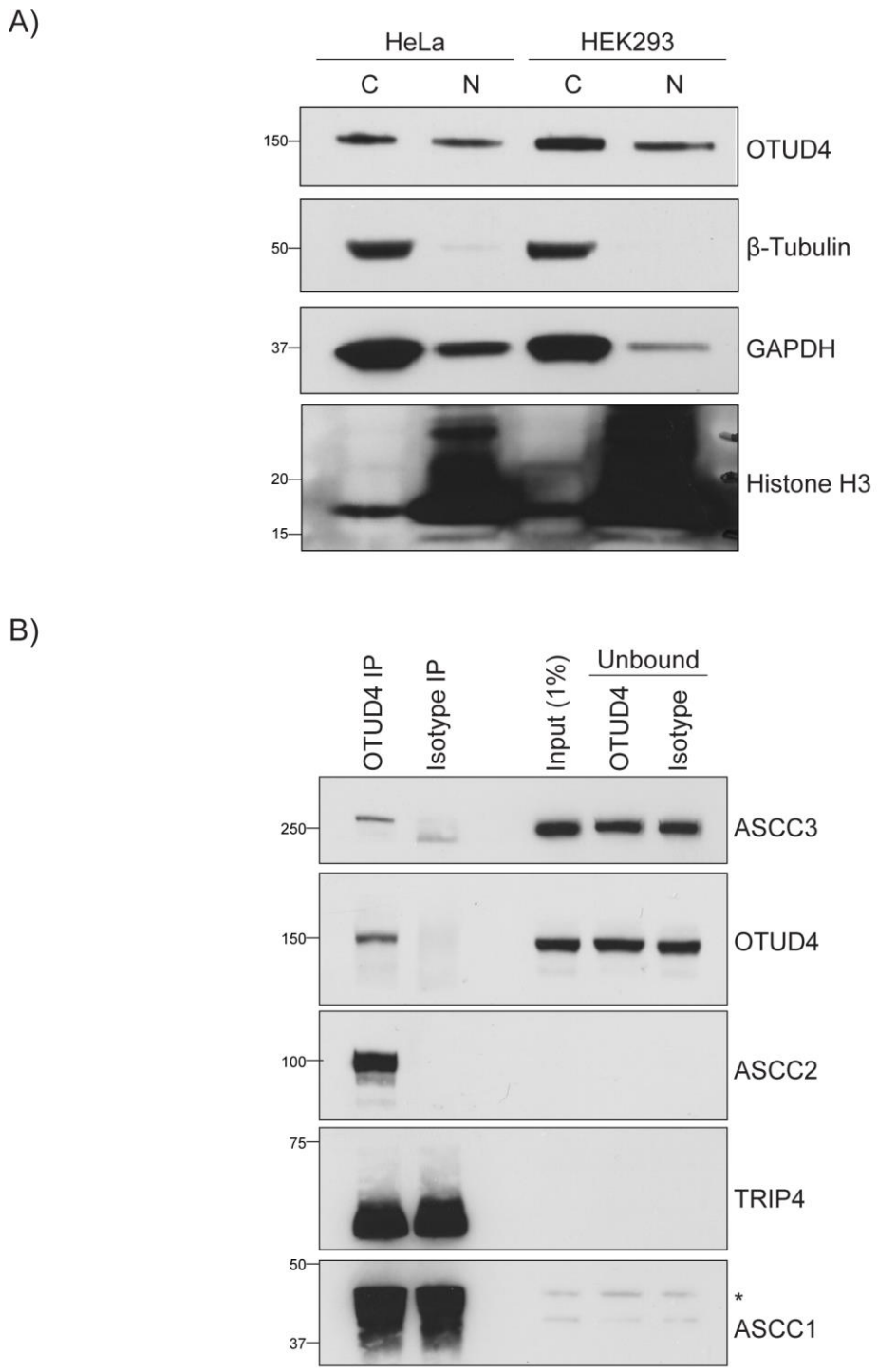

Figure 5-5. Validation of the interaction between OTUD4 and the ASC-1 complex

A) Cytoplasmic/nuclear fractionation of HeLa and HEK293 cells examining the distribution of OTUD4 shows its presence in both cellular compartments. B) Immunoaffinity purification of OTUD4 shows co-purification of ASCC3 and ASCC2, but these proteins are not depleted in the unbound fractions. * = non-specific band.

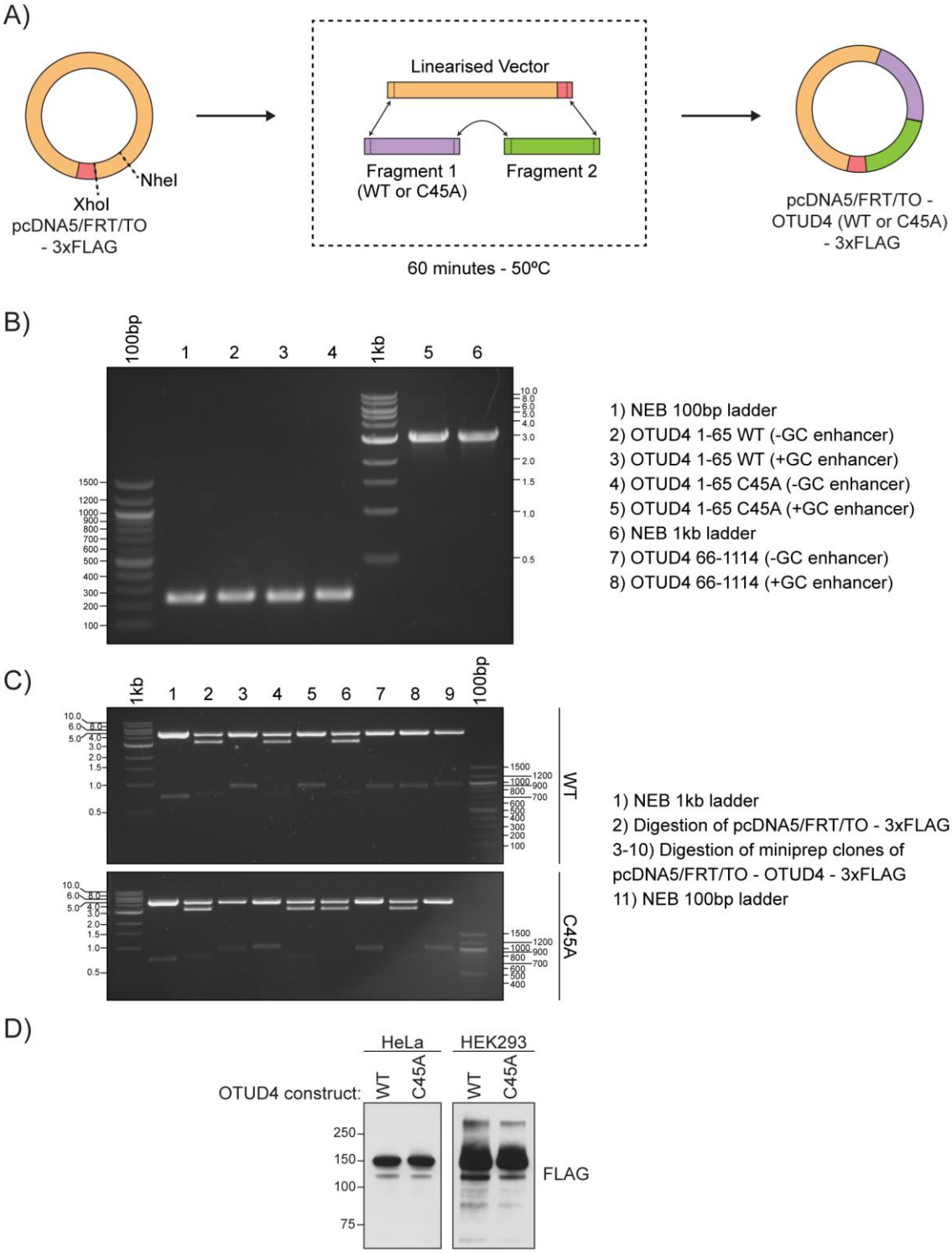

Figure 5-6. Construction of a pcDNA5/FRT/TO – OTUD4 (Wt/C45A) construct

A) Schematic of Gibson assembly to create pcDNA5/FRT/TO – OTUD4 (WT/C45A) – 3xFLAG construct creation. B) Agarose gel showing products of PCR amplification for OTUD4 (WT/C45A) gBlocks that encode the first 1-65 amino acids (lane 2-3 and 4-5 respectively), and amplification of OTUD4 DNA that codes for 66-1114 amino acids (lane 7-8). C) Agarose gel showing diagnostic digest of miniprep clones for pcDNA5/FRT/TO – OTUD4 (WT/C45A) – 3xFLAG using HindIII and XbaI. Clones 2, 3, and 5, and clones 1, 4, 5, and 7, for WT and C45A OTUD4 constructs respectively show the correct band pattern. D) Immunoblot showing transient expression of OTUD4(WT)-3xFLAG and OTUD4(C45A)-3xFLAG exogenous proteins in Flp-In T-REx HeLa and Flp-In T-REx HEK293 cells.

5.4.4 Generation of a wild-type and catalytic mutant OTUD4 inducible stable cell line

As described previously, plasmids were generated that express OTUD4(WT)-3xFLAG and OTUD4(C45A)-3xFLAG in HeLa and HEK293 cells (Figure 5-6). To generate an inducible stable cell line, plasmids were co-transfected in Flp-In T-REx HeLa cells, followed by incubation in hygromycin selection media until individual colonies were formed. Colonies were picked and expanded, then examined for their ability to express the OTUD4(WT)-3xFLAG or OTUD4(C45A)-3xFLAG following incubation with doxycycline (Figure 5-7A). All OTUD4(WT)-3xFLAG clones expressed the exogenous protein and all OTUD4(C45A)-3xFLAG clones, except 1 and 4, expressed the exogenous 3xFLAG tagged protein (Figure 5-7A). Densitometric analysis of FLAG detected exogenous OTUD4 normalised to β-tubulin loading, showed that clone 8 for OTUD4(WT)-3xFLAG and clone 3 for OTUD4(C45A-3xFLAG) expressed the most exogenous protein (Figure 5-7B, orange bars). Zeocin resistance was lost upon incorporation of the plasmid DNA into chromatin; examination of each clone's sensitivity to zeocin demonstrated that clones 1, 8, and 9 for OTUD4(WT)-3xFLAG and clones 2, 6, 9, and 10 for OTUD4(C45A-3xFLAG) were Zeocin resistant and therefore discarded (Figure 5-7C). Despite clone 8 for OTUD4(WT)-3xFLAG showing the most robust exogenous protein expression, because of its Zeocin resistance, the clone was discarded. Therefore, clone 6, that demonstrated the second highest expression of exogenous protein for OTUD4(WT)-3xFLAG (Figure 5-7B) and clone 3 for OTUD4(C45A)-3xFLAG were selected for further examination.

5.4.5 Immunoaffinity purification of exogenous OTUD4 from an inducible stable cell line

Generation of an inducible stable cell line for OTUD4(WT)-3xFLAG and for OTUD4(C45A)-3xFLAG enables a highly specific immunoaffinity purification by FLAG antibody, while gaining further understanding on whether the catalytic activity of OTUD4 is required for ASC-1 complex interaction. Non-covalent immunoaffinity purification of OTUD4(WT)-3xFLAG or OTUD4(C45A)-3xFLAG demonstrated purification of exogenous OTUD4 in both instances, however, ASC-1 complex components did not co-purify with OTUD4 under these conditions (Figure 5-8A). Detection of these components in the input demonstrated that immunoblotting was successful. Interestingly, covalent immunoaffinity purification of exogenous OTUD4(WT)-3xFLAG or OTUD4(C45A)-3xFLAG using magnetic epoxy beads, demonstrated a small amount of ASCC3, ASCC2, and TRIP4 co-purification with both wild-type and catalytic mutant OTUD4 (Figure 5-8B). However, these components were not depleted from unbound samples, which may indicate that the interaction of OTUD4 with the ASC-1 complex is transient or requires post-translational

modifications that are removed in the lysate. This data demonstrates that OTUD4 interacts with the ASC-1 complex and that the catalytic activity of OTUD4 is not required for this interaction. Furthermore, the reason behind the differential ASC-1 complex interaction with exogenous OTUD4(WT)-3xFLAG or OTUD4(C45A)-3xFLAG between the non-covalent and covalent immunoaffinity purification remains unknown.

A)

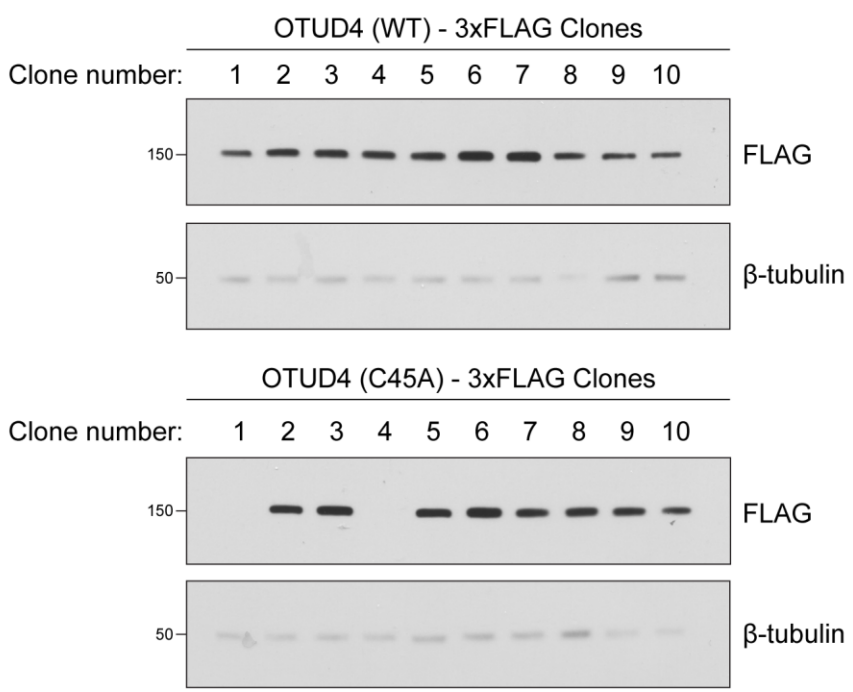

B)

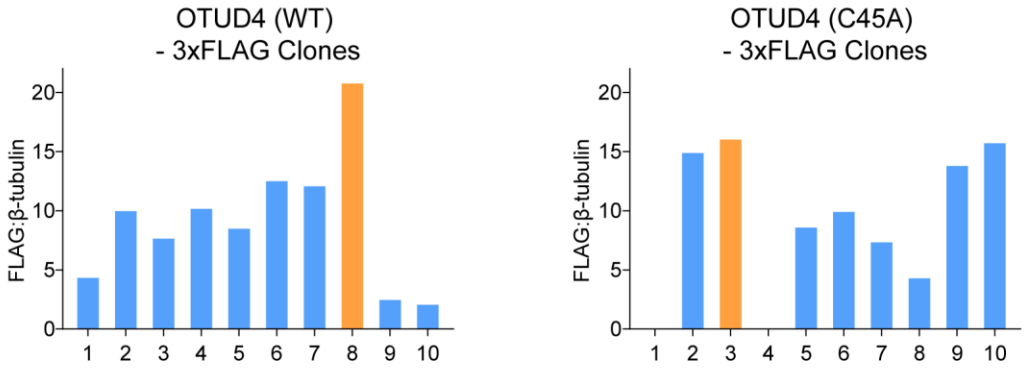

C)

OTUD4 WT clone	Zeocin Sensitive	Protein induction
1	×	✓
2	✓	✓
3	✓	✓
4	✓	✓
5	✓	✓
6	✓	✓
7	✓	✓
8	×	✓
9	×	✓
10	✓	✓

OTUD4 C45A clone	Zeocin Sensitive	Protein induction
1	✓	×
2	×	✓
3	✓	✓
4	✓	×
5	✓	✓
6	×	✓
7	✓	✓
8	✓	✓
9	×	✓
10	×	✓

Figure 5-7. Generation of OTUD4 (WT/C45A) inducible stable HeLa cell lines

A) Immunoblot analysis of exogenous OTUD4 (WT/C45A) expression following addition of 250 ng/ml doxycycline in the culture media for 24 hours prior to lysis. B) Densitometric analysis of (A) creating a ratio of FLAG detected exogenous OTUD4 to the β-tubulin loading control to show which clones express the most exogenous protein (highlighted in orange). C) Table showing which clones were Zeocin sensitive and were able to express exogenous protein. Clones selected for further study are highlighted in green.

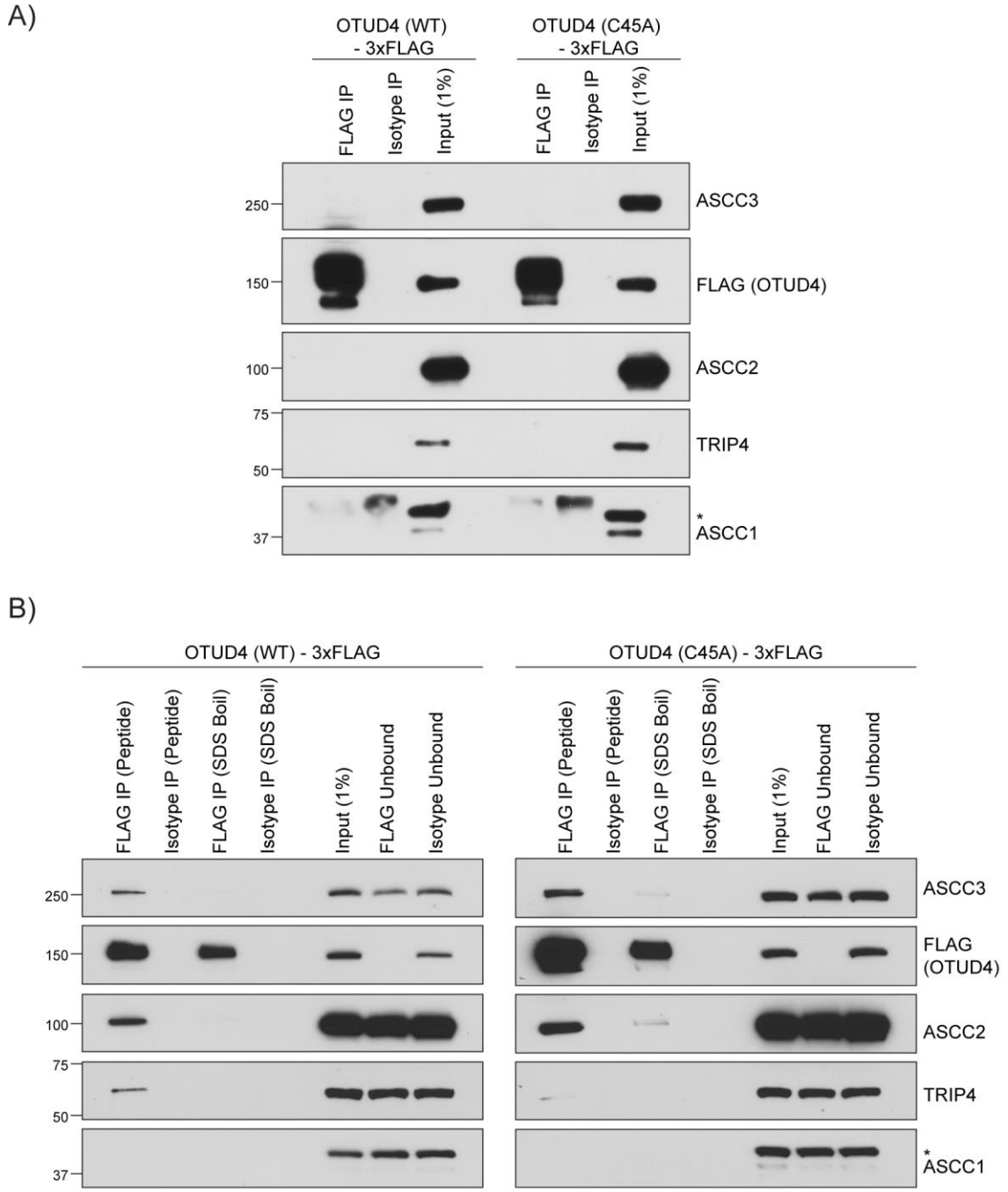

Figure 5-8. Immunoaffinity purification of exogenous OTUD4 (WT/C45A) from inducible stable HeLa cells

A) Non-covalent FLAG immunoaffinity purification of exogenous OTUD4(WT)-3xFLAG or OTUD4(C45A)-3xFLAG using protein G Dynabeads shows ASC-1 complex components are absent from the co-purification. B) Covalent FLAG immunoaffinity purification of exogenous OTUD4(WT)-3xFLAG or OTUD4(C45A)-3xFLAG co-purifies a limited amount of ASCC3, ASCC2, and TRIP4 while maintaining its population in the FLAG unbound fraction in both cases. * = non-specific band.

5.5 The effect of ASC-1 complex component depletion on ASC-1 complex formation

5.5.1 ASC-1 complex component depletion

Previous work has determined that Slh1 was essential for the stability of proteins homologous to ASCC2 and TRIP4 (Matsuo *et al.* 2017), therefore it was important to understand the effect of ASC-1 complex depletion on complex stability. Reverse transfection was carried out on HeLa cells with 10 nM siRNA for either OTUD4, ASCC3, ASCC2, TRIP4, ASCC1, scramble negative control DsiRNA, or lipofectamine (untreated) for 72 hours before extraction of the cytoplasmic fraction. Immunoblot analysis demonstrated that depletion of ASCC3 led to a reduction of ASCC2, TRIP4, and ASCC1 when compared to control samples (Figure 5-9). Depletion of ASCC2 also resulted in the reduction of ASC-1 complex components, albeit to a lesser extent than depletion of ASCC3. Interestingly, the crude ASC-1 complex model generated from immunoaffinity purification studies (Figure 3-6), showed ASCC3 as the backbone of the ASC-1 complex. It is therefore logical that ASCC3 would be required for complex stability and function. Interestingly, depletion of ASCC3 has no effect on detected OTUD4, showing that the interaction of OTUD4 with the ASC-1 complex is not required for complex stability.

5.5.2 SEC analysis of ASC-1 complex and OTUD4

To further determine whether OTUD4 is present in the ASC-1 complex, cytoplasmic HeLa cell lysate was analysed using SEC with a Superose 6 (increase 3.2/300) column. SEC eluates were analysed by immunoblot (Figure 5-10A), with preliminary data demonstrating co-elution of ASCC3, OTUD4, ASCC2, TRIP4, ASCC1, RPS6, and RPL27A at 0.6 ml. Additional enriched co-elution of ASCC3, ASCC2, TRIP4, and ASCC1 was also demonstrated at 1.0-1.05 ml in untreated cells (Figure 5-10A). A plot of log-molecular weight against elution volume was created using pre-determined molecular weight standards as described previously (Section 4.3) (Figure 5-10B). Moreover, the predicted elution volume of ASCC3, ASCC2, TRIP4, ASCC1, the ASC-1 complex, OTUD4, and ASC-1 complex including OTUD4 was calculated by extrapolation (Figure 5-10C). Interestingly, the ASC-1 complex had a predicted elution volume of 1.03 ml, which coincides with data from the immunoblot (Figure 5-10A). Overall, these data show that OTUD4 co-localises in the same high-molecular weight fractions as the ASC-1 complex (0.6 ml), but OTUD4 does not co-localise with a second population of the ASC-1 complex (1.0-1.05 ml) that is predicted to be a 1:1:1:1 ratio of ASCC3, ASCC2, TRIP4, and ASCC1. This may indicate that OTUD4 is only able to interact with the higher order ASC-1 complex that may contain ribosomal components, as demonstrated by co-localisation with RPS6 and RPL27A.

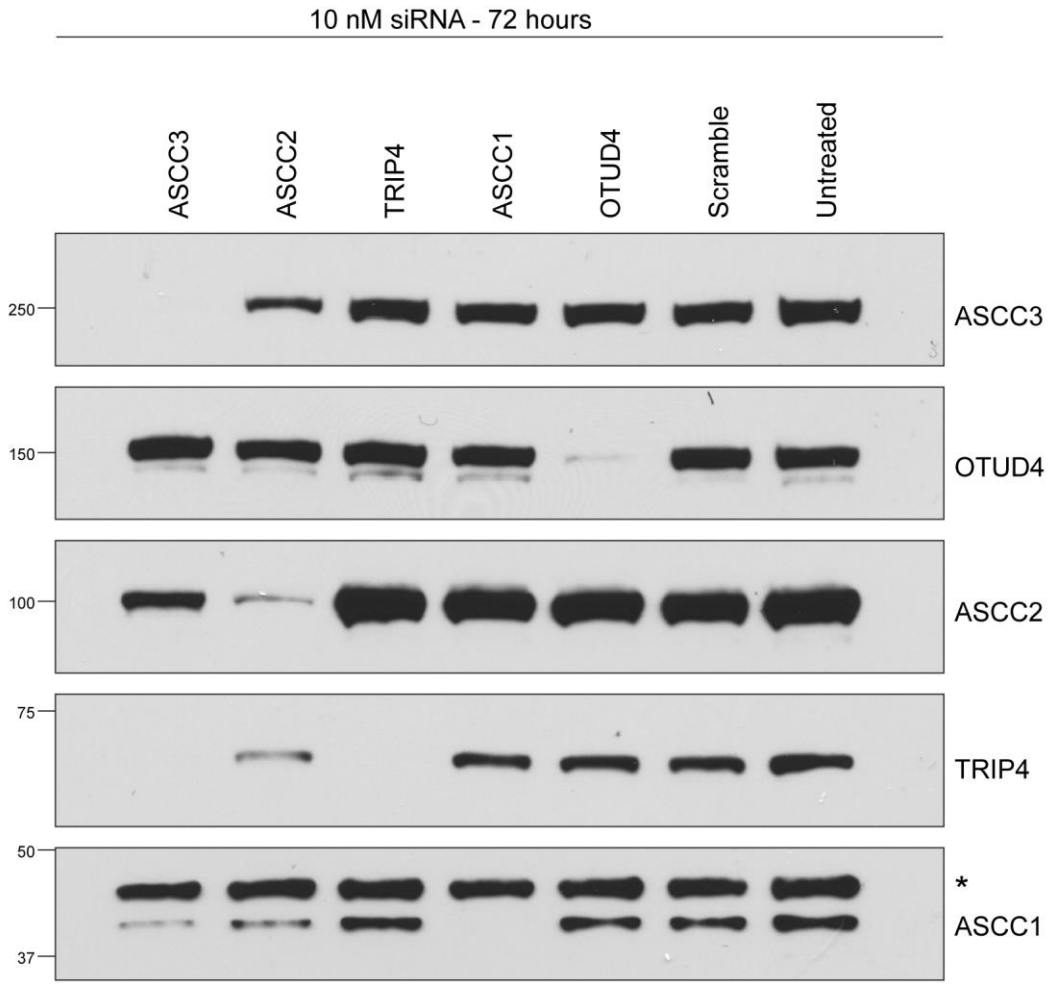

Figure 5-9. ASC-1 complex stability following siRNA component depletion
Reverse siRNA transfection of HeLa cells with 10 nM siRNA for ASCC3, ASCC2, TRIP4, ASCC1, OTUD4, and scramble negative control DsiRNA for 72 hours. Showing effective protein depletion in their respective samples when compared to the untreated or scrambled. * = non-specific band.

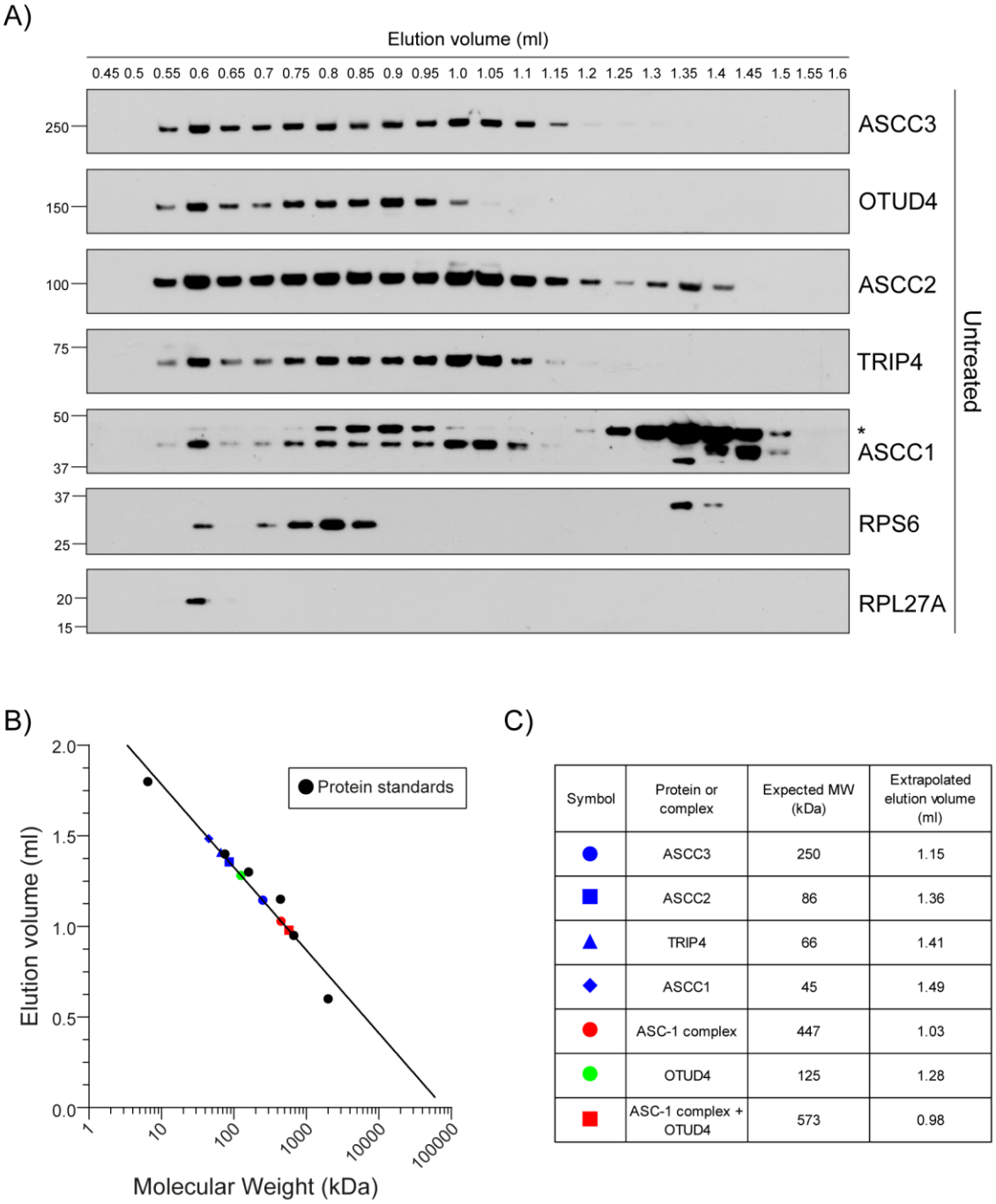

Symbol	Protein or complex	Expected MW (kDa)	Extrapolated elution volume (ml)
●	ASCC3	250	1.15
■	ASCC2	86	1.36
▲	TRIP4	66	1.41
◆	ASCC1	45	1.49
●	ASC-1 complex	447	1.03
●	OTUD4	125	1.28
■	ASC-1 complex + OTUD4	573	0.98

Figure 5-10. SEC analysis and elution predictions of the ASC-1 complex with OTUD4

A) Immunoblot of untreated samples separated by SEC using a Superose 6 (increase 3.2/300) column showing proteins detected in eluted fractions by volume. ASC-1 complex co-localises between 1.0-1.05 ml, and at 0.6 ml with OTUD4 and RPL27A. B) The relationship between protein standard molecular weight and elution volume was used to generate a standard curve which allows extrapolation of elution volume values deduced by molecular weight. C) Predicted elution volumes of ASC-1 complex components, the ASC-1 complex, OTUD4, and ASC-1 complex with interacting OTUD4 are shown as a table. * = non-specific band.

5.6 OTUD4 sucrose gradient analysis

Work within the Willis laboratory has demonstrated using sucrose density gradient ultracentrifugation that ASCC3 and other components of the ASC-1 complex change localisation from sub-polysome to polysome containing fractions in response to UVB irradiation or 4NQO treatment when compared to control (Stoneley *et al*, unpublished data). ASCC3-3xFLAG interaction data suggests that OTUD4 is a putative protein interactor, however, further immunoaffinity purification data (Figure 5-8) and ASC-1 complex depletion (Figure 5-9) studies suggest that OTUD4 has limited interaction with the ASC-1 complex, and is not required for ASC-1 complex stability (Figure 5-9). Interestingly, OTUD4 demonstrated co-localisation with the ASC-1 complex at a high molecular weight elution volume using SEC (Figure 5-10). It was therefore important to determine whether OTUD4 demonstrated the same localisation to the polysomes following stress as other ASC-1 complex components (Stoneley *et al*, unpublished data). Furthermore, using cell lines expressing OTUD4(WT)-3xFLAG and OTUD4(C45A)-3xFLAG may aid an understanding of whether OTUD4 catalytic activity is required for this function. Sucrose density gradient analysis was carried out on HeLa cells (Figure 5-11A), HeLa cells expressing OTUD4(WT)-3xFLAG (Figure 5-11B), and HeLa cells expressing OTUD4(C45A)-3xFLAG (Figure 5-11C) which had been untreated or treated with 4NQO. In samples from all HeLa cell variants, a large increase in 80S ribosome population and reduction in polysomes was seen in 4NQO treated cells when compared to control. In all three HeLa cell variants, ASCC3 demonstrated robust re-localisation to the polysome fractions following 4NQO treatment. Endogenous OTUD4 demonstrated a subtler re-localisation to the polysomes than ASCC3, but a proportion was also located in the 80S fraction. Exogenous OTUD4(WT)-3xFLAG recapitulated the result seen by its endogenous counterpart, with a subtle shift into the polysome fractions and small but noticeable 80S ribosome population. OTUD4(C45A)-3xFLAG demonstrated a proportion of detected protein re-localised to the polysome fractions with a limited population present in the 80S fraction.

Densitometric analysis was carried out to show the percentage distribution of ASCC3, RPS6, RPL11, and OTUD4 (endogenous and exogenous) across the gradient fractions. These data show a significant re-localisation of ASCC3 into the polysome fractions and reproducible reduction in polysomes following 4NQO treatment (Figure 5-12A). Analysis of endogenous OTUD4, OTUD4(WT)-3xFLAG, or OTUD4(C45A)-3xFLAG, further reinforced the observations from the immunoblot directly. Endogenous OTUD4 localises to the 80S ribosome fraction following 4NQO treatment, with only a small amount in the polysome fractions, exogenous OTUD4(WT)-3xFLAG

localises to the 80S ribosome fraction and polysome fractions, and exogenous OTUD4(C45A)-3xFLAG localises to the polysome fractions, with only a small amount in the 80S fraction (Figure 5-12B). Overall, these data show that ASCC3 localises to the polysome fractions following 4NQO treatment. OTUD4 also demonstrates a localisation to the 80S and polysomes following 4NQO treatment, albeit to a lesser extent than ASCC3. Comparison of endogenous OTUD4 distribution to OTUD4(WT)-3xFLAG or OTUD4(C45A)-3xFLAG shows that endogenous protein localises more to the 80S fraction than polysome fractions, which is recapitulated by OTUD4(WT)-3xFLAG but not OTUD4(C45A)-3xFLAG. This may indicate that the catalytic activity is required for interaction with the 80S ribosome. However, these small changes may be caused by poor protein recovery following precipitation. Overall, further work is required to adequately determine the exact localisation profile of OTUD4 following conditions of stress.

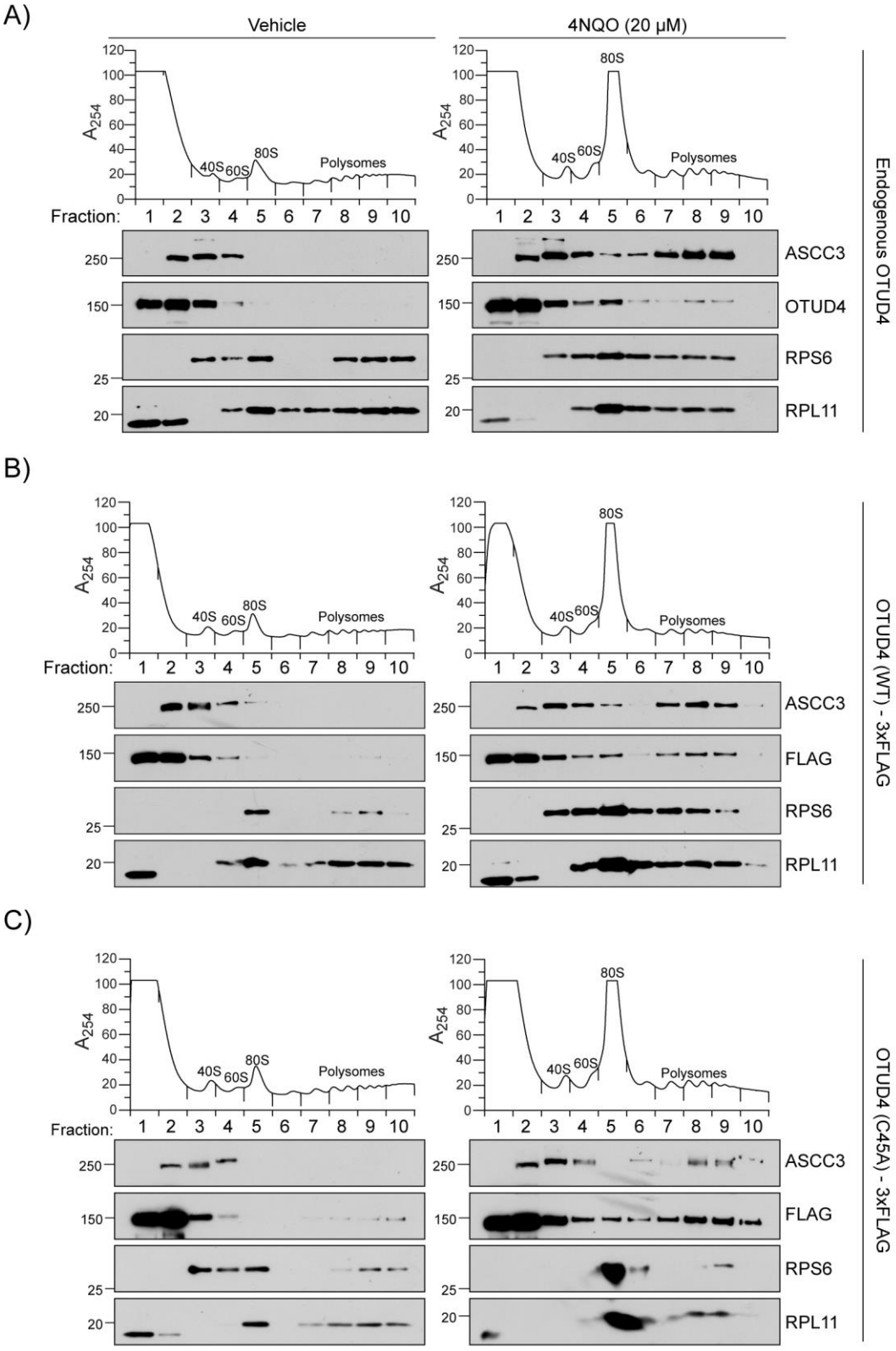

Figure 5-11. ASCC3 and OTUD4 sucrose density gradient profiling

Analysis of ASCC3 and OTUD4 sucrose gradient localisation comparing untreated to 4NQO (20 µM) treated HeLa cells. Endogenous, exogenous WT, and exogenous C45A OTUD4 were all examined in separate samples. ASCC3 reproducibly co-localises to the polysome fractions (fractions 7-9) following 4NQO treatment. OTUD4 follows a similar localisation pattern to ASCC3 but displays small but distinct differences between the samples.

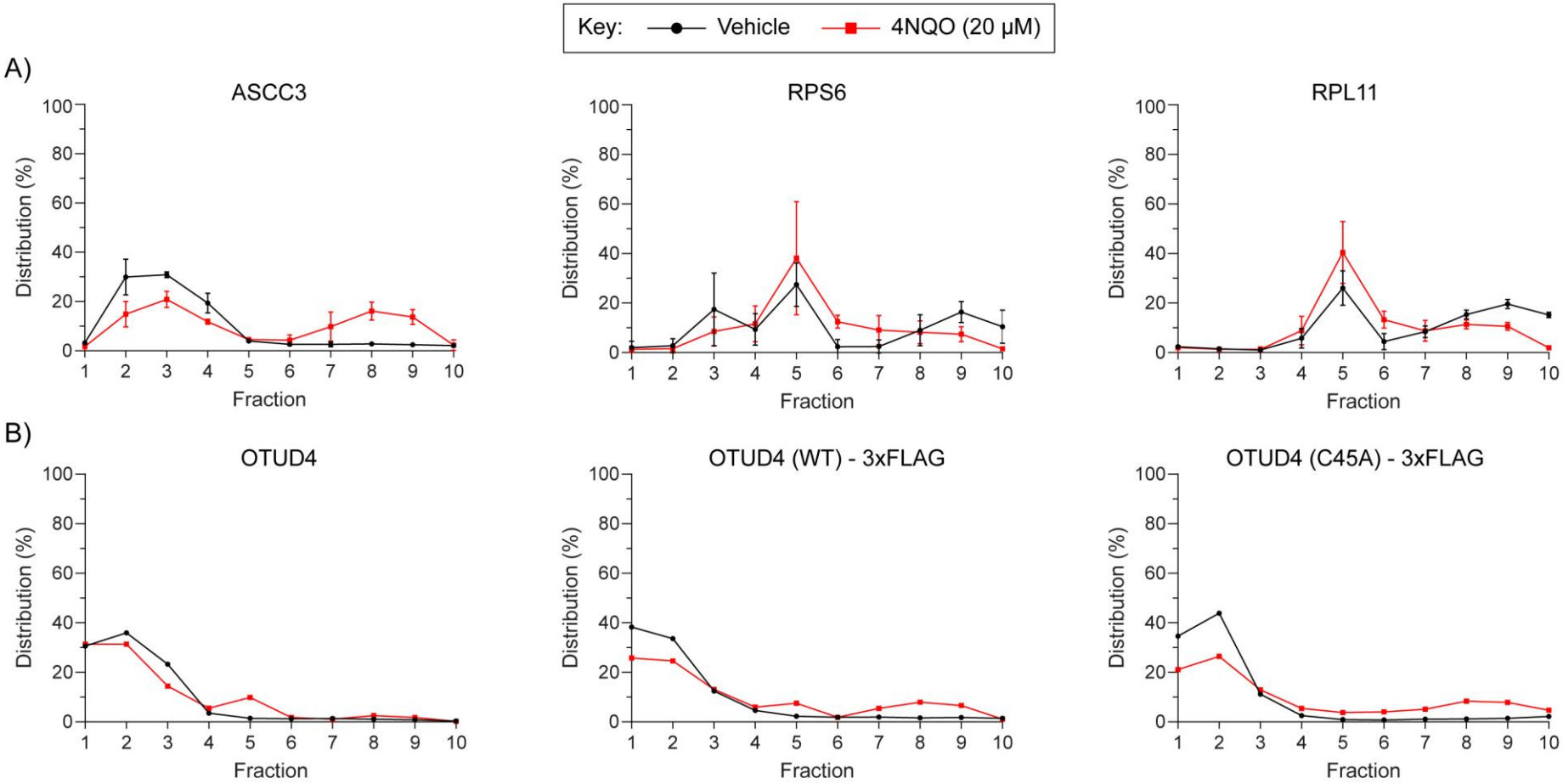

Figure 5-12. Densitometry analysis of ASCC3 and OTUD4 sucrose density gradient profiling

A) Combined polysome profiling densitometry analysis of ASCC3, RPS6, and RPL11, in untreated (black) and 4NQO (20 µM) treated (red) HeLa cells, displaying mean and SD. B) Polysome profiling densitometry analysis of endogenous OTUD4, OTUD4(WT)-3xFLAG, and OTUD4(C45A)-3xFLAG, from untreated (black) and 4NQO (20 µM) treated (red) HeLa cells.

5.7 OTUD4 phenotypic properties

5.7.1 Localisation of OTUD4 following stress

OTUD4 contains the OTUD domain present in its N-terminus, which harbours the catalytic cysteine residue (Zhao *et al.* 2015), and the more central TUDOR domain is thought to enable protein-protein interactions through binding of methyl- arginine and lysine residues (Pek *et al.* 2012). Processing of the OTUD4 amino acid sequence through the NetNES prediction server (La Cour *et al.* 2004) predicted a previously uncharacterized nuclear export signal (NES) (Figure 5-13A). The NES may contribute to the differentiation of the nuclear and cytoplasmic roles of OTUD4. Therefore, to understand the conditions which causes nuclear export of OTUD4 to the cytoplasm, HeLa cell fractionation was carried out following stress induction. Thus, DDR was induced with 4NQO, the unfolded protein response with tunicamycin, and starvation with HBSS, using concentrations previously described (Park 2014; Shinjo *et al.* 2013; Wu *et al.* 2013) (Figure 5-13B). Cells were fractionated following treatment as assessed by the distribution of β-tubulin, GAPDH, and histone H3. Tunicamycin and 4NQO showed no change in nuclear-cytoplasmic distribution of OTUD4 when compared to control, whereas starvation with HBSS caused an increase in the nuclear population of OTUD4. These data were recapitulated by immunofluorescence of HeLa cells under the same conditions (Figure 5-13C). Overall, conditions of cell stress did not cause any re-localisation of OTUD4 from the nucleus to the cytoplasm, in fact, OTUD4 localises to the nucleus during conditions of starvation.

A)

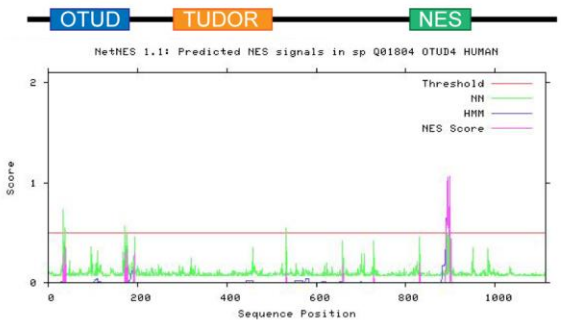

B)

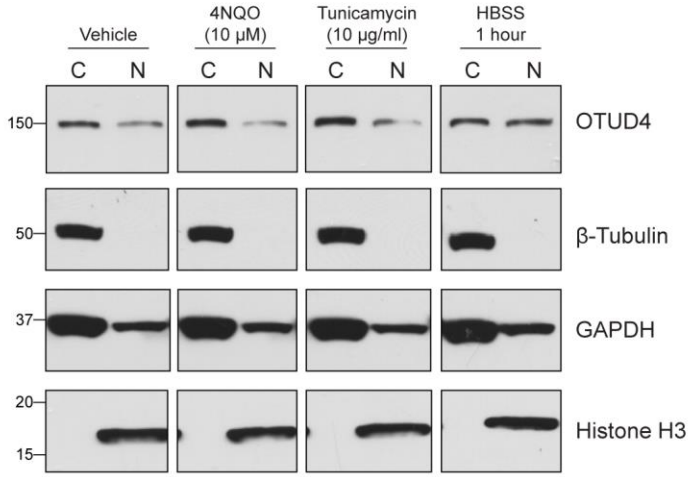

C)

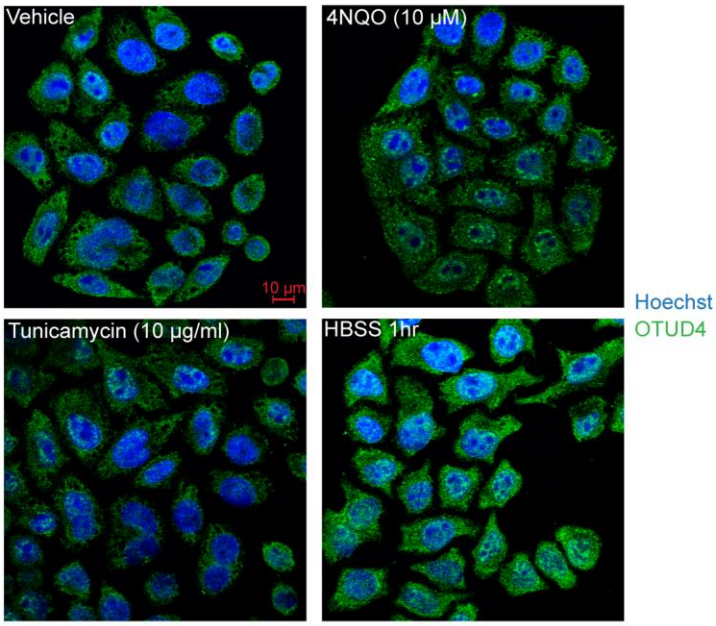

Figure 5-13. Cellular localisation of OTUD4 following stress

A) Domain schematic of OTUD4 showing the NES location that passed the score threshold in NetNES. B) HeLa cell cytoplasmic/nuclear fractionation following 1-hour treatment with vehicle, 4NQO (10 µM), tunicamycin (10 µg/ml), or HBSS. C) HeLa cell immunofluorescence following 1-hour treatment with vehicle, 4NQO (10 µM), tunicamycin (10 µg/ml), or HBSS. Blue shows Hoechst stained DNA, green shows OTUD4 staining (sigma # HPA036623), scale shown in red within the vehicle panel and is uniform across all samples.

5.7.2 Proliferation following OTUD4 depletion

To determine whether OTUD4 was essential for cell growth and survival, the effect on proliferation was monitored following depletion of OTUD4 over 72 hours. Crystal violet staining is a well understood technique for determining cell biomass (Feoktistova *et al.* 2016), leading to a direct correlation between stain intensity and number of cells. Following staining, HeLa cells appeared purple under the microscope (Figure 5-14A). HeLa cells were grown in triplicate in 96 well plates for up to 72 hours, with time points taken at 24, 48, and 72 hours before cell number was inferred from crystal violet absorbance at 540 nm. Cells were RNAiMAX treated (Figure 5-14B, labelled untreated), scramble negative control DsiRNA treated, or treated with one of the three OTUD4 siRNA used previously (Figure 5-1). siRNA concentrations in the range of 50-2.5 nM were used to determine the effect on cell proliferation. Untreated samples were used to determine a baseline level of proliferation for HeLa cells that could be used to understand the effect of siRNA treatment (Figure 5-14B). However, scramble negative control DsiRNA demonstrated a dose-dependent reduction in cell proliferation when compared to untreated cells (Figure 5-14C), with each OTUD4 siRNA recapitulating this result, albeit to a lesser extent. Overall, this data demonstrated that OTUD4 is not essential for cell viability, however, its putative role in cell proliferation is difficult to interpret using siRNAs.

5.7.3 Protein synthesis following OTUD4 depletion

Recent studies identified OTUD4 as an RNA-binding protein, but also demonstrated that OTUD4 was fundamental for global protein synthesis, as demonstrated by puromycylation of endogenous proteins following OTUD4 depletion (Das *et al.* 2019). To measure the effect of OTUD4 depletion on protein synthesis, puromycylation was used. Upon entry into the cell, puromycin is incorporated into newly synthesised proteins and can be detected with anti-puromycin antibodies. Immunoblot analysis, and quantification of puromycylation levels gives a direct measure of protein synthesis rates within a given time. Comparison of puromycylation levels between HeLa cell treated with either 5nM of firefly luciferase siRNA or OTUD4 siRNA #1 for 72 hours, demonstrated no changes in protein synthesis in OTUD4 depleted samples when compared to the firefly luciferase siRNA treated sample. (Figure 5-15A). Firefly luciferase was used as a negative control to prevent off target effects of siRNA sequence, as previously used scramble negative control DsiRNA had demonstrated dose-dependent reduction in HeLa cell proliferation (Figure 5-14C). The inhibitor of elongation, Cycloheximide (10 µg/ml), was used as a positive control and demonstrated a 100% reduction in puromycin incorporation (Figure 5-15A). Densitometry analysis confirmed this interpretation of the data (Figure 5-15B). Overall, depletion of OTUD4 appeared to have no effect on cellular protein synthesis.

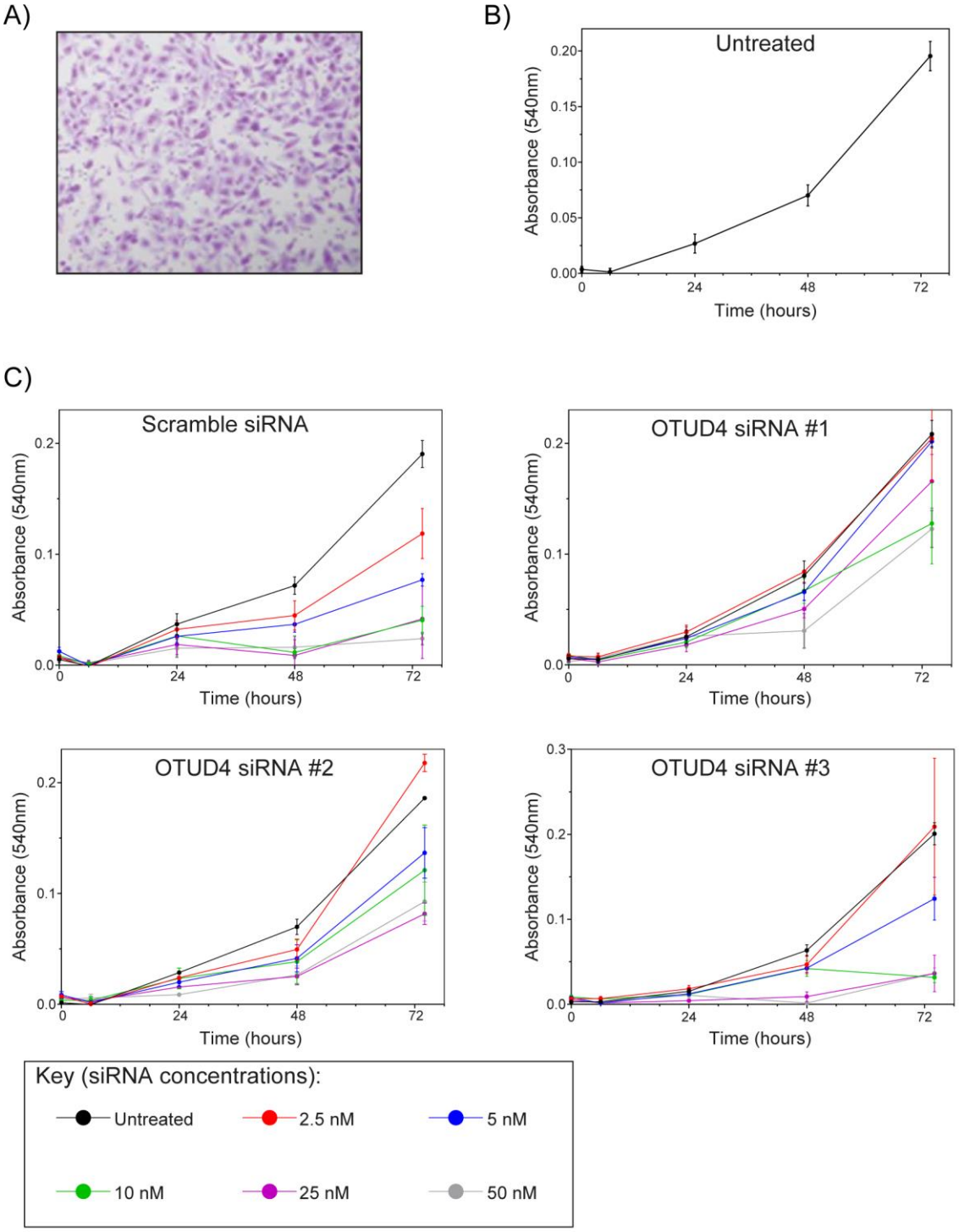

Figure 5-14. Analysis of OTUD4 depletion on HeLa cell proliferation

A) Image of HeLa cells following PFA fixation, staining with crystal violet, and washing with H_2O. B) Crystal violet absorbance of untreated cells grown over 72 hours with a time point taken every 24 hours, representing HeLa cell basal proliferation. C) Graphs showing growth curves for scramble negative control DsiRNA, OTUD4 siRNA #1, #2, and #3 dose dependent treatment of HeLa cells over 72 hours; time points were taken every 24 hours. These data show that each siRNA effects HeLa cell proliferation in a dose dependent manner when compared to untreated cells.

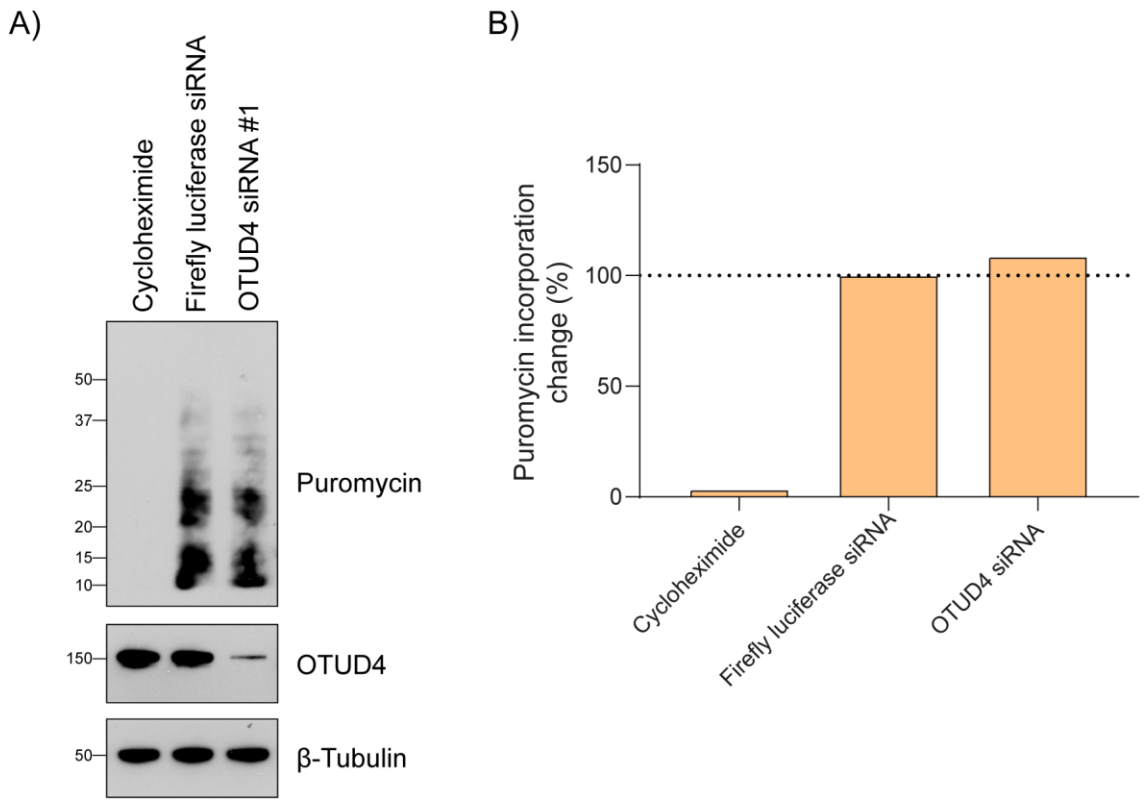

Figure 5-15. Effect of OTUD4 depletion on puromycylation levels

A) Immunoblot analysis of puromycylation levels for cycloheximide (10 µg/ml), firefly luciferase (5 nM), and OTUD4 siRNA #1 (5 nM) treated cells. Showing limited changes in puromycin detection following OTUD4 depletion B) Densitometry analysis showing percentage change in puromycylation levels between the conditions when compared to the firefly luciferase siRNA treated sample.

5.8 Discussion

The main aims of this chapter were to demonstrate the role of OTUD4 as a component of the ASC-1 complex, while also attempting to determine a mechanistic cellular role for OTUD4. OTUD4 has previously been identified in the cytoplasm as a deubiquitinase of MyD88 (Zhao *et al.* 2018) and of MAVs (Liuyu *et al.* 2019), demonstrating a role in immune response signalling. More recent developments identified OTUD4 as an RBP (Baltz *et al.* 2012; Das *et al.* 2019; Liepelt *et al.* 2016), showing localisation to stress granules following stress, and a role in cellular protein synthesis. Furthermore, in support of this data, OTUD4 has been characterised as an RBP here, however, unlike ASCC3 this interaction was not affected by UVB irradiation (Figure 5-4). In a similar manner to the ASC-1 complex, OTUD4 has been identified with roles in both the nucleus (Zhao *et al.* 2015) and the cytoplasm (Das *et al.* 2019; Liuyu *et al.* 2019; Zhao *et al.* 2018), with some data also showing that OTUD4 interacts with ASCC3, ASCC2, and ASCC1 in the mouse cerebellum (Das *et al.* 2019). Therefore, to ensure a focus on cytoplasmic ASC-1 complex and OTUD4 was maintained, isolation of cytoplasmic OTUD4 was demonstrated by fractionation (Figure 5-5A). Immunoaffinity purification of cytoplasmic OTUD4 was inefficient but demonstrated a potential interaction with ASCC3 and ASCC2 (Figure 5-5B). Inducible stable HeLa cell lines for wild-type OTUD4 (OTUD4(WT)-3xFLAG) and catalytic inactive mutant OTUD4 (OTUD4(C45A)-3xFLAG) were created (Figure 5-6 and 5-7), to allow more efficient immunoaffinity purification of OTUD4 and examination of ASC-1 complex co-purification, while also determining if OTUD4 catalytic activity was required for this action. Immunoaffinity purification of these exogenous proteins was initially unable to co-purify ASC-1 complex components (Figure 5-8A). A change of purification conditions demonstrated that both exogenous OTUD4 proteins were able to co-purify ASCC3, ASCC2, and TRIP4 (Figure 5-8B), however, they were not depleted from the unbound fraction, suggesting that a proportion of cellular OTUD4 is not present in the ASC-1 complex, the interaction is transient and is only required under specific conditions, or that this interaction requires other factors, such a post translational modifications which are removed in the lysate. This is further supported by the stability of ASCC2, TRIP4, and ASCC1, but not OTUD4, being dependent on ASCC3, as demonstrated by depletion of ASCC3 (Figure 5-9). SEC analysis of untreated cell lysate demonstrated that OTUD4 co-localises with the ASC-1 complex present in the high-molecular weight fractions, that also co-localises with ribosomal proteins (Figure 5-10). However, OTUD4 does not co-localise with a population of the ASC-1 complex that has a predicted elution volume consisting of a 1:1:1:1 ratio of ASCC3, ASCC2, TRIP4, and ASCC1 (Figure 5-10). Sucrose density gradient analysis of ASCC3 and OTUD4 (endogenous and exogenous) also supported this

hypothesis, firstly showing that a significant population of ASCC3 re-localised from sub-polysome to polysome fractions following 4NQO treatment (Figure 5-11 and 5-12), and secondly, showing that a small amount of total endogenous OTUD4, OTUD4(WT)-3xFLAG, or OTUD4(C45A)-3xFLAG re-localises to the polysome fractions following 4NQO treatment, which may suggest that only a small amount of total OTUD4 interacts with ASCC3.

Domain analysis of OTUD4 revealed a previously undescribed NES in the C-terminal of the protein (Figure 5-13A). Treatments were used to examine the localisation of OTUD4 under conditions of stress by fractionation and immunofluorescence (Figure 5-13B and 5-13C). Interestingly, the distribution of OTUD4 changed upon cell starvation, with more in the nucleus when compared to the control, but no evidence of nuclear export in response to stress was demonstrated. Previous work also demonstrated that depletion of OTUD4 led to a significant reduction in cellular protein synthesis and induced caspase-3 activation (Das *et al.* 2019). Data within this chapter suggests that siRNA depletion of OTUD4 does appear to have an effect on cell proliferation, but this is more likely to be related to the dose of siRNAs used and it may not be a physiological consequence of OTUD4 protein depletion (Figure 5-14). Moreover, depletion of OTUD4 had no effect on protein synthesis levels when compared to control (Figure 5-15).

To conclude, the data in this chapter demonstrates that only a small proportion of cytoplasmic OTUD4 interacts with the ASC-1 complex, the interaction between OTUD4 and the ASC-1 complex is transient, or that specific conditions are required to capture this interaction and are lost upon generation of the cytoplasmic extract. These data also demonstrates that OTUD4 is most likely not essential for cell proliferation or protein synthesis, which challenges previous studies (Das *et al.* 2019). Although these data highlight the interaction between the cytoplasmic ASC-1 complex and the deubiquitinase OTUD4, further work is required to accurately determine the function of the OTUD4 as part of the ASC-1 complex.

6. Post-translational modifications of ASCC3

6.1 Introduction

Previous studies have demonstrated that there are changes in the ubiquitin status of ASCC3 following UVC irradiation (Boeing *et al.* 2016). These data are consistent with the additional bands of RNA-bound ASCC3 of a higher molecular weight, which are induced by UVB, Cisplatin, or 4NQO treatment (Figure 3-11). Other factors that suggest that ASCC3 and or the ASC-1 complex are controlled by ubiquitination include that ASCC2 contains a ubiquitin binding domain (CUE domain), ASCC3 interacts with the deubiquitinase OTUD4, and the role of the ASC-1 complex in RQC, which is a highly ubiquitin dependent process (Juszkiewicz & Hegde 2017; Sundaramoorthy *et al.* 2017). The aims of the research shown in this chapter were to determine if ASCC3 is ubiquitinated in response to 4NQO treatment, and to further understand the function of this modification.

6.2 Deubiquitination of ASCC3

6.2.1 In vitro deubiquitination

As discussed above, a number of lines of evidence suggest that the ASC-1 complex and in particular ASCC3 are ubiquitinated. To confirm that ASCC3 was ubiquitinated, a method determining protein ubiquitination linkage specificity by using specific deubiquitinases was employed (UbiCRest) (Hospenthal *et al.* 2015; Mevissen *et al.* 2013). This method utilises two deubiquitinases, USP21 or USP2, since they display non-specific degradation of ubiquitin chains. In initial control experiments the activity of USP2 catalytic domain ($USP2_{CD}$) was determined using two concentrations of recombinant biotinylated tetra-ubiquitin chains as substrates (Figure 6-1A). Importantly, $USP2_{CD}$ was able to degrade the tetra-ubiquitin chains in a dose dependent manner, with 1 µM of enzyme degrading the most ubiquitin chains into mono-ubiquitin molecules (Figure 6-1A).

6.2.2 Deubiquitination of RNA-bound ASCC3

As shown previously (Figure 3-11), addition bands of RNA-bound ASCC3 at a higher molecular weight are induced by UVB, Cisplatin, or 4NQO treatment. Following successful degradation of ubiquitin chains by $USP2_{CD}$ in a dose dependent manner, the assay was applied to RNA-bound ASCC3, which was isolated by performing RIC on cells treated with 4NQO to determine whether ASCC3 was ubiquitinated. RIC samples were treated with 1, 0.1, or 0 µM $USP2_{CD}$ (Figure 6-1B). Treatment of the samples with $USP2_{CD}$ had no effect on the higher molecular weight bands of

ASCC3 when compared to the untreated sample, suggesting that either ASCC3 was not ubiquitinated, or that $USP2_{CD}$ was unable to remove ubiquitin molecules under these conditions.

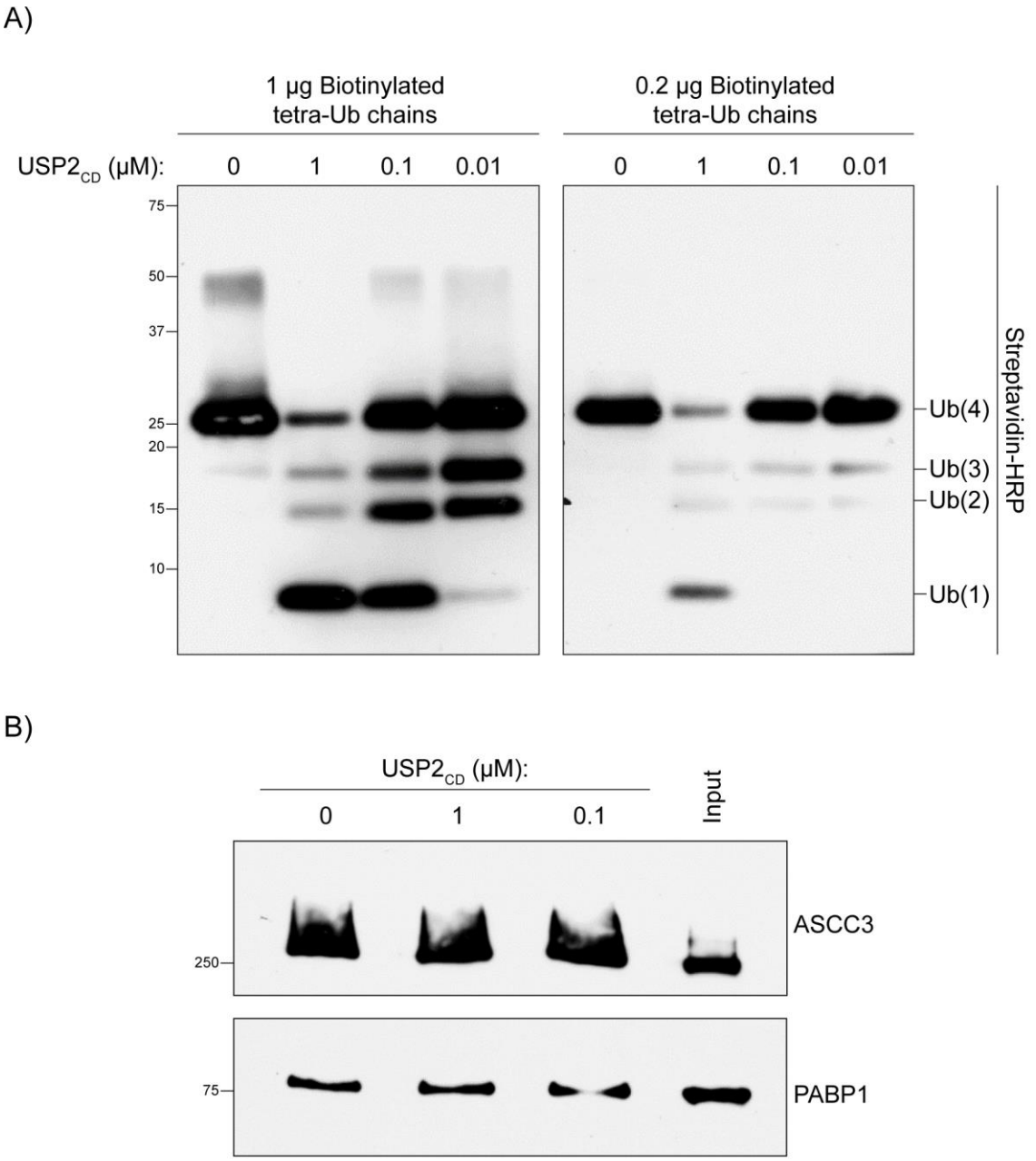

Figure 6-1. Deubiquitination of RNA-bound ASCC3

A) *In vitro* deubiquitination assay using $USP2_{CD}$ at 1, 0.1, and 0.01 µM to degrade 1 and 0.2 µg K63 tetra-ubiquitin chains. Ubiquitin chains are degraded in a $USP2_{CD}$ dose dependent manner to individual ubiquitin molecules. B) A sample from a 4NQO (20 µM) treated RIC assay was treated with varying concentrations of $USP2_{CD}$ using the conditions from (A), showing that the additional series of bands for ASCC3 is not depleted following $USP2_{CD}$ treatment.

6.3 Ubiquitination of ASCC3

6.3.1 6xHis-ubiquitin constructs

To further clarify that ASCC3 was ubiquitinated five ubiquitin constructs were generated with six histidine residues (his-tag) present at the N terminus of the ubiquitin molecule, so as not to interrupt the ubiquitination process. His-tags allow for denaturing purification of exogenous proteins, in this case his-tagged ubiquitin may be isolated with covalently attached proteins.

In total five ubiquitin constructs were created and inserted into the pcDNA5/FRT/TO vector. These constructs consisted of wild-type, and 4 mutants: K48R, K63R, K48R/K63R, or finally K0 (conversion of all lysine residues to arginine) (Figure 6-2A) and were used to determine the ubiquitin linkage specificity of ASCC3. DNA fragments containing the his-tagged ubiquitin constructs were separately cloned into the pcDNA5/FRT/TO vector using restriction enzyme sites present in the multiple cloning site (Figure 6-2B). When transiently expressed and analysed by immunoblot, wild-type exogenous ubiquitin showed expression and incorporation into the proteome, while K0 exogenous ubiquitin showed an extremely poor expression level (Figure 6-2C). The expression levels of these constructs appeared to correlate with the number of lysine to arginine mutations present within the exogenous ubiquitin.

6.3.2 Purification of his-tagged ubiquitin

Purification of expressed his-tag proteins can be carried out using immobilised metal ions such as nickel, cobalt, and copper. Specific buffer conditions allow the interaction of the his-tag with the metal ions, and these buffer conditions can be altered to allow competitive elution of the proteins from the immobilised metal. Commercially available anti his-tagged antibodies allow detection of these proteins.

Proteins were isolated from cells using his-tag lysis buffer (Illana & Farhaeus 2012), and transiently expressed his-tag ubiquitin (WT) was purified from untreated or 4NQO (20 µM) treated samples using magnetic cobalt beads (Figure 6-3A). Preliminary data showed isolation of ASCC3 from cells with expressed his-tag ubiquitin was increased with 4NQO treatment, whereas, cells transfected with an empty plasmid vector showed no isolation of ASCC3 (Figure 6-3A). Detection of his-tag ubiquitin modified proteins by his-tag immunoblot was inefficient for both purification and input, therefore it was suspected that proteins were poorly extracted by this lysis method. The lysis buffer was exchanged for whole cell lysis buffer, and the experiment repeated (Figure 6-3B). His-tag ubiquitin modified proteins were more easily detected in the purification and input samples, and ASCC3 was more easily identified in the input samples.

However, the detection of purified ASCC3 by his-tag ubiquitin was difficult as demonstrated by the short (SE) and long exposures (LE) by immunoblotting. However, this technique still demonstrated increased isolation of ASCC3 in response to 4NQO, importantly, these experiments detail the potential ubiquitination of ASCC3 extracted from a whole cell extract. Further, optimisation is required to determine if this response takes place in the cytoplasm.

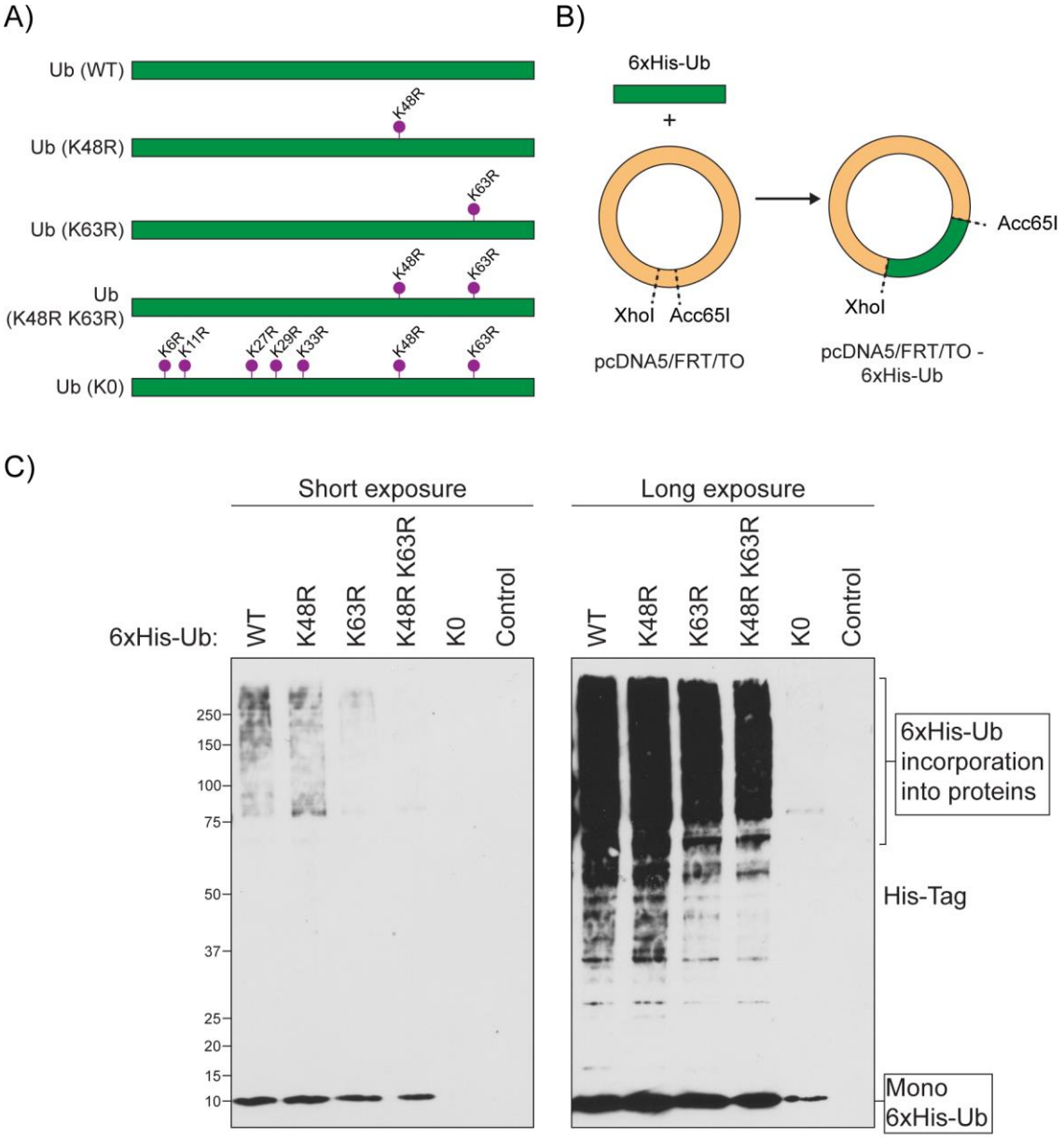

Figure 6-2. Construction and transient expression of his-tagged ubiquitin constructs

A) Five ubiquitin constructs (green) showing the mutated lysine residues (purple). B) Schematic showing the molecular cloning procedure of his-tagged ubiquitin into pcDNA5/FRT/TO. C) Transient expression of the five ubiquitin constructs in HeLa cells showing their relative expression level and incorporation level into the proteome, as determined by his-tag immunoblot. There is correlation between number of ubiquitin mutations and incorporation of ubiquitin into endogenous proteins.

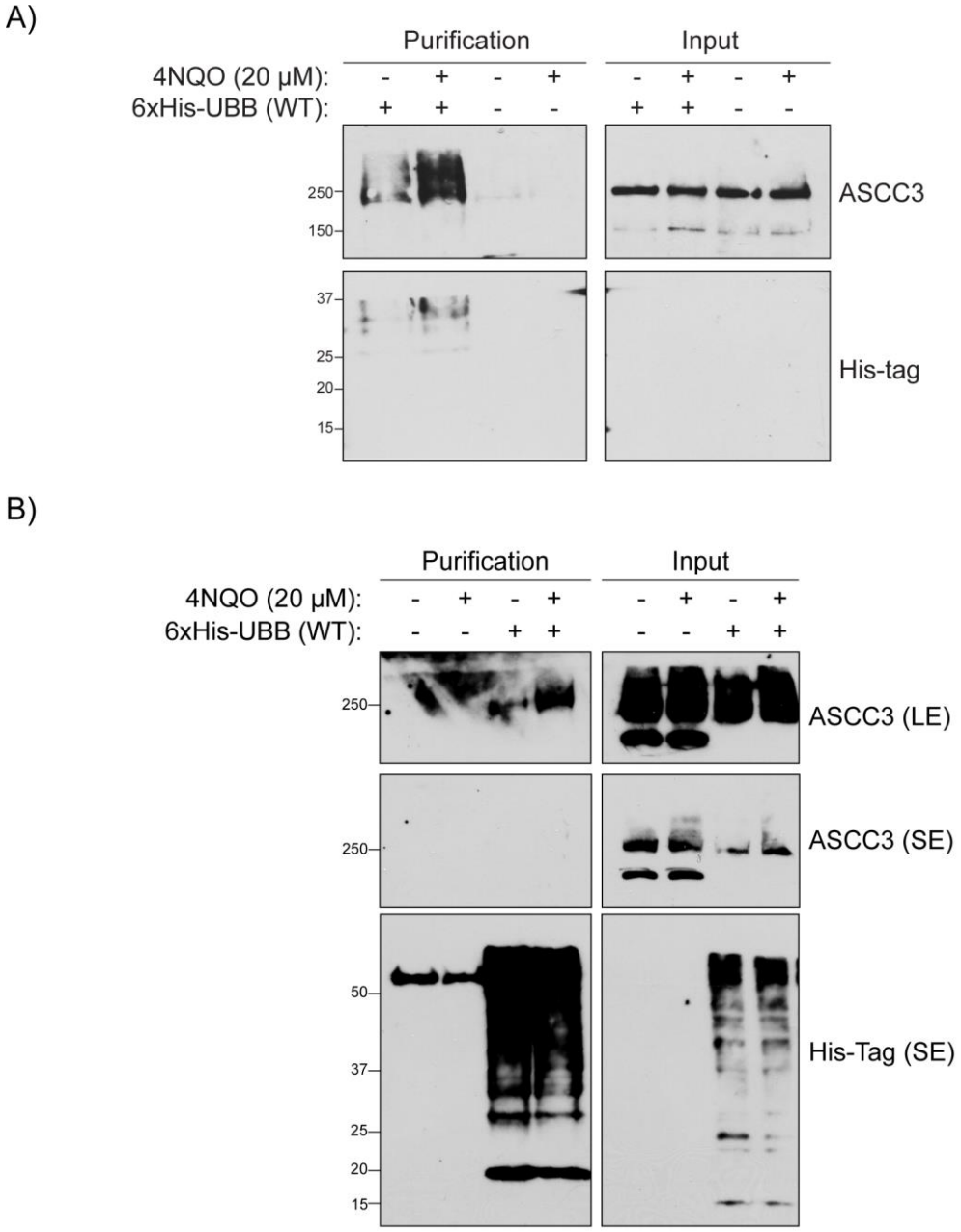

Figure 6-3. Affinity isolation his-tag ubiquitinated proteins

A) Isolation of transiently expressed his-tag ubiquitin and attached proteins from a his-tag lysate using cobalt magnetic beads, comparing samples from untreated to 4NQO (20 µM) treated HeLa cells. Showing an increased purification of ASCC3 following 4NQO treatment. B) Experiment (A) repeated from a whole cell lysate, showing improved detection of his-tag by immunoblot and ASCC3 in the input. Detection of ASCC3 was increased in the 4NQO treated purification but was difficult detect as shown by short (SE) and long (LE) exposures.

6.3.3 Purification of endogenous ubiquitinated proteins

Although the overexpression of ubiquitin with an epitope tag provides preliminary evidence for the ubiquitination potential of a protein of interest, this method does not provide direct evidence of physiological ubiquitination. Tandem ubiquitin-binding elements (TUBEs) are tandem ubiquitin-binding associated (UBA) domains with high specificity to ubiquitin chains (Hjerpe *et al.* 2009). Therefore, TUBEs present in lysis buffers protect ubiquitin chains from native deubiquitinases and can be used for effective isolation of proteins with ubiquitin chains.

His-tagged TUBEs were incubated with lysates from untreated or 4NQO treated cells before their purification using cobalt magnetic beads (Figure 6-4A). Treatment of cells with 4NQO showed increased isolation of ASCC3 when compared to the untreated cells (Figure 6-4A lanes 3 & 4). However, ASCC3 was also purified by the cobalt beads in the absence of TUBEs (Figure 6-4A lanes 1 & 2). Endogenous ubiquitinated proteins are only isolated in this assay when TUBEs are present in the lysis buffer (Figure 6-4A, compare lanes 1 and 2 to 3 and 4), indicating that the TUBEs selectively purify ubiquitinated proteins. Moreover, the input demonstrates there was a small increase in ubiquitinated proteins in lysates containing TUBEs, which suggests that TUBEs are protecting ubiquitin chains from deubiquitinases present within the lysate.

The detection of ASCC3 in the absence of TUBEs suggests potential non-specific interaction between ASCC3 and cobalt magnetic beads. Therefore, equal volumes of His-tag, protein G, and Oligo(dT) magnetic beads were incubated with HeLa cell extracts prepared using TUBEs lysis buffer to assess the background binding of ASCC3 (Figure 6-4B). Detection of ASCC3 and the absence of β-tubulin in His-tag and protein G magnetic bead samples provides evidence for the non-specific binding of ASCC3 to these magnetic beads when isolations are performed using TUBEs lysis buffer. Notwithstanding the above evidence for background binding of ASCC3 to the His-tag magnetic beads, it is clear that more polyubiquitinated ASCC3 is isolated by TUBEs from lysates prepared from 4NQO-treated cells (Figure 6-4A, compare lanes 2 and 4). This observation is consistent with the data from the His-tag ubiquitin purification experiments (Figure 6-3), and suggests that isolation of ubiquitinated ASCC3 using TUBEs warrants further optimisation.

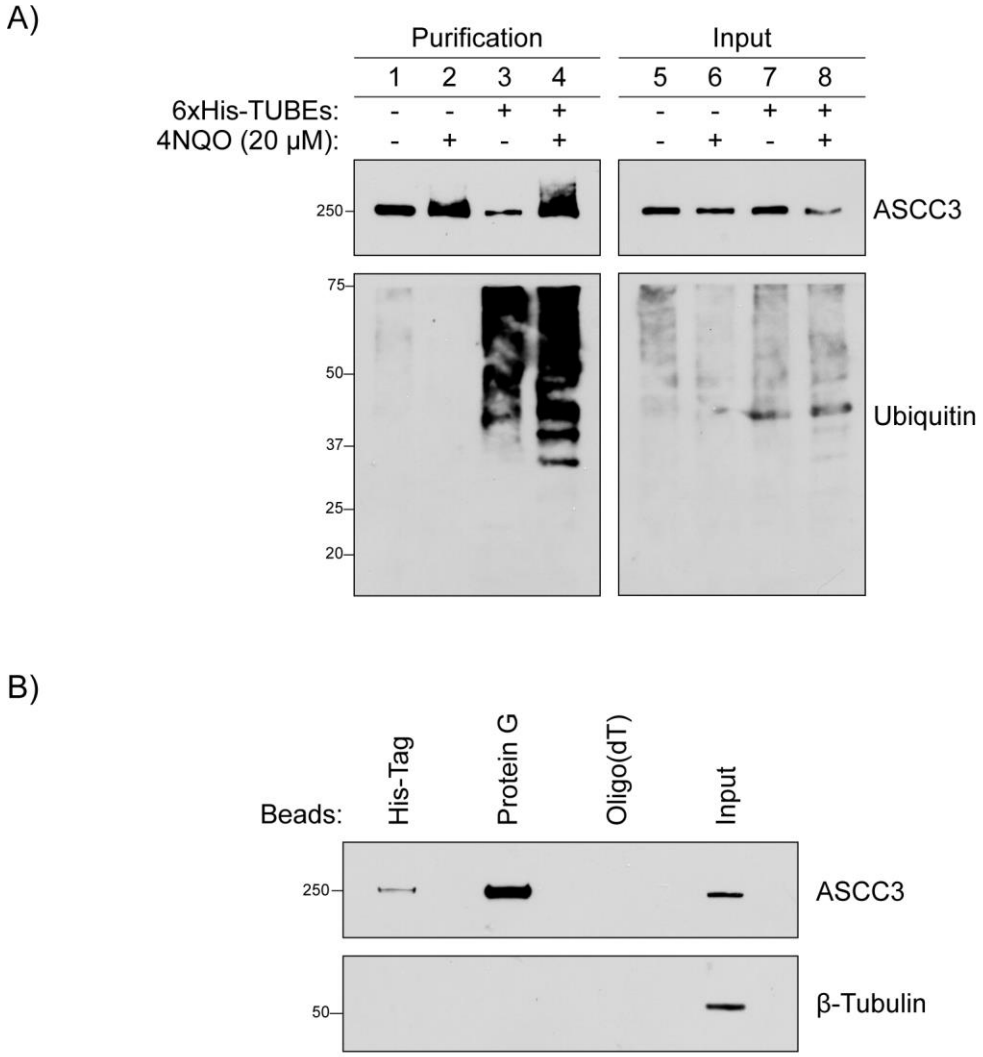

Figure 6-4. Enrichment of ubiquitinated proteins using TUBEs

A) His-tag TUBEs purification of proteins with ubiquitin chains, comparing samples from untreated and 4NQO (20 µM) treated cells, compared this to his-tag purification in the absence of TUBEs. These data show that purification of ubiquitinated ASCC3 is enhanced in response to 4NQO treatment, however, ASCC3 background binding to his-tag beads is a confounding issue. B) Examination of ASCC3 interaction with His-tag, protein G, and Oligo(dT) magnetic beads, showing that ASCC3 can interact with his-tag and protein G magnetic beads.

6.4 Discussion

While previous studies have identified potential ubiquitination sites of ASCC3 in response to UVC irradiation, no direct evidence of ASCC3 ubiquitination has been shown (Boeing *et al.* 2016), together with this data, an additional series of bands detected above RNA-bound ASCC3 (Figure 3-11) was proposed to result from ubiquitin modifications. However, deubiquitination of RNA-bound ASCC3 with non-specific $USP2_{CD}$ caused no change to the migration of ASCC3 (Figure 6-1B). Preliminary his-tag ubiquitin overexpression data suggested ASCC3 was more ubiquitinated in response to 4NQO treatment (Figure 6-3), with direct purification of endogenous ubiquitin using TUBEs also demonstrating that ubiquitin modifications of ASCC3 increased following 4NQO treatment (Figure 6-4A). Unfortunately, technical issues surrounding the detection of purified his-tag ubiquitin, and the non-specific interaction of ASCC3 to magnetic beads (Figure 6-4B), made it challenging to determine whether ASCC3 was ubiquitinated in response to genotoxic stress. Therefore, further technical optimisation is required to adequately determine the ubiquitination status of ASCC3 in response to genotoxic stress.

7. Discussion

In response to agents which result in the addition of bulky adducts to DNA including UVB, Cisplatin and 4NQO, cell survival programs are employed in order to restore and maintain cellular homeostasis. As part of this response, cells change their repertoire of actively synthesised proteins to dictate cell fate (Collier *et al.* 2015; Spriggs *et al.* 2010). While reagents such as UVB, cisplatin and 4NQO are commonly associated with the DDR, these agents are also capable of damaging cytoplasmic RNA by induction of reactive oxygen species (ROS), chemical crosslinking, and bulky adduct addition (Arima *et al.* 2006; Hostetter *et al.* 2012; Wurtmann & Wolin 2009; Yan & Zaher 2019). RNA damage can be detrimental to the cell by preventing base pairing, mRNA decoding, and RNA-binding by RBPs. For example, there is a reduced rate of peptide bond formation by ribosomes on mRNA with 8-oxoG modifications (Simms *et al.* 2014), which are cause by 4NQO treatment (Arima *et al.* 2006), and UVB exposure has been shown to damage ribosome function in prokaryotes and eukaryotes by forming crosslinks in ribosomal RNA (Huggins *et al.* 2005; Iordanov *et al.* 1998). However, the consequences of cytoplasmic RNA damage have not been investigated fully. Any recognition or repair of cytoplasmic RNA damage to rRNA, mRNA, tRNAs, or lncRNAs would require the concerted actions of RNA-binding protein complexes. Therefore, to identify novel proteins involved in these types of process, RIC was carried out following UVB exposure (Stoneley *et al*, unpublished data). ASCC3 was identified as the RBP that showed the greatest change in cytoplasmic RNA-binding in response to UVB irradiation. A number of studies have shown that ASCC3 functions in the nucleus, where it acts as a helicase required for repair of DNA alkylation (Dango *et al.* 2011) and as part of transcription coactivator complexes (Jung *et al.* 2002; Kim *et al.* 1999; Lee *et al.* 2002), however, at the start of this study, a cytoplasmic role for this protein had yet to be fully attributed. On-going research within the Willis laboratory has shown that ASCC3 is present in the ASC-1 complex, and that complex members directly bind RNA in the cytoplasm. The aim of this thesis was to obtain a greater understanding of the cytoplasmic formation of the ASC-1 complex and the role of ASCC3 in this process, and to identify additional binding partners of ASCC3.

The data in this thesis has shown that the response of ASCC3 to UVB exposure was highly conserved, in that ASCC3 increased its affinity for RNA in response to UVB in multiple cell lines derived from different tissues (Figure 3-1). The increased affinity for RNA in response to UVB treatment was also recapitulated with cisplatin and 4NQO, two other reagents known to induce nucleic acid bulky adduct additions (Figure 3-11). Interestingly, modifications which effect the functionality of the decoding centre of the ribosome require Slh1, the yeast homolog of ASCC3, and its ATPase activity to initiate the degradation pathway of non-functional 18S rRNA

(Sugiyama *et al.* 2019). This action also requires rpS3 ubiquitination, which has previously been shown to interact with ASCC3 (Matsuo *et al.* 2017), and was one of the proteins identified by mass spectrometry analysis of immunoaffinity purified ASCC3-3xFLAG (Figure 4-8B). However, the presence of rpS3 in 65% of all immunoaffinity purification datasets within the CRAPome (Table 4-3) (Mellacheruvu *et al.* 2013), made this an unattractive target for further study. During the period that this study was in progress, other research using artificial reporter vectors which cause stalling has shown that Slh1 is required to prevent accumulation of collided ribosomes during NGD (D'Orazio *et al.* 2019). Therefore, it is possible that the increased interaction of ASCC3 with RNA identified herein could result from ribosome stalling induced by chemical damage to mRNA, tRNA, or rRNA. Moreover, as it is well established that di-ribosomes act as the minimal molecular signature to initiate RQC pathways (Ikeuchi *et al.* 2019; Juszkiewicz *et al.* 2018; Simms *et al.* 2017), a possible testable hypothesis is that such di-ribosome formation, as a result of UVB, cisplatin, or 4NQO treatment, could be required for RNA-binding of ASCC3.

Further evidence to support this notion was provided by analysing the distribution of ASCC3 within sucrose density gradients, which showed that a significant proportion of ASCC3 was re-localised to the polysome fractions following 4NQO treatment (Figure 5-11 and 5-12). These fractions could contain collided ribosomes. However, further work would be required to demonstrate that treatment with UVB, cisplatin, or 4NQO causes damage to RNA and thereby induces ribosome stalling and collision. Moreover, identification of the RNA species that are bound by ASCC3 would further advance the understanding of ASCC3 function. This work is currently in progress in the Willis laboratory.

Previous research suggested that the ASC-1 complex is able to interact with the ribosome (Daugeron *et al.* 2011) and polysomes (Matsuo *et al.* 2017), with data from the Willis laboratory (Stoneley *et al* unpublished data) and the data within this thesis providing evidence to support these earlier studies. Thus, the separation of the ASC-1 complex by SEC showed that ASCC3, ASCC2, TRIP4, and ASCC1 co-eluted in high molecular weight fractions (Figure 4-1B). A SEC column that allowed enhanced resolution of high molecular weight macromolecular complexes also demonstrated that ribosomal proteins representative of the 40S and 60S subunits (RPS6 and RPL11 respectively) co-eluted with the ASC-1 complex (Figure 4-2). Furthermore, preliminary data obtained using Mega-SEC analysis (Yoshikawa *et al.* 2018) demonstrated that ASCC3 co-localised with heavy polysomes following 4NQO treatment (data not shown). This co-localisation was lost upon treatment of the sample with RNase T1, indicating that polysomes may be essential for ASCC3 interaction. Again, these data are supported by polysome analysis showing ASCC3 moving into polysome fractions following 4NQO treatment. Interestingly,

preliminary mass spectrometry data was carried out on immunoaffinity isolated ASCC3-3xFLAG from SEC eluates containing the co-localised ASC-1 complex. These data demonstrated an enrichment for ZNF598 and RPS10, two proteins required for induction of the RQC pathway (Juszkiewicz *et al.* 2018; Juszkiewicz & Hegde 2017; Matsuo *et al.* 2017; Sundaramoorthy *et al.* 2017), as well as additional ribosomal protein (data not shown). Further optimisation of this technique may allow identification of other RQC components, elucidating the role of the ASC-1 complex in RQC.

Protein interaction studies of ASCC3-3xFLAG revealed a potential model for ASC-1 complex interaction (Figure 3-6), which challenges previously published data (Brickner *et al.* 2017; Jung *et al.* 2002). Despite this difference, the overall conclusions coincide, showing each component has a direct interaction with ASCC3. siRNA depletion of ASC-1 complex members (Figure 5-9) suggested that the formation and stability of the ASC-1 complex was fundamentally reliant on the presence of ASCC3, and to a lesser degree ASCC2 (Figure 5-9). This recapitulates data from yeast, showing that Slh1 deletion drastically decreased protein levels of Cue3 and YKR023W (ASCC2 and TRIP4 in mammals, respectively), with depletion of Cue3 and YKR023W having only a modest effects on other complex components (Matsuo *et al.* 2017). Interestingly this study also suggests that depletion of Slh1 abolishes the interaction of the ASC-1 complex with the ribosome, which is unsurprising considering the dependency on ASCC3 for complex stability (Figure 5-9). To determine if direct interactions between ASCC2, TRIP4, and ASCC1 are possible, and if ASCC3 is required for these components to interact with the ribosome, further investigation of these interactions in the absence of ASCC3 would be required. The severely reduced complex stability following depletion of ASCC3 in cells suggests that these experiments would be better performed using an *in vitro* system.

Identification of novel interactors of the ASC-1 complex was carried out by FLAG immunoaffinity purification of ASCC3-3xFLAG and led to the identification of OTUD4 as an interactor of ASCC3, which bound following washes of 2.0 M NaCl (Figure 4-7). It has been shown previously that OTUD4 is a deubiquitinase that interacts with the ASC-1 complex in the nucleus, acting as a scaffold protein in the alkylation damage response (Zhao *et al.* 2015). However, recent studies have demonstrated a requirement of OTUD4 K63 deubiquitinase activity for regulation of MyD88 in TLR signalling (Zhao *et al.* 2018) and K48 deubiquitinase activity for MAV regulation in the antiviral response (Liuyu *et al.* 2019), demonstrating a role for OTUD4 in the innate immune response. More recent data have demonstrated that OTUD4 plays a role in neuronal RNA localisation and can be recruited to cytoplasmic stress granules (Das *et al.* 2019). Mass spectrometry data from the same study showed the interaction of OTUD4 with ASCC3, ASCC2,

and ASCC1 in the mouse cerebellum (Das *et al.* 2019). At the time of discovering the interaction of ASCC3 with OTUD4, there was only limited information available about its precise physiological function, making characterisation of OTUD4 challenging. However, a nuclear export signal was observed in its C-terminus using NetNES server prediction (La Cour *et al.* 2004) and OTUD4 has putative mRNA-binding capability (Baltz *et al.* 2012; Liepelt *et al.* 2016), suggesting that it had a cytoplasmic role. The data herein suggest that OTUD4 is a cytoplasmic RBP, however, its RNA-binding characteristics differ from those of ASCC3 in response to UVB exposure (Figure 5-4). Nevertheless, a minor proportion of OTUD4 was shown to co-localise with ASCC3 and the polysomes following treatment with 4NQO, indicating that both ASCC3 and OTUD4 play a role in the response to genotoxic stress (Figure 5-11). Further experiments are required to determine whether the catalytic activity of OTUD4 is responsible for the inefficient accumulation of OTUD4 on the polysomes (Figure 5-11). It should be noted that there is currently no evidence linking OTUD4 with the process of RQC. Therefore, it would be of great interest to determine the effect of OTUD4 depletion on ribosome stalling. For example, the effect of OTUD4 on poly(A)-dependent ribosome stalling could be monitored using well established reporter constructs (Juszkiewicz & Hegde 2017). In addition, a recent assay developed in the Willis laboratory to measure ribosome stalling *in vivo* could be employed to determine the effect of OTUD4 on ribosome stalling after genotoxic stress (Stoneley *et al*, unpublished data). Moreover, another outstanding question is whether OTUD4 plays any role in modulating ASCC3 RNA-binding, or whether this process is independent of OTUD4.

The data in this thesis also demonstrate that depletion of OTUD4 has no effect on cell proliferation (Figure 5-14), or mRNA translation (Figure 5-15), which does not agree with previously published study (Das *et al.* 2019). In this work, depletion of OTUD4 caused caspase 3 cleavage, a marker for apoptosis (Das *et al.* 2019). Protein synthesis has long been known to be inhibited during the process of cell death (reviewed in Morley *et al.* 2005) and therefore it is possible that the depletion conditions in these experiments could account for the discrepancy between these studies. In addition, recent data suggests that OTUD4 is required to stabilise ALKBH3, a demethylase involved in the repair of alkylated DNA adducts (Zhao *et al.* 2015). However, the data in this work show that OTUD4 was not required for the stability of the ASC-1 complex as the abundance of ASC-1 complex components was not affected by depletion of OTUD4 (Figure 5-9).

To further develop and characterise OTUD4 as a component of the ASC-1 complex, the function of its deubiquitinase activity should be explored, and proteomic methods to determine which ubiquitinated lysine residues of endogenous proteins are targeted by OTUD4 (Back *et al.* 2019;

Udeshi *et al.* 2013). Such studies may also uncover a role for OTUD4 in RQC, as this is known to be highly dependent on ubiquitin modifications (Garzia *et al.* 2017; Ikeuchi *et al.* 2019; Juszkiewicz & Hegde 2017; Sugiyama *et al.* 2019; Sundaramoorthy *et al.* 2017). Previous studies have shown that ASCC3 is ubiquitinated at multiple sites in response to UV damage (Boeing *et al.* 2016). Thus, it is possible that OTUD4 regulates the activity of ASCC3 through modulating its ubiquitination. Experiments were carried out to confirm that ASCC3 is ubiquitinated in response to genotoxic stress (Figure 6-3 and 6-4). Unfortunately, determining the exact nature of ASCC3 ubiquitination has proven technically challenging using overexpression of his-tag ubiquitin (Figure 6-3) and capturing endogenous ubiquitinated proteins with TUBEs (Figure 6-4). Nevertheless, these data revealed evidence for increased ASCC3 ubiquitination after 4NQO treatment and suggests that further optimisation of these techniques would be worthwhile to explore the involvement of OTUD4 in ASCC3 ubiquitination. A combination of the CUE domain of ASCC2, the identification the deubiquitinase OTUD4 and the E3 ubiquitin ligase UBR5 as novel protein partners for the ASC-1 complex, and the potential ubiquitin modification of ASCC3, suggests that ubiquitin plays an important role in determining the overall outcome of ASC-1 complex function.

In conclusion, the work carried out in this thesis has led to identification of OTUD4 as a novel interactor of ASCC3, while contributing additional information to further understand ASC-1 complex formation and stability. Although the exact role of the ASC-1 complex, and in particular the function of OTUD4 within this complex, remains undetermined, these new data support recent published studies (D'Orazio *et al.* 2019; Ikeuchi *et al.* 2019; Matsuo *et al.* 2017; Sugiyama *et al.* 2019), suggesting that OTUD4 may function in the process of resolving stalled ribosomes.

8. Appendix

8.1 Primer sequences

Primer name	Primer sequence (5'-3')
ASCC3 forward	CTCGTAGGTACCATGGCTTTACCTCGTCTCACAGG
ASCC3 reverse	CTGTCACTCGAGCTTTAATGCCAGGTCAGTCAG
ASCC3 N-terminal helicase domain reverse	CTTGCACTCGAGTGTATGAGGAGGATGTCTCTC
ASCC3 C-terminal helicase domain forward	CGTAGAGGTACCATGGAATTACTGGATCTTCAGCC
ASCC3 C-terminal domain forward	CGTGAAGGTACCCAGCCGAGGAGAAATGGACAG
ASCC3 N-terminal deletion forward	CTCGTAGGTACCATGCATTATCCCCATGTGTATG
OTUD4 (1-195) forward	TAAGCTTGGTACCGAGCTCGGATCCGCCACCATGGAGGCTG
OTUD4 (1-195) reverse	TACAGGCCATTCTGACTTCAACATGG
OTUD4 forward	TGAAGTCAGAATGGCCTGTATTCACTATCTTCGAGAG
OTUD4 reverse	CGTCATGGTCTTTGTAGTCCTCGAGAGTGTGCTGTCCCCTATGG

Table 8-1. Table of primers and their respective sequences

8.2 DNA fragment sequences

DNA fragment name	DNA fragment sequence (5'-3')
3xFLAG fragment	GTTTCACAATCTCGAGGATTACAAGGATGACGATGACAAGTAAGGGCCC GTGCCAACGG
OTUD4 WT	TCCAGCCTCCGGACTCTAGCGTTTAAACTTAAGCTTGGTACCGAGCTCGG ATCCGCCACCATGGAGGCTGCCGTCGGCGTCCCCGACGGCGGGGACCAG GGCGGCGCGGGGCCCCGCGAGGACGCGACGCCCATGGACGCCTATCTG CGGAAACTGGGCTTGTATCGGAAACTGGTCGCCAAGGACGGGTCGTGCC TGTTCCGGGCCGTGGCGGAGCAGGTATTGCACTCTCAGTCTCGCCATGTT GAAGTCAGAATGGCCTGTATTCACTATCTTCGAGAGAACAGAGAGAAA
OTUD4 C45A	TCCAGCCTCCGGACTCTAGCGTTTAAACTTAAGCTTGGTACCGAGCTCGG ATCCGCCACCATGGAGGCTGCCGTCGGCGTCCCCGACGGCGGGGACCAG GGCGGCGCGGGGCCCCGCGAGGACGCGACGCCCATGGACGCCTATCTG CGGAAACTGGGCTTGTATCGGAAACTGGTCGCCAAGGACGGGTCGGCCC TGTTCCGGGCCGTGGCGGAGCAGGTATTGCACTCTCAGTCTCGCCATGTT GAAGTCAGAATGGCCTGTATTCACTATCTTCGAGAGAACAGAGAGAAA
6xHis-Ubiquitin WT	TGCCGAGGTACCATGCACCACCATCACCATCATATGCAGATCTTCGTGAA AACCCTTACCGGCAAGACCATCACCCTTGAGGTGGAGCCCAGTGACACC ATCGAAAATGTGAAGGCCAAGATCCAGGATAAGGAAGGCATTCCCCCCG ACCAGCAGAGGCTCATCTTTGCAGGCAAGCAGCTGGAAGATGGCCGTAC TCTTTCTGACTACAACATCCAGAAGGAGTCGACCCTGCACCTGGTCCTGC GTCTGAGAGGTGGTtagCTCGAGTCGTAC
6xHis-Ubiquitin K48R	TGCCGAGGTACCATGCACCACCATCACCATCATATGCAGATCTTCGTGAA AACCCTTACCGGCAAGACCATCACCCTTGAGGTGGAGCCCAGTGACACC ATCGAAAATGTGAAGGCCAAGATCCAGGATAAGGAAGGCATTCCCCCCG ACCAGCAGAGGCTCATCTTTGCAGGCAGGCAGCTGGAAGATGGCCGTAC TCTTTCTGACTACAACATCCAGAAGGAGTCGACCCTGCACCTGGTCCTGC GTCTGAGAGGTGGTtagCTCGAGTCGTAC
6xHis-Ubiquitin K63R	TGCCGAGGTACCATGCACCACCATCACCATCATATGCAGATCTTCGTGAA AACCCTTACCGGCAAGACCATCACCCTTGAGGTGGAGCCCAGTGACACC ATCGAAAATGTGAAGGCCAAGATCCAGGATAAGGAAGGCATTCCCCCCG ACCAGCAGAGGCTCATCTTTGCAGGCAAGCAGCTGGAAGATGGCCGTAC TCTTTCTGACTACAACATCCAGAGGGAGTCGACCCTGCACCTGGTCCTGC GTCTGAGAGGTGGTtagCTCGAGTCGTAC
6xHis Ubiquitin K48R K63R	TGCCGAGGTACCATGCACCACCATCACCATCATATGCAGATCTTCGTGAA AACCCTTACCGGCAAGACCATCACCCTTGAGGTGGAGCCCAGTGACACC ATCGAAAATGTGAAGGCCAAGATCCAGGATAAGGAAGGCATTCCCCCCG ACCAGCAGAGGCTCATCTTTGCAGGCAGGCAGCTGGAAGATGGCCGTAC TCTTTCTGACTACAACATCCAGAGGGAGTCGACCCTGCACCTGGTCCTGC GTCTGAGAGGTGGTtagCTCGAGTCGTAC
6xHis Ubiquitin K0	TGCCGAGGTACCATGCACCACCATCACCATCATATGCAGATCTTCGTGAG AACCCTTACCGGCAGGACCATCACCCTTGAGGTGGAGCCCAGTGACACC ATCGAAAATGTGAGGGCCAGGATCCAGGATAGGGAAGGCATTCCCCCC GACCAGCAGAGGCTCATCTTTGCAGGCAGGCAGCTGGAAGATGGCCGTA CTCTTTCTGACTACAACATCCAGAGGGAGTCGACCCTGCACCTGGTCCTG CGTCTGAGAGGTGGTtagCTCGAGTCGTAC

Table 8-2. Table of DNA fragments and their respective sequences

8.3 siRNA sequences

siRNA name	siRNA sequence 5'-3'
Scramble negative control DsiRNA	Sense - CUUCCUCUCUUUCUCUCCCUUGUGA Antisense - AGGAAGGAGAGAAAGAGAGGGAACACU
ASCC1 siRNA	Sense - CCAACAGGCUACAAGAAUUAGUUGA Antisense - UCAACUAAUUCUUGUAGCCUGUUGGAG
TRIP4 siRNA	Sense - UAUAAAUUGACAAACUUUAUACA Antisense - CAAAGUUUGUCAAUUUAUACA
ASCC2 siRNA	Sense - UUGUAUAACACAAAAUACCGG Antisense – GGUAUUUUGUGUUAUACAAAC
ASCC3 siRNA	Sense - UUCAUUAUAAUUAUCUUGCUU Antisense - GCAAGAUAAUUAUAAUGAAGA
OTUD4 siRNA #1	Sense - GUAUUUAAAACUGAUGUUAGUAAAA Antisense - UUUUACUAACAUCAGUUUUAAAUACCU
OTUD4 siRNA #2	Sense - AAAUGGAAAUCAUUAUGAUAUUGTG Antisense - CACAAUAUCAUAAUGAUUUCCAUUUGA
OTUD4 siRNA #3	Sense - CUCCUUCACAAGUAACAGAAAAUAA Antisense - UUAUUUUCUGUUACUUGUGAAGGAGAA
Firefly luciferase siRNA	Dharmacon #P-002099-01-50 Target sequence - CAUUCUAUCCUCUAGAGGAUG

Table 8-3. Table of siRNA's and their respective sequences

References

Absmeier, E., Rosenberger, L., Apelt, L., … Wahl, M. C. (2015a). A noncanonical PWI domain in the N-terminal helicase-associated region of the spliceosomal Brr2 protein. *Acta Crystallographica Section D: Biological Crystallography*, 71, 762–771.

Absmeier, E., Wollenhaupt, J., Mozaffari-Jovin, S., … Wahl, M. C. (2015b). The large N-terminal region of the Brr2 RNA helicase guides productive spliceosome activation. *Genes and Development*, 29(24), 2576–2587.

Acker, M. G., Shin, B. S., Dever, T. E., & Lorsch, J. R. (2006). Interaction between eukaryotic initiation factors 1A and 5B is required for efficient ribosomal subunit joining. *Journal of Biological Chemistry*, 281(13), 8469–8475.

Ahler, E., Sullivan, W. J., Cass, A., … Christofk, H. R. (2013). Doxycycline Alters Metabolism and Proliferation of Human Cell Lines. *PLoS ONE*, 8(5), e64561.

Aksentijevich, I., & Zhou, Q. (2017). NF-κB pathway in autoinflammatory diseases: Dysregulation of protein modifications by ubiquitin defines a new category of autoinflammatory diseases. *Frontiers in Immunology*, 8(APR). doi:10.3389/fimmu.2017.00399

Antrobus, R., & Borner, G. H. H. (2011). Improved elution conditions for native co-immunoprecipitation. *PLoS ONE*, 6(3), 2–7.

Aramburu, J., Ortells, M. C., Tejedor, S., Buxadé, M., & López-Rodríguez, C. (2014). Transcriptional regulation of the stress response by mTOR. *Science Signaling*, 7(332). doi:10.1126/scisignal.2005326

Arima, Y., Nishigori, C., Takeuchi, T., … Miyachi, Y. (2006). 4-Nitroquinoline 1-oxide forms 8-hydroxydeoxyguanosine in human fibroblasts through reactive oxygen species. *Toxicological Sciences*, 91(2), 382–392.

Aulas, A., Fay, M. M., Lyons, S. M., … Ivanov, P. (2017). Stress-specific differences in assembly and composition of stress granules and related foci. *Journal of Cell Science*, 130(5), 927–937.

Baber, J. L., Libutti, D., Levens, D., & Tjandra, N. (1999). High precision solution structure of the C-terminal KH domain of heterogeneous nuclear ribonucleoprotein K, a c-myc transcription factor. *Journal of Molecular Biology*, 289(4), 949–962.

Back, S., Gorman, A. W., Vogel, C., & Silva, G. M. (2019). Site-Specific K63 Ubiquitinomics Provides Insights into Translation Regulation under Stress. *Journal of Proteome Research*, 18(1), 309–318, research-article.

Bagola, K., vonDelbrück, M., Dittmar, G., … Sommer, T. (2013). Ubiquitin Binding by a CUE Domain Regulates Ubiquitin Chain Formation by ERAD E3 Ligases. *Molecular Cell*, 50(4), 528–539.

Baltz, A. G., Munschauer, M., Schwanhäusser, B., … Landthaler, M. (2012). The mRNA-Bound Proteome and Its Global Occupancy Profile on Protein-Coding Transcripts. *Molecular Cell*, 46(5), 674–690.

Batty, D. P., & Wood, R. D. (2000). Damage recognition in nucleotide excision repair of DNA. *Gene*, 241(2), 193–204.

Becker, T., Armache, J. P., Jarasch, A., … Beckmann, R. (2011). Structure of the no-go mRNA decay complex Dom34-Hbs1 bound to a stalled 80S ribosome. *Nature Structural and Molecular Biology*, 18(6), 715–720.

Ben-Asouli, Y., Banai, Y., Pel-Or, Y., Shir, A., & Kaempfer, R. (2002). Human interferon-γ mRNA autoregulates its translation through a pseudoknot that activates the interferon-inducible protein kinase PKR. *Cell*, 108(2), 221–232.

Bleichert, F., & Baserga, S. J. (2007). The Long Unwinding Road of RNA Helicases. *Molecular Cell*, 27(3), 339–352.

Boeing, S., Williamson, L., Encheva, V., … Svejstrup, J. Q. (2016). Multiomic Analysis of the UV-Induced DNA Damage Response. *Cell Reports*, 15(7), 1597–1610.

Brandman, O., & Hegde, R. S. (2016). Ribosome-associated protein quality control. *Nat Struct Mol Biol*, 23(1), 7–15.

Brandman, O., Jacob, S.-O., Wong, D., … Weissman, J. S. (2012). A ribosome-bound quality control complex triggers degradation of nascent peptides and signals translation stress. *Cell*, 151(5), 1042–1054.

Brenner, M., & Hearing, V. J. (2008). The Protective Role of Melain Against UV Damage in Human Skin. *Photochemistry and Photobiology*, 84(3), 539–49.

Brickner, J. R., Soll, J. M., Lombardi, P. M., … Mosammaparast, N. (2017). A ubiquitin-dependent signalling axis specific for ALKBH-mediated DNA dealkylation repair. *Nature Publishing Group*, 551(7680), 389–393.

Brule, C. E., & Grayhack, E. J. (2017). Synonymous Codons: Choose Wisely for Expression. *Trends in Genetics*, 33(4), 283–297.

Bushell, M., Wood, W., Carpenter, G., Pain, V. M., Morley, S. J., & Clemens, M. J. (2001). Disruption of the Interaction of Mammalian Protein Synthesis Eukaryotic Initiation Factor 4B with the Poly(A)-binding Protein by Caspase- and Viral Protease-mediated Cleavages. *Journal of Biological Chemistry*, 276(26), 23922–23928.

Buskirk, A. R., & Green, R. (2017). Ribosome pausing, arrest and rescue in bacteria and eukaryotes. *Philosophical Transactions of the Royal Society B: Biological Sciences*, 372(1716), 20160183.

Buttgereit, F., & Brand, M. D. (1995). A hierarchy of ATP-consuming processes in mammalian cells. *Biochemical Journal*, 312(1), 163–167.

Cai, B., Wang, H., Zheng, H., & Wang, H. (2012). Detection of protein complexes from affinity purification/mass spectrometry data. *BMC Systems Biology*, 6(SUPPL3). doi:10.1186/1752-0509-6-S3-S4

Carell, T., & Epple, R. (1998). Repair of UV Light Induced DNA Lesions: A Comparative Study with Model Compounds. *European Journal of Organic Chemistry*, 1998(7), 1245–1258.

Caruthers, J. M., & McKay, D. B. (2002). Helicase structure and mechanism. *Current Opinion in Structural Biology*, 12(1), 123–133.

Castello, A., Horos, R., Strein, C., … Hentze, M. W. (2015). System-wide identification of RNA-binding proteins by interactome capture. *Methods in Molecular Biology*, 1358(3), 131–139.

Chen, Y., Zhang, L., & Jones, K. A. (2011). SKIP counteracts p53-mediated apoptosis via selective regulation of p21Cip1 mRNA splicing. *Genes & Development*, 1–9.

Chu, J., Hong, N. A., Masuda, C. A., … Kay, S. A. (2009). A mouse forward genetics screen identifies LISTERIN as an E3 ubiquitin ligase involved in neurodegeneration. *Proceedings of the National Academy of Sciences*, 106(7), 2097–2103.

Clague, M. J., Barsukov, I., Coulson, J. M., Liu, H., Rigden, D. J., & Urbé, S. (2013). Deubiquitylases from genes to organism. *Physiological Reviews*, 93(3), 1289–1315.

Cleaver, J. E., Lam, E. T., & Revet, I. (2009). Disorders of nucleotide excision repair: the genetic and molecular basis of heterogeneity. *Nature Reviews. Genetics*, 10(11), 756–768.

Cohen-Chalamish, S., Hasson, A., Weinberg, D., … Kaempfer, R. (2009). Dynamic refolding of IFN-γ mRNA enables it to function as PKR activator and translation template. *Nature Chemical Biology*, 5(12), 896–903.

Collier, A. E., Wek, R. C., & Spandau, D. F. (2015). Translational Repression Protects Human Keratinocytes from UVB-Induced Apoptosis through a Discordant eIF2 Kinase Stress Response. *Journal of Investigative Dermatology*, 135(10), 2502–2511.

D'Orazio, K. N., Wu, C. C.-C., Sinha, N., Loll-Krippleber, R., Brown, G. W., & Green, R. (2019). The endonuclease Cue2 cleaves mRNAs at stalled ribosomes during No Go Decay. *ELife*, 8, 1–27.

da Costa, P. J., Menezes, J., Saramago, M., … Romão, L. (2019). A role for DIS3L2 over natural nonsense-mediated mRNA decay targets in human cells. *Biochemical and Biophysical Research Communications*, 518(4), 664–671.

Dango, S., Mosammaparast, N., Sowa, M. E., … Shi, Y. (2011). DNA Unwinding by ASCC3 Helicase is Coupled to ALKBH3-Dependant DNA Alkylation Repair and Cancer Cell Proliferation. *Molecular Cell*, 44(3), 373–384.

Das, R., Schwintzer, L., Vinopal, S., … Broemer, M. (2019). New roles for the de-ubiquitylating enzyme OTUD4 in an RNA–protein network and RNA granules. *Journal of Cell Science*, 132(12), jcs229252.

Daugeron, M. C., Prouteau, M., Lacroute, F., & Séraphin, B. (2011). The highly conserved eukaryotic DRG factors are required for efficient translation in a manner redundant with the putative RNA helicase Slh1. *Nucleic Acids Research*, 39(6), 2221–2233.

de Laat, W. L., Jaspers, N. G. J., & Hoeijmakers, J. H. J. (1999). Molecular mechanism of nucleotide excision repair. *Genes & Development*, 13, 768–785.

de Nadal, E., Ammerer, G., & Posas, F. (2011). Controlling gene expression in response to stress. *Nature Reviews. Genetics*, 12(12), 833–45.

Defenouillère, Q., & Fromont-Racine, M. (2017). The ribosome-bound quality control complex: from aberrant peptide clearance to proteostasis maintenance. *Current Genetics*, 1–9.

Defenouillere, Q., Yao, Y., Mouaikel, J., … Fromont-Racine, M. (2013). Cdc48-associated complex bound to 60S particles is required for the clearance of aberrant translation products. *Proceedings of the National Academy of Sciences*, 110(13), 5046–5051.

Defenouillère, Q., Zhang, E., Namane, A., Mouaikel, J., Jacquier, A., & Fromont-Racine, M. (2016). Rqc1 and ltn1 prevent c-terminal alanine-threonine tail (cat-tail)-induced protein aggregation by efficient recruitment of cdc48 on stalled 60s subunits. *Journal of Biological Chemistry*, 291(23), 12245–12253.

Deshaies, R. J., & Joazeiro, C. A. P. (2009). RING Domain E3 Ubiquitin Ligases. *Annual Review of Biochemistry*, 78(1), 399–434.

Dever, T. E., & Green, R. (2015). The Elongation, Termination, and Recycling Phases of Translation in Eukaryotes, 1–16.

Di Liegro, C. M., Schiera, G., & Di Liegro, I. (2014). Regulation of mRNA transport, localizationand translation in the nervous system of mammals (Review). *International Journal of Molecular Medicine*, 33(4), 747–762.

Downes, D. J., Chonofsky, M., Tan, K., Pfannenstiel, B. T., Reck-Peterson, S. L., & Todd, R. B. (2014). Characterization of the Mutagenic Spectrum of 4-Nitroquinoline 1-Oxide (4-NQO) in Aspergillus nidulans by Whole Genome Sequencing. *G3 (Bethesda, Md.)*, 4(December), 2483–2492.

Dutertre, M., Lambert, S., Carreira, A., Amor-Guéret, M., & Vagner, S. (2014). DNA damage: RNA-binding proteins protect from near and far. *Trends in Biochemical Sciences*, 39(3), 141–149.

Elfakess, R., & Dikstein, R. (2008). A translation initiation element specific to mRNAs with very short 5'UTR that also regulates transcription. *PLoS ONE*, 3(8). doi:10.1371/journal.pone.0003094

Fadden, P., Haystead, T. A. J., & Lawrence, J. C. (1997). Identification of phosphorylation sites in the translational regulator, PHAS-I, that are controlled by insulin and rapamycin in rat adipocytes. *Journal of Biological Chemistry*, 272(15), 10240–10247.

Faller, W. J., Jackson, T. J., Knight, J. R. P., … Sansom, O. J. (2015). MTORC1-mediated translational elongation limits intestinal tumour initiation and growth. *Nature*, 517(7535), 497–500.

Feoktistova, M., Geserick, P., & Leverkus, M. (2016). Crystal violet assay for determining viability of cultured cells. *Cold Spring Harbor Protocols*, 2016(4), 343–346.

Garzia, A., Jafarnejad, S. M., Meyer, C., … Sonenberg, N. (2017). The E3 ubiquitin ligase and RNA-binding protein ZNF598 orchestrates ribosome quality control of premature polyadenylated mRNAs. *Nature Communications*, 8(May). doi:10.1038/ncomms16056

Gingold, H., Tehler, D., Christoffersen, N. R., … Pilpel, Y. (2014). A dual program for translation regulation in cellular proliferation and differentiation. *Cell*, 158(6), 1281–1292.

Gossen, M., Freundlieb, S., Bender, G., Muller, G., Hillen, W., & Bujard, H. (1995). Transcriptional activation by tetracyclines in mammalian cells. *Science*, 268(5218), 1766–1769.

Gross, J. D., Moerke, N. J., von der Haar, T., … Wagner, G. (2003). Ribosome Loading onto the mRNA Cap Is Driven by Conformational Coupling between eIF4G and eIF4E. *Cell*, 115, 739–750.

Guhaniyogi, J., & Brewer, G. (2001). Regulation of mRNA stability in mammalian cells. *Gene*, 265(1–2), 11–23.

Harigaya, Y., & Parker, R. (2010). No-go decay: A quality control mechanism for RNA in translation. *Wiley Interdisciplinary Reviews: RNA*, 1(1), 132–141.

Harvey, R., Dezi, V., Pizzinga, M., & Willis, A. E. (2017). Post-transcriptional control of gene expression following stress: the role of RNA-binding proteins. *Biochemical Society Transactions*, 45(4), 1007–1014.

Herhaus, L., & Dikic, I. (2015). Expanding the ubiquitin code through post-translational modification. *EMBO Reports*, 16(9), 1071–1083.

Hinnebusch, A. G. (2005). Translational Regulation of GCN4 and the General Amino Acid Control of Yeast. *Annual Review of Microbiology*, 59(1), 407–450.

Hjerpe, R., Aillet, F., Lopitz-Otsoa, F., Lang, V., England, P., & Rodriguez, M. S. (2009). Efficient protection and isolation of ubiquitylated proteins using tandem ubiquitin-binding entities. *EMBO Reports*, 10(11), 1250–1258.

Hospenthal, M. K., Mevissen, T. E. T., & Komander, D. (2015). Deubiquitinase-based analysis of ubiquitin chain architecture using Ubiquitin Chain Restriction (UbiCRest). *Nature Protocols*, 10(2), 349–361.

Hostetter, A. A., Osborn, M. F., & DeRose, V. J. (2012). RNA-Pt Adducts Following Cisplatin Treatment of Saccharomyces cerevisiae. *ACS Chemical Biology*, 7(1), 218–225.

Huggins, W., Ghosh, S. K., Nanda, K., & Wollenzien, P. (2005). Internucleotide movements during formation of 16 S rRNA-rRNA photocrosslinks and their connection to the 30 S subunit conformational dynamics. *Journal of Molecular Biology*. doi:10.1016/j.jmb.2005.09.060

Ikeuchi, K., Tesina, P., Matsuo, Y., … Inada, T. (2019). Collided ribosomes form a unique structural interface to induce Hel2-driven quality control pathways. *The EMBO Journal*, 38(5), e100276.

Illana, V., & Farhaeus, R. (2012). Purification of His-ubiquitin Proteins from Mammalian Cells. *BIO-PROTOCOL*, 2(17). doi:10.21769/BioProtoc.258

Iordanov, M. S., Pribnow, D., Magun, J. L., Dinh, T. H., Pearson, J. A., & Magun, B. E. (1998). Ultraviolet radiation triggers the ribotoxic stress response in mammalian cells. *Journal of Biological Chemistry*, 273(25), 15794–15803.

Iyer, L. M., Burroughs, A. M., & Aravind, L. (2006). The ASCH superfamily: Novel domains with a fold related to the PUA domain and a potential role in RNA metabolism. *Bioinformatics*, 22(3), 257–263.

Izaurralde, E., Sauliere, J., Huntzinger, E., Fauser, M., & Kashima, I. (2008). SMG6 is the catalytic endonuclease that cleaves mRNAs containing nonsense codons in metazoan. *Rna*, 14(12), 2609–2617.

Izawa, T., Park, S.-H., Zhao, L., Hartl, F. U., & Neupert, W. (2017). Cytosolic Protein Vms1 Links Ribosome Quality Control to Mitochondrial and Cellular Homeostasis. *Cell*, 171(4), 890-895.e18.

Jackson, R. J., Hellen, C. U. T., & Pestova, T. V. (2010). The mechanism of eukaryotic translation initiation and principles of its regulation. *Nature Reviews Molecular Cell Biology*, 11(2), 113–127.

Jackson, R. J., Hellen, C. U. T., & Pestova, T. V. (2012). *Termination and post-termination events in eukaryotic translation*. *Advances in Protein Chemistry and Structural Biology*, 1st edn, Vol. 86, Elsevier Inc. doi:10.1016/B978-0-12-386497-0.00002-5

Joazeiro, C. A. P. (2017). Ribosomal Stalling During Translation: Providing Substrates for Ribosome-Associated Protein Quality Control. *Annual Review of Cell and Developmental Biology*, 33(1), 343–368.

Johnson, S. J., & Jackson, R. N. (2013). Ski2-like RNA helicase structures: Common themes and complex assemblies. *RNA Biol*, 10(1), 33–43.

Jung, D.-J., Sung, H.-S., Goo, Y.-W., … Lee, Y. C. (2002). Novel Transcription Coactivator Complex Containing Activating Signal Cointegrator 1. *Molecular and Cellular Biology*, 22(14), 5203–11.

Juszkiewicz, S., Chandrasekaran, V., Lin, Z., Kraatz, S., Ramakrishnan, V., & Hegde, R. S. (2018). ZNF598 Is a Quality Control Sensor of Collided Ribosomes. *Molecular Cell*, 1–13.

Juszkiewicz, S., & Hegde, R. S. (2017). Initiation of quality control during poly(A) translation requires site-specific ribosome ubiquitination. *Molecular Cell*, 65(4), 743-750.e4.

Karamyshev, A. L., & Karamysheva, Z. N. (2018). Lost in translation: Ribosome-associated mRNA and protein quality controls. *Frontiers in Genetics*, 9(OCT), 1–13.

Kashima, I., Yamashita, A., Izumi, N., … Ohno, S. (2006). Binding of a novel SMG-1-Upf1-eRF1-eRF3 complex (SURF) to the exon junction complex triggers Upf1 phosphorylation and non-sense-mediated mRNA decay. *Genes & Development*, 355–367.

Khong, A., Matheny, T., Jain, S., Mitchell, S. F., Wheeler, J. R., & Parker, R. (2017). The Stress Granule Transcriptome Reveals Principles of mRNA Accumulation in Stress Granules. *Molecular Cell*, 68(4), 808-820.e5.

Kim, H.-J., Yi, J.-Y., Sung, H.-S., … Lee, J. W. (1999). Activating Signal Cointegrator 1, a Novel Transcription Coactivator of Nuclear Receptors, and Its Cytosolic Localisation under Conditions of Serum Deprivation. *Molecular and Cellular Biology*, 19(9), 6323–32.

Kim, H. H., Abdelmohsen, K., & Gorospe, M. (2010). Regulation of HuR by DNA Damage Response Kinases. *J. Nucleic Acids*, 2010, 1–8.

Kimball, S. R. (1999). Eukaryotic initiation factor eIF2. *Journal of Biochemistry and Cell Biology*, 31, 25–29.

Kimura, Y., & Tanaka, K. (2010). Regulatory mechanisms involved in the control of ubiquitin homeostasis. *Journal of Biochemistry*, 147(6), 793–798.

Kirkwood, K. J., Ahmad, Y., Larance, M., & Lamond, A. I. (2013). Characterization of native protein complexes and protein isoform variation using sizefractionation- based quantitative proteomics. *Molecular and Cellular Proteomics*, 12(12), 3851–3873.

Komander, D. (2009). The emerging complexity of protein ubiquitination. *Biochemical Society Transactions*, 37(5), 937–953.

Komander, D., Clague, M. J., & Urbé, S. (2009). Breaking the chains: Structure and function of the deubiquitinases. *Nature Reviews Molecular Cell Biology*, 10(8), 550–563.

Kootstra, A. (1994). Protection from UV-B-induced DNA damage by flavonoids. *Plant Molecular Biology*, 26(2), 771–774.

Kostova, K. K., Hickey, K. L., Osuna, B. A., … Weissman, J. S. (2017). CAT-tailing as a fail-safe mechanism for efficient degradation of stalled nascent polypeptides. *Science*, 357(6349), 414–417.

Kozak, M. (1987). At least six nucleotides preceding the AUG initiator codon enhance translation in mammalian cells. *Journal of Molecular Biology*, 196(4), 947–950.

Kozak, M. (1991). Structural features in eukaryotic mRNAs that modulate the initiation of translation. *Journal of Biological Chemistry*, 266(30), 19867–19870.

Kurosaki, T., & Maquat, L. E. (2016). Nonsense-mediated mRNA decay in humans at a glance. *Journal of Cell Science*, 129(3), 461–467.

Kurosaki, T., Popp, M. W.-L., Ermolenko, D. N., … Tian, B. (2014). A Post-Translational regulatory switch on UPF1 controls targeted mRNA degradation. *Genes and Development*, 28(17), 1900–1916.

La Cour, T., Kiemer, L., Mølgaard, A., Gupta, R., Skriver, K., & Brunak, S. (2004). Analysis and prediction of leucine-rich nuclear export signals. *Protein Engineering, Design and Selection*, 17(6), 527–536.

Lal, S., Burkhart, R. A., Beeharry, N., … Brody, J. R. (2014). HuR Posttranscriptionally Regulates WEE1: Implications for the DNA Damage Response in Pancreatic Cancer Cells. *Cancer Research*, 74(4), 1128–1140.

Lange, S. S., Takata, K., & Wood, R. D. (2011). DNA polymerases and cancer. *Nature Reviews. Cancer*, 11(2), 96–110.

Lee, J. W., Choi, H. S., Gyuris, J., Brent, R., & Moore, D. D. (1995). Two classes of proteins dependent on either the presence or absence of thyroid hormone for interaction with the thyroid hormone receptor. *Molecular Endocrinology*, 9(2), 243–254.

Lee, Y. S., Kim, H.-J., Lee, H. J., … Lee, K. (2002). Activating Signal Cointegrator 1 Is Highly Expressed in Murine Testicular Leydig Cells and Enhances the Ligand-Dependent Transactivation of Androgen Receptor. *Biology of Reproduction*, 67(5), 1580–1587.

Leppek, K., Das, R., & Barna, M. (2018). Functional 5′ UTR mRNA structures in eukaryotic translation regulation and how to find them. *Nature Reviews Molecular Cell Biology*, 19(3), 158–174.

Leprivier, G., Remke, M., Rotblat, B., … Sorensen, P. H. (2013). The eEF2 Kinase Confers Resistance to Nutrient Deprivation by Blocking Translation Elongation. *Cell*, 153(5), 1064–1079.

Liao, Y., Castello, A., Fischer, B., … Preiss, T. (2016). The Cardiomyocyte RNA-Binding Proteome: Links to Intermediary Metabolism and Heart Disease. *Cell Reports*, 16(5), 1456–1469.

Liaud, N., Horlbeck, M. A., Gilbert, L. A., Gjoni, K., Weissman, J. S., & Cate, J. H. D. (2019). Cellular response to small molecules that selectively stall protein synthesis by the ribosome. *PLoS Genetics*, 15(3), 1–30.

Liepelt, A., Naarmann-De Vries, I. S., Simons, N., … Ostareck-Lederer, A. (2016). Identification of RNA-binding proteins in macrophages by interactome capture. *Molecular and Cellular Proteomics*, 15(8), 2699–2714.

Linder, P., & Jankowsky, E. (2011). From unwinding to clamping - the DEAD box RNA helicase family. *Nature Reviews. Molecular Cell Biology*, 12(8), 505–16.

Liu, Y., & Lu, X. (2012). Non-coding RNAs in DNA damage response. *American Journal of Cancer Research*, 2(6), 658–75.

Liuyu, T., Yu, K., Ye, L., … Zhong, B. (2019). Induction of OTUD4 by viral infection promotes antiviral responses through deubiquitinating and stabilizing MAVS. *Cell Research*, 29(1), 67–79.

Lu, J., & Deutsch, C. (2008). Electrostatics in the Ribosomal Tunnel Modulate Chain Elongation Rates. *Journal of Molecular Biology*, 384(1), 73–86.

Lubin, A., Zhang, L., Chen, H., White, V. M., & Gong, F. (2013). A human XPC protein interactome-A resource. *International Journal of Molecular Sciences*, 15(1), 141–158.

Maag, D., Fekete, C. A., Gryczynski, Z., & Lorsch, J. R. (2005). A conformational change in the eukaryotic translation preinitiation complex and release of eIF1 signal recognition of the start codon. *Molecular Cell*, 17(2), 265–275.

Madronich, S., Mckenzie, R. L., Björn, L. O., Caldwell, M. M., Bjorn, L. O., & Caldwell, M. M. (1998). Changes in biologically active ultraviolet radiation reaching the Earth's surface. *Journal of Photochemistry and Photobiology B: Biology*, 46(1–3), 5–19.

Marengo, M. S., & Garcia-Blanco, M. A. (2009). Shedding UV Light on Alternative Splicing. *Cell*, 137(4), 600–602.

Margolin, D. H., Kousi, M., Chan, Y.-M., … Seminara, S. B. (2013). Ataxia, Dementia, and Hypogonadotropism Caused by Disordered Ubiquitination. *New England Journal of Medicine*, 368(21), 1992–2003.

Marintchev, A., Edmonds, K. A., Marintcheva, B., … Wagner, G. (2009). Topology and Regulation of the Human eIF4A/4G/4H Helicase Complex in Translation Initiation. *Cell*, 136(3), 447–460.

Marteijn, J. a, Lans, H., Vermeulen, W., & Hoeijmakers, J. H. J. (2014). Understanding nucleotide excision repair and its roles in cancer and ageing. *Nature Reviews. Molecular Cell Biology*, 15(7), 465–81.

Mata, J., Marguerat, S., & Bähler, J. (2005). Post-transcriptional control of gene expression: A genome-wide perspective. *Trends in Biochemical Sciences*, 30(9), 506–514.

Matsuo, Y., Ikeuchi, K., Saeki, Y., … Inada, T. (2017). Ubiquitination of stalled ribosome triggers ribosome-associated quality control. *Nature Communications*, 8(1), 159.

Mazan-mamczarz, K., Lal, A., Martindale, J. L., Kawai, T., & Gorospe, M. (2006). Translational Repression by RNA-Binding Protein TIAR. *Molecular and Cellular Biology*, 26(7), 2716–2727.

Mellacheruvu, D., Wright, Z., Couzens, A. L., … Nesvizhskii, A. I. (2013). The CRAPome: A contaminant repository for affinity purification-mass spectrometry data. *Nature Methods*, 10(8), 730–736.

Merrick, W. C. (1992). Mechanism and Regulation of Eukaryotic Protein Synthesis. *Microbiological Reviews*, 56(2), 291–315.

Mevissen, T. E. T., Hospenthal, M. K., Geurink, P. P., … Komander, D. (2013). OTU deubiquitinases reveal mechanisms of linkage specificity and enable ubiquitin chain restriction analysis. *Cell*, 154(1), 169–184.

Mevissen, T. E. T., & Komander, D. (2017). Mechanisms of Deubiquitinase Specificity and Regulation. *Annual Review of Biochemistry*, 86(1), 159–192.

Meyer, H. J., & Rape, M. (2014). Enhanced protein degradation by branched ubiquitin chains. *Cell*, 157(4), 910–921.

Miao, Z. H., Rao, V. A., Agama, K., Antony, S., Kohn, K. W., & Pommier, Y. (2006). 4-Nitroquinoline-1-oxide induces the formation of cellular topoisomerase I-DNA cleavage complexes. *Cancer Research*, 66(13), 6540–6545.

Milek, M., Imami, K., Mukherjee, N., … Landthaler, M. (2017). DDX54 regulates transcriptome dynamics during DNA damage response. *Genome Research*, 27(8), 1344–1359.

Molliex, A., Temirov, J., Lee, J., … Taylor, J. P. (2015). Phase Separation by Low Complexity Domains Promotes Stress Granule Assembly and Drives Pathological Fibrillization. *Cell*, 163(1), 123–133.

Montecucco, A., & Biamonti, G. (2013). Pre-mRNA processing factors meet the DNA damage response. *Frontiers in Genetics*, 4, 1–14.

Morley, S. J., Coldwell, M. J., & Clemens, M. J. (2005). Initiation factor modifications in the preapoptotic phase. *Cell Death and Differentiation*, 12(6), 571–584.

Moser, J. J., Chan, E. K. L., & Fritzler, M. J. (2009). Optimization of immunoprecipitation–western blot analysis in detecting GW182-associated components of GW/P bodies. *Nature Protocols*, 4(5), 674–685.

Mu, D., & Sancar, A. (1997). Model for XPC-independant Transcription-coupled Repair of Pyrimidine Dimers in Humans. *Journal of Biological Chemistry*, 272(12), 7570–7573.

Muñoz, M. J., Santangelo, M. S. P., Paronetto, M. P., … Kornblihtt, A. R. (2009). DNA Damage Regulates Alternative Splicing through Inhibition of RNA Polymerase II Elongation. *Cell*, 137(4), 708–720.

Myllykoski, M., Raasakka, A., Han, H., & Kursula, P. (2012). Myelin 2′,3′-cyclic nucleotide 3′-phosphodiesterase: Active-site ligand binding and molecular conformation. *PLoS ONE*. doi:10.1371/journal.pone.0032336

Nag, N., Lin, K. Y., Edmonds, K. A., … Marintchev, A. (2016). EIF1A/eIF5B interaction network and its functions in translation initiation complex assembly and remodeling. *Nucleic Acids Research*, 44(15), 7441–7456.

Nakada, S., Tai, I., Panier, S., … Durocher, D. (2010). Non-canonical inhibition of DNA damage-dependent ubiquitination by OTUB1. *Nature*, 466(7309), 941–946.

Nanda, J. S., Saini, A. K., Muñoz, A. M., Hinnebusch, A. G., & Lorsch, J. R. (2013). Coordinated movements of eukaryotic translation initiation Factors eIF1, eIF1A, and eIF5 trigger phosphate release from eIF2 in response to start codon recognition by the ribosomal preinitiation complex. *Journal of Biological Chemistry*, 288(8), 5316–5329.

O'Driscoll, M. (2012). Diseases associated with defective responses to DNA damage. *Cold Spring Harb Perspect Biol*, 4(12), 1–25.

Park, M. H., Nishimura, K., Zanelli, C. F., & Valentini, S. R. (2010). Functional significance of eIF5A and its hypusine modification in eukaryotes. *Amino Acids*, 38(2), 491–500.

Park, W. H. (2014). Anti-apoptotic effect of caspase inhibitors on H2O2-treated HeLa cells through early suppression of its oxidative stress. *Oncology Reports*, 31(5), 2413–2421.

Parker, S. H., Parker, T. A., George, K. S., & Wu, S. (2006). The roles of translation initiation regulation in ultraviolet light-induced apoptosis. *Molecular and Cellular Biochemistry*, 293(1–2), 173–181.

Parsyan, A., Svitkin, Y., Shahbazian, D., … Sonenberg, N. (2011). mRNA helicases: The tacticians of translational control. *Nature Reviews Molecular Cell Biology*, 12(4), 235–245.

Pascucci, B., Versteegh, A., van Hoffen, A., van Zeeland, a a, Mullenders, L. H., & Dogliotti, E. (1997). DNA repair of UV photoproducts and mutagenesis in human mitochondrial DNA. *Journal of Molecular Biology*, 273(2), 417–427.

Passos, D. O., Doma, M. K., Shoemaker, C. J., … Parker, R. (2009). Analysis of Dom34 and Its Function in No-Go Decay. *Molecular Biology of the Cell*, 20(13), 3025–3032.

Pek, J. W., Anand, A., & Kai, T. (2012). Tudor domain proteins in development. *Development (Cambridge)*, 139(13), 2255–2266.

Pestova, T. V., & Kolupaeva, V. G. (2002). The roles of individual eukaryotic translation initiation factors in ribosomal scanning and initation codon selection. *Genes & Development*, 16, 2906–2922.

Pfeifer, G. P. (1997). Formation and Processing of UV Photoproducts: Effects of DNA Sequence and Chromatin Environment. *Photochemistry and Photobiology*, 65(2), 270–283.

Piñeiro, D., Stoneley, M., Ramakrishna, M., … Willis, A. E. (2018). Identification of the RNA polymerase I-RNA interactome. *Nucleic Acids Research*, 46(20), 11002–11013.

Pinol-Roma, S., Adam, S. A., Choi, Y. Do, & Dreyfuss, G. (1989). Ultraviolet-induced cross-linking of RNA to proteins in vivo. *Methods in Enzymology*, 180(1981), 410–418.

Pisareva, V. P., Pisarev, A. V., Komar, A. A., Hellen, C. U. T., & Pestova, T. V. (2008). Translation Initiation on Mammalian mRNAs with Structured 5'UTRs Requires DExH-Box Protein DHX29. *Cell*, 135(7), 1237–1250.

Popp, M. W.-L., & Maquat, L. E. (2014). The Dharma of Nonsense-Mediated mRNA Decay in Mammalian Cells. *Molecules and Cells*, 37(1), 1–8.

Powley, I. R., Kondrashov, A., Young, L. A., … Willis, A. E. (2009). Translational reprogramming following UVB irradiation is mediated by DNA-PKcs and allows selective recruitment to the polysomes of mRNAs encoding DNA repair enzymes. *Genes and Development*, 23(10), 1207–1220.

Ramachandran, S., Tran, D. D. H., Klebba-Faerber, S., Kardinal, C., Whetton, A. D., & Tamura, T. (2011). An ataxia-telangiectasia-mutated (ATM) kinase mediated response to DNA damage down-regulates the mRNA-binding potential of THOC5. *RNA (New York, N.Y.)*, 17(11), 1957–66.

Ramanathan, A., Robb, G. B., & Chan, S. H. (2016). mRNA capping: Biological functions and applications. *Nucleic Acids Research*, 44(16), 7511–7526.

Reeve, B., Hargest, T., Gilbert, C., & Ellis, T. (2014). Predicting translation initiation rates for designing synthetic biology. *Frontiers in Bioengineering and Biotechnology*, 2(JAN), 1–6.

Richter, J. D., & Coller, J. (2015). Pausing on Polyribosomes: Make Way for Elongation in Translational Control. *Cell*, 163(2), 292–300.

Ronen, A. A., & Glickman, B. W. (2001). Human DNA repair genes. *Environmental and Molecular Mutagenesis*, 37(3), 241–283.

Ryazanov, A. G., Shestakova, E. A., & Natapov, P. G. (1988). Phosphorylation of elongation factor 2 by EF-2 kinase affects rate of translation. *Nature*, 334(6178), 170–173.

Saito, S., Hosoda, N., & Hoshino, S. I. (2013). The Hbs1-Dom34 protein complex functions in non-stop mRNA decay in mammalian cells. *Journal of Biological Chemistry*, 288(24), 17832–17843.

Sancar, A., Lindsey-Boltz, L. A., Unsal-Kaçmaz, K., & Linn, S. (2004). Molecular Mechanisms of Mammalian DNA Repair and the DNA Damage Checkpoints. *Annu Rev Biochem*, 73, 39–85.

Santos, K. F., Jovin, S. M., Weber, G., Pena, V., Luhrmann, R., & Wahl, M. C. (2012). Structural basis for functional cooperation between tandem helicase cassettes in Brr2-mediated remodeling of the spliceosome. *Proceedings of the National Academy of Sciences*, 109(43), 17418–17423.

Scheerlinck, E., Dhaenens, M., Van Soom, A., … Deforce, D. (2015). Minimizing technical variation during sample preparation prior to label-free quantitative mass spectrometry. *Analytical Biochemistry*, 490, 14–19.

Schofield, J. P. R., Cowan, J. L., & Coldwell, M. J. (2015). G-quadruplexes mediate local translation in neurons. *Biochemical Society Transactions*, 43, 338–342.

Schuller, A. P., Wu, C. C. C., Dever, T. E., Buskirk, A. R., & Green, R. (2017). eIF5A Functions Globally in Translation Elongation and Termination. *Molecular Cell*, 66(2), 194-205.e5.

Schwertman, P., Lagarou, A., Dekkers, D. H. W., … Marteijn, J. a. (2012). UV-sensitive syndrome protein UVSSA recruits USP7 to regulate transcription-coupled repair. *Nature Genetics*, 44(5), 598–602.

Searfoss, A. M., & Wickner, R. B. (2000). 3' poly(A) is dispensable for translation. *Proceedings of the National Academy of Sciences of the United States of America*, 97(16), 9133–7.

Sfakianos, A. P., Whitmarsh, A. J., & Ashe, M. P. (2016). Ribonucleoprotein bodies are phased in. *Biochemical Society Transactions*, 44(5), 1411–1416.

Shao, S., Brown, A., Santhanam, B., & Hegde, R. S. (2015). Structure and assembly pathway of the ribosome quality control complex. *Molecular Cell*, 57(3), 433–445.

Shao, S., & Hegde, R. S. (2014). Reconstitution of a Minimal Ribosome-Associated Ubiquitination Pathway with Purified Factors. *Molecular Cell*, 55(6), 880–890.

Shao, S., Von der Malsburg, K., & Hegde, R. S. (2013). Listerin-dependent nascent protein ubiquitination relies on ribosome subunit dissociation. *Molecular Cell*, 50(5), 637–648.

Shearer, R. F., Iconomou, M., Watts, C. K. W., & Saunders, D. N. (2015). Functional Roles of the E3 Ubiquitin Ligase UBR5 in Cancer. *Molecular Cancer Research*, 13(12), 1523–1532.

Shen, P. S., Park, J., Qin, Y., … Frost, A. (2015). Rqc2p and 60S ribosomal subunits mediate mRNA-independant elongation of nascent chains. *Science (New York, N.Y.)*, 3471(6217), 75–78.

Shinjo, S., Mizotani, Y., Tashiro, E., & Imoto, M. (2013). Comparative analysis of the expression patterns of UPR-target genes caused by upr-inducing compounds. *Bioscience, Biotechnology and Biochemistry*, 77(4), 729–735.

Simms, C. L., Hudson, B. H., Mosior, J. W., Rangwala, A. S., & Zaher, H. S. (2014). An Active Role for the Ribosome in Determining the Fate of Oxidized mRNA. *Cell Reports*, 9(4), 1256–1264.

Simms, C. L., Yan, L. L., & Zaher, H. S. (2017). Ribosome Collision Is Critical for Quality Control during No-Go Decay. *Molecular Cell*, 68(2), 361-373.e5.

Sinha, R. P., & Häder, D.-P. (2002). UV-induced DNA damage and repair: a review. *Photochemical & Photobiological Sciences*, 1(4), 225–236.

Sitron, C. S., Park, J. H., & Brandman, O. (2017). Asc1, Hel2, and Slh1 couple translation arrest to nascent chain degradation. *Rna*, 23(5), 798–810.

Soll, J. M., Brickner, J. R., Mudge, M. C., & Mosammaparast, N. (2018). RNA ligase-like domain in activating signal cointegrator 1 complex subunit 1 (ASCC1) regulates ASCC complex function during alkylation damage. *Journal of Biological Chemistry*, 293(35), 13524–13533.

Sonenberg, N., & Hinnebusch, A. G. (2009). Regulation of Translation Initiation in Eukaryotes: Mechanisms and Biological Targets. *Cell*, 136(4), 731–745.

Sowa, M. E., Bennett, E. J., Gygi, S. P., & Harper, J. W. (2009). Defining the Human Deubiquitinating Enzyme Interaction Landscape. *Cell*, 138(2), 389–403.

Spriggs, K. A., Bushell, M., & Willis, A. E. (2010). Translational Regulation of Gene Expression during Conditions of Cell Stress. *Molecular Cell*, 40(2), 228–237.

Stoneley, M., & Willis, A. E. (2004). Cellular internal ribosome entry segments: structures, trans-acting factors and regulation of gene expression. *Oncogene*, 23(18), 3200–3207.

Sudhakar, A., Ramachandran, A., Ghosh, S., Hasnain, S. E., Kaufman, R. J., & Ramaiah, K. V. A. (2000). Phosphorylation of Serine 51 in Initiation Factor 2α (eIF2α) Promotes Complex Formation between eIF2α(P) and eIF2B and Causes Inhibition in the Guanine Nucleotide Exchange Activity of eIF2B. *Biochemistry*, 39, 12929–38.

Sugasawa, K., Masutani, C., Uchida, A., … Hanaoka, F. (1996). HHR23B, a Human Rad23 Homolog, Stimulates XPC Protein in Nucleotide Excision Repair In Vitro. *Molecular and Cellular Biology*, 16(9), 4852–61.

Sugiyama, T., Li, S., Kato, M., … Inada, T. (2019). Sequential Ubiquitination of Ribosomal Protein uS3 Triggers the Degradation of Non-functional 18S rRNA. *Cell Reports*, 26(12), 3400-3415.e7.

Sundaramoorthy, E., Leonard, M., Mak, R., Liao, J., Fulzele, A., & Bennett, E. J. (2017). ZNF598 and RACK1 Regulate Mammalian Ribosome-Associated Quality Control Function by Mediating Regulatory 40S Ribosomal Ubiquitylation. *Molecular Cell*, 65(4), 751-760.e4.

Thoma, F. (1999). Light and dark in chromatin repair: repair of UV-induced DNA lesions by photolyase and nucleotide excision repair. *The EMBO Journal*, 18(23), 6585–98.

Thomas, M. P., & Lieberman, J. (2013). Live or let die: posttranscriptional gene regulation in cell stress and cell death. *Immunological Reviews*, 253(1), 237–252.

Thomas, P., & Smart, T. G. (2005). HEK293 cell line: A vehicle for the expression of recombinant proteins. *Journal of Pharmacological and Toxicological Methods*, 51(3 SPEC. ISS.), 187–200.

Tremblay, M., Toussaint, M., D'Amours, A., & Conconi, A. (2009). Nucleotide excision repair and photolyase repair of UV photoproducts in nucleosomes: assessing the existence of nucleosome and non-nucleosome rDNA chromatin in vivo. *Biochemistry and Cell Biology*, 87(1), 337–46.

Tsao, Y. S., Condon, R., Schaefer, E., Lio, P., & Liu, Z. (2001). Development and improvement of a serum-free suspension process for the production of recombinant adenoviral vectors using HEK293 cells. *Cytotechnology*, 37(3), 189–198.

Tse, W. K. F., Eisenhaber, B., Ho, S. H. K., Ng, Q., Eisenhaber, F., & Jiang, Y. J. (2009). Genome-wide loss-of-function analysis of deubiquitylating enzymes for zebrafish development. *BMC Genomics*, 10, 1–15.

Tse, W. K. F., Jiang, Y. J., & Wong, C. K. C. (2013). Zebrafish transforming growth factor-β-stimulated clone 22 domain 3 (TSC22D3) plays critical roles in Bmp-dependent dorsoventral patterning via two deubiquitylating enzymes Usp15 and Otud4. *Biochimica et Biophysica Acta - General Subjects*, 1830(10), 4584–4593.

Udeshi, N. D., Mertins, P., Svinkina, T., & Carr, S. A. (2013). Large-scale identification of ubiquitination sites by mass spectrometry. *Nature Protocols*, 8(10), 1950–1960.

Verma, R., Oania, R. S., Kolawa, N. J., & Deshaies, R. J. (2013). Cdc48/p97 promotes degradation of aberrant nascent polypeptides bound to the ribosome. *ELife*, 2013(2), 1–17.

Verma, R., Reichermeier, K. M., Burroughs, A. M., … Deshaies, R. J. (2018). Vms1 and ANKZF1 peptidyl-tRNA hydrolases release nascent chains from stalled ribosomes. *Nature*, 557(7705), 446–451.

Wang, Y., & Taniguchi, T. (2013). MicroRNAs and DNA damage response: Implications for cancer therapy. *Cell Cycle*, 12(1), 32–42.

Wawer, I., Golisz, A., Sulkowska, A., Kawa, D., Kulik, A., & Kufel, J. (2018). mRNA Decapping and 5'-3' Decay Contribute to the Regulation of ABA Signaling in Arabidopsis thaliana. *Frontiers in Plant Science*, 9(March), 1–12.

Wek, R. C., Jiang, H.-Y., & Anthony, T. G. (2006). Coping with stress: eIF2 kinases and translational control. *Biochemical Society Transactions*, 34(Pt 1), 7–11.

Wiederhold, K., & Passmore, L. A. (2010). Cytoplasmic deadenylation: regulation of mRNA fate. *Biochemical Society Transactions*, 38(6), 1531–1536.

Wilczynska, A., & Bushell, M. (2015). The complexity of miRNA-mediated repression. *Cell Death and Differentiation*, 22(1), 22–33.

Williamson, L., Saponaro, M., Boeing, S., … Svejstrup, J. Q. (2017). UV Irradiation Induces a Non-coding RNA that Functionally Opposes the Protein Encoded by the Same Gene. *Cell*, 168(5), 843-855.e13.

Wolfe, A. L., Singh, K., Zhong, Y., … Wendel, H. G. (2014). RNA G-quadruplexes cause eIF4A-dependent oncogene translation in cancer. *Nature*, 513(7516), 65–70.

Wood, R. D. (1997). Nucleotide Excision Repair in Mammalian Cells. *J Biol Chem*, 272(38), 23465–8.

Wood, R. D., Mitchell, M., Sgouros, J., & Lindahl, T. (2001). Human DNA Repair Genes. *Science*, 291(5507), 1284–1289.

Wu, C. A., Chao, Y., Shiah, S. G., & Lin, W. W. (2013). Nutrient deprivation induces the Warburg effect through ROS/AMPK-dependent activation of pyruvate dehydrogenase kinase. *Biochimica et Biophysica Acta - Molecular Cell Research*, 1833(5), 1147–1156.

Wurtmann, E. J., & Wolin, S. L. (2009). RNA under attack: Cellular handling of RNA damage. *Critical Reviews in Biochemistry and Molecular Biology*, 44(1), 34–49.

Xu, P., Duong, D. M., Seyfried, N. T., … Peng, J. (2009). Quantitative Proteomics Reveals the Function of Unconventional Ubiquitin Chains in Proteasomal Degradation. *Cell*, 137(1), 133–145.

Yan, L. L., & Zaher, H. S. (2019). How do cells cope with RNA damage and its consequences? *Journal of Biological Chemistry*, (1), jbc.REV119.006513.

Yip, M. C. J., Keszei, A. F. A., Feng, Q., Chu, V., McKenna, M. J., & Shao, S. (2019). Mechanism for recycling tRNAs on stalled ribosomes. *Nature Structural and Molecular Biology*, 26(May). doi:10.1038/s41594-019-0211-4

Yoshikawa, H., Larance, M., Harney, D. J., … Lamond, A. I. (2018). Efficient analysis of mammalian polysomes in cells and tissues using ribo mega-SEC. *ELife*, 7, 1–26.

Young, D. J., Guydosh, N. R., Zhang, F., Hinnebusch, A. G., & Green, R. (2015). Rli1/ABCE1 Recycles Terminating Ribosomes and Controls Translation Reinitiation in 3'UTRs In Vivo. *Cell*, 162(4), 872–884.

Zhang, X., Smits, A. H., Tilburg, G. B. A. van, … Vermeulen, M. (2017). An Interaction Landscape of Ubiquitin Signaling. *Molecular Cell*, 0(0), 941-955.e8.

Zhang, Z., Ye, Y., Gong, J., … Han, L. (2018). Global analysis of tRNA and translation factor expression reveals a dynamic landscape of translational regulation in human cancers. *Communications Biology*, 1(1), 1–11.

Zhao, Y., Majid, M. C., Soll, J. M., Brickner, J. R., Dango, S., & Mosammaparast, N. (2015). Noncanonical regulation of alkylation damage resistance by the OTUD4 deubiquitinase. *The EMBO Journal*, 34(12), 1687–1703.

Zhao, Y., Mudge, M. C., Soll, J. M., … Mosammaparast, N. (2018). OTUD4 Is a Phospho-Activated K63 Deubiquitinase that Regulates MyD88-Dependent Signaling. *Molecular Cell*, 69(3), 505-515.e5.

Zhou, B. S., & Elledge, S. J. (2000). The DNA damage response: putting checkpoints in perspective. *Nature*, 408(November), 433–439.